

Department of Chemical and Environmental Engineering

Transitional two-phase flow around 90° bends of different orientations

By

Rajab Abulgasem Omar

Thesis submitted to the University of Nottingham for the degree of Doctor of Philosophy

January 2017

ABSTRACT

Considering the gap in available information and the need of the industries such as oil and gas production, energy, and food processing, this study focuses on the two phase flows around bends in process pipe lines. The aim of this study is to investigate the influence of 90° bends on the gas-liquid two phase flow behaviour in vertical and horizontal orientations using advanced two-phase flow measuring techniques.

An experimental study has been conducted using silicone oil with a viscosity of 5 mPa.s and air to examine the transitional flows around 90° bends of 68 mm internal diameter (ID) with different configurations. Experiments were conducted at ambient conditions in an open system which consists of a 68 mm ID riser of 4.5 m long, vertical upward 90° bend and two horizontal sections of a 9.2m and 5.5m long in series with a horizontal 90° bend in between. The experimental matrix comprises 60 combinations of gas and liquid superficial velocities, ranging from 0.045 $m.s^{-1}$ to 3.21 $m.s^{-1}$ and 0.15 $m.s^{-1}$ to 0.53 $m.s^{-1}$ respectively. The phase distributions within the pipes were measured using Electrical Capacitance Tomography (ECT) and Wire Mesh Sensors (WMS). The behaviour of the flow was examined qualitatively using high speed imaging. To study the flow development in the riser, both ECT and WMS were placed in series and moved along three axial locations downstream of the mixing section. During the experiments at the bends, the ECT was kept immediately upstream while the WMS was moved to different positions downstream of the bend.

The cross-sectional void fraction time series from the ECT and the WMS were used to quantify the main hydrodynamic parameters of the flow including cross-sectional averaged void fraction, bubble size distribution, radial void fraction profiles, slug length, slug frequency, void fraction in liquid slugs, and the slug bubble velocity. Results were compared against the available slug flow correlations.

The results show that the phases separate shortly after the vertical to horizontal bend leading to stratified or wavy stratified flow. Beyond a certain threshold of the gas flow rate and liquid level, onset of slugs can be observed at a certain distance downstream of the vertical upward bend. This work suggests that the formation of hydrodynamic slugs downstream of the vertical upward bend is independent of the inlet conditions upstream. The horizontal bend, unlike the vertical upward bend, has a minor influence on the flow evolution, particularly slug flow. This is due to the influence of gravitational force on phase separation and its subsequent effect on the change of momentum in the vertical bend. The flow structures, mainly slugs and disturbance waves, are slightly accelerated as they pass through the horizontal bend with minimum change to the structure frequency and gas holdup within liquid slugs.

Most of the existing correlations do not predict the measured void fractions in this work as those correlations were essentially limited to the conditions they were developed for as the basis of them lies in the curve fitting. In this work, the higher viscosity and lower surface tension led to higher gas holdup in liquid slugs causing the discrepancy.

LIST OF PUBLICATIONS

Omar, R., B. Azzopardi, and B. Hewakandamby. "Air-Silicone Oil Flow Around a Vertical to Horizontal 90° Bend." 17th International Conference on Multiphase Production Technology. 10-12th June 2015 Cannes, France BHR: BHR Group.

Omar, R., B. Azzopardi, and B. Hewakandamby. "Experimental study on slug flow development in a riser and vertical to horizontal 90° bend ".9th International Conference on Multiphase Flow. May 22 to 27, 2016 in Firenze, Italy.

Zhao, D., Omar, R., Abdulkadir, M., Abdulkareem, L.A., Azzi, A., Saidj, F., Perez, V.H., Hewakandamby, B.N. and Azzopardi, B.J., 2017. The control and maintenance of desired flow patterns in bends of different orientations. Flow Measurement and Instrumentation, 53, pp.230-242

ACKNOWLEDGMENT

I would like to express my sincere gratitude to my advisors, Dr. Buddhika N. Hewakandamby and Prof. Barry J. Azzopardi for their continuous support and guidance throughout the course of my PhD research. My general research skills and multiphase flow knowledge have been greatly improved through their expert advice and constructive feedback.

It is truly important to extend my appreciation to the technical staff of L3 laboratory and L4 work shop, Phil, Mick, Mel, Fred, Marion, Reg and Paul for their effort and help to overcome any technical problem during the construction and operating the experimental facility. A special thanks to Fred and Mel for their endless support.

I would like to thank my fellow doctoral researchers, Josep Escrig, Shara Mohammed, Komonibo Ebiundu, Dr. Katerina Loizou, Abubakr Ibrahim, Mustapha Al-Behadili, Yousuf AlAufi, João Vasques and Matthew Yates for their feedback, cooperation and friendship.

I am especially grateful to all my friends for their help and support throughout my PhD course. Finally, I would like to thank my family for their love, support and encouragement to achieve this aim.

TABLE OF CONTENTS

ABSTRACT ..... **ii**

LIST OF PUBLICATIONS ..... **iv**

ACKNOWLEDGMENT ..... **v**

TABLE OF CONTENTS ..... **vi**

LIST OF FIGURES ..... **x**

LIST OF TABLES ..... **xix**

NOMENCLATURE ..... **xx**

Chapter 1 ..... **1**

Introduction **1**

1.1 The research background 3

1.2 Aims and objectives 6

1.3 Thesis structure 7

Chapter 2 ..... **9**

Literature review **9**

2.1 Basic definitions 9

2.1.1 Void fraction 10

2.1.2 Superficial velocity 10

2.2 Gas-liquid two-phase flow in pipes 11

2.2.1 Flow patterns in vertical and horizontal pipes 12

2.2.2 Flow Pattern Maps 15

2.3 Slug flow in pipes 18

2.3.1 Slug bubble velocity 21

2.3.2 Void fraction in liquid slug 24

2.3.3 Slug frequency 28

2.3.4 Slug length 32

2.4 Flows in curved pipes and bends 34

2.4.1 Two-phase flow through 90°bends 35

2.5 Summary 41
Chapter 3 43
Experimental setup and procedure 43
3.1 Experimental facility design and construction 43
3.1.1 Operating fluid 45
3.1.2 Design of the bends 46
3.1.3 Mixing section design 47
3.2 Description of experimental facility 48
3.3 Flow facility instrumentation 53
3.3.1 Data acquisition 53
3.3.2 Flow rate measurement 55
3.3.3 Temperature measurements 55
3.3.4 Pressure measurements 55
3.3.5 High speed imaging system 56
3.4 Wire Mesh Sensor 57
3.4.1.1 Calibration procedure and void fraction extraction 63
3.5 Electrical Capacitance Tomography 64
3.5.1.1 Image reconstruction 66
3.5.1.2 Calibration procedure and void fraction extraction 68
3.6 Experimental methodology 70
3.7 Signal analysis and data Processing 71
3.7.1 Data Characterisation 72
3.7.1.1 Stationarity test 73
3.7.1.2 Periodicity test 74
3.7.2 Sampling frequency 76
3.7.3 Time averaged void fraction from WMS and ECT 77
3.7.4 Bubble size distribution 79
3.7.5 Liquid level 80
3.7.6 Probability density function 82
3.7.7 Structure Frequency 83
3.7.8 Structure velocity 85
3.7.9 Slug length 87

3.8 Error analysis and uncertainty 87
3.8.1 Systematic uncertainty 88
3.8.2 Random uncertainty 89
3.8.3 Propagation of uncertainties 90
Chapter 4 92
Flow development in 68mm riser 92
4.1 Comparison between WMS and ECT 94
4.2 Flow patterns identification 97
4.3 Flow transition along the axial direction 99
4.3.1 Bubble size distribution and radial void fraction 101
4.4 Cross-sectional averaged void fraction 102
4.5 Slug Unit Characterisation 107
4.5.1 Slug length 108
4.5.2 Slug Frequency 111
4.5.3 Void fraction in liquid slug 114
4.5.4 Taylor bubble velocity 120
4.6 Summary 124
Chapter 5 128
Influence of vertical to horizontal 90◦ bend on gas-liquid flows development 128
5.1 Flow patterns 130
5.2 Axial flow development 136
5.3 Cross-sectional averaged void fraction 140
5.4 Structure Frequency 145
5.5 Structure Velocity 148
5.6 Slug unit characterisation 150
5.6.1 Taylor bubble velocity 151
5.6.2 Slug length 158
5.6.3 Slug frequency 162
5.6.4 Void fraction in liquid slug 168
5.7 Summary 176
Chapter 6 181

Experimental characterisation of air- silicone oil slug flow through a horizontal 90° bend 181

6.1 Onset of Hydrodynamic slugging 182

6.1.1 Visual observations 184

6.1.2 Necessary conditions for slug initiation 187

6.2 Axial flow development 191

6.3 Slug frequency 194

6.4 Slug bubble velocity 200

6.5 Slug length 205

6.6 Void fraction in liquid slug 208

6.7 Summary 214

Chapter 7 217

Conclusion and future wok 217

7.1 Conclusions 217

7.2 Recommendations for future work 221

BIBLIOGRAPHY 223

Appendix A 237

Appendix B 245

LIST OF FIGURES

Figure 2-1: Flow patterns in vertical and horizontal two-phase flow. Adopted from Taitel et al. (1978); (1980). 13

Figure 2-2: Flow pattern map for vertical upward flow Hewitt and Roberts (1969). 16

Figure 2-3:Flow pattern map for vertical upward flow by Taitel et al. (1980). 17

Figure 2-4: Flow pattern map for a horizontal flow system by Baker (1954). 17

Figure 2-5: Mandhane et al. (1974) flow pattern map for gas-liquid flow in a horizontal pipe..... 18

Figure 2-6: Slug Units.(a) vertical flow adopted from Azzopardi (2006), (b) horizontal flow adopted from Al-Safran (2009b). 20

Figure 3-1: A schematic diagram and a picture of the designed bend. 46

Figure 3-2: Schematic diagram of the air-silicone oil mixer. 48

Figure 3-3: A 3D diagram of the flow facility showing the main components. ... 50

Figure 3-4: Pictures of the main parts of the flow rig. 51

Figure **3-5**: A sketch of the ECT and WMS installation around the vertical ben. 52

Figure 3-6: A block diagram of the data acquisitions system. 54

Figure 3-7: Simplified scheme of the Wire Mesh sensor that is proposed by (Prasser et al. (1998). 58

Figure 3-8: A 24×24 Wire Mesh Topographic system. 62

Figure 3-9: Measurement principle of an ECT system (Dyakowski et al., 2000). 65

Figure 3-10: Electrical Capacitance Tomography system 65

Figure 3-11: The moving average and variance of 1 minute signal divided into 6 intervals of 5 second length. 74

Figure 3-12: Autocorrelation sequence for time averaged void fraction signal recorded at 1000Hz frequency for 1 minute. 75

Figure 3-13: Weight coefficients for estimating the time averaged local void fractions, adopted from Prasser et al. (2002). 77

Figure: 3-14: Coordinates of the measuring points used in identifying the interface height between phases in a horizontal pipe. (Black and red colours represents liquid and gas phase respectively)..... 80

Figure 3-15: The vertical mean chordal profiles of the void fraction at several time frames. 81

Figure 3-16: Identification of flow structures in the calculation of the structure frequency. 83

Figure 3-17: A sample of the time series (a) and the autocorrelation sequence (b) of cross-sectional averaged void fraction sampled at 1000Hz. 84

Figure 3-18: Power spectral density of the void fraction time series. 85

Figure 3-19:A sample of the void fraction time series received by the dual plane ECT, indicating the time delay. 86

Figure 3-20: The cross-correlation function of the void fraction signal obtained from the ECT system. 86

Figure 4-1: The PDF plots of the cross-sectional averaged void fraction for ECT and WMS at 45D downstream the mixer. The liquid superficial velocity= 0.22 m s^{-1}. 95

Figure 4-2: Radial void fraction profile and bubble size distribution obtained from WMS at 45D downstream of the mixer. Liquid superficial velocity = 0.22 $m.s^{-1}$.96

Figure 4-3: Cross-sectional averaged time series of void fraction and the corresponding PDFs for each flow pattern..... 98

Figure 4-4: Probability density function of a developed slug and an undeveloped slug. 99

Figure 4-5: PDF plots for different flow condition at 15D, 30D and 45D downstream the mixer. 100

Figure 4-6: Bubble size distribution for different flow patterns. 101

Figure 4-7: The variation of the averaged void fraction with superficial gas velocity for several liquid superficial velocities in the riser. 103

Figure 4-8: The axial variation of mean void fraction at Uls = 0.3 m s^{-1}. 104

Figure 4-9 Comparison of experimentally measured void fraction and predicted void fraction using drift flux model at 15D and 45D downstream of the mixer. 106

Figure 4-10: The axial development of the mean liquid slug length in the riser, at liquid superficial velocity=0.3ms^{-1}. 109

Figure 4-11: Liquid slug variation at different flow conditions..... 110

Figure 4-12: Comparison of experimentally measured slug length and predicted slug length using (Khatib and Richardson, 1984) correlation. 110

Figure 4-13: Frequency variation as a function of the axial distance in the riser at U_{ls}=0.3ms^{-1}. 112

Figure 4-14: Slug frequency variation with air and oil superficial velocity in the riser..... 112

Figure 4-15: Comparison of the experimental slug frequency with the available correlation. 113

Figure 4-16: Void fraction in the liquid slug along the axial direction..... 115

Figure 4-17: The effect of superficial gas velocity on the void fraction within the body of slugs. 116

Figure 4-18: Comparison of void fraction in liquid slugs with empirical correlations. 119

Figure 4-19: Taylor bubble velocity variation as a function of the axial distance in the riser at liquid superficial velocity = 0.3ms^{-1} 120

Figure 4-20: Taylor bubble velocity variation at 45D downstream of the mixer. 121

Figure 4-21: Experimental Taylor bubble velocity against the predicted values.123

Figure 5-1: Flow patterns observed in the riser. 130

Figure 5-2: Flow patterns observed in the horizontal section. 131

Figure 5-3:Flow condition in the riser superimposed on the flow patterns map of (Taitel et al., 1980). 133

Figure 5-4: Flow condition in the riser superimposed on the flow patterns map of (Mandhane et al., 1974). 134

Figure 5-5: Tomographic images from positions along the pipe system. Liquid superficial velocity = 0.22 m s^{-1} and gas superficial velocity = 0.05 m s^{-1}..... 138

Figure 5-6: Probability Density Function of void fraction time series at axial positions along the pipeline. Liquid superficial velocity = 0.15 m s^{-1} and gas superficial velocity = 0.05 m s^{-1}..... 138

Figure 5-7: Tomographic images from positions along the pipe system. Liquid superficial velocity = 0.53 m s^{-1} and gas superficial velocity = 0.45 m s^{-1}..... 139

Figure 5-8: Probability Density Function of void fraction time series at axial positions along the pipeline. Liquid superficial velocity = 0.53 m s^{-1} and gas superficial velocity = 0.45 m s^{-1}..... 139

Figure 5-9: Tomographic images from positions along the pipe system. Liquid superficial velocity = 0.53 m s^{-1} and gas superficial velocity = 3.21 m s^{-1}..... 140

Figure 5-10: Probability Density Function of void fraction time series at axial positions along the pipeline. Liquid superficial velocity = 0.53 m s^{-1} and gas superficial velocity = 3.21 m s^{-1}. 140

Figure 5-11: Effect of gas flow rate on the Cross-sectional averaged void fraction along the pipe system. Liquid superficial velocity = 0.45 m s^{-1}. 141

Figure 5-12: Effect of liquid flow rate on the cross-sectional averaged void fraction along the pipe system. Gas superficial velocity = 0.91 m s^{-1}. 142

Figure 5-13: The variation of the averaged void fraction with gas superficial velocity at 5D upstream (a) and 98D downstream (b) of the vertical bend. 143

Figure 5-14: Effect of gas flow rate on the characteristic frequency along the pipe system. Liquid superficial velocity = 0.45 m s^{-1}. 146

Figure 5-15: Effect of liquid flow rate on the characteristic frequency along the pipe system. Gas superficial velocity = 1.83 m s^{-1}..... 146

Figure 5-16: Frequency variation with air and oil superficial velocity at 5D (a) upstream and 98D (b) downstream of the vertical bend. 148

Figure 5-17: Structure velocity for several air and oil superficial velocities at 5D upstream (a) and 98D downstream (b) of the vertical bend. 149

Figure 5-18: Slugs velocity variation at 5D upstream of the bend (filled symbols) and 128D downstream of the bend (empty symbols)..... 152

Figure 5-19: Regression analysis on the measured Taylor bubble velocity in the horizontal section downstream of the bend. 155

Figure 5-20: Theoretical prediction of the experimental Taylor bubble velocity. 156

Figure 5-21: The axial development of the mean liquid slug length at the horizontal section, liquid superficial velocity=0.53 m s^{-1}. 158

Figure 5-22: Slug length variation at 5D upstream of the bend (filled symbols) and 128D downstream of the bend (empty symbols). 161

Figure 5-23: Frequency variation as a function of gas superficial velocity along the pipe system. Liquid superficial velocity=0.53 m s^{-1}. 163

Figure 5-24: Frequency variation at 5D upstream of the bend (filled symbols) and 128D downstream of the bend (empty symbols). 164

Figure 5-25: prediction of slug frequency at 128D downstream of the bend. 166

Figure 5-26: Axial development of the void fraction in slug length at the horizontal section, Uls=0.53 m s^{-1}. 170

Figure 5-27: Void fraction in liquid slug variation at 5D upstream of the bend (filled symbols) and 128D downstream of the bend (empty symbols). 171

Figure 5-28: Void fraction ratio between liquid slug and Taylor bubble against gas superficial velocities..... 172

Figure 5-29: Predicted void fraction in liquid slug using the available correlations. 174

Figure 6-1: Slug flow and disturbance waves observed during the experiments.183

Figure 6-2: Photographs illustrating the onset of a slug at; U_{ls} = 0.15 $m.s^{-1}$, U_{gs} = 1.37 $m.s^{-1}$.The direction of the flow from left to right. 185

Figure 6-3: Photographs illustrating the onset of a slug at; U_{ls} = 0.45 $m.s^{-1}$, U_{gs} = 1.37 $m.s^{-1}$. The direction of the flow from left to right. 187

Figure6-4: Liquid height measurements at L/D = 69 and U_{ls} = 0.53 $m.s^{-1}$: (a) U_{gs} = 0.36 $m.s^{-1}$,(b) U_{gs} = 0.91 $m.s^{-1}$, (c) U_{gs} = 1.83 $m.s^{-1}$, (d) U_{gs} = 2.75 $m.s^{-1}$..... 188

Figure 6-5: Liquid height at three different locations from the vertical 90° bend; U_{gs} = 1.37 $m.s^{-1}$, U_{ls} = 0.53 $m.s^{-1}$. 189

Figure 6-6: The variation of liquid height with the increase of gas superficial velocity at L/D=69. 190

Figure 6-7: Tomographic images from positions along the horizontal pipe system. Liquid superficial velocity = 0.53 m s^{-1} and gas superficial velocity = 0.55 m s^{-1}. 191

Figure 6-8: Probability Density Function of void fraction time series from positions along the horizontal pipe system. Liquid superficial velocity = 0.53 m s^{-1} and gas superficial velocity = 0.55 m s^{-1}. 192

Figure 6-9: Tomographic images from positions along the horizontal pipe system. Liquid superficial velocity = 0.53 m s^{-1} and gas superficial velocity = 3.21 m s^{-1}. 193

Figure 6-10: Probability Density Function of void fraction time series from positions along the horizontal pipe system. Liquid superficial velocity = 0.53 m s^{-1} and gas superficial velocity = 3.21 m s^{-1}. 193

Figure 6-11: Frequency variation against the gas superficial velocity along the pipe system. Liquid superficial velocity=0.45 m s^{-1}. 195

Figure 6-12: Frequency variation at 5D upstream of the bend (a) and 69D downstream of the bend (b)..... 196

Figure 6-13: Prediction of slug frequency at 5D upstream and 69D downstream of the bend. 197

Figure 6-14: Experimental slug frequency at 69D downstream of a horizontal bend is correlated in term of Strouhal number. 199

Figure 6-15: Slug bubble velocity variation at 5D upstream of the bend (a) and 69D downstream of the bend (b)..... 201

Figure 6-16: Regression analysis on the measured slug bubble velocity at 5D upstream and 69D downstream of the horizontal bend. 203

Figure 6-17: Theoretical prediction of the experimental slug bubble velocity at 5D upstream and 69D downstream of the horizontal bend. 204

Figure 6-18: The axial development of the mean liquid slug length around the horizontal bend, liquid superficial velocity = 0.45 $m.s^{-1}$. 206

Figure 6-19: Slug length variation at 5D upstream of the horizontal bend (a) and 69D downstream of the horizontal bend (b). 207

Figure 6-20: Axial development of the void fraction in liquid slug around the horizontal bend. Liquid superficial velocity = 0.45 $m.s^{-1}$. 209

Figure 6-21: Axial development of the void fraction in liquid slug around the horizontal bend. Gas superficial velocity = 1.83 $m.s^{-1}$..... 210

Figure 6-22: Void fraction in liquid slug variation at 5D upstream (a) and 69D downstream (b) of the horizontal bend. 211

Figure 6-23: Predicted void fraction in liquid slug at 5D upstream and 69D downstream of the horizontal bend, using the available correlations. 212

Figure A-1: The main valves of the flow rig..... 240

Figure A-2: Silicone oil tank..... 240

Figure A-3: Shutdown buttons at the upper platform (left) and the lower platform (right)..... 241

Figure A-4: High speed imaging system..... 241

Figure A-5: The differential pressure measurements system..... 242

Figure A-6: A schematic of the circuit showed in figure A-5, adopted from Recktenwald (2013). 242

Figure A-7: The LabVIEW block diagram used for data acquisition..... 243

Figure A-8: The LabVIEW block diagram used for data acquisition and valve control. 244

Figure B-1: The discrepancy of void fraction measurements between the WMS and the ECT..... 246

Figure B-2: The effect of gas superficial velocity on the average error. 247

Figure B-3: The fractional uncertainty of gas superficial velocities. 251

Figure B-4: The fractional uncertainty of gas superficial velocities. 252

Figure B-5: The fractional uncertainty of mixture superficial velocities. 253

Figure B-6: Calibration curve of a temperature sensor. 255

Figure B-7: Calibration curve of a pressure transmitter..... 255

LIST OF TABLES

Table 2-1: void fraction in liquid slug correlations 27

Table 2-2: Slug frequency correlations 31

Table 3-1: Fluid properties at ambient conditions 45

Table 3-2: the systematic error and the uncertainty associated with the corrected values through calibration. 89

Table 3-3: The fractional random uncertainty of the measured flow parameters. 90

Table 4-1: The statistical results for the applied two-phase flow correlations. .. 127

Table 5-1: The statistical measures for the employed two-phase flow correlations. 180

Table 6-1: Statistical results of the slug frequency correlations (top values are for upstream and bottom values are for downstream) 198

Table 6-2: Statistical results of the estimated void fraction in liquid slugs (top values are for upstream and bottom values are for downstream)..... 213

Table A-1: The experimental matrix. 237

Table B-1: Random uncertainty of the measured flow parameters..... 249

NOMENCLATURE

A	Cross section area, (m^2)
C_0	Distribution parameter of Taylor bubble velocity, (Dimensionless)
D	Internal pipe diameter, (m)
D_b	Bubbles diameter, (m)
f_s	Slug frequency, (1/s)
g	Gravity constant, (ms^{-2})
G	Mass flux, ($Kg/m^2.s$)
L	Length of the pipe, (m)
L_{su}	Length of the slug unit, (m)
L_S	Length of liquid slug, (m)
L_B	Length of Taylor babble, (m)
L_m	Length of the mixing zone, (m)
Q	Volumetric flow rate, (m^3/s)
R, r	Pipe radius, (m)
R_c	Curvature radius, (m)
u	Velocity, (m/s)

u_{gs} Gas superficial velocity, (m/s)

u_{ls} Liquid superficial velocity, (m/s)

u_g Taylor bubble velocity, (m/s)

u_{gSL} Gas superficial velocity in liquid slug, (m/s)

u_{lSL} Liquid superficial velocity in liquid slug, (m/s)

u_m Mixture velocity, (m/s)

U_d Drift velocity, (m/s)

U_{sg} Gas superficial velocity, (m/s)

U_{sl} Liquid superficial velocity, (m/s)

U_0 Terminal velocity of a bubble rising through fluid, (m/s)

x Mass quality, (Dimensionless)

Greek Symbols

μ Viscosity, (mPa.s)

ρ Density, (Kg/m^3)

σ Surface tension, (N/m)

ε_g Averaged void fraction, (Dimensionless)

ε_{gSL} Void fraction in liquid slug, (Dimensionless)

ε_{gTB} Void fraction in Taylor bubble, (Dimensionless)

θ	Bend angle, inclination angle (Degree)
$\emptyset$	Dimensionless ratio, $\emptyset = \varepsilon_{gSL}/\varepsilon_{gTB}$
ψ	Baker correction factor $\psi = \left(\frac{73}{v}\right)\left[\mu_L\left(\frac{62.3}{\rho_L}\right)^2\right]^{1/3}$, (Dimensionless)
λ	Baker correction factor $\lambda = \left[\left(\frac{\rho_G}{0.075}\right)\left(\frac{\rho_L}{62.3}\right)\right]^{0.5}$ (Dimensionless)

Subscripts

d	Drift
g	Gas phase
gls	Gas in liquid slug
l	Liquid phase
lls	Liquid in liquid slug
m	Mixture
s	Slug
su	Slug unit
tb	Taylor bubble

Dimensionless numbers

De	Dean Number, $De = Re(R/R_c)^2$
E_{ov}	Eotvos number, $E_{ov} = \rho_l g\, d^2/\sigma$

Fr	Froude Number, $Fr = u_m^2/gd$
Re	Reynolds number, $Re = \rho du/\mu$
St	Strouhal number, $St = fD/U_{ls}$

Chapter 1

Introduction

Multi-phase flows occur in a diverse range of industrial equipment, such as pipelines, boilers, condensers, reactors and phase separators. Although, the combination of gas-liquid is the most common case of multiphase flows; there are other mixtures that can possibly be encountered; such as gas-solid, liquid-solid and to a lesser extent (gas-liquid-water) flow. In the oil and gas industry, gas-liquid flow is often apparent throughout the different stages of production. The importance of multiphase flow in the oil industry was recognised over the last decades as a crucial parameter in equipment sizing such as pipes and separators. The understanding of the hydrodynamics of two-phase flow and hence the underlying fluid dynamics and heat transfer is a real challenge due to the complicity of the flow behaviour. In two-phase flow systems, gas and liquid phases are continuously redistributed, around the cross-section and the length of the pipe, in different structures known as flow patterns, while the change from one configuration to another is called flow patterns transition. Flow transition from one flow pattern to another affects the physical properties of the mixture and the expected flow rate of a specific phase. Thus, flow patterns play a major role in the design and operation of the industrial equipment. The importance of an accurate prediction of flow transition has been identified; several studies have presented the transition boundaries between different flow patterns, either in vertical or

horizontal pipes, on 2D plots known as flow pattern maps (Taitel et al., 1980; Mandhane et al., 1974).

The intermittent flows occur over a broad range of flow rates and are associated with high void fraction fluctuations. Slug flow is dominantly apparent in the pipelines of the gas and oil industry. It is generally characterised by large elongated bubbles separated by liquid slugs. The existence of slug flow in transportation pipelines causes high fluctuations in oil and gas flow rate at downstream facilities. The void fluctuations generate severe vibration that may cause damage especially at bends and other pipe fitting, moreover, corrosion can be accelerated with existence of slug flow (Gopal et al., 1995). It is recommended to minimise the occurrence of slug flow in the industrial pipelines to avoid the high impact of liquid slugs on pipe fittings such as bend and T-junctions (Miwa et al., 2015). The detailed monitoring of the slug behaviour can enhance the prediction of corrosion rate and pipe fatigue. Therefore in this work advanced instrumentations were used to obtain an accurate data set.

The spontaneous monitoring of the flow patterns in chemical processes is highly desired for quality control purposes. This requires realtime measurements devices that can offer void fraction measurements and phase distribution without disturbing the process. Visual observation based on the observer judgment, has been the main procedure to observe the flow behaviour, although it is impractical in most of the industrial applications due to the opaque nature of pipes and vessels. Several two phase measuring techniques have been proposed and developed over the past decades; all of those techniques have their own advantages and limitations. Therefore the selection of the appropriate measuring

techniques depends particularly on the nature of the process including, fluid properties, vessel size and the space available, in addition to the required measurements.

The chaotic transition of flow patterns in straight pipes is further enhanced during two-phase flow in pipe fittings such as bends and tees. Pipe fittings are widely used in the oil industry production pipelines. Bends dramatically influence the distribution of gas and liquid phases and the pressure losses. Predicting the behaviour of gas-liquid mixtures around bends require high quality quantitative measurements with reliable instrumentations. Therefore this work is devoted to the air-silicone oil flow experiments in 90° bends of different orientations, in order to gain more understanding of the effects on the gas-liquid flow development, bends would impart.

1.1 The research background

The gas and the liquid phases tend to flow in different configurations along the pipeline system mainly due to the difference in flow rates, densities as well as the pipes size and orientation. Pipe fittings including bends are widely used in most of the industrial process such as evaporation, condensation, and refrigeration. The complex nature of gas-liquid flow behaviour increases in the presence of bends, due to the effect of centrifugal force induced by curvature. Therefore, predicting the unsteady hydrodynamics of the flow around bends is crucial for process design and flow control. This becomes more demanding in offshore location where pipe failure due to vibration and flooding incidents are unaffordable.

As the flow passes through the bend, a secondary flow in the form of two identical vortices is imposed to the main stream, due to the imbalance of radial pressure created by the centrifugal force at the bend. The secondary flow in single phase flow was theoretically proven by (Dean, 1927). It is known as Dean Motion and its intensity is measured by a dimensionless group called a Dean's Number(De). The flow separation due to the secondary flow induced by the curvature has a significant influence on the distribution of phases. It results in higher energy dissipation than that of straight pipes and hence higher pressure loss. Moreover, the secondary flow is associated with pressure fluctuations and flow pattern transition which may enhance corrosion and cause problems such as burn out and pipe failure. In a vertical configuration, the flow in bends is more complex, where a combination of centrifugal and gravitational forces acts simultaneously, in addition to buoyancy forces. The effect of bends is more pronounced within the intermittent flow region, particularly slug flow. The current work realised the importance of the experimental characterisation of slug flow through bends, using high temporal and spatial resolution instruments. The prediction of slug flow characterises is of a great interest to the gas and oil industries. The experimental data was analysed in order to examine the behaviour of liquid slugs around 90 bends of different orientations.

Slug flow is a complex flow pattern that is commonly encountered in oil and gas transportation and production. The prediction of hydrodynamic parameters of liquid slug, mainly frequency and maximum length, is necessary in order to avoid some operational issues such as flooding and high pressure fluctuations. The slug flow enhances the corrosion rate in pipes, due to the turbulent region at the front

of the slug which increases the shear stress at the pipe wall (Sun and Jepson, 1992). Slug flow characteristics, such as frequency and gas holdup are required as inputs for two-phase flow predictive models (Dukler and Hubbard, 1975). The presence of bends increases the potential risk of slugging phenomenon; for instance, the direct impact of liquid slugs on bends increases vibrations in the pipe structure.

Single flow in bends and curved pipes has been extensively investigated over the last century, where most of the available literature about the secondary flow in bends is mainly focused on single phase flow (Berger et al., 1983; Spedding et al., 2004). Fewer papers are dedicated to two-phase gas-liquid flows, most of which are focused on two-phase pressure drop across bends. A limited number of publications have investigated the effect of bends on gas-liquid flow development (Saidj et al., 2014; De Oliveira et al., 2014). In addition, the effect of flow obstruction on the hydrodynamics of slug flow has not been fully exposed.

The publications that have realised the importance of the subject are few and restricted to small pipe diameter (< 40 mm) and fluids with physical properties incomparable to the industrial fluids. In small pipes the Taylor bubble is well defined, in contrast to large pipes where the Taylor bubble is deformed and hence the behaviour of liquid slugs can be totally different. Water was extensively used as the liquid phase for most of the previous studies. This provokes the need to investigate fluids with different physical properties, particularly fluids comparable to the hydrocarbons encountered in the oil and gas industry. Therefore, this work considers the investigation of air-silicone oil two-phase flows in relatively large diameter pipes (68mm ID), using a vertical upward and horizontal 90° bend in

series. It aims to overcome the limitations of the previous studies and provide a reliable database, employing advanced instrumentations. The behaviour of slug in 68mm ID can be comparable to the slug occurring in the industries pipeline. While the low surface tension silicone oil is comparable to the industrial hydrocarbon fluids. The work also provides a detailed analysis of the main slug characteristics at after and before 90° bends.

1.2 Aims and objectives

The design and operation of two-phase flow facilities is restricted to the limitation of existence theoretical models in predicting two-phase flow behaviour as well as the small range of the reliable data on two-phase gas-liquid flow. Therefore, the motive of this work is the need of reliable data of two-phase flow in pipes comparable to those employed in industrial piping system with fluids of relatively high viscosity. The main aims of this work are:

- To observe the flow transition throughout vertical and horizontal 90° bends.
- To investigate the effect of gas and liquid superficial velocities on the flow development through 90° bends of different orientations.

Objectives contributing to achieve the aims are:

- To design and commission a two-phase flow facility with flow control and instrumentation.
- To test the capability of the experimental rig for the achievable flow rates.
- To study the flow development in a vertical riser.
- To evaluate the effects of the primary operation conditions on the flow development in vertical upward and horizontal 90° bends.

- To examine the effects of 90° bends of different orientations on the hydrodynamics of slug flow.
- To test the available slug flow models.

1.3 Thesis structure

This thesis is divided into seven chapters:

Chapter one: Introduction

This chapter contains a general introduction to multi-phase flow systems. Furthermore, the research background is highlighted, while the problem, as well as the main aims and objectives of this work, are defined.

Chapter two: Literature review

In this chapter, the main flow patterns in vertical and horizontal pipes are described, where the widely used flow pattern maps are highlighted. The major works on slug flow in straight pipes are reviewed, while the main correlations of slug flow are discussed. The gas-liquid flow around 90° bends is extensively and critically reviewed and the limitations of the previous studies are identified.

Chapter three: Experimental setup and procedure

It presents the design and construction process of the flow rig including the description of the important parts such as bends and gas-liquid mixing section. This chapter also provides the experimental procedure followed during the experimental runs, in addition to the rig instrumentation. Finally, the methods of data analysis and error estimation are explained in details.

Chapter four: Flow development in 68mm riser

This chapter contains a comparison between the wire mesh sensor and Electrical capacitance system. It presents the flow transition along the pipe at three axial locations (15, 30 and 45 pipe diameter) downstream of the mixing section. The change in void fraction with gas and liquid superficial velocities is also presented. A detail analysis of the liquid slug characterises along the pipe is demonstrated while the validation of the available slug flow correlations is discussed.

Chapter five: Gas-liquid flows development through vertical to horizontal 90° bend

This chapter offer a detail investigation about the air-silicone oil flow evolution through vertical upward 90° bend. The observed flow patterns are reported and compared with established flow pattern maps. The flow transition at 3 positions upstream and 6 position downstream of the bend is presented. The effects of the bend on the hydrodynamics of the slug unit are interrogated.

Chapter six: Experimental characterisation of air- silicone oil slug flow through a horizontal 90° bend

This chapter presents detailed experimental results of air-silicone oil two-phase flows through a horizontal 90° bend. It includes the visual observations and a comprehensive analysis of the slug characteristics at 4 locations before and 5 locations after the bend.

Chapter seven: Conclusion and future work

It includes the main findings of this work as well as the recommendations of future work.

Chapter 2

Literature review

Two phase gas-liquid flow through straight pipes have been widely studied over the last several decades. Several models were developed to predict the gas-liquid flow behaviour, however, none of those models can be generalised. The gas and liquid phases tend to flow in different configurations along the pipe system mainly due to the difference in flow rates, densities as well as the pipes size and orientation. Pipe fittings including bends are widely used in most of the industrial process where the complexity of the flow behaviour is increased due to the effect of centrifugal force induced by curvature. Therefore predicting the unsteady hydrodynamics of the flow is crucial for the process design and flow control.

This chapter provides an overview of the gas-liquid flow in straight pipes as well as the main flow pattern maps available for two phase flow classification and prediction section 2.2. The slug flow characteristics are described in Section 2.3, where the main studies on slug flow through vertical and horizontal pipes are reviewed. The gas-liquid flow through 90° bends is critically reviewed in Section 2.4.

2.1 Basic definitions

Before proceeding through the main chapters of this wok, it is crucial to define some of the related terminology.

2.1.1 Void fraction

Void fraction (ε_g) is one of the main parameter to characterise the behaviour of gas–liquid two phase flows. It represents the volumetric concentration of the gas phase over a sufficient length of a pipe (L) (Wallis, 1969). This can be achieved only by isolating the test section, using quick closing valve. The void fraction is defined as:

$$\varepsilon_g = Q_g/AL \tag{2.1}$$

where; Q_g is the volume of the trapped gas and A is the cross-sectional area of the pipe. It is not always practical to conduct such measurements, thus the averaged void fraction can be obtained through enormous number of instantaneous measurements at certain location in the test section. The void fraction is a dimensionless quantity with values ranging between 0 and 1. It is often called as gas holdup and interchangeably used with the liquid holdup. In this work, the term void fraction and gas holdup are used.

2.1.2 Superficial velocity

The superficial velocity represents the volumetric flow rate of a given phase per unit area. It can be termed as gas volume flux. The superficial velocity is calculated based on the hypothesis that a single phase flows alone in the cross section area as:

$$u_{gs} = Q_g/A \tag{2.2}$$

$$u_{ls} = Q_l/A \tag{2.3}$$

In practice such velocity does not exist, since the both phases flow simultaneously in the same channel, however, it is a useful parameter for flow characterisation. In single phase flow the superficial velocity is equal to the mean velocity of the given phase. The sum of gas and liquid superficial velocity gives the total volume flux which is referred to as the mixture velocity.

$$u_m = u_{gs} + u_{ls} \tag{2.4}$$

The average velocity of each phase can be found using the following expressions (Azzopardi, 2006):

$$u_g = u_{ls}/\varepsilon_g \tag{2.5}$$

$$u_l = u_{ls}/(1 - \varepsilon_g) \tag{2.6}$$

2.2 Gas-liquid two-phase flow in pipes

Gas-liquid tow-phase flow is a special case of the multi-phase flow in which the gas and liquid flow concurrently along the pipe. Gas-liquid flows are commonly encountered in different industrial application such as gas-oil industries, power generation, and food processing. Therefore, a sufficient knowledge on the behaviour of two-phase mixtures is a primary requirement in engineering design and operation for these industrial processes. In gas-liquid flows, phases change progressively along the pipe with time and distance exhibiting several geometric configurations which are broadly known as flow regimes or patterns. This change in flow regimes is significantly influenced by the pipe orientation, pipe size, flow

rates, and the difference in phase densities. The area of multiphase flow in pipes has received great attention due to ubiquitous industrial applications. Different flow regimes are observed in horizontal and vertical pipes, while several approaches were proposed to identify and predict the flow regimes including flow pattern maps and theoretical correlations. This section provides a brief description of the different flow regimes occurring in vertical and horizontal pipes, while the corresponding flow pattern maps are highlighted.

2.2.1 Flow patterns in vertical and horizontal pipes

The flow regimes that can be expected in vertical upward flow are classified into four main regimes according to Hewitt and Hall-Taylor (1970) including bubble, slug, churn and annular as illustrated in Figure 2-1.

In horizontal pipes, the gravity acts perpendicular to the flow direction. Thus, the liquid tends to accumulate at the bottom of the pipe while the gas tends to flow above the liquid. According to Alves (1954), the main flow regimes in horizontal pipes can be described as, bubbly, plug, stratified, slug, annular flows as shown in Figure 2-1.

Bubbly flow: In this pattern, the gas phase is almost uniformly distributed within the continuous liquid phase in the form of small discrete bubbles of non-uniform size. The bubbles can coalesce and break up as they travel along the pipe. In the case of upward flows, the large bubbles tend to flow in the centre while the smaller bubbles move to the pipe wall, due to the change in the lift force. It was reported that the critical bubble size at which a transition from wall to core peak occurs is around 5-6mm (Tomiyama, 1998; Lucas et al., 2005; Lucas et al., 2010).

Griffith and Snyder (1964) and Taitel et al. (1980) suggested that bubble/slug transition occurs at void fraction value of around 0.25 to 0.3. In horizontal configuration the gas bubbles tend to flow at the upper part of the pipe, due to the bouncy effects

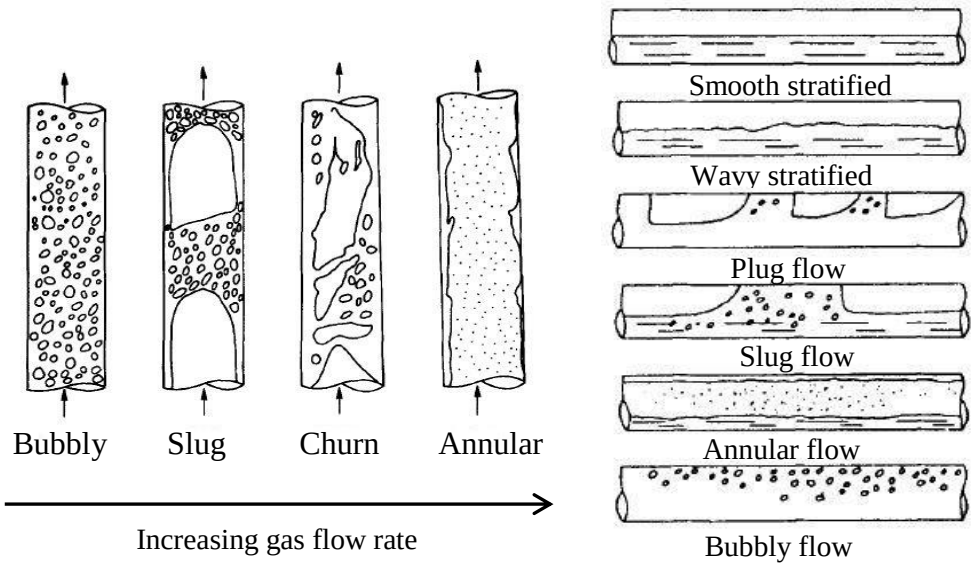


Figure 2-1: Flow patterns in vertical and horizontal two-phase flow. Adopted from Taitel et al. (1978); (1980).

Plug flow: It is characterised by gas plugs moving along the upper part of the pipe alternatively with liquid plugs. Gas plugs velocities are almost equal to the velocity of the liquid.

Stratified flow: In this configuration, the gas phase flows above a liquid layer with a smooth interface.

Wavy stratified flow: It is similar to the stratified flow except that at high gas velocity the interface is disturbed and waves are formed along the flow direction.
Slug flow: This configuration is characterised by bullet shape bubbles, usually known as Taylor bubbles that is almost equivalent to the size of the pipe. These

large bubbles travels upward surrounded with a thin liquid film. The bubbles are separated by liquid slugs that are more likely to contain small dispersed gas bubbles. Different slug-churn transition models have been proposed, the main ones are described in (Jayanti and Hewitt, 1992).On the other hand, several studies reported the absence of slug flow in large diameter pipes (~200mm) (Ohnuki and Akimoto, 2000; Omebere-Iyari et al., 2007; Omebere-Iyari et al., 2008).

Churn flow: It is described as unstable pattern of liquid oscillation. Churn flow is a chaotic intermittent flow which covers wide range of gas flow rates, where in some cases can be referred to as froth or semi-annular flow. Slug-churn transition has been a controversial topic. Churn flow was considered as an entrance phenomenon (Taitel et al., 1980) or a manifestation of slug (Mao and Dukler, 1993). In contrast, Brauner and Barnea (1986) considered churn flow as an independent and developed flow pattern. In response to this argument, Hewitt and Jayanti (1993) reported that churn flow can occur as an entry phenomenon or an independent region between slug and annular flow.

Annular flow: In this flow pattern, the gas phase flow along the pipe core, while the liquid phase travels upward as liquid film around the pipe and partially in form of entrained droplets in the gas core. At specific gas and liquid flow rates, other sub-flow patterns are observed such as mist flow and wispy-annular flow. In the horizontal configuration, the liquid film is thicker in the lower part of the pipe due to the effect of gravity. As the gas velocity increases, most of the liquid phase is entrained into the gas forming a spray or dispersed flow.

It can be noted that there are sub-flow regimes that can be observed within the main flow regimes mentioned above. Flow patterns identification is subjected to the observer judgment and experience; hence it is challenging to construct a general flow pattern map.

2.2.2 Flow Pattern Maps

Over a half century, several flow pattern maps have been developed. Most of those maps were generated from experimental data of adiabatic two-phase flow systems. Those maps present the transitional boundaries between the different flow patterns in 2D plots. The selection of the two coordinates is usually based on dimensional parameters including superficial phase velocities, mass flow rate and mass velocity. In some cases dimensionless groups are employed (Taitel et al., 1980). The different parameters that can be used to identify the flow transition were reviewed by (Spedding and Nguyen, 1980). Spedding and Spence (1993) reviewed around 40 flow pattern maps. They concluded that neither the empirical flow pattern maps nor the theoretical transitional models are able to consider the difference in pipe size or phase properties. Spedding et al. (1998) reported that there is no existing flow regimes map that can be generalised to predict the vertical two-phase flow. It can be said that the transitional boundaries in the flow pattern maps should not be treated as sharp distinct transitional lines, but as transitional zones. However, there is no universal flow pattern map that can predict the two-phase flow patterns accurately; there are several reliable flow pattern maps that can give a satisfactory prediction within a specific range of experimental data.

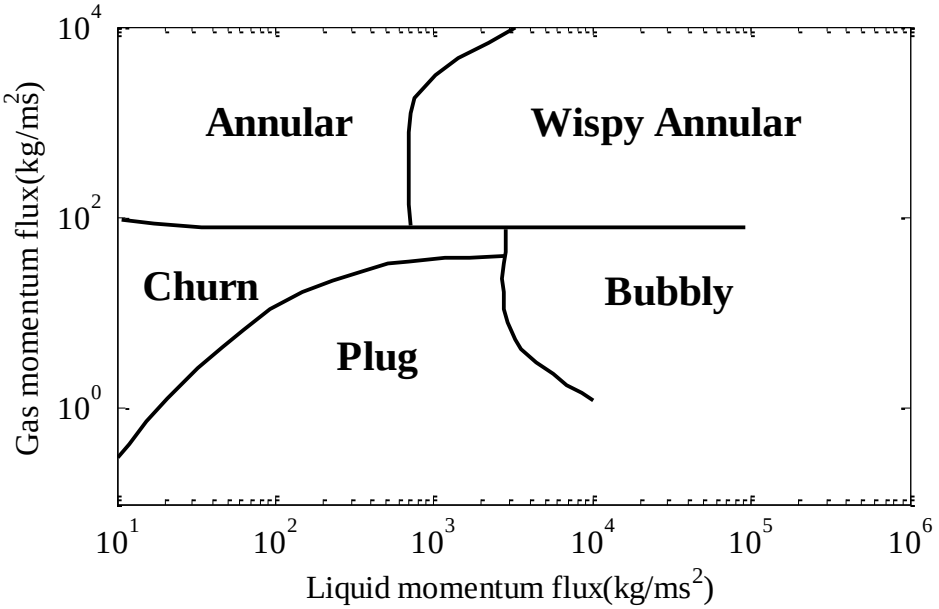


Figure 2-2: Flow pattern map for vertical upward flow Hewitt and Roberts (1969).

For vertical upward flow, Hewitt and Roberts (1969) map, as illustrated in Figure 2-2, is considered one of the commonly used flow pattern maps. They used air-water data at a pressure of 3 bar and steam-water data at a pressure of 35 and 70 bar, where the overall data was presented as liquid flux against gas flux.

The well-kwon map of Taitel et al. (1980), as shown in Figure 2-3, was developed for air-water flow in a vertical 50 mm pipe. This map unlike others is based on theoretical models similar to the approach of Taitel and Dukler (1976) for horizontal systems. Therefore, it is expected to be valid for a wider range of flow conditions. Oshinowo and Charles (1974) and Spedding and Nguyen (1980) developed their flow pattern maps, using Froude number and the volumetric ratio as coordinates.

For horizontal flow, the flow pattern map proposed by Baker (1954) is the most widely accepted, particularly in industrial application, as illustrated in Figure 2-4. It was developed from experimental data comparable to the industrial conditions.

The data was plotted as gas mass velocity against the mass ratio. Correction factors (λ and ψ) were introduced to compensate for the difference in physical properties. Baker flow patterns map was modified later by Scott (1963) who extended the sharp boundaries to transitional zones.

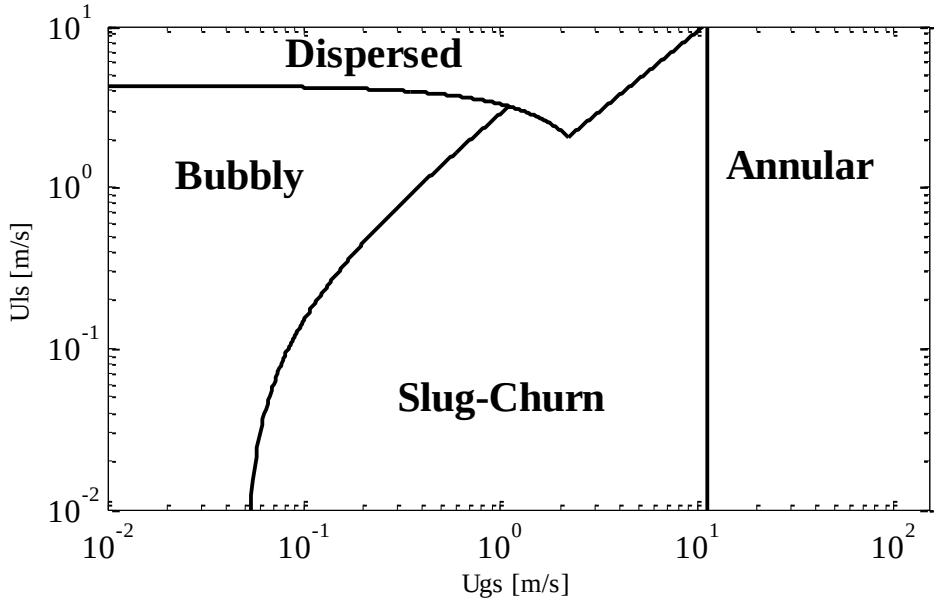


Figure 2-3:Flow pattern map for vertical upward flow by Taitel et al. (1980).

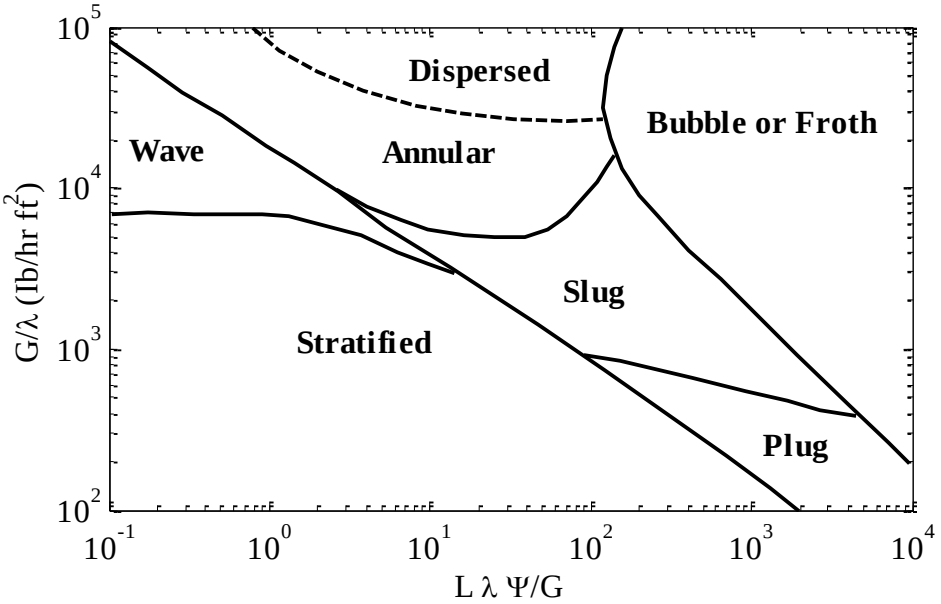


Figure 2-4: Flow pattern map for a horizontal flow system by Baker (1954).

Mandhane et al. (1974) developed a flow pattern map based on nearly six thousands visual observations (Figure 2-5). It is the most widely used amongst the available flow pattern maps for horizontal flows. Mandhane et al. (1974) suggests that changes in pipe diameter and fluid properties have no dramatic effects on the transition boundaries, if superficial gas velocity and superficial liquid velocity are used as coordinates. Taitel and Dukler (1976) argued that two axes are not enough to predict the different transitional boundaries. Therefore, they developed a theoretical flow patterns map that considers different dimensional coordinates for different transitional boundaries.

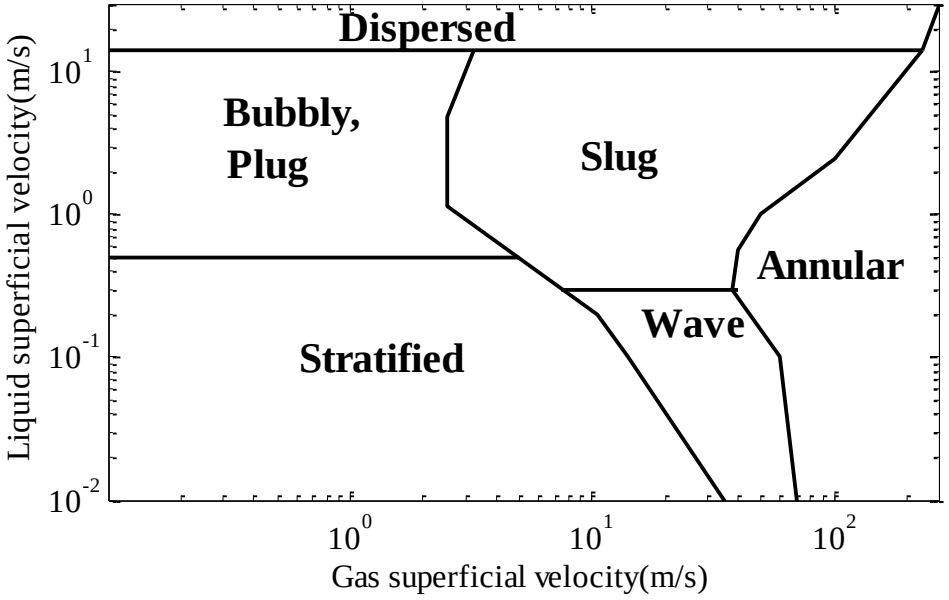


Figure 2-5: Mandhane et al. (1974) flow pattern map for gas-liquid flow in a horizontal pipe.

2.3 Slug flow in pipes

Slug flow is commonly encountered in many of the industrial applications, in particular the oil and gas industries. It occurs over a wide range of liquid and gas superficial velocities and at different pipe orientations including vertical, horizontal and inclined pipes. It is an intermittent flow pattern that causes

fluctuations in void fraction, velocity and pressure. Therefore the presence of slug flow in industrial pipelines is unfavourable due to the damages that can be caused, such as burnout and pipe failure, mainly at pipe fittings. The estimation of the liquid holdup and the maximum slug length during slugging conditions is crucial for process design and flow control.

Slugging phenomenon is categorised, based on the formation mechanism, into two main types; hydrodynamic slugging and terrain slugging. Hydrodynamic slugging is the common slug flow pattern that occurs in straight pipes due to a growing disturbance over a stratified interface. This type of slugs is short and high in frequency. Terrain induced slugging is more complex and a transient flow that forms by the accumulation of liquid phase at the bottom of a pipeline that passes through a hilly terrain. The pressure upstream of the liquid bridge continuously increases to the point that it blows the liquid along the pipeline forming a long slug. More details about the terrain induced slugging is available in (Schmidt et al., 1980; Taitel and Barnea, 1990; Zheng et al., 1994; Al-Safran et al., 2005).

Slug flow in vertical pipes is characterised by large bullet shape bubbles sometimes known as Taylor bubbles surrounded by thin liquid film, these large bubbles are separated by liquid slugs that usually contains dispersed small bubbles Figure 2-6(a). Horizontal slug flow is described as an alternating appearance of aerated liquid slugs over a stratified liquid layer Figure 2-6 (b).

Slug flow in straight pipes has been studied extensively over the last decades. Several theoretical models have been developed in order to provide a reliable estimate to the complex behaviour of liquid slugs. Dukler and Hubbard (1975)

has developed the first comprehensive model for horizontal flow. They suggested that the slug flow can be described by a sequence of similar slug units moving at constant transitional velocity where the slip ratio is equal to unity, while the film around the Taylor bubble is free of any dispersed bubbles. A modified version of this model is presented by Nicholson et al. (1978), while Andreussi et al. (1993) developed more simplified version of the original model. Fernandes et al. (1983) have presented a model that can be used for slug flow in vertical pipes.Taitel and Barnea (1990) used a unified model that is applicable for pipes with different inclinations.

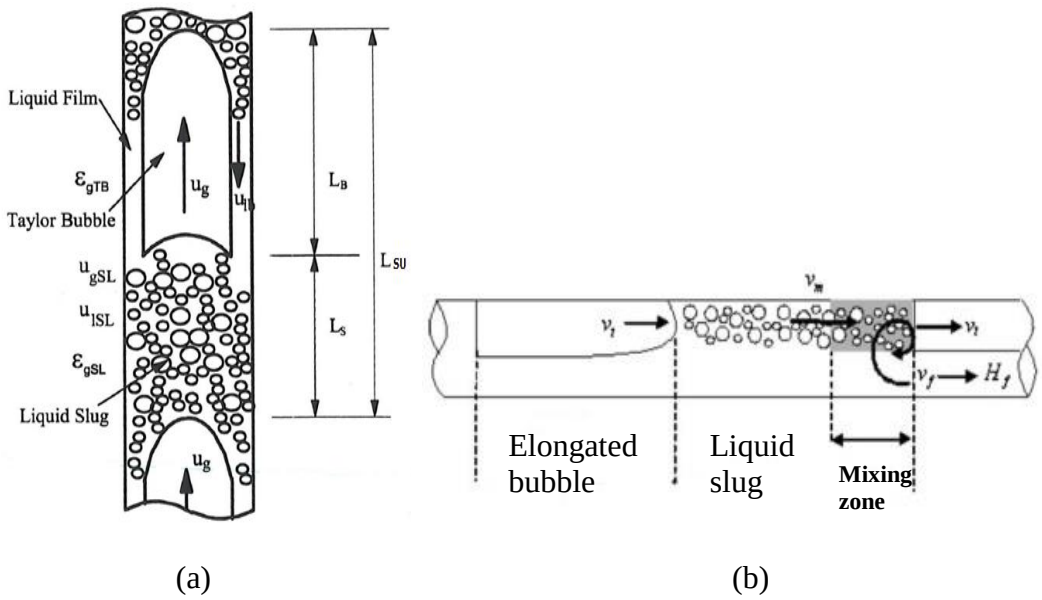


Figure 2-6: Slug Units.(a) vertical flow adopted from Azzopardi (2006), (b) horizontal flow adopted from Al-Safran (2009b).

The Kelvin-Helmholtz instability was primarily considered to be the cause of slugging in horizontal pipes (Taitel and Dukler, 1976). This theory fails at high pressure and for viscous fluids, where it underpredicts the minimum gas velocity at which the slugging occurs. Hence a similar approach to the linear stability theory, that includes viscosity and inertia terms, has been suggested by Lin and

Hanratty (1986). It was found that although inviscid theory predicts the onset of slugging at low gas flow rate and atmospheric pressure, it is more likely that the instability at this conditions will lead to 2D waves and not necessarily to slugs (Andritsos and Hanratty, 1987).

They main hydrodynamic parameters of slug flow have been continuously investigated over years. The main works that examined the different slug features are highlighted in the next subsections, while the widely used empirical correlations are discussed.

2.3.1 Slug bubble velocity

Slug bubble is widely known as Taylor bubble in vertical flow and either elongated or Benjamin bubble in horizontal flow. A large volume of publications have been dedicated to study the behaviour of Taylor bubbles either in stagnant or continuous slug flow. Morgado et al. (2016) have provided a comprehensive review on these papers.

The transitional velocity of a rising bubble in a continuous flow is adequately correlated in terms of the slug mixture velocity and the rise velocity of a bubble in a stagnant liquid, namely drift velocity as suggested by Nicklin et al. (1962):

$$u_{gTB} = C_0\left(u_{gs} + u_{ls}\right) + U_d \tag{2.7}$$

Where; U_d is the drift velocity and C_0 is the distribution parameter. C_0 is equal to the ratio of centreline velocity at the front of the bubble to the mixture velocity of slug flow (U_{max}/U_m). The value of C_0 varies from 1.2 for fully developed turbulent flow to 2 for laminar flow (Nicklin et al., 1962). Fernandes et al. (1983)

found that C_0 is equal to 1.29 for larger diameter pipe. This difference is related to the expansion effects and the interaction of consecutive bubbles. Mao and Dukler (1985) suggested that the higher value of C_0 in Fernandes et al. (1983) work is due to the effect of the gas holdup in liquid slugs. The propagation velocity of a Taylor bubble increases with the increase of gas holdup. They proposed a correlation that accounts for the dispersed bubbles in a liquid slug as:

$$u_{gTB} = \left[(C_0 - \Phi)\left(u_m - U_o \varepsilon_{gSL} + U_d - U_o \Phi\right)\right](1 - \Phi)^{-1} \tag{2.8}$$

Where; $\Phi = \varepsilon_{gSL}/\varepsilon_{gTB}$ and U_o is the rise velocity of a bubble in the presence of a swarm of bubbles as presented by Zuber and Hench (1962):

$$U_o = 1.53\left[\frac{\sigma g(\rho_L - \rho_G)}{\rho_L^2}\right]^{0.25}\left(1 - \varepsilon_g\right)^{0.5} \tag{2.9}$$

Where ε_g is the averaged void fraction. Generally, there is no a precise value for the distribution parameter C_0. Bendiksen (1984) has suggested a strong dependency of C_0 on Froude Number, he reported that C_0 =1.05 for (Fr < 3.5) and C_0 =1.2 for (Fr ≥ 3.5). For horizontal slug flow, the value of C_0 was reported to vary between 1.28 and 1.35 (Gregory and Scott, 1969; Mattar and Gregory, 1974; Dukler and Hubbard, 1975).

The drift velocity is a function of the buoyancy force. It has been experimentally approved that it mainly depends on the orientation of the pipe and gas superficial velocity. The maximum drift velocity is reported at an angle of around 40° to 45° from the horizontal (Zukoski, 1966; Bendiksen, 1984; Van Hout et al., 2002a). In vertical flow, the drift velocity is estimated by eq. (2.10) based on the theoretical

work of (Dumitrescu, 1943) and (Davies and Taylor, 1950). This equation was confirmed experimentally by the work of (Nicklin et al., 1962) in 26mm ID pipe.

$$U_d = 0.35\sqrt{(g * D)} \tag{2.10}$$

Where; D is the pipe diameter. For horizontal flow, although a non-zero drift velocity is usually considered (Mattar and Gregory, 1974; Nicholson et al., 1978; Weber, 1981), several studies argued that the absence of buoyancy in the horizontal pipes suggests a zero drift velocity (Dukler and Hubbard, 1975; Gregory and Scott, 1969). The drift velocity was estimated experimentally by Zukoski (1966). It is equal to the velocity of an elongated bubble moving opposite the liquid flow in a horizontal pipe open at one end. The work of Zukoski was later verified theoretically by Benjamin (1968)who presented the drift velocity in horizontal circular pipes as:

$$U_d = 0.75\sqrt{gr} \tag{2.11}$$

Where; r is the radius of the pipe. The widely used estimate of drift velocity based on Benjamin's work is presented in terms of the pipe diameter (Weber, 1981; Van Hout et al., 2002a; Fabre, 2003) as:

$$U_d = 0.54\sqrt{gD} \tag{2.12}$$

The drift velocity reaches zero in small pipes (< 5 mm ID), according to Weber (1981). He suggested a critical Eotvos number (E_{Ov}) value of 12, below which the drift velocity is negligible. According to Bendiksen (1984), the drift velocity has a

value only at Froude number below 3.5, while it approaches zero at high mixture velocities.

The physical properties of the fluids and the pipe diameter seem to have a great influence on the velocity of Taylor bubble. Therefore, it is beneficial to extend the available data base of two-phase flow experiments as an attempt to reach a final and solid conclusion on the behaviour of slug bubbles at different flow conditions.

More details on the rise velocity of Taylor bubble and the interaction between consecutive bubbles in continuous slug flow can be found in (Moissis and Griffith, 1962; Mao and Dukler, 1991; Polonsky et al., 1999; Van Hout et al., 2002b; Pringle et al., 2015; Morgado et al., 2016; Lizarraga-Garcia et al., 2017).

2.3.2 Void fraction in liquid slug

Void fraction in liquid slug (ε_{gSL}) is one of the main hydrodynamic characteristics of slug flow. It influences the average gas fraction and can be used to identify the transition to churn flow. The void fraction in liquid slug is an interchangeable parameter to the liquid holdup. Therefore, the prediction of the gas holdup within the body of the liquid slug is vital for the design and operation of the downstream separators in the oil and gas industry. An accurate estimation of ε_{gSL} is also required as an input to the mechanistic models of slug flow (Dukler and Hubbard, 1975; Fernandes et al., 1983).

Gas bubbles are entrained in a liquid slug due to turbulence created by the wall jet effect of the falling liquid film in vertical flow. The mixing eddies in the front of the liquid slug also enhances the rate of entrainment. Moreover, for viscous fluids bubbles can be entrained through an aerated liquid film that is absorbed by the

liquid slug. Similar mechanisms are applicable for horizontal slug flow (Fernandes et al., 1983; Al-Safran et al., 2015).

Various models have been proposed to estimate the gas hold up in liquid slug. These predictive models ranges from simple empirical correlations (Gregory et al., 1978) to more complex models (Zhang et al., 2003). Table 2-1 contains most of the common correlations for void fraction estimation in liquid slug.

It is clear that the correlations of vertical slug flow are developed from air-water flow in small pipes, mostly 25mm ID pipes. Akagawa and Sakaguchi (1966) and Mori et al. (1999) simply correlated the void fraction in liquid slug as a function of the mean void fraction (ε_g). Sylvester (1987) developed a closure relationship to estimate the void fraction in liquid slugs a function of the gas and mixture velocities.

The most common correlation for horizontal flow was developed by Gregory et al. (1978). They empirically correlated their experimental results as function of the mixture velocity only. The correlation is simple and widely used, but it ignores the effect of other flow parameters, such as the geometrical and physical properties parameters. Andreussi and Bendiksen (1989) developed a semi-empirical correlation that considers the effects of the pipe size, the inclination angle from horizontal and fluid properties. The inclination angle from the horizontal has a significant influence on the gas holdup in liquid slugs, the gas holdup increase with the increase of the inclination angle (Felizola and Shoham, 1995; Gomez et al., 2000; Barnea et al., 2013). Nydal et al. (1992) reported that in horizontal flow, the gas holdup in a liquid slug is weakly dependent on the pipe

diameter and liquid superficial velocities. Gomez et al. (2000) proposed a correlation based on six data sets with pressure ranges of 1.5 to 20 bar. They reported a strong dependency of liquid holdup in liquid slug on the inclination angle and Reynolds number. Malnes (1983) used the data of Gregory et al. to develop an empirical correlation that considers the surface tension and the density of the liquid phase.

Barnea and Brauner (1985) suggested that the gas in the liquid slug can be treated as dispersed bubbly flow, therefore the void fraction in a liquid slug can be estimated from the balance between breakage and coalescence forces. Brandt and Fuchs (1989) debated that this assumption is not valid for air-oil flow in a large diameter pipe, where a highly aerated mixture can be generated.

The surface tension and viscosity of the liquid phase has significant effect on the gas holdup in liquid slug. The gas holdup increases with the increase of surface tension (Andreussi and Bendiksen, 1989; Nydal et al., 1992; Nädler and Mewes, 1995), while it decreases with the increase of viscosity, as reported by Nädler and Mewes (1995) Al-Safran et al. (2015) and Zhao et al. (2015), for horizontal flow with a viscosity range of 14 to 37 mPa.s, 180 to 587 mPa.s and 919 to 6226 mPa.s respectively. The effect of viscosity on slug liquid holdup is negligible below a mixture velocity of 2 $m.s^{-1}$, according to Kora et al. (2011) and Al-Safran et al. (2013a) for a horizontal flow with a viscosity range of 181 to 587 mPa.s. The effects of viscosity on the gas holdup in liquid slugs have not been fully investigated. This leads to the necessity of investigating different grade of oils in order to cover the full range of viscosities.

Table 2-1: void fraction in liquid slug correlations

Source; Correlation	Angle (degree)	Pipe diameter (mm)	Fluids
(Akagawa and Sakaguchi, 1966) $\varepsilon_{gsl} = \varepsilon_g^{1.8}$	90	27.6	air/water
(Sylvester, 1987) $\varepsilon_{gSL} = \frac{u_{gs}}{0.425 + 2.65(u_{gs} + u_{ls})}$	90	25 to 75	gas/water gas/oil
Mori et al. (1999) $\varepsilon_{gsl} = 0.523\varepsilon_g$	90	25.8	air/water
(Gregory et al., 1978) $\varepsilon_{gSL} = 1 - \frac{1}{1 + \left(\frac{u_m}{8.66}\right)^{1.39}}$	0	51.2, 25.8	air/light oil
(Marcano et al., 1998) $\varepsilon_{gsl} = 1 - \frac{1}{(1.001 + 0.0179u_m + 0.0011u_m^2)}$	0	77.9	air/ kerosene
Malnes (1983) $\varepsilon_{gSL} = 1 - \frac{u_m}{\left[83\left(\frac{g\sigma_{gl}}{\rho_l}\right)^{0.25} + u_m\right]}$	0	51.2, 25.8	air/light oil
(Andreussi and Bendiksen, 1989) $\varepsilon_{gSL} = \frac{Fr_m - F_0}{Fr_m - F_1}$ $Fr_m = \frac{U_m}{\sqrt{gD}}$, $F_0 = 2.6\left(1 - 2\frac{D_0^2}{D^2}\right)$ $F_1 = 2400\left(1 - \frac{\sin\Theta}{3}\right)Bo^{-0.75}$	0	50, 90	Air/water
(Gomez et al., 2000) $\varepsilon_{gsl} = e^{-(0.45\theta + 2.48\times10^{-6}\,Re)}$ $R_{el} = \frac{\rho_l u_m d}{\mu_l}$	0 - 90	51to 200	Air/water air/ kerosene N_2/diesel

Al-Safran et al. (2015) proposed a semi-empirical model for liquid holdup of liquid slug in viscous fluid (180 to 587 mPa.s), based on the viscous and inertia effects. Although, they claimed that the model showed a good accuracy when it

was tested against a selected set of independent data (400 mPa.s), a validation against a wider range of the available experimental data could have reinforced the reliability of this claim.

Abdul-Majeed (2000) tested several models for predicting the gas hold up in liquid slug ε_{gsl} in horizontal and slightly inclined pipes, using 435 data points from different sources. It was reported that none of the available models is capable of predicting the gas holdup, in inclined pipes($\theta = \mp 10°$). He developed a model in which the viscosity and the inclination angle were considered. Al-Safran (2009b) proposed a semi mechanistic correlation based on the momentum transfer between the body of the slug and the liquid film. This model requires an iterative solution, using Taitel and Barnea (1990) slug flow model.

Pereyra et al. (2012) presented a comprehensive validation between the available correlations and models of gas holdup in liquid slug, excluding the complex correlation of Al-Safran (2009b). The Gregory et al. (1978) correlation showed the best performance for horizontal data, while unified model of Zhang et al. (2003) was the best for the whole range of the tested data.

2.3.3 Slug frequency

The frequency of liquid slug indicates the number of liquid slugs occurring at a certain location within a period of time. It is a critical parameter that is related to inherent instability of slugging conditions. An accurate estimation of slug frequency can reduce the risk of several operational issues such as flooding of two-phase separators and pressure pulsations and pipe failure due to severe

vibration. Several empirical correlations and models have been proposed to estimate the frequency of liquid slugs in pipes.

Table 2-2 summarises the main slug frequency correlations. The most widely used slug frequency correlation is developed by Gregory and Scott (1969). They showed that the frequency can be correlated in terms of the liquid Froude number. This correlation was modified by Greskovich and Shrier (1972), by considering the mixture Froude number Fr_m and the liquid volume fraction. They claimed that their correlation and the original correlation are applicable for large diameter pipe. Legius et al. (1997) adopted almost identical correlation to Greskovich and Shrier, for their work in vertical pipe.

Taitel and Dukler (1977) proposed the first theoretical model for slug frequency prediction in horizontal pipes, based on the time required for a slug to be formed at the entrance region. The formed slug swipes the slow liquid film in front leaving a shallow liquid layer behind. They suggested that the slug frequency is the reciprocal of the time required for the swept liquid layer to rebuild to its equilibrium value. This model requires a prior estimation of the minimum and the equilibrium height of the liquid layer, by solving the momentum equation of stratified configuration. Trononi (1990) suggested that the slug frequency is equal to half the frequency of the unstable waves responsible for slug initiation.

Zabaras (2000) presented a comprehensive study on the available slug frequency correlations. He proposed a modified version of Gregory and Scott (1969) correlation where the effect of inclination angle (0° to 11°) from horizontal was included. The correlation produced 0% average error when it was validated

against the original data bank. This claim should be verified, by testing the correlation against independent experimental data. Hernandez-Perez et al. (2010) proposed an empirical correlation for air-water flow in an inclinable 67mm ID pipe, covering inclination angles from 0 °to 90°. This correlation seems a pure mathematical fit of the experimental data to the Gregory and Scott (1969) correlation.

Fossa et al. (2003) showed that the slug frequency can be correlated in terms of a dimensionless Strouhal number and liquid volume fraction. Wang et al. (2007) and Abdulkadir et al. (2016) showed that the criterion proposed by Fossa et al. (2003) can be applied to independent frequency data.

Al-Safran (2009a) reported that the initiation mechanism has a significant influence on the slug frequency. The experimental results, in a 420 m long flow loop of 50.8mm, showed that the frequency of hydrodynamic slugs is higher than that of terrain slugs for a Froude number greater than 3 and vice versa. He proposed a predictive model for slug frequency in horizontal flow. This model considers the effect of pipe diameter, actual liquid velocity and the slip ratio.

More detailed descriptions of the existing slug frequency correlations and models can be found in (Zabaras, 2000; Al-Safran, 2009a; Hernandez-Perez et al., 2010). It is obvious that most of the available correlations are restricted to horizontal flow. None of those correlations has shown an accurate agreement when compared to independent experimental data. More recently, Al-Safran (2016) has reviewed the most recent correlations, mainly those developed for high viscosity flows. Al-Safran identified the random nature of slug frequency, due to

dissipation, merging and regeneration of liquid slugs along the pipeline. Therefore, he proposed a model based on the Poisson probability theory to predict the probability of a certain slug frequency to occur. The mean slug frequency, which is required as an input to this model, was correlated in terms of the pipe diameter, liquid superficial velocity and slip ratio.

Table 2-2: Slug frequency correlations

Source; Correlation	Angle (degree)	Pipe diameter (mm)	Fluids
Sylvester (1987) $f_s = \frac{U_{tb}(1-\beta)}{L_{ls}}$ $\beta = l_{tb}/l_s$	90	25 to 75	gas/water gas/oil
Legius et al. (1997) $f_s = 0.0543\frac{u_{ls}}{u_m}\left(\frac{2.02}{D}+\frac{u_m^2}{gD}\right)^{1.02}$	90	50	air/water
Gregory and Scott (1969) $\mathrm{f_s} = 0.0226\left[\frac{\mathrm{u_{sl}}}{\mathrm{gd}}\left(\frac{19.75}{\mathrm{u_m}}+\mathrm{u_m}\right)\right]$	0	19, 38	CO_2/water air/water
Zabaras (2000) $\mathrm{f_s} = 0.0226\left[\frac{\mathrm{u_{sl}}}{\mathrm{gd}}\left(\frac{212.6}{\mathrm{u_m}}+\mathrm{u_m}\right)\right]^{1.2}[0.836 + 2.75\sin(\Theta)]$	0 - 11	25to100	air/water air/oil
Nydal (1991) $\mathrm{f_s} = 0.088\frac{(u_{ls}+1.5)^2}{\mathrm{gd}}$	0	53, 90	air/water
Fossa et al. (2003) $St = \frac{\mathrm{f_s}D}{u_{gs}} = \frac{0.044X_L}{1-1.71X_L+0.70(X_L)^2}$ $X_L = \frac{u_{ls}}{u_{ls}+u_{gs}}$	0	40, 60	air/water

Nydal et al. (1992), Wang et al. (2007) and Al-Safran (2009a) reported that slug frequency is insensitive to flow development along the pipeline. On the other hand, it has been reported that the frequency of a liquid slug decreases along the

axial distance in a long pipeline (Scott et al., 1987). More recently Thaker and Banerjee (2015) reported a decrease in frequency with the axial distance from the inlet. Taitel (1987) argued that the slug length increases in long pipes due to coalescence of consecutive elongated bubbles, and hence the frequency should decrease. This argument was experimentally confirmed by Grenier et al. (1997) as reported in Al-Safran (2009a). The minimum slug frequency occurs at slug velocity of 6 $m.s^{-1}$ according to Gregory and Scott (1969) and Heywood and Richardson (1979).

2.3.4 Slug length

Slug length is inversely proportional to the slug frequency, thus both quantities are interrelated. Knowledge about the maximum slug length is significant for the design of downstream facilities in the oil and gas industries. It is acknowledged that liquid slugs are short and unstable in the developing region. Short slugs shed more liquid than long slugs, thus a bubble behind a short slug travels faster and overtake the leading bubble. In the process, short slug disappears and merges with the upstream slug. The merging process continues until the slug length reaches a stable length (Moissis and Griffith, 1962).

The stable length has been reported to be around 8D to16D for vertical flow (Moissis and Griffith, 1962; Akagawa and Sakaguchi, 1966; Barnea and Shemer, 1989))and 12D to 30D for horizontal flow (Dukler and Hubbard, 1975; Nicholson et al., 1978; Barnea and Brauner, 1985; Andreussi and Bendiksen, 1989; Nydal et al., 1992).Theoretically, the stable slug length is defined as the length required to attain a fully developed velocity profile at the rear of the liquid slug i.e. the length required to absorb the wall jet created by the liquid film. The

simulations showed similar results to the experimental observations (Moissis and Griffith, 1962; Taitel et al., 1980; Dukler et al., 1985). Barnea and Taitel (1993) proposed a model to estimate the slug length distribution, based on the velocity of a bubble behind short slug.

Brill et al. (1981) proposed a correlation to predict the mean slug length in horizontal large diameter pipes (10 cm to 41 cm), based on experimental data of Prudhoe Bay. They found that the slug length is a function of the pipe diameter and mixture velocity. The correlation was modified by Norris (1982) who excluded the mixture velocity term, while Scott et al. (1989) improved the correlation even further by expanding the data base and considering the slug growth. Khatib and Richardson (1984) proposed a correlation to predict the mean length of liquid slugs in vertical pipes based on a mass balance around slug units.

Due to the transient behaviour of slug flow, the statistical distribution of the main slug flow parameters is desirable, particularly for design and operation of gas-liquid separators. For horizontal flow, it was reported that that the slug length data fits a log-normal distribution (Brill et al., 1981; Nydal et al., 1992). While for vertical flow, the slug lengths seem to follow a normal distribution. Van Hout et al. (1992) reported that the standard deviation from the mean slug length varies from 30% to 40%, while Costigan and Whalley (1997) reported a standard deviation of 40% to 50% from the mean of a normally distributed slug length.

Although , the slug length is considered insensitive to the change in gas and liquid superficial velocities (Nicholson et al., 1978; Nydal et al., 1992; Woods et al., 2006), other studies reported an increase in slug length as the gas superficial

velocity increased (Ferré, 1979; Wang et al., 2006). Losi et al. (2016) have reported a strong dependency of slug length on gas superficial velocity, using air and high viscosity oil (37 to 804 mPa.s) in a relatively small pipe (22mm ID) of 9m length. Al-safran et al. (2013b) reported a reduction in the average slug length with the increase of liquid viscosity.

2.4 Flows in curved pipes and bends

Curved pipes and bends are unavoidable parts in the piping system of different industrial process such as boilers, heat exchangers and in the transportation pipelines of the oil and gas industries. It is widely known that the flow in pipe fittings is more complicated than the flow in straight pipe due to generation of the secondary flow which is well established for single phase flow. As the fluid passes through the bend, the centrifugal force induced by the curvature acts stronger on the fluid at the pipe core than that at the pipe wall creating a radial pressure difference. This difference in pressure causes the faster fluid to flow near the outside of the bend while slow fluid switches to the inside wall in order to maintain the momentum balance (Berger et al., 1983). Consequently secondary flow is imposed to the main stream in a form of two symmetrical vortices forcing the flow to maintain a helical shape. The intensity of secondary flow is usually defined by the Dean Number (De) (Spedding et al., 2004).

$$De = Re\left(\frac{R}{R_c}\right)^{0.5} \tag{2.13}$$

Where R and R_c are the pipe and the curvature radius respectively, Re is the Reynolds number. The flow in curved channels was first reported by Thomson (1876) who explained the behaviour of the river water through a curved path.

(Eustice, 1910; 1911) was the first to study the effects of changing the pipe curvature on the flow resistance. The pioneer work of Dean (1927) is the first to theoretically confirm the secondary flow in curved pipe discovered by Eustice.

Over the decades most of the research efforts were devoted to study single phase flow in bends and curved pipes. Extensive reviews on the subject can be found in Berger et al. (1983); Itō (1987); Spedding et al. (2004).

2.4.1 Two-phase flow through 90°bends

Knowledge about the effect of pipe fittings on the flow development is required for the design and operation of two-phase flow system. Bends are commonly used in several industrial processes including evaporation, condensation, refrigeration and gas-liquid transportation. The secondary flow, induced by the bend curvature results in a higher energy dissipation than that of straight pipes, and hence a higher pressure drop is expected in bends. The secondary flow usually associates with flow separation and flow pattern transition which may enhance corrosion and cause problems such as burn out and pipe failure (Azzopardi, 2006). The flow separation at the bend causes instability to the void fraction and flow regimes, especially at short distance after the bend.

The complex effects of the bends on the two phase flow is a common issue in a wide range of industrial applications, nevertheless the available studies have not fully exposed the subject. Some studies have investigated the effect of return bends on the flow structure; (Banerjee et al., 1967; Traviss and Rohsenow, 1971; Oshinowo and Charles, 1974; Usui et al., 1980; 1981; 1983; Abdulkadir et al., 2012; De Oliveira et al., 2014). It was reported that the phase distribution of

phases within return bends can be predicted based on a modified Froude number (Oshinowo and Charles, 1974; Usui et al., 1983; Abdulkadir et al., 2012). The main observations for gas-liquid flows in return bends were phase separation, dryout zone, flow reverse in slug flow, film inversion in annular and stratified flow (Banerjee et al., 1967; Usui et al., 1980; Usui et al., 1981).

Several attempts have been conducted to predict the two-phase flow pressure drop in bends (Fitzsimmons, 1964; Das et al., 1991; Paliwoda, 1992; Mandal and Das, 2001; Azzi and Friedel, 2005; Benbella et al., 2009; Kim et al., 2010; Sánchez Silva et al., 2010). Chisholm in a series of publications (Chisholm, 1967; 1971; 1980) has proposed the well-known B-type and C-type models.

Fitzsimmons (1964) generated a useful two phase pressure drop data set from a vertical upward 90° bend of 50.8 mm ID and curvature radius of 50, 76 and 254 mm. The system operated with steam and water at high pressures. The main observation was that the pressure drop increases with the reduction of curvature radius of the bend due to increase in the intensity of secondary flow.

A critical review of the available two-phase flow correlations to predict the pressure drop in bends is published by Azzi et al. (1999). They emphasised the inconsistency of most of the equations especially at zero bend angle and zero mass flow rate. Ultimately the B- type model of Chisholm is considered the best available correlation at the time. The accuracy of the Chisholm B-type model was confirmed in Azzi et al. (2002) through comparison with experimental results of two-phase pressure drop across 90° bends with 30mm ID and four curvature ratios. Azzi and Friedel (2005) proposed a new model to estimate the twophase

pressure losses in vertical 90° bends. This model is based on two-phase flow multiplier, where the Beij (1938) model is used to estimate the single phase pressure loss in the bend. Spedding and Benard (2007) concluded that the orientation of the bend has a significant effect on the total pressure drop. Benbella et al. (2009). found that pressure drop in a wavy bend is 2-5 time higher than that of smooth bends. This is mainly due to the increase of the vortexes in the internally wavy bends which causes an increase in the friction between phases. Sánchez Silva et al. (2010) modified the Chisholm B-type model and also developed a new correlation. Both models showed an improvement in pressure prediction. Hsu et al. (2015) reported a good agreement between their experimental results of two-phase flow in small 90° bends with the prediction of Sánchez Silva et al. (2010) correlation.

It is apparent that two-phase flow pressure around bends has received a great attention over the past years. Several empirical and theoretical models are developed to predict the pressure drop across bends. Some of those models have been widely accepted for pressure drop prediction in industrial applications. On the other hand, the effects of bends of the flow evolution seem to not being fully exposed yet, in particular the influence of bends on the slug flow behaviour.

The air-water flow distribution around bends in a upflow bend system was investigated by Gardner and Neller (1969) using two 76 mm ID 90° bends with a curvature radius of 305 and 610 mm. They reported that the liquid phase can move inside or outside of the bend depending on the dominant force within the bend. They found that the interaction between the two forces can be expressed in the form of critical Froude number:

$$(Fr)_{\theta} = u_m^2/gR\ sin\theta \tag{2.14}$$

Where, u_m is the average mixture velocity, g is the gravitational constant, R is the curvature radius and θ is the deflection angle of the bend. It was observed that the air moves to inside of the bend at $(Fr)_{\theta} > 1$ and to the outside when $(Fr)_{\theta} < 1$. Whilst the radial equilibrium between phases exists when $(Fr)_{\theta}$ is equal to unity, since it was assumed that the two phases flow at the same axial velocity. Abdulkadir et al. (2011) reported that the modified Froude number of Gardner and Neller predicts well the phase distribution of air-silicone oil flow in 67mm ID bend to an acceptable accuracy.

The capability of the numerical simulation to study the two phase flow behaviour through bends was demonstrated by Carver (1984) who conducted numerical two dimensional simulations in order to predict the interaction between the centrifugal and gravitational forces. The results showed a relative discrepancy with the experiments of Gardner and Neller (1969). The discrepancy was reduced using three dimensional model by Carver and Salcudean (1986).

The advances in CFD technique increased the potential of the analysis to simulate the two-phase flow in bends especially by improving the performance of the available models. Mazumder (2012) conducted CFD simulation of single and two-phase flow through 90° horizontal to vertical bend of 12.7 mm ID. The results were in acceptable agreement in comparison with the available empirical models such as Chisholm B-type and Benbella et al. (2009) models. Hamad et al. (2013) simulated the Kerosene-water two-phase flow in vertical pipe downstream of a 90° bend, using FLUENT 12.0. The CFD analysis offered satisfactory agreement with the experimental results except at short distance downstream of the bend due

to the effect of the secondary flow. This might indicate the limitations of the existing CFD models to simulate two-phase flow around bends.

The erosion due to the presence of solid particles in pipe 90 elbows has been also investigated experimentally and numerically in several publications, using air-sand flows (Pereira et al., 2014; Mansouri et al., 2015; Solnordal et al., 2015; Vieira et al., 2016). All studies showed the ability of appropriate CFD models to predict the erosion in 90 degree elbows. Pereira et al. (2014) suggested that the empirical model proposed by Oka et al. (2005) as the most suitable for erosion prediction industrial applications. They also found that the wall roughness diminishes the rate of erosion. Solnordal et al. (2015) reported that the maximum erosion depth occurs at 55° to 60° around the bend. Vieira et al. (2016) suggested that the location of the maximum erosion rate is insensitive to the particle size. They identified the maximum erosion rate at 45° to the bend.

The 90° elbows were found to enhance the bubble interaction of horizontal bubbly flow, either by coalescence or fragmentation subjected to the flow conditions, which significantly alters the interfacial area (Kim et al., 2006; 2007). The effect of bends on the mass transfer, in annular flow regions, was studied by Mazhar et al. (2014). They have reported two maximum areas of enhanced mass transfer; one was in middle of the outer wall of the bend and the other occurred slightly downstream.

Yadav et al. (2014a) examined the effect of a vertical upward 90° bend of 50.8mm ID on the main characteristics of bubbly flow, using four pin conductance probes. The main observation was that regardless of the upstream conditions, the

secondary flow of the liquid phase at the bend forces the bubbles to form a bimodal distribution in the vertical plane to the flow direction. Yadav et al. (2014b) found that the intensity of the bend region decays exponentially along the axial distance downstream. More recently, Qiao and Kim (2016) extended the work of Yadav et al. (2014a) and Yadav et al. (2014b) to develop a model that can estimate the interfacial area in vertical to horizontal air-water flow.

Silva et al. (1999) experimentally studied the effect of a sharp horizontal 90° elbow on the main features of slug flow, using ring conductive probes in air-water system of 41mm ID. It was reported that slug characteristics are considerably altered due to the presence of the elbow. They observed a random behaviour of liquid slugs after the bend. The hydrodynamics of slugs downstream of the elbow are certainly influenced by the momentum transfer and gas expansion at the bend. Abdulkadir et al. (2011) conducted air-silicone oil flow experiments in an inclinable flow facility which consisted of a 6 m long pipe with 67 mm ID and 90° bend of 150 mm curvature radius. Similar flow patterns were reported before and after the horizontal bend, whereas the vertical bend showed significant influence on the flow development downstream.

The behaviour of an air-water mixture through horizontal to vertical 90° bends of 34 mm diameter was studied by Saidj et al. (2014) for 5 curvature ratios. Conductance probes were used to estimate the cross-sectional averaged void fraction at six positions downstream the bend. They suggested that the structure frequency is persistent to the presence of the bend at high liquid superficial velocity; while it rises at the lowest gas and liquid superficial velocity. They also observed an increase in the slug length downstream of the bend.

Tay and Thorpe (2014) have developed a one dimensional theoretical model as an attempt to estimate the magnitude of the forces acting on a horizontal 90 bend during slug flow conditions. They reported a good agreement with their experimental results for air-water flow in a horizontal 70mm ID pipeline. In a related work, Tay and Thorpe (2015) found that the force traces due to the impact of liquid slugs on the bend can be correlated by a normal distribution. A comprehensive literature survey on the two-phase flow induced vibration can be found in (Miwa et al., 2015).

It was noticed that the effects of flow obstacles such as bends on slug flow have received less attention in the previous studies. In addition, water has been usually used as the liquid phase. This indicates the need of novel experimental data that consider the effect of bends in more details, employing other fluids than water.

2.5 Summary

It is evident that in the recent years, the importance of two phase flow behaviour around bends has been identified. Nevertheless, most of the available studies are limited to small pipe diameter and water as the liquid phase. Developed slug flow in straight pipes has been the focus of researchers over the past decades. In contrast the effects of obstruction and fittings, such as bends, on the evolution of slug flow have been only investigated in a limited number of papers. More over those publications that considered slug characteristics through bends were conducted in relatively small pipes and with water as a liquid phase.

This work investigates the effect of 90° bends of different orientations on the development of air-silicone oil flow in relatively large diameter pipes (68mm ID).

In particular, it sheds more light on the effects of vertical and horizontal 90° bends on the evolution of the slug flow. This experimental campaign aims to generate a reliable database that might overcome some of the limitation of the previous studies, using advance instrumentation such as WMS and ECT. It provides more detailed analysis of slug characteristics before and after 90° bends, in order to evaluate the significance of bends on flow alteration.

Chapter 3

Experimental setup and procedure

This chapter illustrates the design and construction process of the flow rig that was used to study the two-phase flow behaviour in vertical upward and horizontal 90° bends in series (section3.1). It also provides a general description of the experimental arrangement (section3.2). A detailed description of instruments employed on the flow facility is available in section 3.3, whilst the experimental procedure is demonstrated in section 3.4. Finally, data processing methods and error analysis are described in section 3.5 and section 3.6 respectively.

3.1 Experimental facility design and construction

The two-phase flow facility was designed and built at the L3 laboratories in the department of Chemical and Environmental Engineering at University of Nottingham. This rig was specifically commissioned to achieve the aims of this project. During the design of the rig the safety and the available space were effectively managed and a detailed cad drawing was produced. The required length of flow development at the downstream of the mixing section and bends was considered based on previous works in the field. The amount of silicone oil required to run the rig was estimated in addition a suitable pump was selected to circulate the liquid around. The flow rig consists of, a storage tank, a liquid centrifugal pump, a mixing section, a vertical riser 4.5 m long, a 90° bend, two horizontal sections of 9.2 m and 5.5 m long respectively with a 90° bend between them. The test sections are made of transparent acrylic pipes with an average inner

diameter 0.068 m. The riser and the horizontal sections are constructed using a number of short pipe lengths connected with flanged joints to allow the installation of the measurement equipment at various axial distances and also to prevent risk of pipe failure due to vibration. The pipes have been smoothed at their ends to ensure that there are no steps and hence disturbance to flow. The return section is made of PVC pipes since observations in the return section are of less importance in these experiments. The pipes and the bends are supported with clamping rings mounted on steel stands that are fixed around the balcony of L3 laboratories. The two-phase mixer is made of a machined Polyvinyl chloride (PVC) block. Two sections of 0.75m length with pressure taps at both ends are installed downstream of the vertical and horizontal bends, to allow the variation of measuring point downstream of the bends in order to investigate the flow behaviour. The pipe section of the electrical capacitance sensor upstream of the bends has two pressures taps at both bends for simultaneous pressure and voidage measurements. The pressure taps were connected to the differential pressure transducer through a Perspex manifold which offered an easy control of the measurements, using automated solenoid valves and allowed sequential pressure measurements at the desired locations. The pipes and the bends are supported with clamping rings mounted on steel stands that are fixed around the balcony of the L3 laboratories. The experiments were conducted at atmospheric pressure and the ambient temperature. The flow rig was earthed using a copper strip, to eliminate the effect of static charges on the measurements of the flow sensors. A cooling system is available in the tank to keep the oil temperature at an acceptable range around the lab temperature, particularly after long experimental campaigns. The

choice of the operating fluid with the design of the mixing section and the bends are demonstrated in following subsections.

3.1.1 Operating fluid

Silicone oil was selected as the liquid phase, due to several considerations. The production of an oil well is commonly associated with a ratio of water to the total volume of the produced hydrocarbons called as water cut. Water has been widely studied as a liquid phase in two-phase flow experiments because of the simplicity in handing water within laboratory environment. Therefore there is a need to investigate fluids comparable to the hydrocarbons produced in the oil and gas industries. The silicone oil used is this work has a viscosity five times higher than that of water with noticeably lower surface tension, which makes it comparable to the industrial fluids (hydrocarbons). Air from the central compressor is used for the gas phase. Table 3-1 summaries the physical properties of the operating fluids used in these experiments.

Table 3-1: Fluid properties at ambient conditions

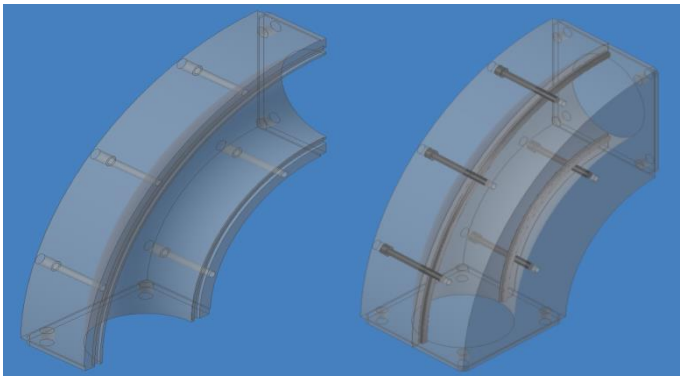
Fluid	Density (kg/m3)	Viscosity (mPa.s)	Surface tension (N/m)
Air	1.18	0.018	0.02
Silicone oil	915	5.25	

Silicone oil is not a hazardous material as defined in the OSHA Hazard Communication Standard. It is nontoxic and thermally stable. The dielectric properties of the silicone oil are detectable using several proven advanced instrumentation including WMS and ECT systems.

3.1.2 Design of the bends

The bends were designed in a way that allows easy visual observation. They were fabricated by machining and polishing a block of transparent acrylic (Perspex). Each bend is made of two arched slabs on which a channel with semi-circular cross section is machined. The two slabs bolted together with a rubber seal to form the pipe bend. Two flanges are bolted at the both ends as illustrated in Figure 3-1.

(a) Conceptual design using AutoCAD.



(b) Fabricated bend using acrylic.

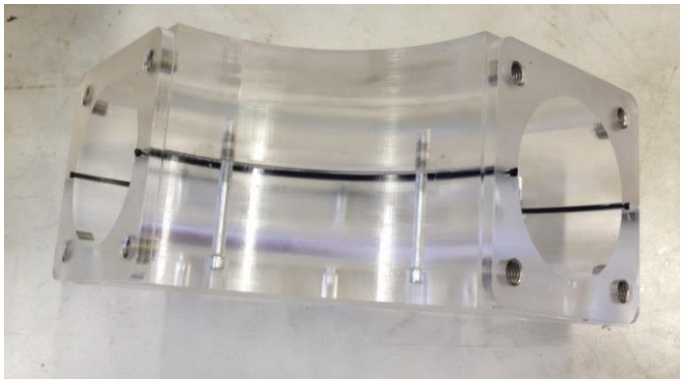


Figure 3-1: A schematic diagram and a picture of the designed bend.

One pair of bends was designed with internal diameter of 68 mm and curvature ratio of 3. One bend is installed vertically at the end of riser while the other is placed horizontally downstream of the first bend. The coincided connection between inner wall of the bend and that of the connected straight pipe is required

to avoid the excessive pressure drop, therefore the pipe sections before and after the bend are smoothed to match the bend bore.

3.1.3 Mixing section design

The mixing process in two-phase flow should be performed in a way that ensure fast flow stability and prevents high pressure drops in order to achieve flow development within a minimum distance. The flow patterns depend mainly on the primary bubble size (Lucas et al., 2005), however, this effect is pronounced only for a short distance. The selection of the appropriate geometry of the mixing chamber is governed by the flow patterns of the primary concern. In this study a range of flow regimes are studied, thus the design of the mixer considered the size and the number of gas distributor holes that can provide the required gas flow rate with minimum pressure drop.

The two-phase mixer is made of a machined Polyvinyl chloride (PVC) block. It consist of two parts; main pipe section of 68 mm internal diameter with a tangential entry pipe of 42 mm ID for the liquid inlet. A 33 cm long concentric PVC pipe (45mm OD) with 96 holes of 3 mm diameter is used for the gas inlet. The holes are distributed uniformly around the cylindrical surface of the concentric pipe in 8 rows of 12 holes each, for uniform air distribution as shown in Figure 3-2. The air enters the bottom of the mixer through a tube of 28 mm ID. During the experiments, air injected through the concentric distributor flow into the annulus through the holes mixing well with the liquid introduced through the radial inlet.

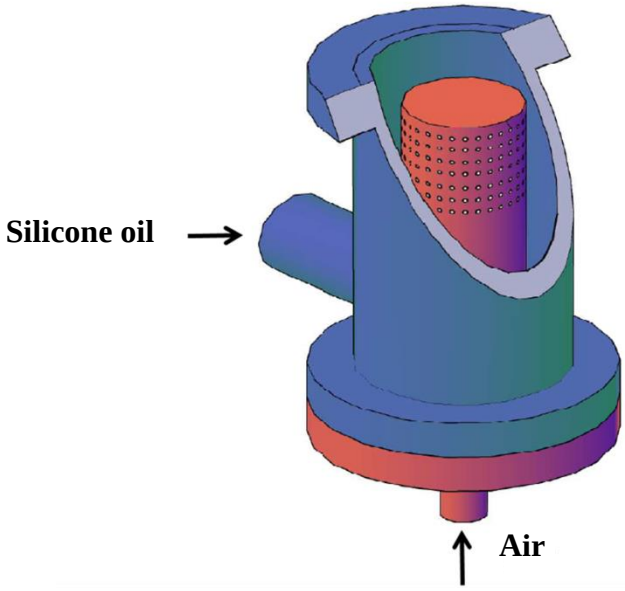


Figure 3-2: Schematic diagram of the air-silicone oil mixer.

3.2 Description of experimental facility

The two-phase air-silicone oil flow experiments were conducted in the flow rig illustrated in Figure 3-3. The flow facility consists mainly of a liquid tank, a liquid centrifugal pump, a mixing section, a vertical riser, two horizontal sections, two 90° bends, air and liquid flowmeters, electronic temperature sensors and pressure transmitters. The main pipe section has an average internal diameter of 68mm, while the air and the liquid inlets to the mixing section are 28 mm and 42 mm diameter respectively.

During the experiments, the silicone oil is pumped from the storage tank using the centrifugal pump into the mixing section. A bypass line with appropriate valve arrangement is installed for a better liquid flow control and to boost the flow stability. The start-up and shut down procedure is available in Appendix A. The air is supplied from a central compressed air line. Temperature and pressure of both the liquid and the gas streams are measured prior to the mixing section by electronic temperature sensors and pressure transmitters respectively. The silicone

oil and air are well mixed within the mixing section and then the mixture flows along a vertical riser of 4.5 m before it reaches the bend. This offers a 66 pipe diameter length which should be enough for the flow development (Azzi and Friedel, 2005; Benbella et al., 2009; Abdulkadir et al., 2012). The two-phase flow in the vertical section is passed into the 9.2 m long horizontal test section through the vertical upward 90° bend, and then the mixture is diverted to a second horizontal section of 5.5 m long downstream of a horizontal to horizontal 90° bend. The flow is returned, through a return PVC pipes that passes beneath the main test section, to the holding tank where the phases separate. The air is vented into the atmosphere while the silicone oil is returned to the bottom of the storage tank prior to its reuse.

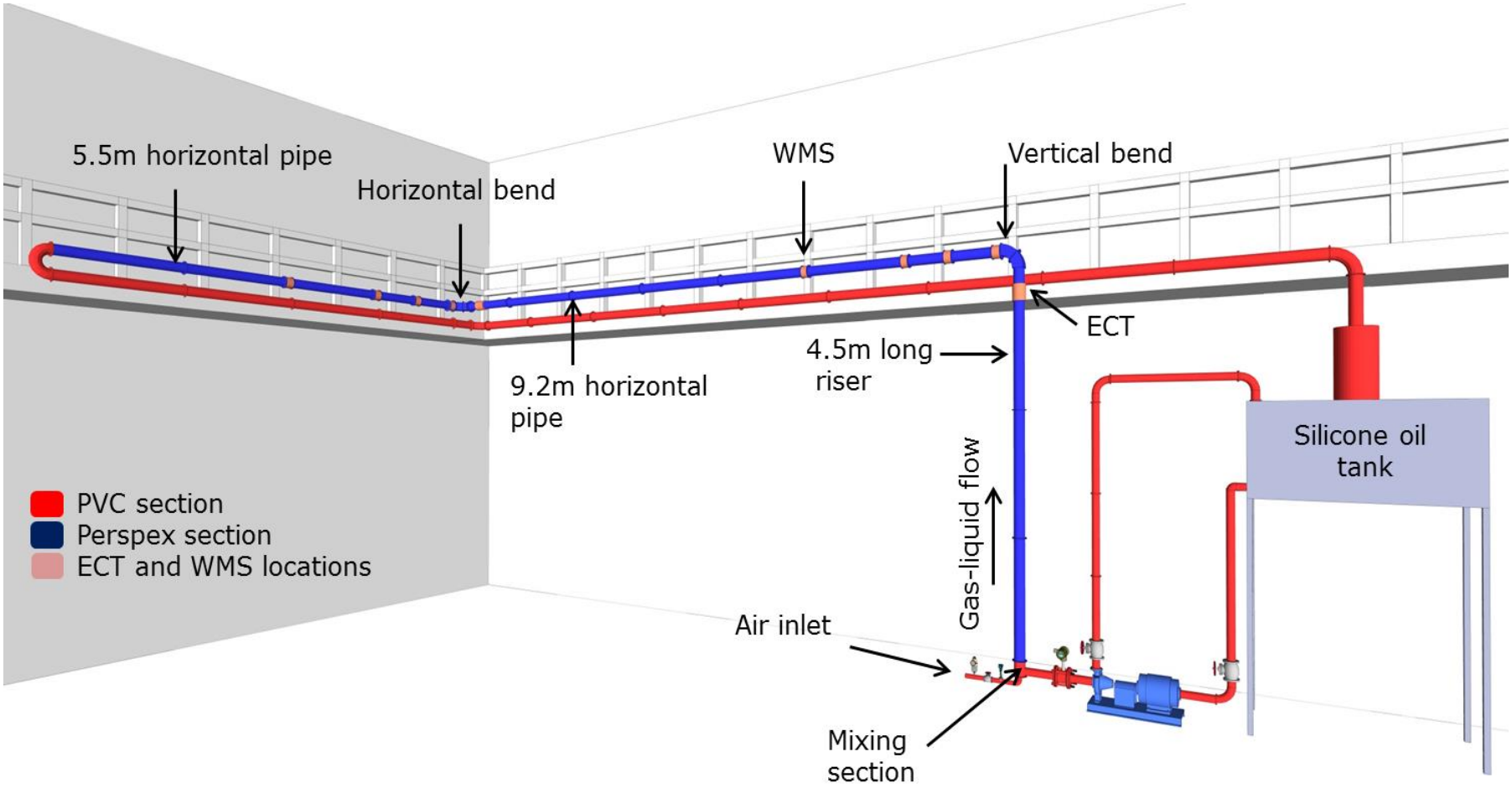


Figure 3-3: A 3D diagram of the flow facility showing the main components.

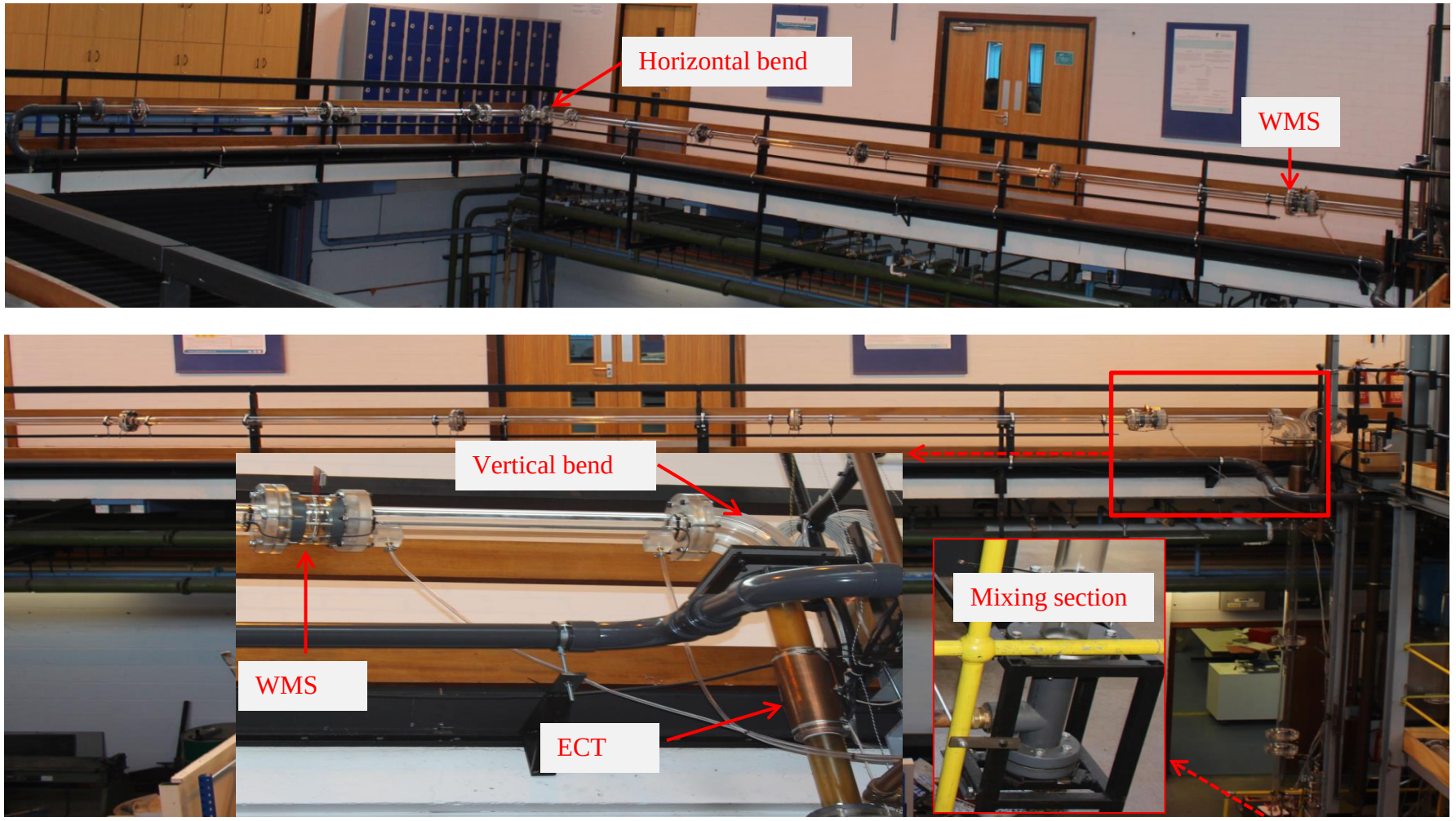


Figure 3-4: Pictures of the main parts of the flow rig.

In all experiments, the Electrical Capacitance tomography probe (ECT) and the Wire Mesh Sensor (WMS) are installed upstream and downstream of the bend respectively as illustrated in Figure **3-5**. It should be noted that the WMS is an intrusive technique that could cause distortion of the flow structures and bubble fragmentation as mentioned in Chapter 2, thus it is usually installed downstream of the non-intrusive ECT system. During the flow measurements around the vertical and the horizontal bends, the ECT was fixed immediately upstream of the bend while the WMS was moved at six and four axial locations downstream of the bend respectively. This allowed the investigation of the flow behaviour downstream of the bend and examining the effects of secondary flow on the flow structure. Similar procedure was repeated for the horizontal to horizontal bend, where the WMS was located at five different axial positions downstream of the horizontal bend.

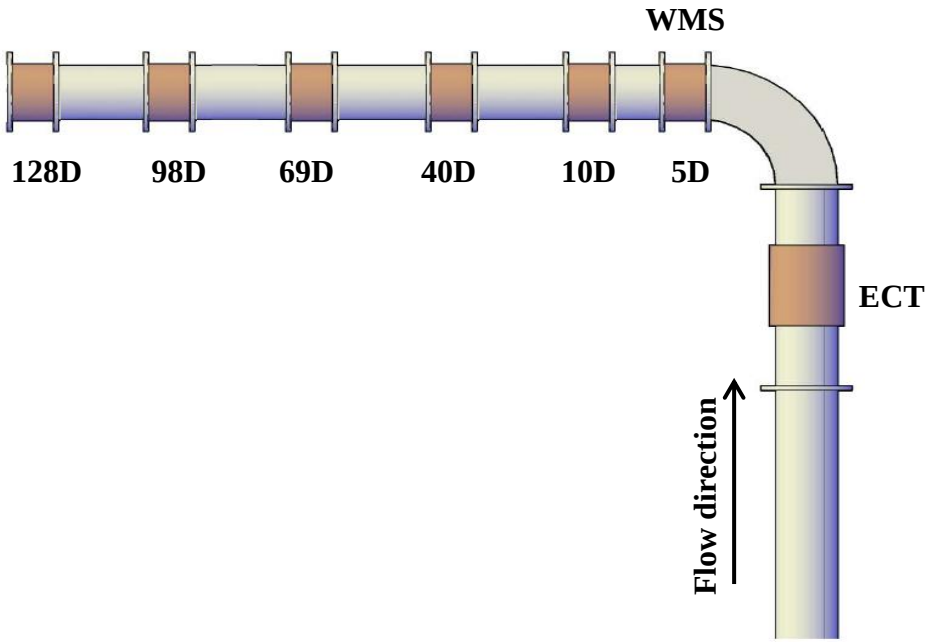


Figure **3-5**: A sketch of the ECT and WMS installation around the vertical ben.

3.3 Flow facility instrumentation

Advanced instrumentations, including WMS and ECT system were used to measure the void fraction along the flow facility. Flow rates, temperatures and pressure of gas and liquid streams were measured prior to the mixing section using, flow meters, electronic temperature sensors and pressure transmitters respectively. All measurements were acquired simultaneously through a data acquisition system. This section provides description of all devices used in the flow facility and the data acquisition system.

3.3.1 Data acquisition

The data acquisition process involves data collection and processing which includes calibration and signal conditioning. The data acquisition system (DAQ) consists of a sensor, a DAQ hardware, a personal computer and software as illustrated in Figure 3-6. The sensor measures a physical phenomenon and provides an electrical signal that its amplitude is usually proportional to the change in magnitude of measured parameter. The electrical signal undergoes the required signal conditioning, such as amplification and filtering prior to its arrival to the DAQ hardware. The DAQ hardware determines the resolution, sampling rate and the input range of the signal. It converts the Analog signal from the sensor to a binary digital code that is transmitted to the personal computer. The software works and an interface between the DAQ hardware and the personal computer, it allows an easy control over the data acquisition process by integrating the DAQ hardware and computer resources.

In these experiments, NI cDAQ-9178 Compact DAQ 8-Slot USB chassis was used along with NI9203 module DAQ hardware purchased from National

Instruments. The NI9203 module offers 8 analog channels with an input range of ± 20 mA and 16-bit resolution. NI9472 module was used to generate the signal required to actuate the solenoid valves. It is an 8chnnel model that provides digital output signals in the range of 6 to 30 V.

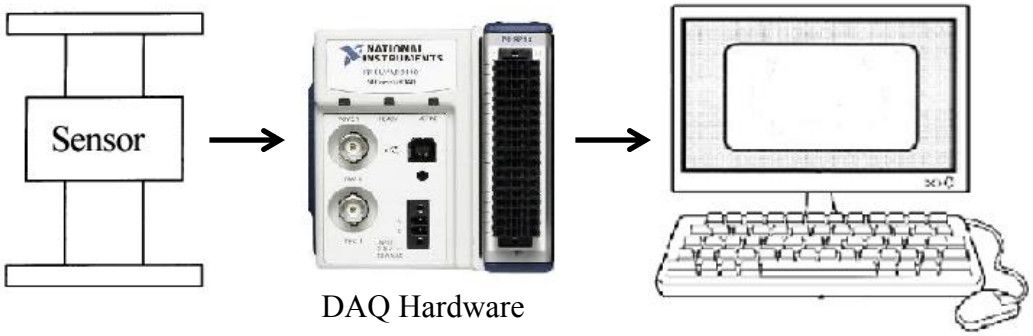


Figure 3-6: A block diagram of the data acquisitions system.

Each instrument was wired to a single Analog channel while all channels were earthed using the common terminal, which is designed to isolate the ground reference of the module. It should be noted that WMS and ECT have their own hardware and were not wired to the NI module. The end to end electrical calibration was conducted when the acquisition system was in its final configuration to avoid any alteration in the signal output during the actual measurements. The output current span of all devices is 4mA to20 mA which corresponds to the lower and upper limit of the measurements.

LabVIEW 2013 software, offered by National Instruments, was used to create an interface with a personal computer for data acquisition and control. The LabVIEW is designed to convert the electrical signals to the physical values of the corresponding measurements based on the calibration files obtained for each measuring device, where the measurement rate is easily controlled during the experiments and data is directly saved in Excel format for offline data analysis.

A trigger signal from the WMS electronics was connected to the ECT hardware and the NI cDAQ-9178 base through a BNC wire. The built-in trigger function in LabVIEW 2013 was used to facilitate the trigger signal and initiate the data acquisition system simultaneously with the WMS and the ECT. The LabVIEW block diagram used to run and control the data acquisition system is available in the Appendix A.

3.3.2 Flow rate measurement

A metal tube variable area flowmeter (Flotrak MT-50-P-TiA) with a flow range of 2-16 m^3/hr and a thermal mass compressed air flowmeter (MCF0150) with a flow range of 0 to 1000 l/min were used to measure the flow rate of liquid and air prior to the mixing section with measurement accuracy of ±2% and ±3% of full scale respectively. Both flowmeters provide direct flow reading and also output a signal of 4-20 mA. The bore size of the liquid flowmeter was larger than the cross section, thus a divergent and convergent section was designed at the inlet and outlet of the flow meter respectively. This might cause a slight increase in the pressure drop; however the accuracy of the readings should not be altered.

3.3.3 Temperature measurements

The temperature of the silicone oil and the air was measured before the mixing section with an electronic temperature sensor (TDA-L3M) with a measurement range of -50 to+125° C and accuracy of ± 0.5° C. It offers a direct reading display and an analogue output of 4 to 20 mA.

3.3.4 Pressure measurements

Pressure transmitters with digital display (PDA-15) were used for pressure measurements at the liquid and the air inlet immediately before the mixing

section. The device offers measurement range of 0 to 6 bar with accuracy of ± 0.5% FS, it also provide a signal output of 4-20 mA. Differential pressure transmitter with measuring range of 0 to 0.865 bar was used to estimate the pressure loss across the bends, it offers digital display as well as electronic output signal of 4-20 mA with accuracy of ±0.075% of the calibrated span.

The differential pressure system consists of a differential pressure sensor with low and high pressure ports, a manifold with six ports and normally closed solenoid valves of type (PU220) with a maximum opening time of 50 msec. Images of the pressure system and the solenoid valves circuit are available in the Appendix A. The reference pressure tap (i.e. lowest pressure) is connected to the low pressure port of the sensor, while the other pressure taps are connected the high pressure port through the manifold. The (normally closed) solenoid valves are located at the inlet ports of the manifold to control the measuring location. A digital output signal, from NI9472 module is used to sequentially energise the electromagnetic coil of the valves. Therefore only one valve is open at the time. The opening and closing of valves was programmed in LabVIEW, to allow automated switching from one pressure tap to another. The LabVIEW block diagram and images of the system are available in the Appendix A.

3.3.5 High speed imaging system

A high speed video system was used to observe the flow in the pipe sections and around the vertical bend. The system consists of a Phantom V12.1 Camera, Macro105 mm and Nikon 28 mm lenses, tripod of the camera, laptop with phantom milt cam application software installed and Dedocool cold lighting system. The quality of the videos was enhanced by the use of LED backlighting.

The images were taken at a frame rate of 2000 frame/s and full frame resolution was 1280 × 800 pixels while the exposure time was 160.85 µs. The camera was placed at the bend and far downstream of the bend in order to capture the flow behaviour. The Macro 105 mm lens was used throughout since it gave the best focus. An image of the system arrangement is available in the Appendix A.

3.4 Wire Mesh Sensor

Wire Mesh Sensors (WMS) were initially developed to overcome the limitations in spatial resolution of the flush mounted electrodes. The first mesh sensor was introduced by Johnson (1987). Reinecke et al. (1998) developed a three planes conductance mesh sensor that provides spatial resolution of 100 pixels with an imaging rate of 120 frames per second. The phase distribution maps are reconstructed through image reconstruction algorithms. Prasser et al. (1998) introduced a new wire mesh sensor that offers direct conductivity measurements with relatively high resolution (1024 frames per second). This sensor does not require the image reconstruction process. The simplified operating procedure of the sensor is illustrated in Figure 3-7.

The conductive WMS mainly consists of two planes of parallel wires that are positioned, in the cross-section of the pipe, perpendicular to each other with axial separation of around 2mm. The sensor electronics measures local conductivity in the space between all the crossing points. This is achieved by activating a single wire of the wires in one plane (transmitters), using a rectangular voltage pulse, while keeping all other transmitters grounded and measuring the currents which flow into the wires in the other plane (receivers). Amplifier circuits are used to convert the analogue current from the receivers to voltage. The voltage signal is

then sampled and passed to analogue to digital converts before it is stored on a computer, through a data acquisition unit. The void fraction distribution and bubble size measurements can be obtain with spatial resolution of 2mm and the time resolution of up to 10000 frames per second (Pietruske and Prasser, 2007).

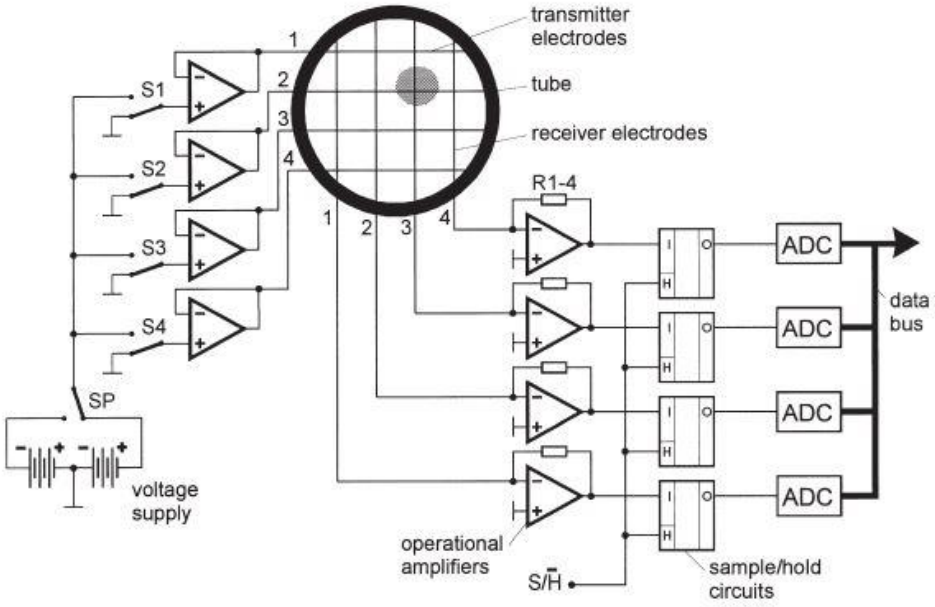


Figure 3-7: Simplified scheme of the Wire Mesh sensor that is proposed by (Prasser et al. (1998).

Da Silva et al. (2007) have extended the application of the conductance WMS to the capacitance measurements. The developed sensor measures the capacitance values at the crossing point of the electrodes. It follows a similar excitation procedure to the conductive sensor except that a sinusoidal voltage is applied for excitation and a logarithmic detector is used to receive the output voltage in the case of permittivity measurements. The capacitance distribution through the cross-section of the sensor is represented by a two dimensional matrix of the current values between all the crossing points of the electrodes. The obtained matrices can be interpreted to a void fraction distribution by considering the proportional relation between the electrical permittivity and the local void fraction, using the

calibration data. The initial time resolution was 625 frames per second which was improved later to 5000 frames per second, by using a faster analogue to digital converter and improving the electronic circuit (Da Silva et al., 2010).

The wire mesh sensor is considered as an intrusive technique which disturbs the flow and may cause bubbles fragmentation. Nonetheless, the obtained bubble size measurements demonstrate an original representation of the flow structure before deformation (Prasser et al., 2001).

The WMS can provide detail information about the flow structure. The chordal and cross-sectional void fraction can be obtained at high temporal and moderate spatial resolutions. The spatial resolution of the sensor is sufficient to identify individual bubbles of the size of the grid and above. The measurements of the bubble size distribution showed satisfactory agreement with those obtained by the high speed imaging (Prasser et al., 2001). The radial void fraction profiles can also be estimated as described in (Prasser et al., 2002). In horizontal flow, the WMS can be used to estimate the liquid level through the chordal distribution measurements (Salve et al., 2012; Rodriguez et al., 2015). The local gas velocity and individual bubble velocities can be measured using a multi-plane sensor as in (Manera et al., 2009).

The uncertainties of wire mesh sensor measurements are mainly attributed to the deceleration of bubbles at the mesh at low flow velocity, in addition to the escape of bubbles that are smaller than the spatial resolution of the sensor. More recently, Banowski et al. (2016) reported that the loss of small bubbles can be overcompensated by the deceleration of bubbles at the crossing point. Ito et al.

(2011) evaluated the performance of triple plane WMS against a high speed camera. They found that the intrusiveness of the sensor causes an obvious discrepancy in the measurements of bubble diameter and velocity. This was mainly due to the deceleration of small and the acceleration of large bubbles at low and high liquid flowrates respectively. Banowski et al. (2016) suggested the WMS performs best at a liquid superficial velocity above 0.4 $m.s^{-1}$.

The reliability of the WMS measurements has been extensively evaluated over the last decade. The first validation of the WMS performance was conducted against a single beam gamma-ray densitometry (Prasser et al., 1998). The results of vertical air-water flow showed that the WMS estimated the volumetric void fraction with an absolute relative error of 8%. The WMS sensor has been tested against several established measuring systems, including; high speed imaging (Prasser et al., 2001), ultrafast X-ray tomography (Prasser et al., 2005; Zhang et al., 2013; Banowski et al., 2016), conductive needle probes (Manera et al., 2009), gamma densitometry (Sharaf et al., 2011), quick closing valves (Salve et al., 2012) and electrical capacitance tomography (Azzopardi et al., 2010).

The WMS showed a good agreement with ultrafast X-ray tomography in terms of void fraction measurements and the radial void fraction profiles. It also showed a satisfactory agreement with the conductive four tips needle probes for measurement of two-phase parameters such as void fraction, bubble velocities and interfacial area in a vertical upward flow, where WMS offers higher spatial resolution. In the comparison with quick closing valves, the WMS showed higher deviation in the intermittent flow region while the agreement was highly improved in annular flow. It might be said that the quick closing valves is not be

the best option for intermittent flow, since different lengths of the test section may give different measurements. Both the ECT and the WMS give similar same mean void fraction and frequency. One advantage of the WMS is the capability to provide detailed bubble size measurements, whereas the ECT can provide the structure velocity without disturbing the flow. A detailed and quantitative comparison between dual mode WMS and gamma densitometry (GD) showed an acceptable agreement for void fraction measurement at the pipe core with a deviation of ±10%, while the deviation increases at the pipe wall (Sharaf et al., 2011).

Pietruske and Prasser (2007) demonstrated the ability of WMS to operate at high pressure (7Mpa) and temperature (286 °C). Recently, Kipping et al. (2016) have designed an industrial WMS that can provide online void fraction measurements. They also claimed that the main gas-liquid flow patterns in vertical upward flows can be identified, using an algorithm based on the probability distribution of the measured void fraction. More details about the application of the WMS in multiphase flow can be found in (Velasco Peña and Rodriguez, 2015). They have presented a comprehensive critical review about the performance and application of the WMS in different flow environments.

It can be concluded that the WMS has been tested and used successfully for two-phase flow measurements over the last 15 years. Despite being intrusive, it can be considered a reliable and safe alternative to the available measurement techniques. It offers high temporal and spatial resolution measurements at a lower cost in comparison to Gamma radiography and X-ray tomography. The WMS offers spontaneous void fraction measurements over the pipe or the vessel cross section.

It can also identify single bubbles due to its high temporal and spatial resolution; therefore bubble size distribution can be obtained. While the structure velocity and can be estimated using dual plane sensors.

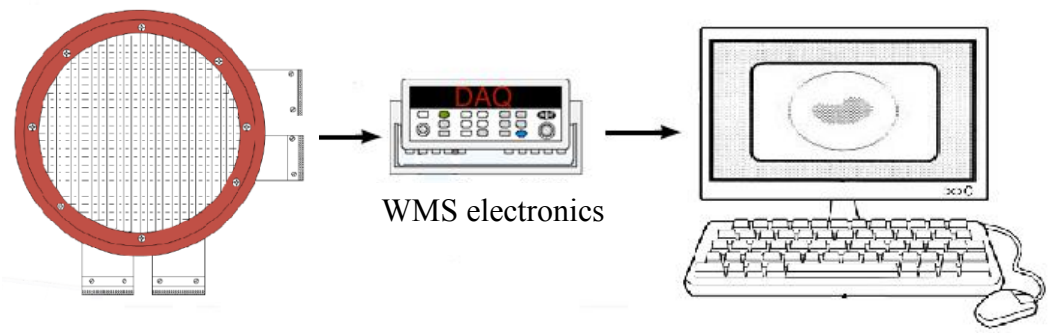


Figure 3-8: A 24×24 Wire Mesh Topographic system.

The capacitance WMS that was developed by Da Silva et al. (2007) was used in this work due to the low relative permittivity of the silicone oil. The sensor that was employed in this work consists of two electrodes. Each electrode has 24 parallel stainless steel wires of 0.12mm diameter separated by a lateral distance of 2.8 mm (Figure 3-8). Electrodes were placed perpendicular to the flow direction with an axial spacing of 2mm. The measuring points that were out of the pipe cross-section were eliminated during the data processing. The sensor is able to obtain data with a frequency of 1000 Hz and spatial resolution of 2.8mm. Due to the fact that the wire mesh sensor disturbs the flow and induces the breakup of the bubbles as reported by Prasser et al. (2001), it is not practical to use two sensors in series for simultaneous measurements and hence in this work, the ECT system was used in combination with WMS. The WMS was placed downstream of the bend while the ECT is fixed at immediately upstream of the bend for the vertical and horizontal configurations.

3.4.1.1 Calibration procedure and void fraction extraction

Calibration procedure was conducted prior to the main experimental runs, in which the measurement is taken first for pipe full with low permittivity fluid (air) and then the process is repeated for the pipe full with high permittivity fluid (silicone oil). The calibration files are saved separately and then used to obtain the void fraction data from the raw files.

The WMS generates data in a form of 3D matrix V(*i,j,k*) which corresponds to the voltage measurements at each crossing point (i,j) at time interval of k, where i and j represent the thin wire of each plane. According to Da Silva et al. (2010) the voltage measurements are proportional to the fluid permittivity and can be represented by:

$$V = a\ ln(\varepsilon_m) + b \tag{3.1}$$

Where; a and b are constants that can be determined through the calibration measurements. The measurements first conducted for the pipe filled with the gas phase with permittivity ε_G, resulting in a reference voltage matrix $V^G(i,j)$. The same procedure is repeated for the pipe full with liquid phase with permittivity of ε_L. This generates a reference data matrix $V^L(i,j)$. The mixture permittivity can be estimated based on equation (3.1).

$$V(i,j,k) = a\ ln\varepsilon_m(i,j,k) + b \tag{3.2}$$

By applying the boundary conditions to the equation (3.2), the constant can a and b can be calculated. The permittivity distribution in the sensor cross section can be represented as:

$$\varepsilon_m(i,j,k) = exp\left[\left(\frac{V(i,j,k) - b(i,j)}{a(i,j)}\right)\right] \tag{3.3}$$

Since the effective permittivity is linearly dependent of the phase fraction, then the void fraction can be measured from the obtained permittivity using parallel model as given in equation (3.4).

$$\alpha(i,j,k) = \frac{\varepsilon_{r,L} - \varepsilon_m(i,j,k)}{\varepsilon_{r,L} - \varepsilon_{r,G}} \tag{3.4}$$

3.5 Electrical Capacitance Tomography

Electrical capacitance tomography (ECT) is a non-intrusive technique in which the sensor electrodes are equally distributed around the exterior of the test section (non-invasive). The capacitance is measured between all pair of electrodes. The ECT system is described in details in Hammer (1983) and Huang (1986).

The ECT sensor operating principle is based on measuring the dielectric properties (permittivity distribution) of the fluid within the sensing area of the electrodes which are distributed on the exterior of the pipe cross section as shown in Figure 3-9. The electrodes are excited sequentially while the capacitance between the excited electrode and the all remaining electrodes is measured. This means that for sensor with N electrodes, N (N-1)/2 measurements are obtained. The acquired measurements are used to extract the permittivity distribution using an appropriate image reconstruction system. The ECT system consists of

capacitance sensor, data acquisition unit and data processing unit as shown in Figure 3-10.

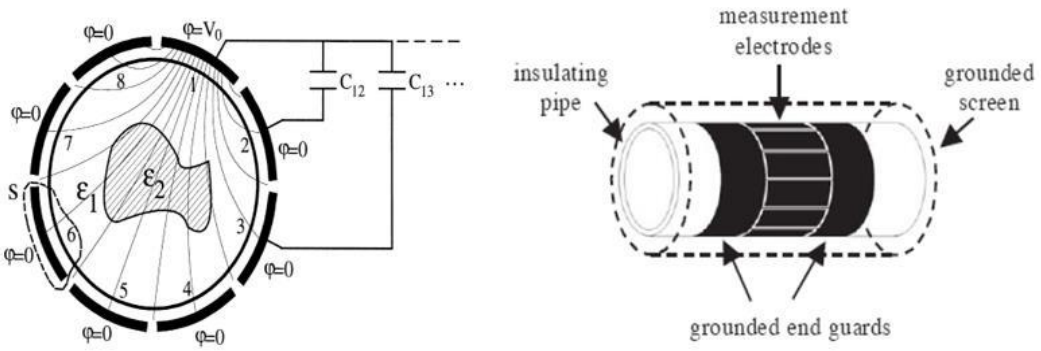


Figure 3-9: Measurement principle of an ECT system (Dyakowski et al., 2000).

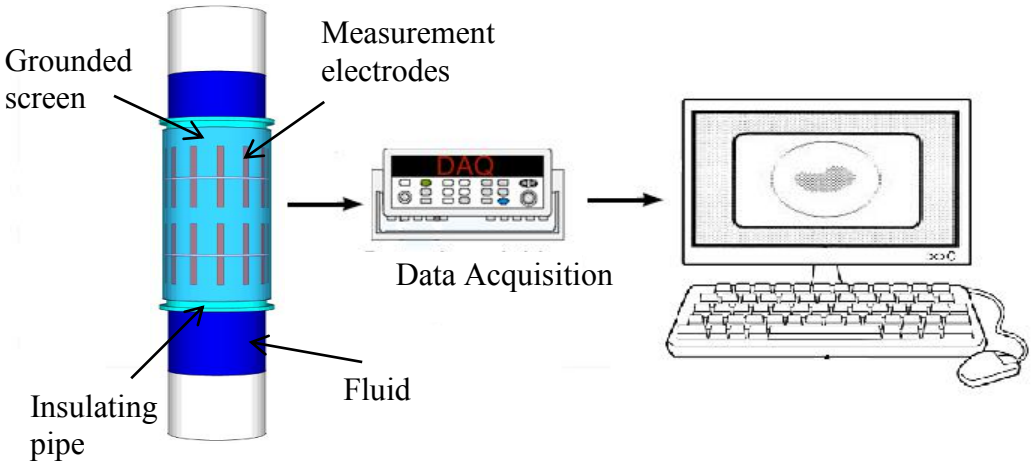


Figure 3-10: Electrical Capacitance Tomography system

The ECT sensor consist of 8 to 16 electrodes (Rautenbach et al., 2013) arranged around the exterior of an insulated section, earthed guards are used between the electrodes to minimise the capacitances between the adjacent electrodes. An overall screen is employed to shield the sensor from the external electromagnetic fields (Beck and Williams, 1995). A stray immune circuit is usually implemented to acquire the capacitance between the selected electrodes only. It ignores the stray capacitance between the selected electrodes and earth as well as between the selected and unselected electrodes (Huang et al., 1988). Calibration procedure is

required to maintain the offset and gain balance due to the change in sensitivity between different electrodes. The capacitance measurements for sensor full with the lower permittivity are stored as offset (zeros) values and those for the sensor full with higher permittivity fluid are stored as gain values. A data acquisition unit is employed to collect data , control the excitation process, digitise the capacitance value and send them to the computer (Huang et al., 1992). An appropriate interface is required to send obtained data from the data acquisition unit to image reconstruction computer in which image reconstruction algorithms are applied.

3.5.1.1 Image reconstruction

The image reconstruction (the inverse problem) is a complex process which requires estimating the permittivity distribution from the obtained capacitance values. The opposite procedure is called the "forward problem", which involves obtaining the measured capacitance values from an identified image (or permittivity distribution). The inverse problem has no analytical solution due to non-linearity of the governing equation (Poisson's equation). Therefore, an appropriate algorithmic should be applied. The linear back-projection (LBP) is the first and most commonly used algorithm for image reconstruction, despite the low resolution resulting from signal deformation. It is simple and fast and can be used as iterative or non-iterative technique (Huang et al., 1989; Xie et al., 1992; Isaksen, 1996). Yang and Peng (2003) have reviewed most of the available image reconstruction algorithms for ECT system. More details on the electrical capacitance tomography, particularly on the electrode design, data acquisition system, image reconstruction algorithms and applications can be found in (Beck

and Williams, 1995; Isaksen, 1996; Reinecke and Mewes, 1996; Dyakowski et al., 2000; York, 2001; Rasteiro et al., 2011).

The ECT has been developed over the past years. It has been widely used for flow imaging and void fraction measurements in various processes, including fluidized bed (Wang et al., 1995), fluidized bed dryer (Chaplin and Pugsley, 2005), oil pipelines (Yang et al., 1995), pneumatic conveying (Azzopardi et al., 2008), cyclone dipleg (Sun et al., 2008), vertical gas-liquid flow (Azzopardi et al., 2010), flow separation in T-junction (Baker, 2003) and it has been employed successfully in combination with WMS to study two-phase flow in bends (Abdulkadir, 2011). More recently, Sardeshpande et al. (2015) reported the ability of ECT to obtain void fraction measurements in opaque flow of bubble column. Mohamad et al. (2016) demonstrated the capability of ECT system to visualise oil-water flow and provide consistent phase distribution measurements.

Although, the ECT technique provides a low resolution imaging, generally it gives accurate volume fraction measurements in the disperse system. In addition, a dual plane ECT sensor can provide velocity information, using correlation function (Azzopardi et al., 2010). Rautenbach et al. (2013) summarised the advantage and the limitation of the ECT system in comparison to X-ray tomography. The main advantage of the ECT system is the capability of an online imaging which makes it suitable for process control. The main drawback is the limited spatial resolution for large pipes.

It can be concluded that the recent development of the ECT system especially in term of spatial resolution makes it a reliable non-intrusive technique. It is highly

tested and can provide velocity and void fraction information. The ECT system is easy to operate and can be used safely in laboratory applications.

In this work, a twin plane sensor was used. The sensor consists of 8 electrodes mounted around the outer circumference of the pipe. The sensor was mounted around an insulating pipe, with an axial distance of 89 mm between the measuring planes. A brass sheet was placed around the sensor; it was designed to work as a stray immune capacitance measuring circuit to isolate the selected electrodes.

The TFLR5000 ECT system used in these experiments is supplied by Process Tomography LTD. It consists of 8 electrode twin-plane sensor, data acquisition unit and personal computer (PC) for data processing. The data acquisition unit contains 8 capacitance nodes and 8 driven guard excitation nodes for each plane to ensure uniform electric field over the cross section of the sensor. It is controlled by a PC through ECT32 control software operates under windows XP operation system. The ECT 32 software control the twin plane sensor to measure the capacitances between ungrounded electrode pairs at a speed up to 5000 frame per second. The captured data can be saved and played back at adjustable frame rates either in a form of images or normalised capacitance. TFLR5000 ECT system applies the linear back projection algorithm to reconstruct the cross-sectional distribution of the capacitance values inside the pipe. The measurements were recorded at sampling frequency of 1000 Hz for 60 seconds.

3.5.1.2 Calibration procedure and void fraction extraction

The calibration procedure is conducted in a similar way to the WMS, where the sensor is filled with the low and the high permittivity fluids in turn, and then

measuring the capacitance values at these to limit values. The calibration data is then saved as a reference file that is used to normalise the unique capacitance measurements between all pairs of electrodes.

According to Huang et al. (2003), the normalised capacitance can be represented by:

$$Cr_i = \frac{C_i - C_{oi}}{C_{mi} - C_{oi}} \tag{3.5}$$

where C_i is the *ith* measured capacitance between the electrodes, C_{oi} and C_{mi} are the i_{th} measured capacitances for sensor full with low and high permittivity material respectively. Since the capacitance is proportional to the material permittivity equation (3.5) can be written as:

$$Cr_i = \frac{\varepsilon_m - \varepsilon_l}{\varepsilon_h - \varepsilon_l} \tag{3.6}$$

Where; ε_l and ε_h are the permittivity of low and high permittivity phases, while ε_m is the effective permittivity of the mixture within the sensor. When the sensor is full with the low permittivity phase, the volume fraction of the high permittivity material will be zero, while the volume fraction will be one when the sensor is full with high permittivity material. The volume fraction for sensor contains both low and high permittivity material can be calculated, assuming a linear relation between the lower and higher permittivity limits during the calibration (Huang et al., 1989).

3.6 Experimental methodology

The two-phase flow development through vertical and horizontal 90° bends was investigated experimentally. Electrical Capacitance Tomography (ECT) which is described in detail by Hammer (1983) and Huang (1986) and the Wire Mesh Sensor tomography (WMS), that introduced by Prasser et al. (1998) and developed for capacitance measurement by Da Silva et al. (2007), were used to obtain real-time void fraction measurements in these experiments. These measurements techniques have been widely tested over the years. For instance WMS measurements showed a good agreement with X-ray tomography and Gamma radiography for void fraction measurements as reported by Prasser et al. (2005) and Prasser (2000), whereas Azzopardi et al. (2010) concluded that the ECT and WMS give similar mean void fraction, they also highlighted the advantage of each technique. The ECT and WMS are installed upstream and downstream of the bends respectively. It should be noted that the WMS is an intrusive technique that could cause distortion of the flow structures, thus it is usually installed downstream of the non-intrusive ECT system.

To investigate the two-phase flow around the vertical 90° bend, experiments are designed using ten gas superficial velocities in conjunction with six liquid phase superficial velocities giving a total of 60 conditions. The experimental matrix is available in the Appendix A. This flow range corresponds to bubble and intermittent flow (slug and churn) in the vertical pipe. A data acquisition system using LabVIEW software was developed for simultaneous acquisition of data from all devices. A trigger signal from the WMS is used to initialise the ECT and the other measuring devices including flowmeters. The pressure drop across the

bend is measured using a smart differential pressure transmitter with range of 0 to 0.865 bar. The differential pressure transmitter was connected to the pressure tappings, through a manifold; this allows measuring the pressure difference at different locations sequentially and offered simultaneous measurements with the WMS and ECT system.

During each experiment the flow rate, pressure, temperature and void fraction were measured after allowing the flow to stabilise. The process was repeated for each run until the full set of experiments was completed.

The cross-sectional void fraction data was averaged over a period of 60 seconds at an acquisition rate of 1 kHz. The consistency of the results was checked through data analysis process which included estimating the probability density functions (PDF), frequency and structure velocities. The PDF plots of cross section averaged void fraction time series data was used to identify the relevant flow pattern. The power spectral density method is applied to obtain the frequency of the time series data that describe the periodicity of the flow structure such as slugs whilst structure velocity was determined by cross correlating the time averaged void fraction distribution of the twin-plane ECT sensor.

3.7 Signal analysis and data Processing

The instrumentations that were used in this work such as the capacitance WMS and ECT system offer a wide range of detailed data about the two-phase flow structure at remote locations. Real-time measurements in the form of void fraction time series were obtained from both sensors.

The time series data of the void fraction distribution was used to estimate several flow parameters including; the probability density functions (PDFs), radial void fraction, bubble size distribution, structure frequency and structure velocity. This section explains the procedure that was employed to process the raw data obtained from the measuring devices in order to generate expressive results.

3.7.1 Data Characterisation

Signals obtained from any experiment are generally classified to either random or deterministic signals, in other words, non-predictable or predictable data. Most of the physical processes produce non-deterministic data. The understating of the nature of the generated data is essential for selecting the appropriate methods of analysis.

A random signal represents a random change in the frequency and the amplitude of the physical phenomenon. Random data cannot be predicted mathematically in time and it can be either stationary or nonstationary.

Data obtained from this work exhibit a random nature where the void fraction signal is varying randomly with time. It can be presented by the probability of occurrence or the mean averaged values of the void fraction. This randomness of the void fraction signal can be identified through the probability density function, power spectral analysis and the autocorrelation of the time series sequence of the void fraction data (Bendat and Piersol, 2011).

The analysis procedure employed is often justified based on the type of the random signal as being either stationary or nonstationary. The following subsections illustrate the main tests that were conducted to characterise the

generated data. Detailed information about random data processing is available in (Bendat and Piersol, 1980; Bendat and Piersol, 2011)

3.7.1.1 Stationarity test

A random signal is considered to be stationary if the mean values $\mu_x(\bar{x})$ and the variance of the random data stay unchanged with time. In order to perform the test of stationarity, the recorded signal should be divided into smaller intervals (n) of size (N). Then the mean value and the variance of the intervals can be estimated by:

$$\mu_x(\bar{x}) = \frac{1}{N}\sum_{i=1}^{N} x_i \tag{3.7}$$

$$\sigma_x^2(\bar{x}) = \frac{1}{N}\sum_{i=1}^{N} (x_i - \bar{x})^2 \tag{3.8}$$

In this work, the void fraction time series was split into several intervals of similar sample sizes. It is noted that the change in the mean and variance was almost constant, for a sample size greater than or equal to 5000 data point and at measuring frequency of 1000Hz. The results indicate that all the averaged values are almost invariant with time, and hence the data can be considered stationary, as illustrated in Figure 3-11. The stationarity test can also be conducted using nonparametric methods such as the reverse arrangement test detailed in (Bendat and Piersol, 2011). Autocorrelation function can be used as well to identify stationary data, where the autocorrelation sequence should decay to zero with the increase of time delay, in case of random stationary data.

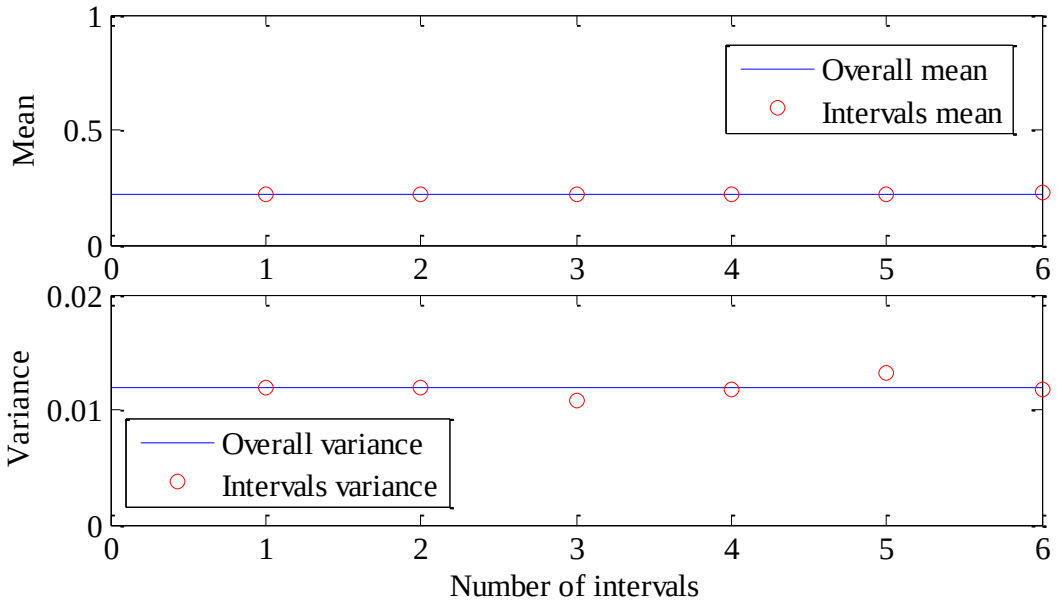


Figure 3-11: The moving average and variance of 1 minute signal divided into 6 intervals of 5 second length.

3.7.1.2 Periodicity test

There are several different methods to identify the periodic nature of a signal, including; visual observation of the time series or the power of the probability density function, the autocorrelation function and the spectral density function.

In this work, the autocorrelation function R_{xx} was used to identify the periodic structure of the void fraction time series which subsequently was used to estimate the frequency implementing the power spectral density analysis as explained later in this chapter.

Autocorrelation function of stationary random process is a measure of the dependency of the future data on the previous observation. It can be estimated by multiplying a delayed signal by its original record (Bendat and Piersol, 2011).

$$R_{xx}(t_1, t_1 + \tau) = \frac{1}{N}\sum_{i=1}^{N} x(t_1)x(t_1 + \tau) \tag{3.9}$$

Figure 3-12 shows clearly the periodic nature of the void fraction time series of 60000 data point obtained at 1000Hz frequency. Similar procedure was applied to all cross-sectional averaged records of the void fraction.

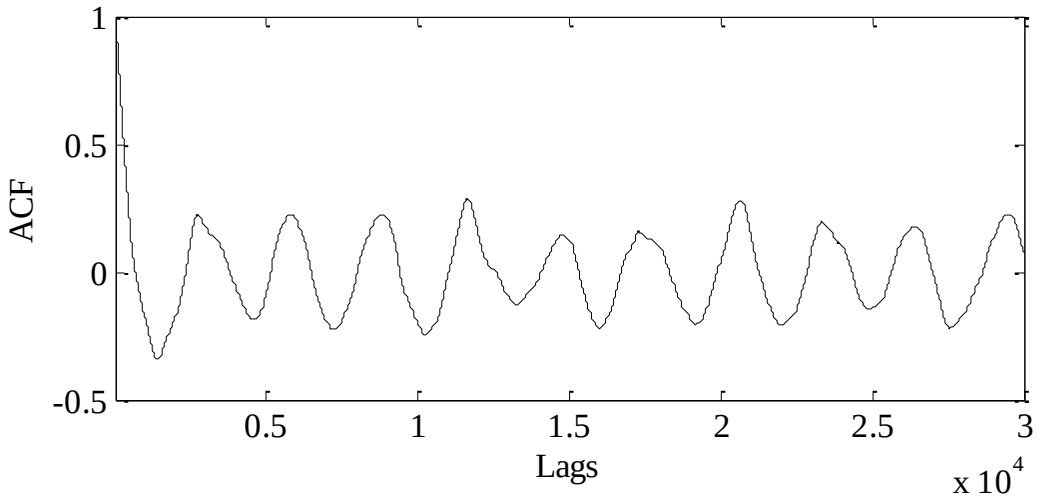


Figure 3-12: Autocorrelation sequence for time averaged void fraction signal recorded at 1000Hz frequency for 1 minute.

Since the mean values of the void fraction time series is invariant with time and the autocorrelation function depends on the time delay and it decays at time delay $\tau > 0$, the data is considered to be weakly stationary.

Generally the weakly stationary data, that fits normal distribution, denotes strongly stationary data as suggested by Bendat and Piersol (2011), since the probability distribution is derived from the mean values and correlation functions. In this work, due to the existence of bimodal distribution that is associated with the intermittent flows, the averaged time series void fraction signal varies from strongly stationary to weakly stationary. In both cases, the analysis methods that were used in this chapter are valid and justified.

3.7.2 Sampling frequency

The void fraction data was captured at sampling frequency of 1000Hz for 1 minute for the most of flow patterns except in the case of intermittent flows (i.e. slug flow). for intermittent flows the measuring time was increased to 5 minutes and the frequency was reduced to 400Hz, in order to capture meaningful statistical representation of the flow. The selected sampling frequency is sufficient to capture the fast moving structure and fulfils the sampling theorem; hence spectral density analysis can be performed to the signal.

Sampling theorem suggests that the sampling frequency should be at least twice the maximum frequency of the signal (Nyquist frequency), in order to avoid the issue of aliasing.

$$f_s \geq 2f_{max} \tag{3.10}$$

Therefore, in order to avoid misinterpreting the contribution of any possible frequency components, the time series signal should be constructed with an interval size equal to Nyquist interval:

$$\Delta_t \geq \frac{1}{2f_{max}} \tag{3.11}$$

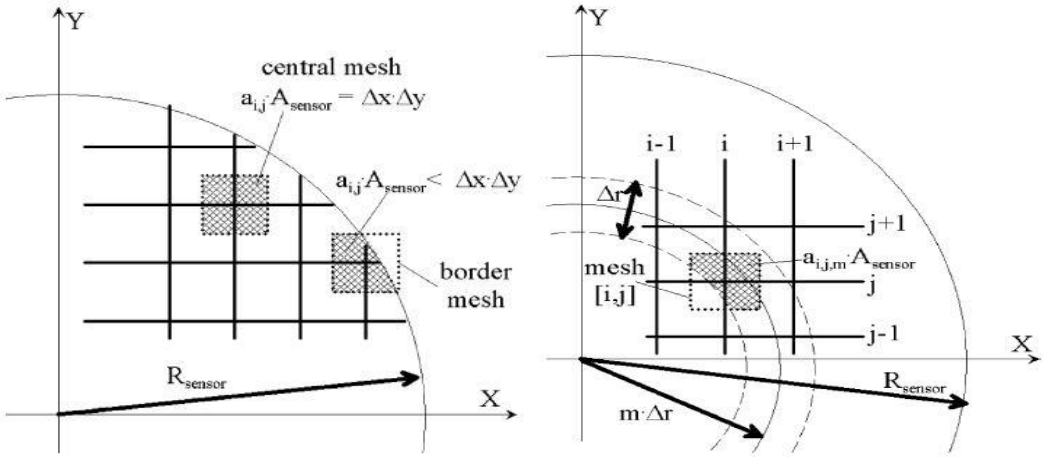
In this work, 1000Hz and 400Hz are much higher than the maximum dominant frequency of the void fraction time series; though, it was required to capture the fast moving structures. Consequently, the computational time of the data processing was increased.

3.7.3 Time averaged void fraction from WMS and ECT

For the WMS, both time and cross-sectional averaging of the void fraction were calculated as illustrated by Prasser et al. (2002). The total time averaged void fraction distribution of each individual sampling period can be estimated through averaging over the cross section.

$$\varepsilon_{i,j} = \frac{1}{k_{max}} \sum_{i=1}^{imax} \sum_{j=1}^{j\,max} \sum_{k=1}^{kmax} a_{ij} \,.\, \varepsilon_{i,j}, k \tag{3.12}$$

This averaging is based on weight coefficients a_{ij} that incorporate the contribution of each crossing point (i,j) to the total cross sectional area of the sensor (Figure 3-13-a). Where k_{max} is the number of instantaneous void fraction distribution, i_{max} and j_{max} are the total wire in both planes.



a. Weight coefficients $a_{i,j}$ for the averaged cross-sectional void fraction

b. Weight coefficients $a_{i,j},m$ for the averaged radial void fraction profiles

Figure 3-13: Weight coefficients for estimating the time averaged local void fractions, adopted from Prasser et al. (2002).

On the other hand, the radial void fraction profiles can be obtained by averaging the local instantaneous void fraction over measured period and over a number of radius intervals (m). The sensor is divided into a number of ring-shaped intervals

with increment of $\Delta r = R_{sensor}/m$ as shown in Figure 3-13-b. The weight coefficients $a_{i,j,m}$ represent the contribution of each measuring point to a ring of number (m). The radial time averaged void fraction can be written as:

$$\varepsilon_m = \frac{1}{k_{max}} \sum_{i=1}^{imax} \sum_{j=1}^{j\,max} \sum_{k=1}^{kmax} a_{i,j,m} \,.\, \varepsilon_{i,j}, k \tag{3.13}$$

For ECT system, the void fraction can be obtained using the method suggested by Huang et al. (2003) for void fraction measurement which is based on the reconstructed images of the ECT system. The void fraction can be estimated through analysing the reconstructed images, since the grey level (f) of the image represents the distribution of the phases. Therefore the void fraction can be estimated as:

$$\varepsilon = 1 - \frac{\left(\sum_{j=1}^{N} f_j A_j\right)}{A} \tag{3.14}$$

where N is the number of pixels, A_j is the area of *jth* pixel and *A* is the pipe cross section area. The voidage can be also estimated from the normalised capacitance measurements by calculating the average of the normalised capacitance values in a single image frame as:

$$\varepsilon = \frac{(\sum_{i=1}^{M} Cr_i)}{M} \tag{3.15}$$

where, M is the total number of the measurements between all electrode pairs and Cr_i is the normalised capacitance between *i* electrode pairs.

3.7.4 Bubble size distribution

Bubble size measurement and bubble size distribution can be obtained from the WMS void fraction measurement as illustrated by Prasser et al. (2001), where bubbles diameter can be calculated from the bubbles volume as:

$$D_b = \sqrt[3]{6/\pi \,.\, V_b} \tag{3.16}$$

Where V_b is the volume of a given bubble that can be estimated by identifying the corresponding local instantaneous void fraction. Then the equivalent bubble diameter can be used to obtain the statistical distribution.

The procedure requires identifying the individual bubbles first and then estimating the volume of each bubble through the integration of the local gas fraction. Prasser et al. (2001) used the recursive fill algorithm to identify the bubbles from a 3D array of local void fraction. The filling procedure initiates at a local gas fraction maxima (i.e. highest gas fraction within its neighbourhood) and it is stops when the gas fraction is lower than the local maxima with a certain threshold, called the differential threshold. An optimum threshold value of 10% is recommended. It was reported that at lower value, below 10%, unrealistic artefacts are identified as individual bubbles, whilst at higher threshold value unrealistic coalescence was reported.

Similar procedure was implemented in this work to estimate the bubble size distribution from a 3D array of instantaneous void fraction measurements. The fill algorithm was included in the data processing software package provided by Institute of Fluid Dynamics, Helmholtz-Zentrum Dresden-Rossendorf, Germany. The obtained bubble size distribution from this method represents the partial

contribution of a class of bubbles to the total gas volume fraction, instead of the number of bubbles distribution.

3.7.5 Liquid level

The WMS sensor generates a three-dimensional void fraction array $\varepsilon_{i,j,k}$ as explained earlier where the indices [i,j] indicate the local void fraction in the cross-section of the pipe (i.e. crossing points of the electrode wires) and k is the represents the variation of the voidage in the time domain. Figure: 3-14 shows the cross-sectional coordinates of the (24X24) WMS sensor.

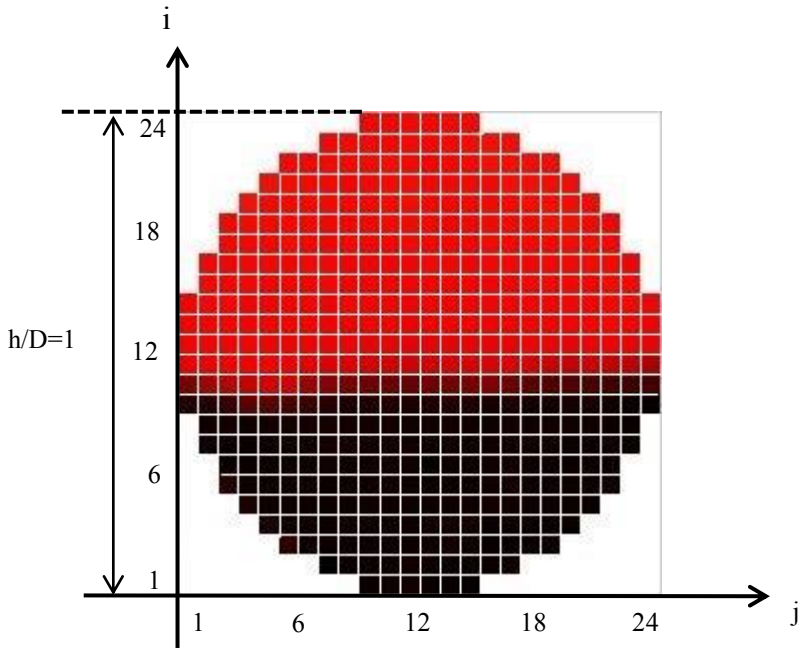


Figure: 3-14: Coordinates of the measuring points used in identifying the interface height between phases in a horizontal pipe. (Black and red colours represents liquid and gas phase respectively).

The averaged chordal void fraction profiles were used to estimate the liquid level. The void fraction was averaged in the horizontal plane producing a 24x1 matrix for each time frame. The vertical distance is normalised by the pipe diameter where h/D= 0 at the bottom and equal to 1 at the top of the pipe.

The results of the chordal void fraction profiles in the vertical direction exhibit three regions; a low void fraction region at the bottom of the pipe, a high void fraction region at the top and an intermediate region in between as illustrated in Figure 3-15.

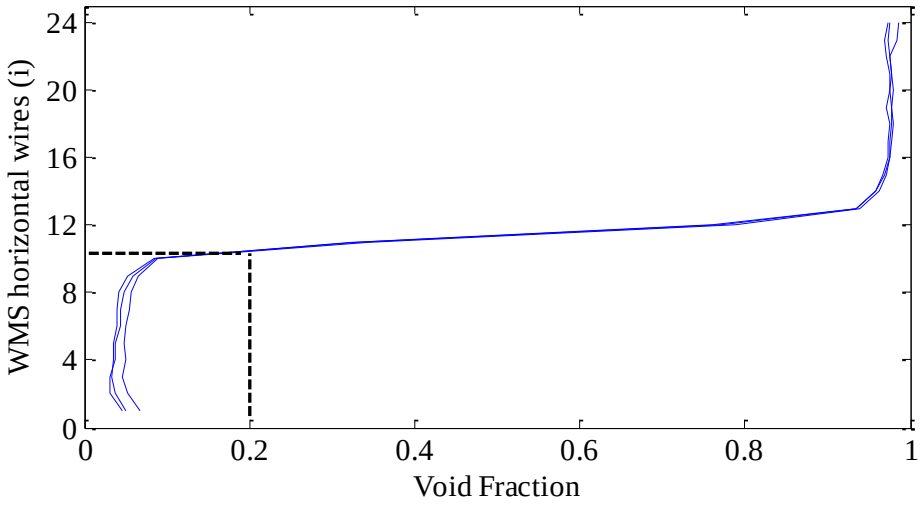


Figure 3-15: The vertical mean chordal profiles of the void fraction at several time frames.

Stratified flow pattern is associated with a sharp change in void fraction at the interface. The void fraction value at which the sharp change occurs is around 0.2. Therefore, the interface height was identified from the vertical chordal void profile, using a voidage threshold value of 0.2. When this threshold value was increased up to 0.5, an insignificant change in the interface height estimation was recorded. This indicates that the measuring points are more likely to be immersed in liquid if the local void fraction is below 0.5. This procedure was implanted in MATLAB and the time series of the liquid level was obtained at all flow conditions.

3.7.6 Probability density function

Probability density functions (PDF) demonstrates how often each value of void fraction occurs within a particular range. PDF plots show the rate of change of probability with void fraction values, where the total area under the PDF plot should be equal to one. The PDFs has been widely used to identify the relevant flow patterns. It has showed the ability to discriminate between the main flow patterns. In addition, PDFs can be also used to estimate different flow parameters such as film thickness, slug length and bubble length in slug flow (Jones and Zuber, 1975).

The PDFs plots of the cross-sectional averaged void fraction are used to identify the corresponding flow patterns based on the work of Jones and Zuber (1975) and Costigan and Whalley (1997) in which they pointed out that the PDFs of the void fraction data can be used to discriminate quantitatively the main flow patterns. Bubbly flow is associated with a single peak at low void fraction, while churn flow is represented by a single peak with a wide band at high void fraction and a tail stretched to low void fraction. Slug flow, as internment flow pattern between bubbly and churn flow, is identified by a twin peak PDF signature, one at low void fraction corresponding to the void fraction in liquid slug while the other at high void fraction representing Taylor bubble.

The PDF of the cross-sectional averaged void fraction was estimated using the hist function in MATLAB. The void data was distributed to 100 bins to produce the histograms. A histogram is a specific type of bar chart that indicates the number of occurrences of void values within a certain range. A histogram is created by distributing the measurements into intervals, where the rate of change

of the probability in the ordinate plotted against the void fraction values in the abscissa.

3.7.7 Structure Frequency

The frequency of the structures was estimated using the method proposed by Hazuku et al. (2008) for large disturbance waves. The void fraction signal from the WMS and ECT was used to estimate the front and the tail of the liquid slug as illustrated in Figure 3-16. A liquid slug is defined as a part of the signal whose peak is higher than the upper average of the liquid holdup and both ends are lower than the average of the liquid holdup. The part of the signal between two trailing liquid slugs represents a Taylor bubble. A MATLAB script was developed to implement this method.

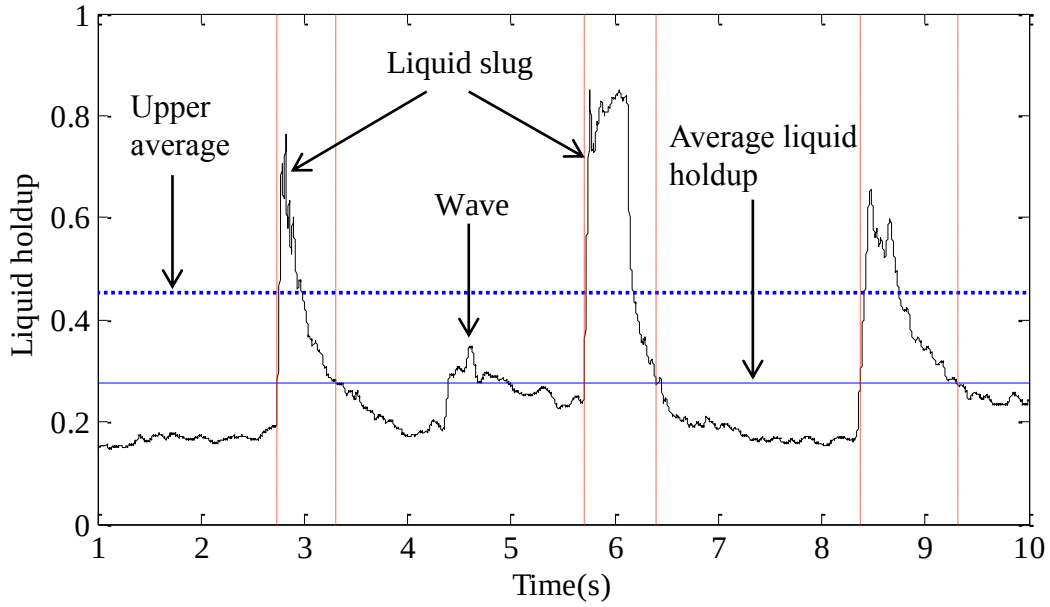


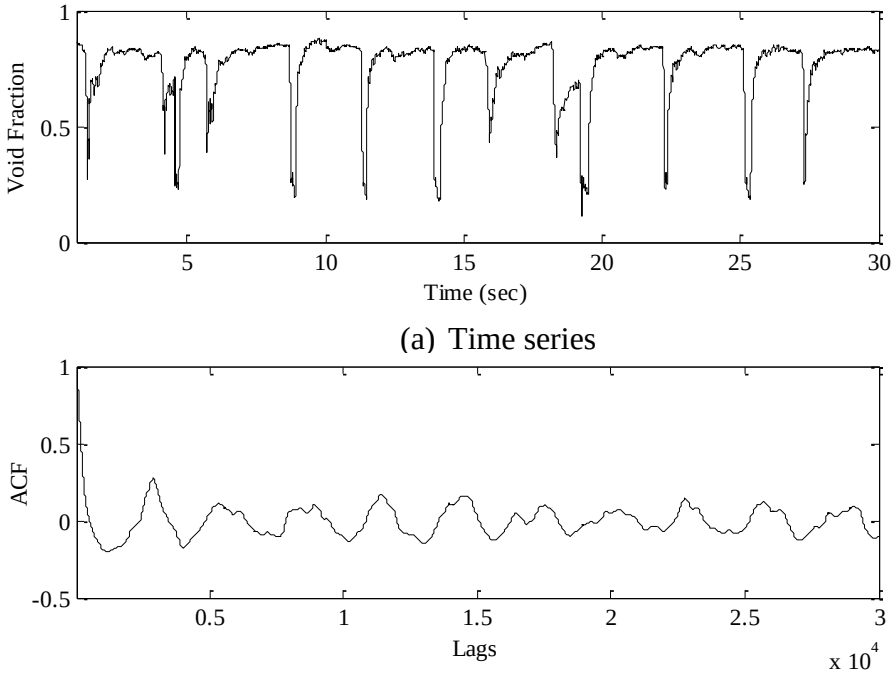
Figure 3-16: Identification of flow structures in the calculation of the structure frequency.

The power spectral density (PSD) method was also applied to obtain the frequency of the time series data that describe the periodicity of the flow structure such as slugs. The PSD was estimated through discrete Fourier transform of the

autocorrelation sequence of the time series, according to Wiener-Khinchine theorem, as shown in equation (3.17):

$$S_{xx}(f) = \int_{-\infty}^{+\infty} R_{xx}(\tau) e^{-j2\pi f\tau} d\tau \tag{3.17}$$

Where; R_{xx} is the autocorrelation function of the void fraction time series as described by equation (3.9) while $S_{xx}(f)$ is the power spectral density as reported by (Bendat and Piersol, 1980). This procedure was implemented in MATLAB using fast Fourier transform (FFT) algorithm. Fourier analysis transforms the void fraction data from its time domain into the frequency domain. Figure 3-17 and Figure 3-18 show an example of the PSD analysis that was applied to the recorded void fraction time series signals.



(a) Time series

(b) Autocorrelation function

Figure 3-17: A sample of the time series (a) and the autocorrelation sequence (b) of cross-sectional averaged void fraction sampled at 1000Hz.

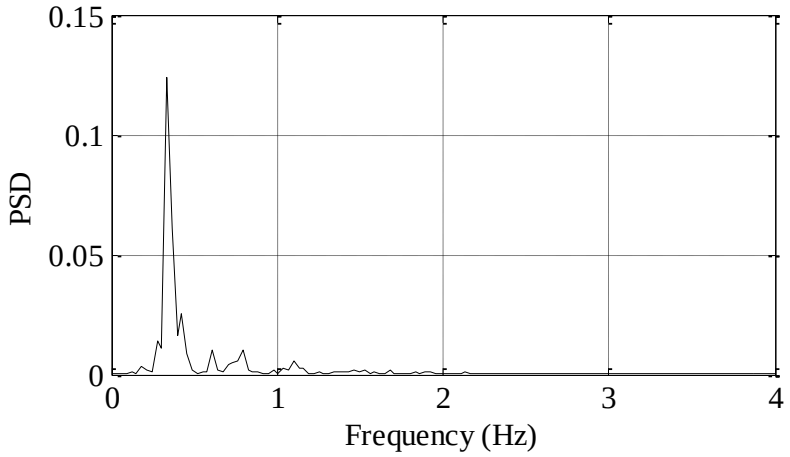


Figure 3-18: Power spectral density of the void fraction time series.

The results from described methods were in a good agreement with the manual counting of the peaks in the time series signal of the cross-sectional averaged void fraction.

3.7.8 Structure velocity

The structure velocity was determined by cross correlating the void fraction time series obtained from the twin-plane ECT sensor. The sensor planes are located at 0.089m apart, hence the signal recorded by the first plane will be received at the second plane at a time delay of ΔT without any significant distortion as shown in Figure 3-19. The cross-correlation function is, in fact, the autocorrelation of a signal delayed by certain time τ as in equation (3.18). In this case x and y represent the signal at the first and second plane of the ECT system respectively. Thus the cross-correlation is given by:

$$R_{xy}(t_1, t_1 + \tau) = \frac{1}{N}\sum_{i=1}^{N} x(t_1)y(t_1 + \tau) \tag{3.18}$$

The cross-correlation sequence exhibits a sharp peak at the time of delay; thus the peak occurs at zero only if there is no delay in the signal. In these experiments, the

cross-correlation peak indicates the lag in the number of data points received by both sensors as illustrated in Figure 3-20. The first sensor always leads the second sensor by certain number of data points. This value of data points is divided by the sampling frequency (fs) to obtain the actual time delay (τ).

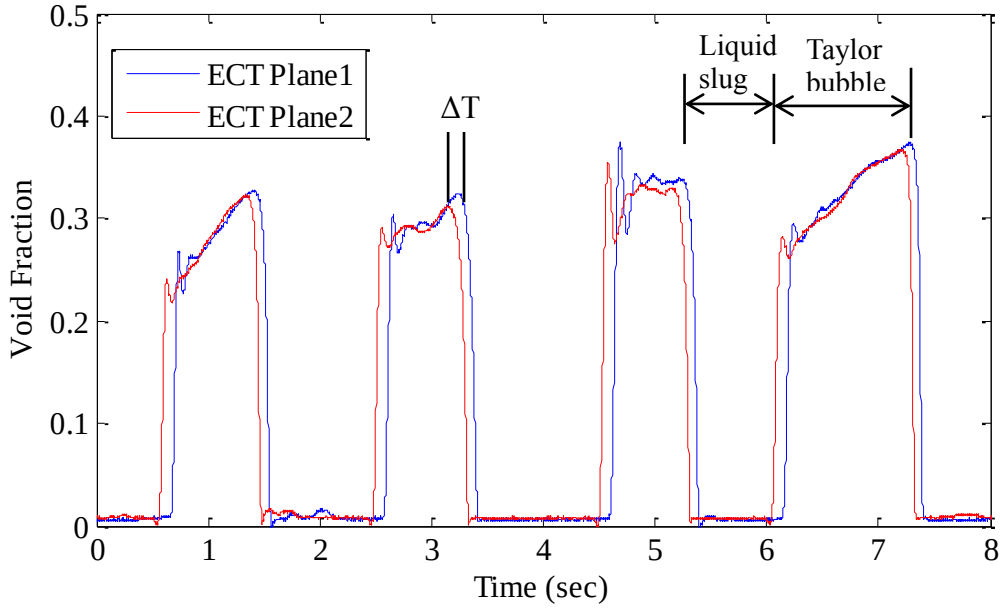


Figure 3-19:A sample of the void fraction time series received by the dual plane ECT, indicating the time delay.

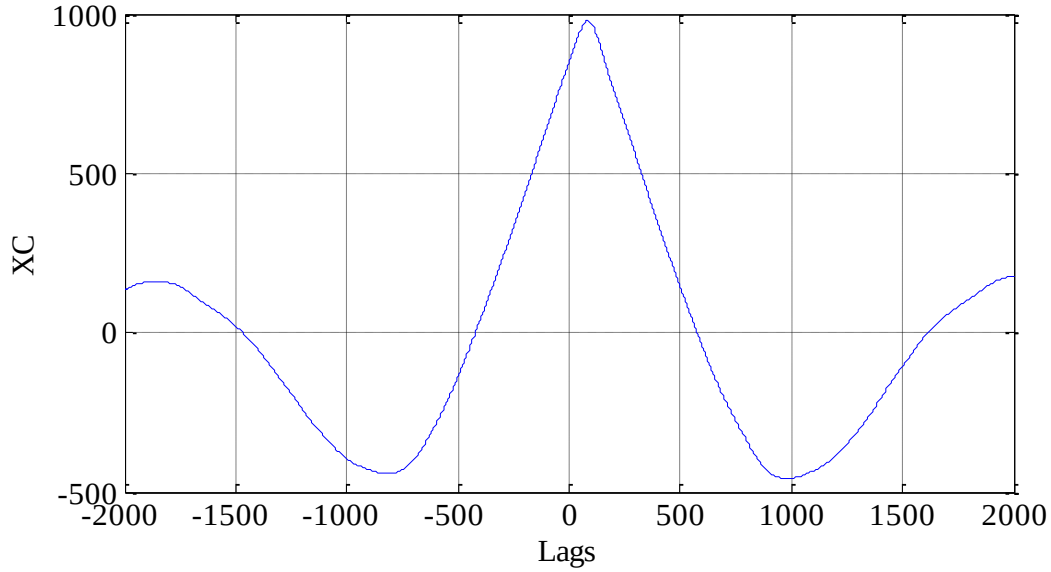


Figure 3-20: The cross-correlation function of the void fraction signal obtained from the ECT system.

The propagation velocity of the flow structure is estimated by:

$$U = \frac{d}{\tau} \tag{3.19}$$

Where; d is the distance between the two sensors (d=0.089m) and τ is the time delay estimated by the cross correlation function.

3.7.9 Slug length

The length of slugs was estimated using the averaged transitional velocity of slugs and the resident time of slugs at the measuring plane (τ). The velocity was assumed to be constant throughout the test section and the following equation was used:

$$L_s = \tau \ . U_s \tag{3.20}$$

Where; L_s is the slug length, τ is the resident time of slugs at the sensor and U_s is the velocity of slugs.

3.8 Error analysis and uncertainty

In practice, no experiments can be conducted free of error, regardless how carefully the measurements are made. The error is commonly defined as the difference between the measured value and the true value. The experimental error is evaluated by its accuracy and precision.

Accuracy forecasts the difference between measured and true value. It is impossible to predict the accuracy of a measurement when the true value is unknown. Precision refers to the reoccurrence of measurements within a certain range when the experiment is repeated. Precise measurements tend to generate values close together.

In engineering analysis, error refers to uncertainty since the true value is hardly known. In fact, the identifiable mistakes or errors in measurements should be eliminated prior to the uncertainty estimation. For instance, calibration curves can be used to correct the output of the measuring devices before starting the experiments. Therefore the measured value should be equal to the best measurement plus the uncertainty.

Experimental uncertainties are inherited in the measurements of the physical quantities and cannot be avoided by experimental repetition. There are two types of experimental uncertainty: systematic uncertainty and random uncertainty.

It is worth mentioning that any instrument has a limited resolution and can be used to measure with a certain degree of excellence. However, the resolution of an instrument is not connected to the accuracy of the measurements.

3.8.1 Systematic uncertainty

Systematic uncertainty affects the accuracy of the measurements. It is consistent and cannot be improved by repeating the experiments. Systematic errors are commonly caused by an inaccurate calibration of a measuring device, a change in the experimental conditions and a wrong reading by the observer. The systematic error can be diminished by refining the source of error and repeating the measurements (Kirkup and Frenkel, 2006).

In this work, the systematic error information is supplied by manufacturers for all measuring devices except the WMS and ECT system. Therefore; the WMS and ECT were compared and the relative uncertainty between both sensors is considered to be the systematic uncertainty of void fraction measurements.

The systematic uncertainty is successfully removed through the calibration procedure. However, there is still a margin of uncertainty associated with the corrected values. Table 3-2 summaries the systematic error of the used instruments and the associated uncertainty with calibration procedure. The calibration details are available in Appendix B.

Table 3-2: the systematic error and the uncertainty associated with the corrected values through calibration.

Measurement	Systematic Uncertainty ±	Uncertainty after correction (±of the calibrated span)
Temperature (°C)	0.5°C	0.5° C
Pressure (bar)	0.5% FS	0.5% FS
Differential pressure (bar)	1% FS	0.075%
Air flow (l/min)	3% FS	1%
Silicone oil flow (m^3/hr)	2%	1%
Void fraction (-)	5%	5%

3.8.2 Random uncertainty

Random errors affect the precision of the data. For a random process, the random uncertainty estimates the scatter of the measurements around the best estimate (i.e. the mean value). Random uncertainty is caused mainly by an inherent fluctuation in the measurements. The effect of random errors can be reduced by increasing the number of repetition of the measurements (Taylor, 1997).

In these experiments, the measurements were repeated two to three times for each location. The repeatability of the measurements (i.e. precision) at different

locations was confirmed through estimating the random uncertainty of different flow parameters upstream the test section for six different runs.

Random errors are estimated statistically using the mean and the standard deviation of the mean, the details of the calculations are presented in Appendix B. Since the fractional uncertainty, as described in Appendix B, is more expressive than just the uncertainty interval. The results are summarised in Table 3-3, in term of fractional uncertainty. The results indicate notably a low random uncertainty which suggests high precision measurements and hence repeatable runs are justified.

Table 3-3: The fractional random uncertainty of the measured flow parameters.

Measurement	Fractional uncertainty ($\frac{\delta x}{\lvert x_{best}\rvert}$)	The mean of ($\frac{\delta x}{\lvert x_{best}\rvert}$)
Air flow (l/min)	$2 \times 10^{-4} \leq \frac{\delta Qa}{\lvert Qa_{best}\rvert} \leq 7 \times 10^{-3}$	1×10^{-3}
Liquid flow (m^3/hr)	$4 \times 10^{-4} \leq \frac{\delta Ql}{\lvert Ql_{best}\rvert} \leq 4 \times 10^{-3}$	1×10^{-3}
Pressure (bar)	$2 \times 10^{-3} \leq \frac{\delta P}{\lvert P_{best}\rvert} \leq 2 \times 10^{-2}$	8×10^{-3}
Void fraction (-)	$2 \times 10^{-4} \leq \frac{\delta VF}{\lvert VF_{best}\rvert} \leq 1 \times 10^{-2}$	2×10^{-3}
Frequency (Hz)	$1 \times 10^{-3} \leq \frac{\delta F}{\lvert F_{best}\rvert} \leq 1 \times 10^{-2}$	4×10^{-3}

3.8.3 Propagation of uncertainties

Certain physical quantities are often measured indirectly through a combination of independent measured quantities, due to the difficulty or impossibility of a

direct measurement. Each of those independent quantities has an uncertainty; therefore the uncertainty of the resulting estimate is a combination of the error associated with the independent measurements (Taylor, 1997).

The propagated uncertainty (i.e. combined uncertainty) was measured for gas and liquid superficial velocities as well as mixture velocity. The results and the detail analysis of the experimental uncertainty are available in Appendix B.

Chapter 4

Flow development in 68mm riser

Vertical pipes of different sizes, lengths and inclinations are common in many industrial applications, such as reactors, heat exchangers, gas-lift pumps. In oil and gas pipelines, particularly offshore platforms, prior knowledge of the flow structure (slugs) is crucial for the design of equipment and safe operation. Bends are usually required to connect pipes at different orientations, and their effect on the flow evolution should not be ignored. Therefore, the knowledge of two-phase flow development in risers is crucial from the perception of research as well as industrial applications.

Flow regime transition due to the variation of the flow parameters and the layout of the pipes, in addition to the forces acting on the phases, are of primary interest. Local measurements of flow parameter at different locations in co-current gas-liquid flow are desirable for development and validation of computational fluid dynamics (CFD) codes. Reliable two-phase flow data is required for developing flow models and validating the existing models. The characterisation of axial flow evolution has a crucial industrial application, especially in gas and oil industry where the transition between flow patterns has a direct influence on the design of the downstream equipment.

The majority of the available literature is focused on air-water flow experiments. In fact, most of the available models are based on air-water flows experiments.

The models that developed based on such data are devoid of the dependency on the physical properties of the process fluids used in many industrial settings. This has raised the demand of experiments that employ fluids with viscosity, density and surface tension different to that of water. Thereby the experiments presented in this work were designed to provide more accurate and high-resolution database, employing advanced instrumentation and using oil with physical properties different to water. This data will expand the range of published results and could be used to evaluate the available flow transition models. The data will also be used to compare the evolution of the flow before and after the bend in the next chapter.

In this chapter axial flow development in 4.5 m long riser with 68mm internal diameter (ID) is examined. The chapter describes how the flow structures in the vertical section develop as it moves downstream of the mixer. It also presents a detailed investigation of the axial flow development of slug flow. The experimental results were obtained from the two-phase facility described in Chapter 3. Air and 5 mPa.s silicone oil experiments were conducted at ambient pressure and temperature for 60 different flow combinations.

The time series of the averaged void fraction was obtained at three different locations (15D, 30D and 45D) downstream of the mixer. For all experiments, the WMS was placed immediately after the ECT sensor, to eliminate the impact of the intrusive nature of the former. Detailed analysis of the void fraction time series signal (as described in Chapter 3) was performed. The characteristic parameters are reported including, cross-sectional averaged void fraction, probability density functions, structure frequency and velocity, slug length, Taylor bubble velocity,

and the void fraction in the body of slugs. The available flow models and existing empirical correlations were tested using the experimental data at 45ID downstream of the mixer. The comparison between the experimental and predicted results is presented.

4.1 Comparison between WMS and ECT

Electrical Capacitance Tomography (ECT) and Wire Mesh Sensor (WMS) tomography have been widely tested over the last years. For instance WMS measurements showed good agreement with X-ray tomography and Gamma radiography for void fraction measurements as reported by Prasser et al. (2005) and Prasser (2000). Whereas Azzopardi et al. (2010) concluded that the ECT and WMS give a similar mean void fraction, they also highlighted the advantage of each technique. For all experiments reported in this thesis, the WMS was placed downstream of the ECT sensor in order to minimise the intrusive nature of the WMS and also to limit the change in the vertical distribution of the void fraction between the two measuring planes.

The void fraction data gathered from both sensors showed a reasonable agreement for all experiments. Figure 4-1 shows PDFs of the cross section averaged void fraction time series data simultaneously collected using WMS and ECT at the given flow conditions.

The comparison illustrates that at liquid superficial velocity, U_{ls}, 0.22 m s^{-1} and gas superficial velocity, U_{gs}, 0.045 m s^{-1} the PDF corresponds to bubbly flow. For this flow pattern, the WMS seems to give higher void fraction which might be due to the drag effects triggered by the intrusive nature of the sensor, where at low

flow rates the bubbles decelerate at the measuring plane causing an increase in average void fraction.

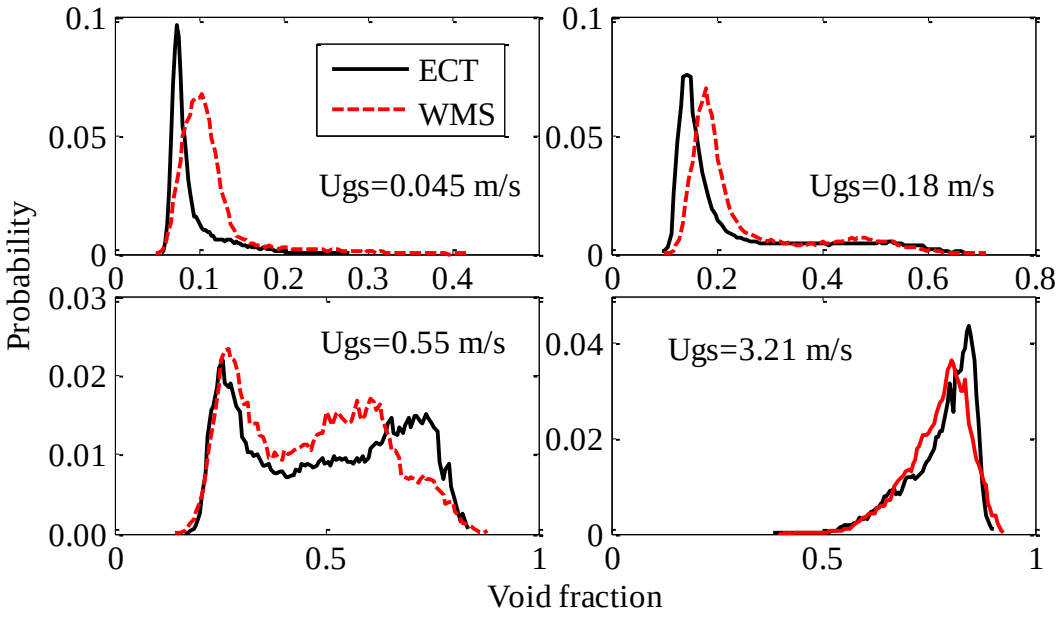
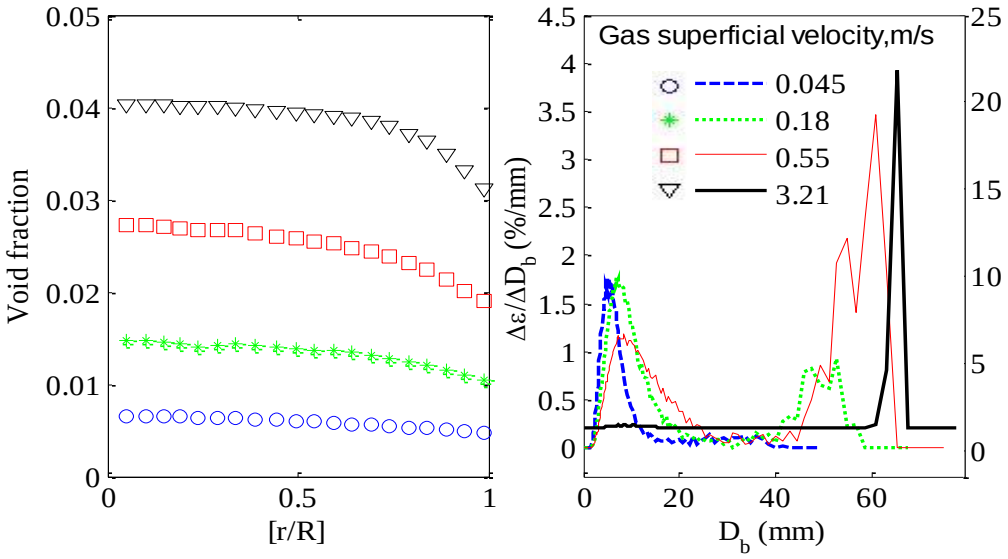


Figure 4-1: The PDF plots of the cross-sectional averaged void fraction for ECT and WMS at 45D downstream the mixer. The liquid superficial velocity= 0.22 m s^{-1}.

At liquid superficial velocity, U_{ls} 0.15 m s^{-1} and gas superficial velocity, U_{gs} 0.36 m s^{-1}, both sensors show almost similar PDF plots which indicate Slug flow. For the maximum flow condition achievable in the experimental rig (U_{ls}=0. 53m s^{-1}, U_{gs}=3.21 m s^{-1}), the PDF signatures for ECT and WMS characterise churn flow, where ECT provides a higher peak at slightly higher void fraction than the WMS. It is obvious that the difference between the PDF plots created using the two sensors reduces as the gas superficial velocity increases. Generally, the PDF signatures for both devices indicate similar flow patterns (Omar et al., 2015).

The radial void fraction profile and bubble size distribution at liquid superficial velocity 0.22 m.s^{-1} and different gas superficial velocity are illustrated in Figure 4-2. The radial distribution of the gas fraction shows a flat profile at low gas superficial velocity (Ugs=0.045 m s^{-1}); this corresponds to a dispersed bubbly

flow, in which small gas bubbles are uniformly distributed throughout the cross section of the pipe. As the gas superficial velocity increases, the uniform distribution disappear and the radial void profile tends to indicate a local maxima at the core of the pipe. At these conditions large bubbles are formed and rapidly shifted to the centre of the pipe. At U_{gs} = 0.18 m s^{-1} and 0.55 m s^{-1} the bubble size distribution switched from single to bimodal, indicating the transition to cap bubble and slug flow regime respectively. The most significant observation from these results is that the bubble size at the measuring plane is greater than the wire spacing of the WMS and hence the error due to the sub-resolution bubble sizes is considered to be minimum. This is expected since the initial bubble size is 3mm while the spatial resolution of the sensor is 2.8 mm. It seems that small bubbles are deaccelerated at the sensor wires while the large bubbles are accelerated as reported by (Ito et al., 2011). This hypothesis explains the reduction in the difference between the two sensors as the gas superficial velocity increases.



a. Radial void fraction b. Bubble size distribution

Figure 4-2: Radial void fraction profile and bubble size distribution obtained from WMS at 45D downstream of the mixer. Liquid superficial velocity = 0.22 m.s^{-1}.

Banowski et al. (2016) suggested the best working range of the WMS. They also reported that the sensor insensitiveness of small bubbles could be overcompensated by the deceleration of bubbles at the crossing point. Therefore, in this case, the WMS is expected to overestimate the averaged void fraction at a low gas flow rate. On the other hand, the limited spatial resolution of the ECT sensor should not be ignored. It is a non-invasive sensor and hence the void fraction at the core of the pipe may not be accurately represented, especially when the gas phase is not uniformly distributed. On the other hand, a twin plane ECT system can provide velocity information without altering the flow structure.

In conclusion, it can be said that both sensors can give an acceptable and comparable estimation of the cross-sectional average void fraction. The high temporal and spatial resolution of the WMS can provide detailed information of the flow and can detect bubbles within its spatial resolution. The dual plane ECT sensor offers the prediction of the structure velocity without disturbance of the flow. Both sensors have strengths and weaknesses due to the limitations in the design and it is difficult to select one over the other. It is obvious that if both sensors are integrated, a considerable amount of flow information can be obtained.

4.2 Flow patterns identification

The PDFs signature of the cross-sectional averaged void fraction, obtained from the WMS and ECT, is used to identify the corresponding flow patterns based on the work of Jones and Zuber (1975). They reported that the PDFs of the void fraction data could be used to discriminate the main flow patterns quantitatively. Visual observations corroborated the statistical analysis and have been in use

since. The main flow patterns observed in the riser are bubbly, cap bubbles, slug and churn. For gas superficial velocity ranges from 0.45 to 3.21 $m.s^{-1}$ and liquid superficial velocities from 0.15 to 0.53 $m.s^{-1}$. Figure 4-3 shows the time series of the main flow pattern and their PDFs. The results show that each flow regime has a unique probability density function distribution comparable to those reported in the literature.

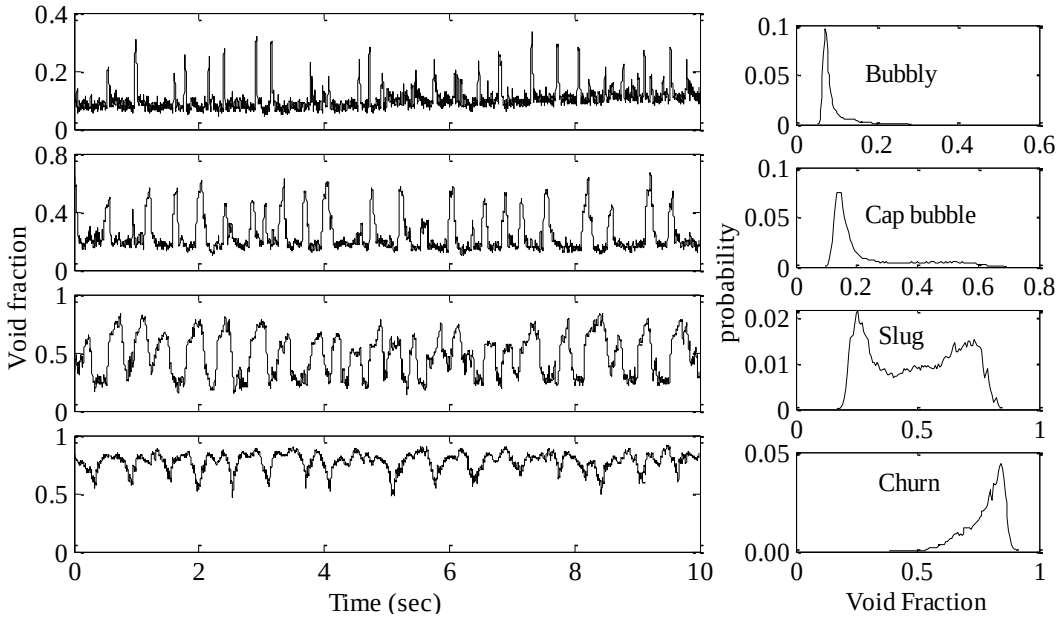
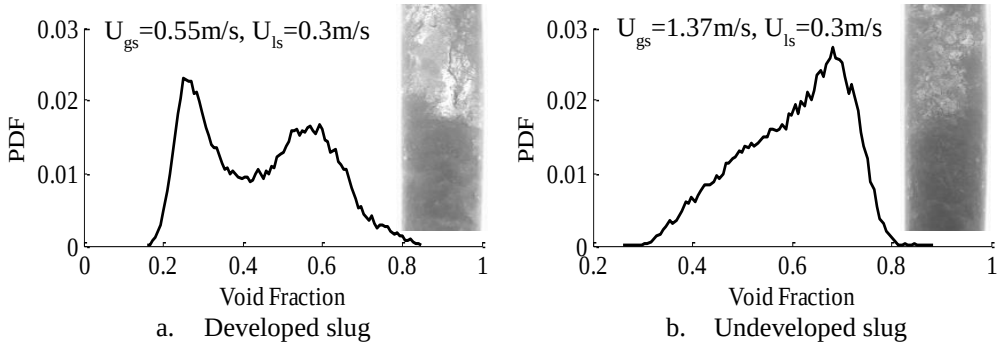


Figure 4-3: Cross-sectional averaged time series of void fraction and the corresponding PDFs for each flow pattern.

According to Costigan and Whalley (1997), slug flow is identified by twin peak PDF, one at low void fraction corresponding to the smaller bubbles in the liquid slug, while the other at high void fraction corresponding to the Taylor bubble. The most remarkable observation in the riser was the undeveloped slugs; they are short and highly aerated slugs, similar to those reported by Nydal et al. (1992) in horizontal pipes.

Undeveloped slugs in the riser are more likely to occur near the transition to churn flow at high gas flow rates. This type of slug is characterised by a single wide

peaked PDF. Therefore it can be inaccurately identified as churn flow. Figure 4-4 illustrates the difference between developed slugs and undeveloped slugs.



a. Developed slug b. Undeveloped slug

Figure 4-4: Probability density function of a developed slug and an undeveloped slug.

4.3 Flow transition along the axial direction

Void fraction measurements at three different locations upstream of the bend (the vertical pipe section) were initially conducted. The time series of the averaged void fraction was obtained at three different locations (15D, 30D and 45D) downstream of the gas injection point (mixer).

It can be seen from Figure 4-5 that at the lowest gas superficial velocity (case a), the averaged void fraction near the mixer (at 15D) is the highest, while at the second location (30D) the void fraction reaches the lowest values before increasing again at 45D downstream of the mixer. Since the PDF plots, as well as the visual observation, indicate bubbly and cap bubble flow, it can be reasoned that at low gas superficial velocity, finer bubbles forms near the mixer resulting dispersed bubbly flow. Furthermore, the bubble density is high making the mixture to appear like a foam. As the bubbles move up to the second position, 30D, larger bubbles formed due to coalescence and these bubbles moves to the centre of the pipe occupying a smaller area of the cross section of the pipe. The

observation is in agreement with Prasser et al. (2002) and Lucas et al. (2005) for multi-disperse bubbles and Tomiyama (1998) for a single bubble. As the large bubbles move upward at relatively higher velocity, more coalescence occurs forming larger cap bubbles and hence the void fraction increases again (Omar et al., 2015).

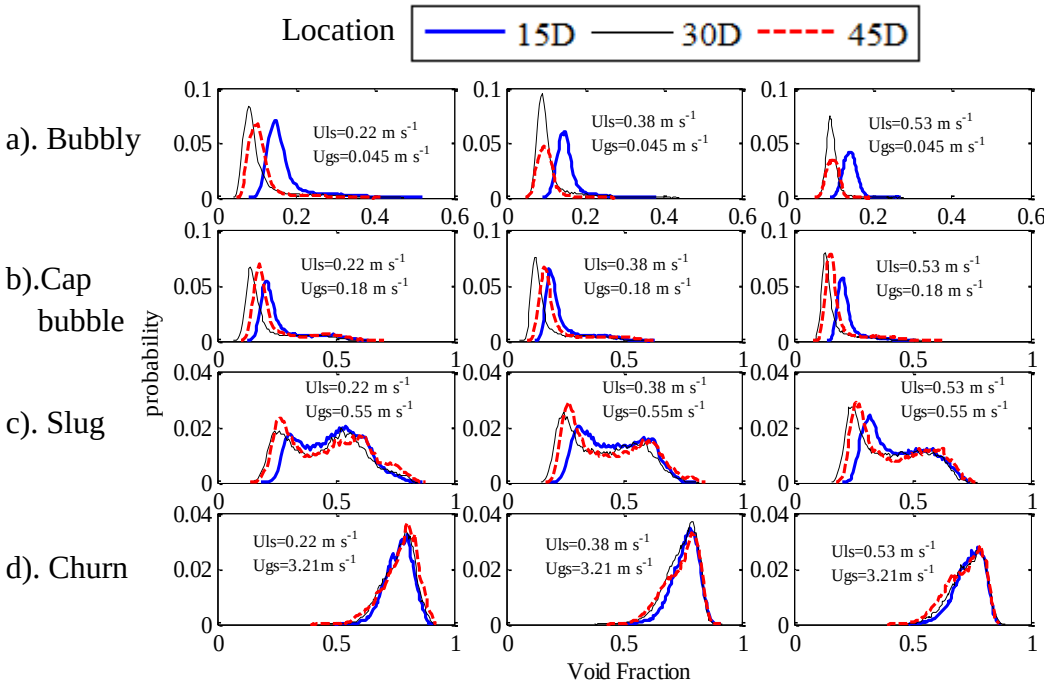


Figure 4-5: PDF plots for different flow condition at 15D, 30D and 45D downstream the mixer.

PDF plots were generated for superficial gas velocities 0.045 m s^{-1}, 0.18 m s^{-1}, 0.55 m s^{-1}, and 3.21 m s^{-1} and superficial liquid velocities 0.22 m s^{-1} 0.38 m s^{-1} and 0.53 m s^{-1} at selected axial positions. The flow pattern changes with different combinations of the liquid and gas superficial velocities as shown in Figure 4-5 Several flow patterns such as bubbly (Figure 4-5-a), cap bubbles (Figure 4-5-b), slug (Figure 4-5-c) and churn (Figure 4-5-d) could be attained in the riser. As the gas superficial velocity increases, the PDFs produced for the three measurement locations are almost similar (Omar et al., 2015). It seems that at high gas flow

rates the change in the averaged void fraction along the axial length is insignificant thus the required length for flow development is expected to be shorter under these conditions. However, the interaction between phases is considered to continue in risers, regardless their length, due to the change in pressure and forces acting on bubbles.

4.3.1 Bubble size distribution and radial void fraction

Bubble size distribution is obtained from the WMS data using the algorithm developed by (Prasser et al., 2001) as detailed in Chapter 3. It is based on the gas volume fraction contained in each class of bubbles instead of the number of bubbles. Figure 4-6 illustrates the bubble size distribution at three different flow conditions.

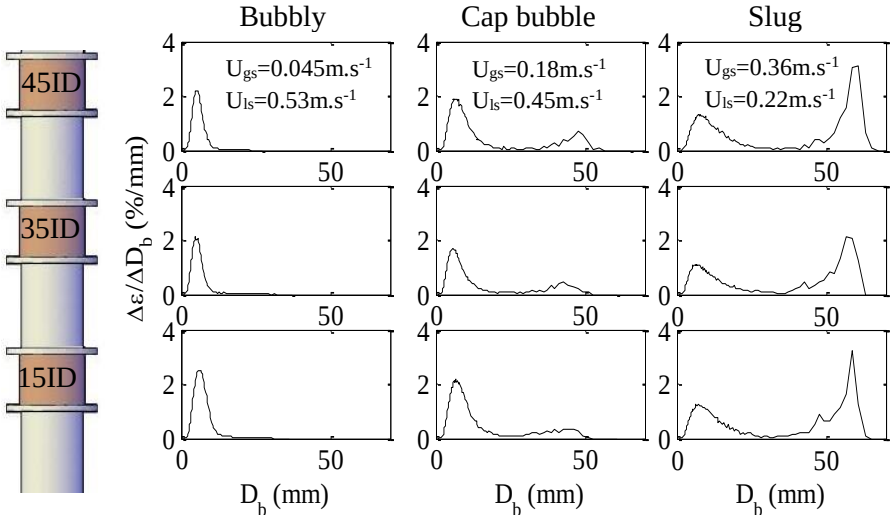


Figure 4-6: Bubble size distribution for different flow patterns.

It is obvious that in the bubbly flow region the distribution displays a single peak at small bubble size, this peak is shifted to the right as the bubbles move upwards due to the coalescence. At bubble/cap bubble transition, the distribution of the first location shows a single peak indicating small bubble sizes and a long tail

extended to relatively large bubbles. This represents a nonhomogeneous bubbly flow. As the flow develops in the axial direction, a second peak becomes apparent, this peak shows that large cap bubbles become more frequent. It is clear that the estimated diameter of these bubbles is around 50 mm, slightly below the pipe diameter. In slug flow region the bubble size distribution is characterised by double peak one at small bubble size, similar to that of bubbly flow, and the other for bubble diameters equivalent to the size of the pipe representing the distorted Taylor bubbles. It is possible to use the bubble size distribution to discriminate between steady flow patterns, such as bubbly, cap bubbles and slug flow. There is an agreement between the bubble size distribution and PDFs results, both plots could give a clearer image of the axial evolution of the flow. The case is slightly complicated for slug-churn transition, since both regimes are represented by almost similar distribution, especially near the transition boundary. At the upper end of slug flow conditions and throughout the churn conditions the distribution is represented by a single peak at large bubble size with a tail extending to the small bubble size. It is worth mentioning that at high gas hold up in liquid slug, unrealistic bubbles coalescence might be identified by the filling algorithm used is this work.

4.4 Cross-sectional averaged void fraction

The superficial gas velocity has a significant influence on the subsequent flow development in the riser. Figure 4-7 shows the mean void fraction for the range of gas and liquid flow rates at 45D downstream of the gas injection point. The curves indicate a continuous increase in the void fraction with increasing superficial gas velocity. It can be seen that the void fraction is sensitive to the change of

superficial gas velocity at low values. Figure 4-7 clearly indicates that the curves tend to level off beyond the superficial gas velocity 1.5 m s^{-1}. This trend can be interpreted as the change in flow patterns with the increase of superficial gas velocity. The transition from bubbly to slug flow is associated with a considerable shift in the rate of change of the void fraction, w.r.t. the superficial gas velocity. The higher gradient up to superficial gas velocity of 0.55 m s^{-1} explains bubbly to slug transition, whereas the transition from slug to churn incorporates a slight variation in the rate of change of void fraction beyond U_{gs} > 1.5 m s^{-1}. If the superficial gas velocity increases further, the curve is expected to have another distinguish increase at the annular flow tarnation (Omar et al., 2015).

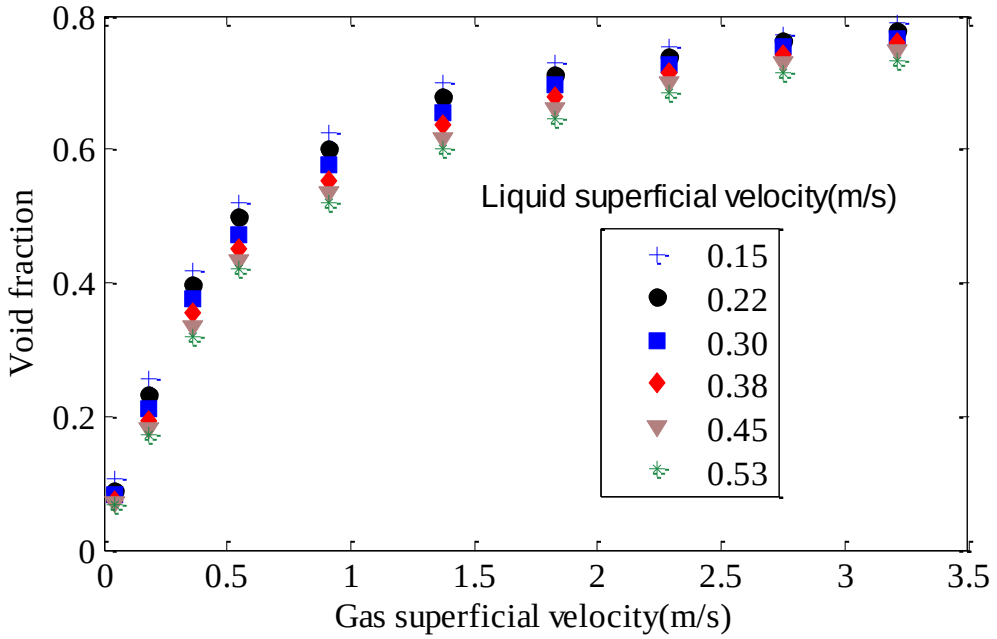


Figure 4-7: The variation of the averaged void fraction with superficial gas velocity for several liquid superficial velocities in the riser.

The influence of the superficial liquid velocity on the mean void fraction shows a decrease in the void fraction as the liquid superficial velocity increases. However, it can be said that the superficial liquid velocity has a weaker influence on the void fraction comparing to that of superficial gas velocity.

Figure 4-8 illustrates the axial propagation of the cross-sectional void fraction at U_{ls} = 0.3 m s^{-1}. Generally, at low gas superficial velocity, the change in void fraction along the axial length does not follow a clear trend. This part of data represents bubbly flow. Therefore the change in bubble size and population could be responsible for this transient behaviour.

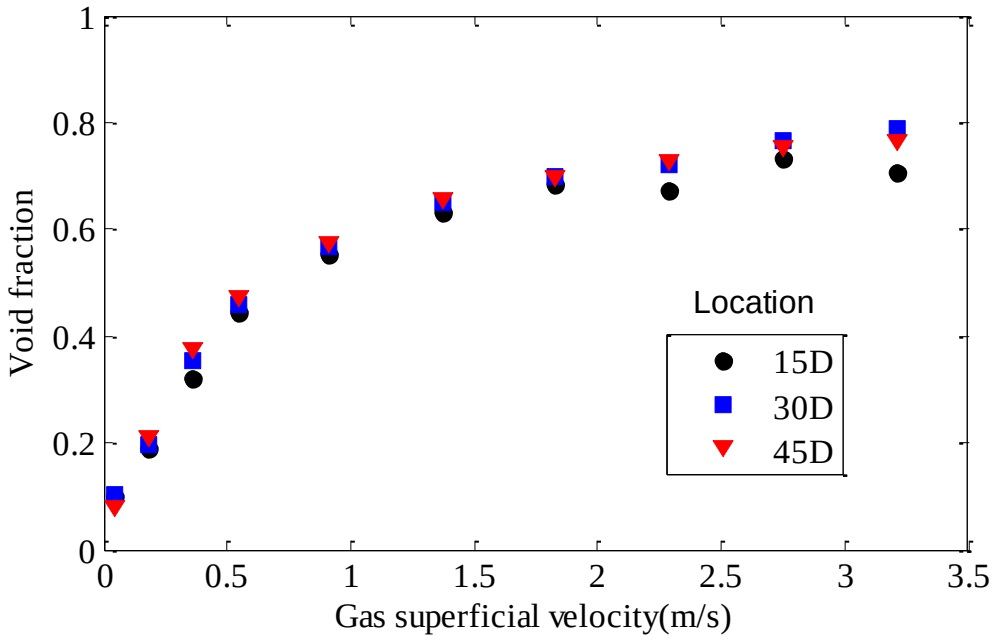


Figure 4-8: The axial variation of mean void fraction at Uls = 0.3 m s^{-1}.

As the superficial gas velocity increases, the change in void fraction become consistent and increases in the axial direction. It should be noted that the difference in averaged void fraction at the second and third positions is small. The PDF plots at 30D and 45D are identical in shape as explained earlier, and no change in the flow structure were visually observed. Therefore, the flow development is considered to be insignificant at those locations. Although the void fraction distribution is expected to evolve continuously in long vertical pipes due to the change in pressure, the changes on average would be small beyond certain pipe length.

The void fraction is a crucial parameter in characterising two-phase flow; therefore an accurate prediction of void fraction is of great interest in industrial applications. In this work, Drift-flux model was used to estimate the void fraction in the region of slug flow. Drift-flux model considers the mixture as whole, instead the two-phase separately. The one-dimensional drift-flux model is widely used to estimate the averaged void fraction. It is usually preferred over the two-fluid models for its simplicity and applicability in a wide range of flow conditions. The general form of the one-dimensional drift-flux model is represented by Eq. (4.1) (Bhagwat and Ghajar, 2014).

$$\varepsilon_d = \frac{U_{gs}}{C_0 U_m + U_d} \tag{4.1}$$

Where U_d and C_0 are the drift velocity and distribution parameter respectively. The drift velocity is the relative velocity between the gas phase and mixture velocity at the centreline. While the distribution parameter accounts for the distribution of the gas phase through the cross section of the pipe. The drift velocity is estimated by the equation proposed experimentally by Nicklin et al. (1962) eq. (4.2) which is in agreement with the theoretical work of Dumitrescu (1943) and Davies and Taylor (1950).

$$U_d = 0.35\sqrt{(g * D)} \tag{4.2}$$

The distribution parameter C_0 was found to have different values with respect to the corresponding flow patterns. For slug flow it is widely acceptable that C_0 is equal to 1.2, however in this work the equation proposed by Hibiki and Ishii (2003), that accounts for density differences, is used.

$$C_0 = \left(1.2 - 0.2\sqrt{\frac{\rho_g}{\rho_l}}\right) \tag{4.3}$$

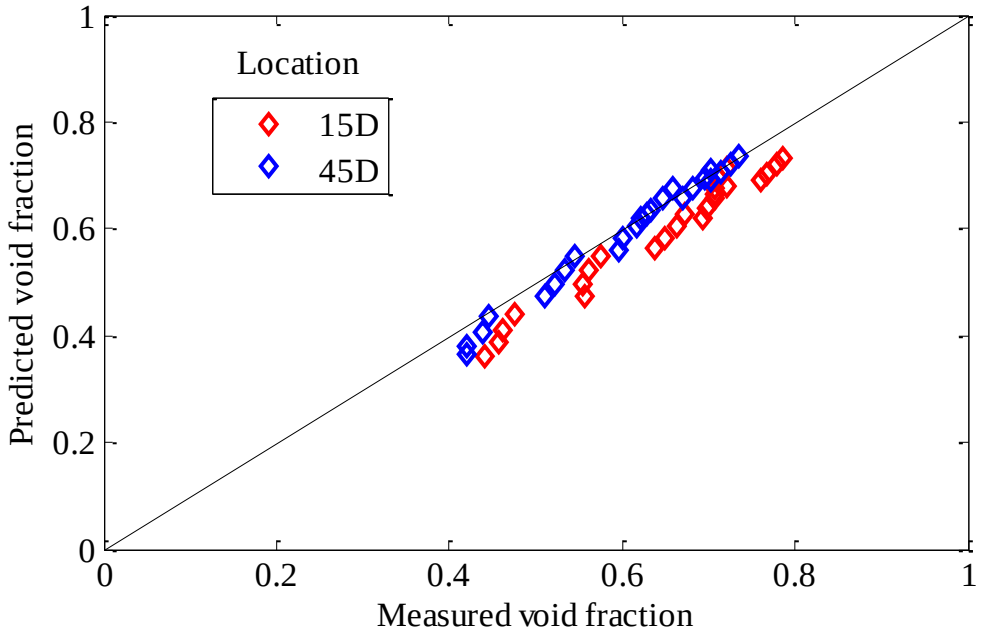


Figure 4-9 Comparison of experimentally measured void fraction and predicted void fraction using drift flux model at 15D and 45D downstream of the mixer.

The Drift-flux model results were compared to the experimentally estimated averaged void fraction at 45D downstream of the mixing section, as presented in Figure 4-9. The figure shows a good agreement between the predicted and experimental data with an average percentage error of -2.38% and standard deviation of 0.6. The accuracy of the model decreases for data obtain at a shorter distance from the mixing section. For instance, at 15D the cross-sectional void fraction data was visibly under predicted with an average percentage error of -8.5% and standard deviation of 0.6. It is evident that highly aerated underdeveloped slugs were more dominant at 15D from the mixing section leading to underestimation of the void fraction. As the slugs move upward towards 45D downstream of the mixer, developed slugs become more frequent leading to improved accuracy of the predicted data.

4.5 Slug Unit Characterisation

A slug unit consists of an elongated bubble called Taylor bubble followed by a liquid slug which usually contains dispersed bubbles. In this work, a distorted Taylor bubble was observed, due to the relatively large diameter pipe. In vertical pipes, Taylor bubble is surrounded by a thin liquid which flows downwards in the space confined between the bubble and the pipe wall. Taylor bubbles behind short slugs travels faster than the leading bubbles. Therefore, consecutive slug units tend to merge. During this process, the length of Taylor bubble and liquid slug increases. The increase in slug length continues, until the separation between two successive bubbles is long enough so that the transitional velocity of bubble behind the liquid slug is unaffected by the wake region of the leading bubble (Moissis and Griffith, 1962). Therefore stable slug length is considered equal to the minimum separation distance between two bubbles, that able to absorb the jet formed by the falling film around the leading bubble (Moissis and Griffith, 1962; Taitel et al., 1980; Barnea and Brauner, 1985).

One dimensional model is commonly used to model slug flow, in which the slug phenomenon is simplified to a sequence of identical units flowing at constant velocity (Wallis, 1969; Fernandes et al., 1983; Taitel and Barnea, 1990). Due to the intermittency of the slugging phenomenon, the estimation of slug characteristics, such as slug frequency and length, is a crucial factor for industrial design and operation. For instance, the maximum length of liquid slugs is important for the design of slug catchers and two-phase separators. These flow characteristics vary in time and space, therefore several correlations were proposed in order to predict the main features of slugs in vertical pipes, such as

Taylor bubble velocity, gas hold up within the body of liquid slugs, length of liquid slugs and the frequency of slugs (Nicklin et al., 1962; Sylvester, 1987; Khatib and Richardson, 1984; Legius et al., 1997).

In the following subsections, the development of slug flow is investigated; the effects of superficial gas velocity and axial flow position are examined. The experimental results were compared to the available correlations, which are originally proposed for fully developed flow.

4.5.1 Slug length

The length of liquid slugs was estimated using the averaged transitional velocity of slugs and the resident time of slugs at the measurement plane as explained in (Chapter3). Figure 4-10 shows the axial development of the averaged slug length at three different locations in the riser. It can be clearly seen that the averaged slug length increases along the pipe. The rate of increase in slug length is smaller near the pipe exit and at high gas superficial velocity. This increase of the slug length in the axial direction is due to the coalescence of Taylor bubbles. At the first location (15D) the slugs are not fully developed, and the distance between consecutive Taylor bubbles is small. The trailing bubble is influenced by the flow within the preceding liquid slug. As a result, the trailing bubble travels faster than the leading bubble and as a consequence, the rate of slug growth is higher around this location. As the liquid slugs move further upward, the merging process decreases due to the increase in the length of liquid slugs. At 45D, the length of liquid slugs is almost double the size of the slugs at 15D downstream of the mixing section. This indicates clearly the coalescence of two slug units. It can be said that near 45D, the slugs are almost developed, regardless the infrequent

observation of short slugs. However, it could be argued that the merging process may continue in extremely long pipes, due to the energy dissipation and pressure difference.

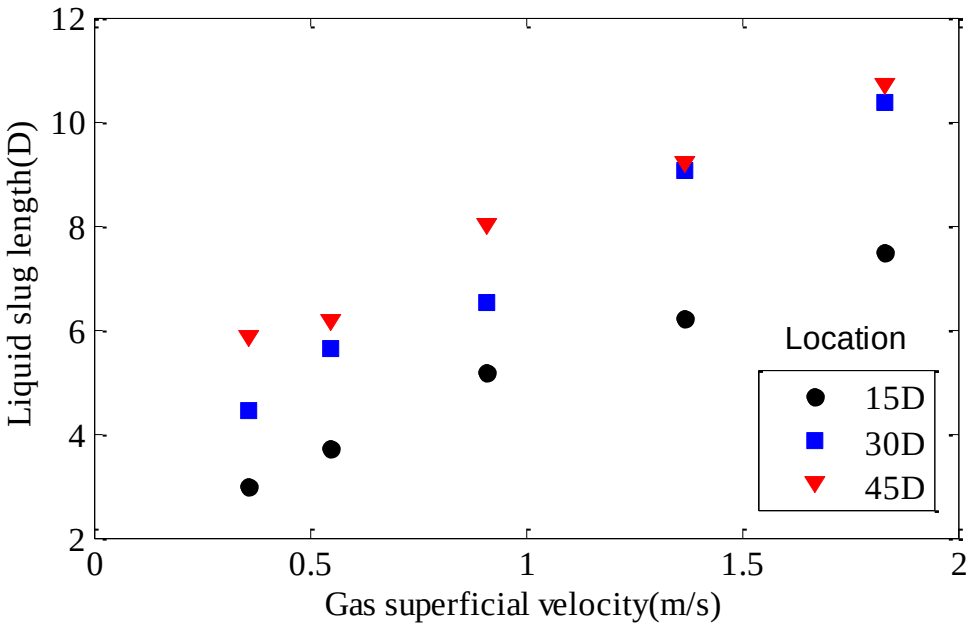


Figure 4-10: The axial development of the mean liquid slug length in the riser, at liquid superficial velocity=0.3ms^{-1}.

It was observed that the length of slugs and Taylor bubbles increase with the increase of superficial gas velocity as shown in Figure 4-11. The slug length, at 45D downstream of the mixing section, was found to vary between 6D and 12D. This is still within the range of the reported minimum stable slug length, about 8 to 16 D (Moissis and Griffith, 1962; Taitel et al., 1980).

Slug length correlation developed by Khatib and Richardson (1984) was used to estimate the experimental results of slug lengths as given in Equation (4.4). The predicted slug length was in an acceptable agreement with experimental data as shown in Figure 4-12. The mean length of the slug body is slightly underestimated, especially at low gas superficial velocities. The whole data was

predicted with an average absolute error of 20.70% and standard deviation of 1.92.

$$L_S = \frac{C_0 U_m + U_0}{f_S}\left[\frac{\varepsilon - \varepsilon_{gTB}}{\varepsilon_{gsl} - \varepsilon_{gTB}}\right] \tag{4.4}$$

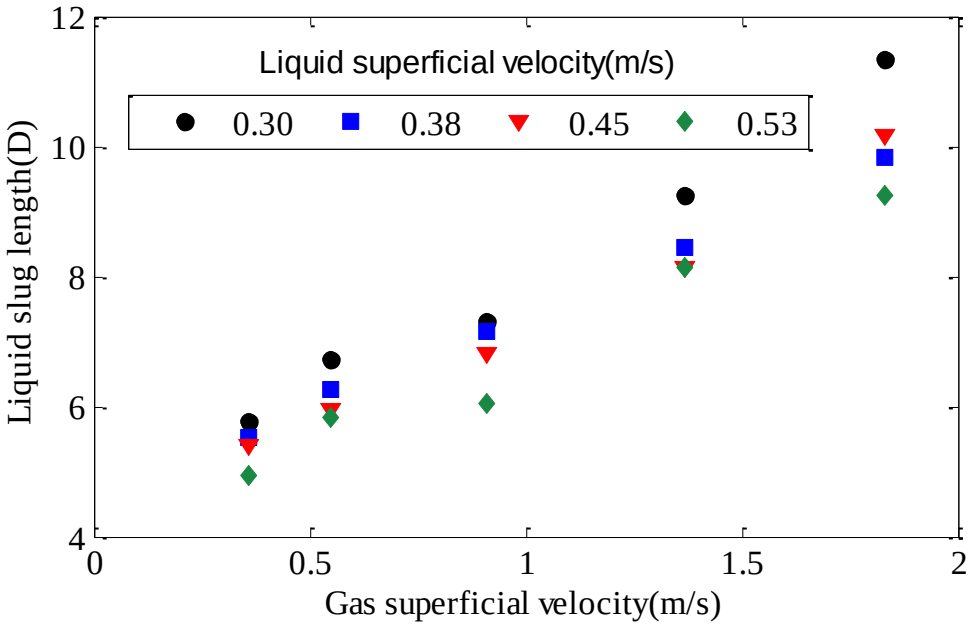


Figure 4-11: Liquid slug variation at different flow conditions.

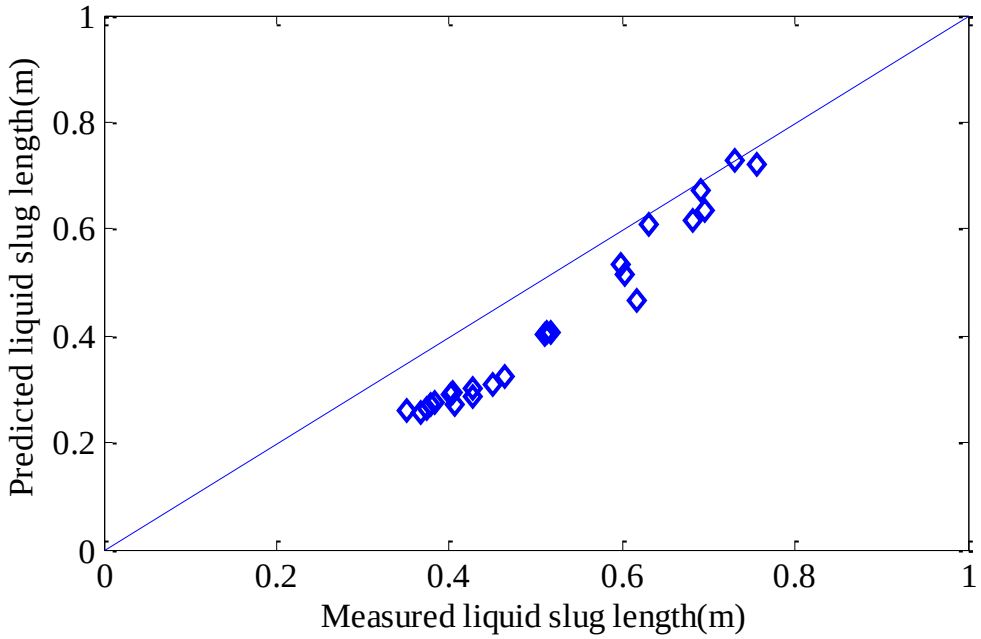


Figure 4-12: Comparison of experimentally measured slug length and predicted slug length using (Khatib and Richardson, 1984) correlation.

The discrepancy between the experimental and predicted values could be attributed to the assumptions made by (Khatib and Richardson, 1984). The correlation was proposed through a simple mass balance around a slug unit, in which the slug unit was assumed to travel at a constant velocity. The effect of physical properties was not included.

It was noticed that the error in estimating slug length can be higher at a high gas flow rate; where Taylor bubbles are distorted and it becomes difficult to distinguish between the Taylor bubble and the wake zone within the liquid slug due to the increase in dispersed gas concentration within the liquid slug.

4.5.2 Slug Frequency

The frequency of liquid slugs was estimated using the modified method of Hazuku et al. (2008) for large structures, as detailed in Chapter 3. The results were compared with the PSD method and a good agreement was obtained. The frequency of liquid slugs was estimated at three different locations in the riser for all the liquid velocities considered. Figure 4-13 illustrates how the frequency of slugs varies along the riser. It is clear that the slug frequency decreases along the pipe and also with the increase of superficial gas velocity. It is generally agreed that bubbles behind short liquid slugs moves faster than the leading one and hence emerging process occurs. In the riser, the slug and Taylor bubble length increase along the pipe due to the merge of two consecutive slug units. Therefore the frequency decreases in the axial direction. It is evident that change in frequency and slug length do not follow a smooth trend, this is directly related to the intermittent nature of slug flow. The uncertainty in distinguishing Taylor bubble from liquid slugs in some cases can contribute to the deviation from the general

trend. It is evident that as the growth rate of slugs increases the frequency decreases.

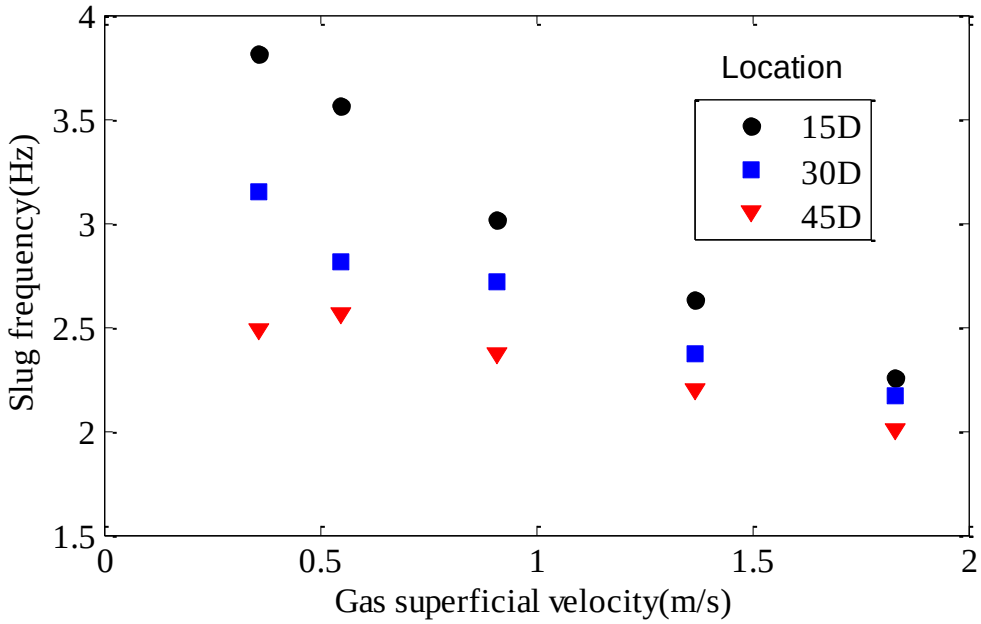


Figure 4-13: Frequency variation as a function of the axial distance in the riser at U_{ls}=0.3ms^{-1}.

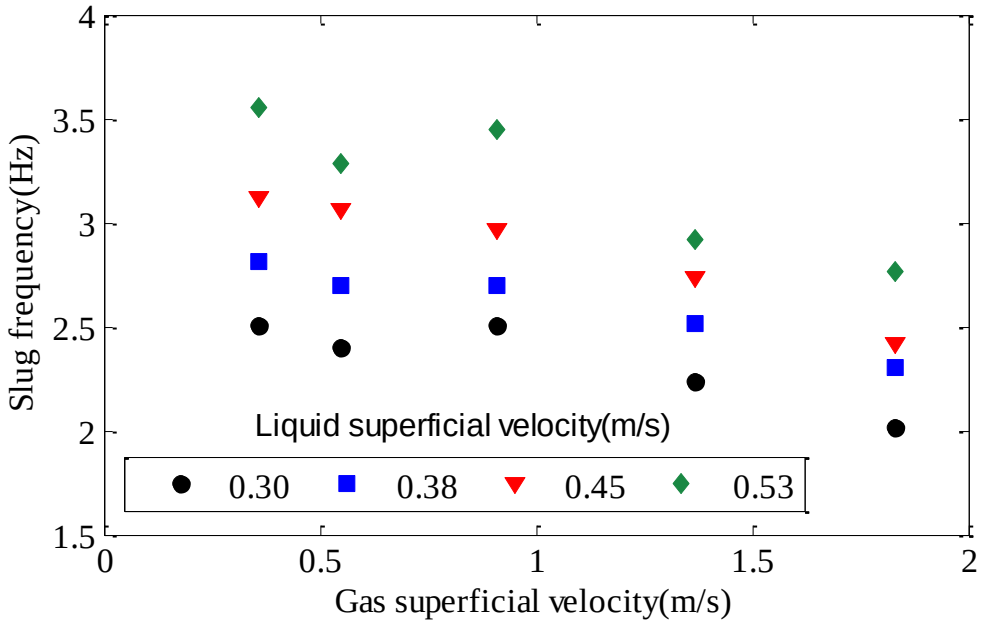


Figure 4-14: Slug frequency variation with air and oil superficial velocity in the riser.

Figure 4-14 shows the effect of the superficial liquid velocity on the frequency of the periodic structure of slugs. It can be clearly seen that the slug frequency

increases with the increase of the superficial liquid velocity while continue to decrease with the increasing superficial gas velocity.

Several empirical correlations have been proposed to estimate the frequency of slugs, most of which are for horizontal or near horizontal flows. Some of the reported correlations in Chapter 2, namely Sylvester (1987), Legius et al. (1997) and Zabaras (2000), were used to predict the frequency obtained experimentally as illustrated in Figure 4-15.

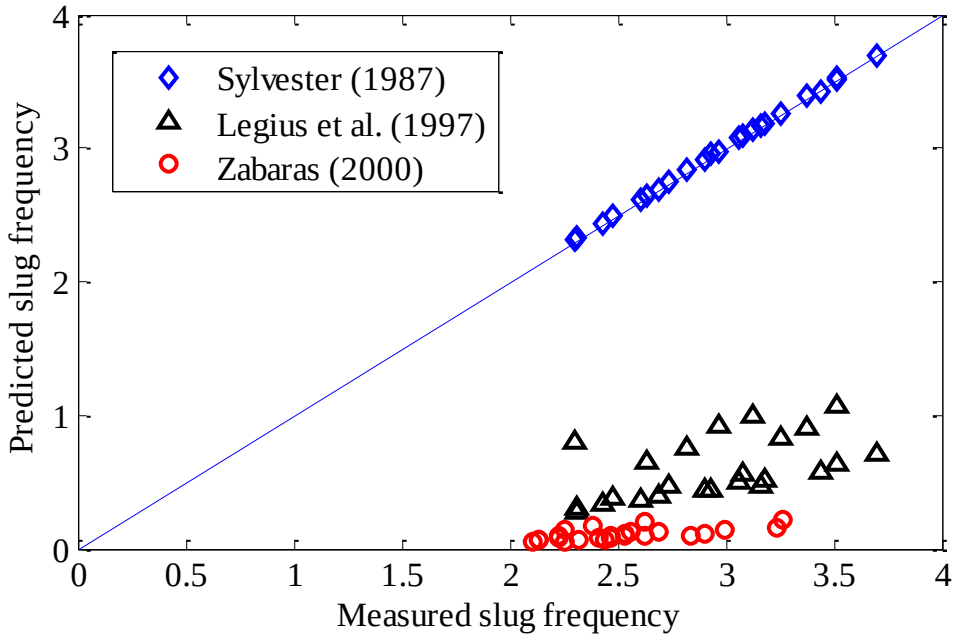


Figure 4-15: Comparison of the experimental slug frequency with the available correlation.

It is remarkable that Sylvester (1987) correlation showed a strong agreement with the experimental results. It is, however, impractical to identify more than one variable in one equation. In fact, it is a simple mathematical correlation that requires the knowledge of slug unit velocity and length as following:

$$f_s = \frac{U_{tb}(1-\beta)}{L_{ls}} \tag{4.5}$$

Where β is the ratio between length of Taylor bubble and length of slug unit. Zabaras (2000) correlation has underestimated the experimental frequency. This is not surprising since, it is a modified version of Gregory and Scott (1969) correlation for horizontal flow, except that the effect of a small inclination up to 9 degrees was included. Legius et al. (1997) correlation has also dramatically underpredicted the experimental data. This clear discrepancy is due to the inherent limitation of this correlation. It is absolutely a replica of Heywood and Richardson (1979) correlation, for horizontal flow with a slightly modified constant.

It seems that most of the available correlations for predicting slug frequency in vertical flow are either mathematical models that include several unknown variables or simple empirical correlations that originally proposed for horizontal flow for a limited range of flow conditions. In order to develop a more general correlation, several parameters should be considered such as the physical properties of the phases and pipe geometry in addition to the variables that are already considered.

4.5.3 Void fraction in liquid slug

Void fraction in liquid slug (ε_{gSL}) is a crucial parameter in characterising slug flow which has a direct influence on the average void fraction. The knowledge of gas hold up within the body of the liquid slug has been considered as an input parameter for the several physical models developed to study slug flow, such as the model of Fernandes et al. (1983). It also can be used to determine the transition from slug to churn flow. In this work, the evolution of void fraction within the body of slugs was studied.

It is acknowledged that the gas phase is dynamically exchanged between the Taylor bubble and liquid slug. Gas bubbles at the rear of liquid slug coalesce with Taylor bubble while small bubbles are entrained into the liquid slug behind it due to the jet effect of the falling liquid film (Fernandes et al., 1983).

The liquid slug can be divided into three main regions based on the voidage profiles. The wake region which is a region of high turbulence and high local gas fraction, it extends to few pipe diameters downstream of the Taylor bubble. The translational region is an intermediate region that separates the wake and the developed region. The developed region starts at around 10D behind the Taylor bubble, It has a void fraction profile similar to that of dispersed bubbly flow (Van Hout et al., 1992).

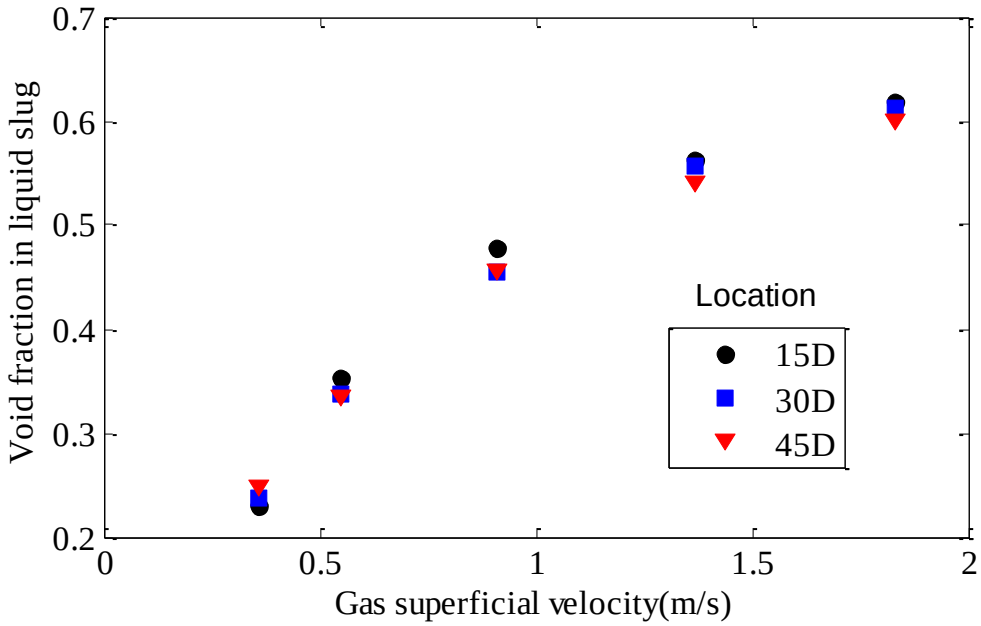


Figure 4-16: Void fraction in the liquid slug along the axial direction.

Figure 4-16 illustrates the change in void faction in liquid slug at three axial positions 15D, 30D and 45D downstream of the mixing section. The figure shows no significant change along the axial direction, particularly between 30D and

45D, however, it is clear that the averaged gas holdup in liquid slug decreased slightly from the 15D to the following axial locations. This is more likely due to the nature of the flow near the entrance being more chaotic where slugs are still developing. At this location, the wake region within liquid slug is expected to be longer and hence the overall gas holdup is higher.

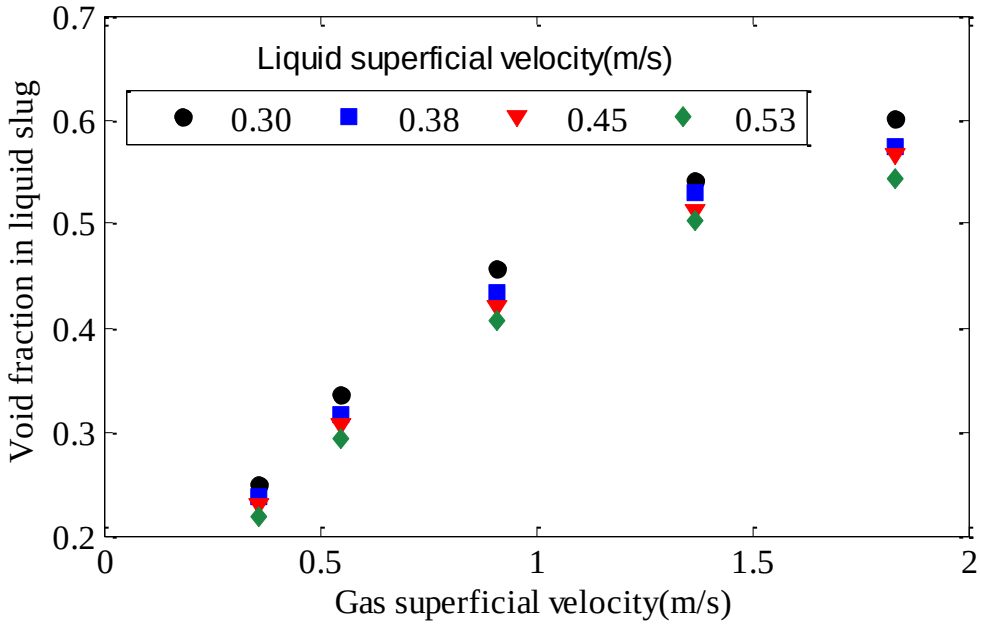


Figure 4-17: The effect of superficial gas velocity on the void fraction within the body of slugs.

The effect of superficial liquid velocity on the void fraction in liquid slugs is shown in Figure 4-17. Void fraction in the liquid slug follow the same trend discussed under Figure 4-16. However it should be noted that with the increase of the superficial liquid velocity, the void fraction within the liquid slug decreases as shown in Figure 4-17. Similar observation is reported by (Akagawa and Sakaguchi, 1966; Barnea and Shemer, 1989; and Mori et al., 1999). It expected that at high gas flow rate, the turbulence force becomes dominant and hence more air is entrained into liquid slugs as a fine dispersion of bubbles. The averaged void fraction within the body of the slug varied from 0.23 to 0.63 over the range of

experimental matrix. This corresponds to the transition border of bubbly and churn flow respectively. Similar observation reported by (Barnea and Shemer, 1989). The lower value of 0.23 is almost equal to the suggested value of bubbly to slug transition (0.25) by (Taitel et al., 1980). The upper value of 0.63 represents the maximum packing of bubbles in the liquid slug, hence the transition from slug to churn flow as suggested by (Brauner and Barnea, 1986).

It is suggested that the liquid slugs can be treated as fully developed bubbly flow. Therefore liquid slugs can only accommodate maximum gas fraction equal to that of fully developed bubbly flow (Barnea and Brauner, 1985). Barnea and Shemer (1989) for air-water flow in 50mm ID pipe, reported that the void fraction in the liquid slug was 0.25 for U_{gs} below 1 $m.s^{-1}$. Beyond U_{gs}=1 $m.s^{-1}$ the void fraction increased up to 0.6 which was considered the upper limit before the onset of the churn flow. Schmidt (1977) indicated that the void fraction in liquid slug varies from 0.2 to 0.8 for a wide range of gas and liquid superficial velocities for air and kerosene mixture in 50 mm ID pipe.

In this work, the voidage in liquid slug continuously increases for the whole range of gas superficial velocity in slug flow region, and hence it eventually exceeds the value suggested for fully developed bubbly flow by (Barnea and Brauner, 1985). This behaviour is similar to Schmidt (1977) observation for the air-kerosene system. It can be said that void fraction in liquid slug is constant, i.e. can be equal to the value of dispersed bubbly flow, only for a limited range of superficial gas velocities. Beyond a critical value of $U_{gs,}$ the air entrainment in the body of the slug constantly increases until slug/churn transition occurs. This value of U_{gs} might vary for different pipe configuration and flow conditions. Silicone oil

has the ability to entrain more bubbles in comparison to water. This can be confirmed by the observation of Schmidt (1977) for air-kerosene system which showed a continuous increase in the void fraction of liquid slugs. Pipe diameter may also have an effect on slug characteristics since slugs appear more aerated in large pipes.

Figure 4-18 illustrates the predicted value of void fraction of liquid slugs as predicted by the available models reported in the literature, namely; Akagawa and Sakaguchi (1966), Sylvester (1987) and Mori et al. (1999) as shown respectively in the following equations:

$$\varepsilon_{gsl} = \varepsilon_g^{1.8} \tag{4.6}$$

$$\varepsilon_{gSL} = \frac{u_{gs}}{0.425 + 2.65\left(u_{gs} + u_{ls}\right)} \tag{4.7}$$

$$\varepsilon_{gsl} = 0.523\varepsilon_g \tag{4.8}$$

It is clear that Akagawa and Sakaguchi (1966) correlation gives the best estimation of void fraction in the body of the slugs, however, it underpredicts the experimental results with an average absolute error of 26.05% and standard deviation of 1.38. Correlations of Sylvester and Mori et al. showed larger drift from the experimental results with an average absolute error of 35.50% and 6.59% respectively. In fact, this was not surprising since correlations (4.6) and (4.8) were pure empirical fits for experimental results that were obtained for air-water system of pipes with smaller diameters (27.6mm ID and 25.8mmID). The equation (4.7)

was theoretically derived while the constants of the equation are based on the experimental work of Fernandes (1981).

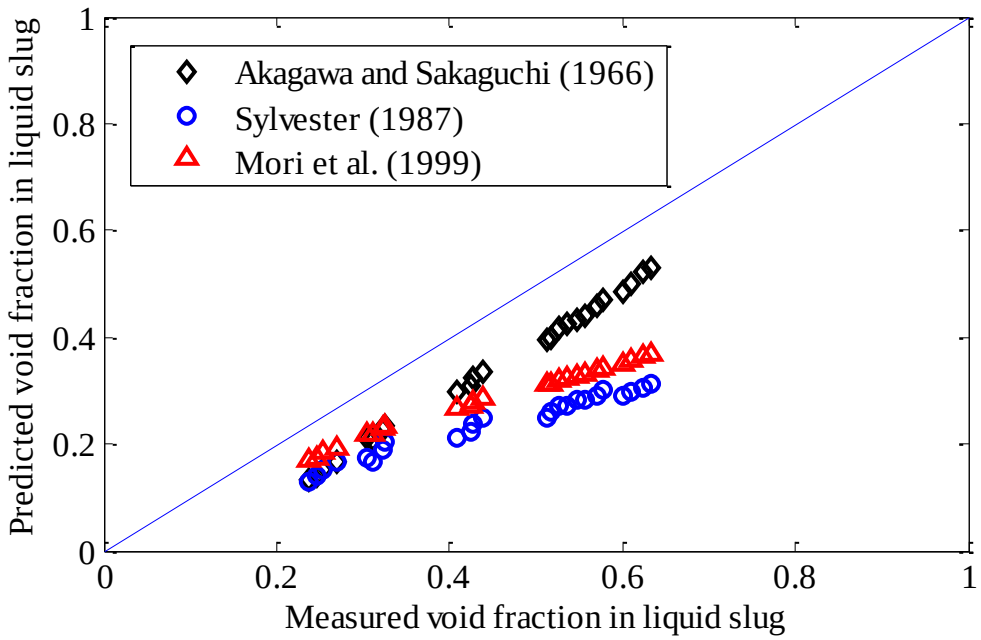


Figure 4-18: Comparison of void fraction in liquid slugs with empirical correlations.

It is obvious that the silicone oil has a higher tendency to entrain more gas bubbles than water, especially at the high gas superficial velocity. The prediction of void fraction in liquid slugs seems better at low superficial gas velocity and continuously deviates as U_{gs} increases, except for equation (4.6) that showed a consistent prediction for the whole range of experiments. The performance of Akagawa and Sakaguchi correlation can be significantly improved if the constant of 1.3 is used instead of 1.8**.** The prediction of the improved constant was in perfect agreement with the current experimental results with averaged absolute error of 2.02% and averaged standard deviation of 0.43.

It can be said that there is no general correlation that predicts the void fraction within the liquid slugs for a wide range of operating conditions. Most of the available correlations were simple fits of experimental data for a limited range of

operating conditions. Therefore, the collective effect of different flow parameters such as pipe diameter and fluid properties should be considered in order to develop more robust correlation.

4.5.4 Taylor bubble velocity

The Signals from the dual plane ECT sensor were cross-correlated to estimate the time delay of slugs at the sensor. The velocity is simply equal to the distance between the two planes divided by the time delay. The slug velocity was measured at three axial locations along the riser, in order to see how the axial velocity influences the evolution of slugs.

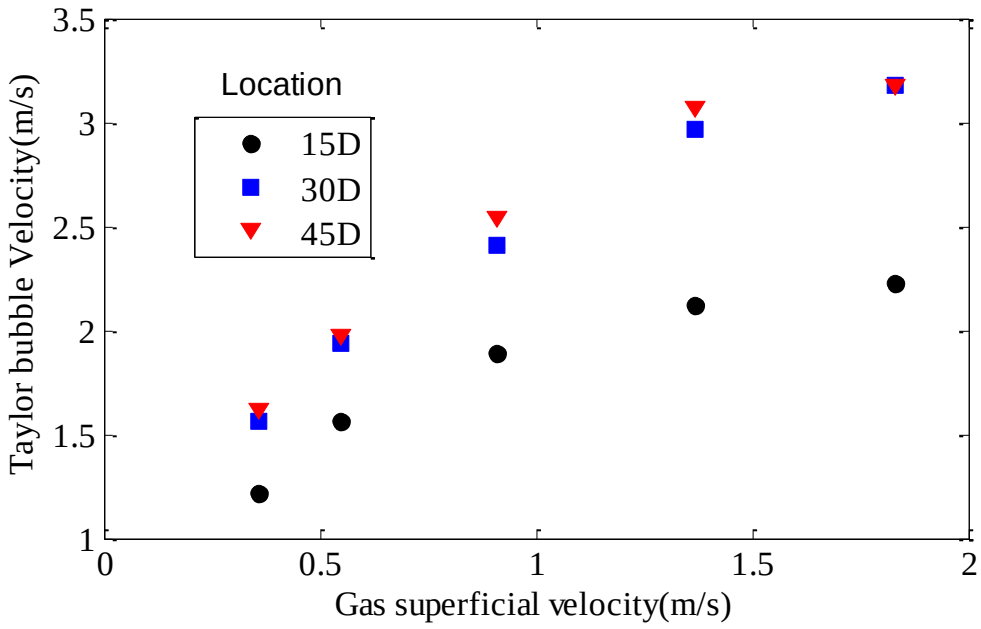


Figure 4-19: Taylor bubble velocity variation as a function of the axial distance in the riser at liquid superficial velocity = 0.3ms^{-1}.

Figure 4-19 demonstrate the difference in the slug velocity in the axial direction. It can clearly be seen that the velocity increases with the increase of superficial gas velocity. It also increases in the axial direction under constant superficial gas velocities. This increase is significant from the first (15D) to the second location (30D), whereas at the third location (45D) the slug velocity showed only a small

increase over that of 30D. This is due to the increase of bubble size as a subsequent merging process between two slug units since larger bubbles travel faster. Based on Bernoulli's principle, the increase of slug velocity along the pipe could be boosted by the decrease in pressure with altitude. In addition, the change in gravitational effect with altitude can also enhance the velocity of Taylor bubbles. The slugs are more stabilised at 45D location, where velocity profile within the slug unit is expected to be fully developed.

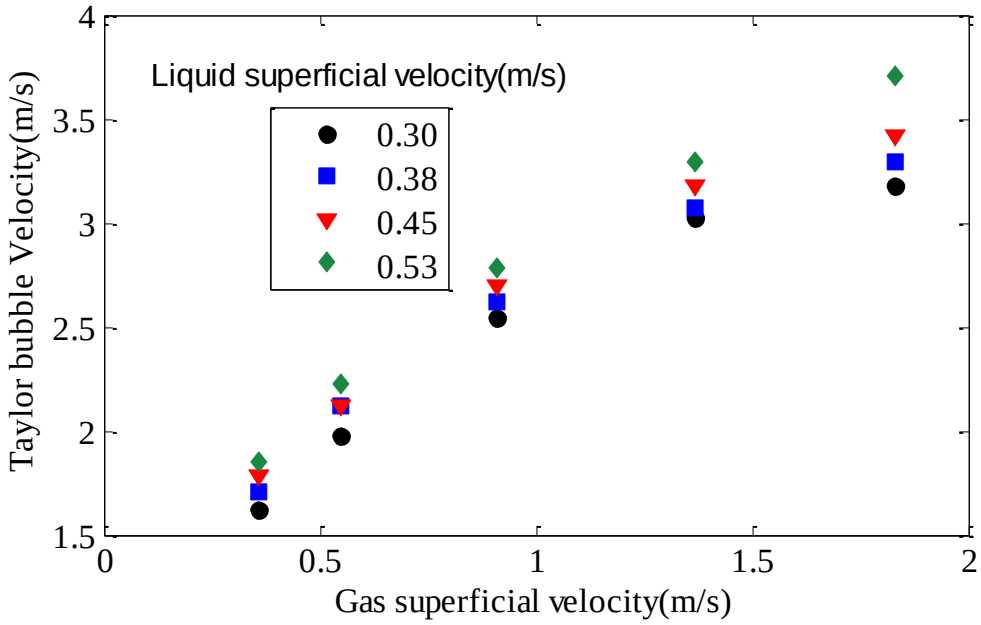


Figure 4-20: Taylor bubble velocity variation at 45D downstream of the mixer.

The effect of the superficial gas velocity on the slug unit at 45D downstream of the mixing section is presented in Figure 4-20. It shows, as expected, an increase in structure velocity of the slugs with the increase in both, the gas and the liquid superficial velocities. In these experiments, it was assumed that the slug unit is traveling at the same velocity. However, in reality, the Taylor bubble and liquid slug may travel at different velocities, which is usually considered to be small and has a negligible effect, since the gas entrainment into and out of the Taylor bubble

should be equal (Fernandes et al., 1983). It is noticeable that the superficial liquid velocity has a weaker effect on the slug velocity in comparison to that of the superficial gas velocity.

Taylor bubble velocity has been investigated extensively over years. The transitional velocity is considered to be a combination of the slug mixture velocity and the velocity of a bubble in a stagnant liquid, namely drift velocity. Nicklin et al. (1962) has suggested the following expression for the velocity of the Taylor bubble:

$$u_{gTB} = C_0\left(u_{gs} + u_{ls}\right) + U_d \tag{4.9}$$

Where; U_d is the drift velocity given by equation (4.2) and C_0 is the distribution parameter. C_0 is the ratio of centreline velocity to the mixture velocity within the liquid slug. It has been found to vary from 1.2 (Nicklin et al., 1962) to 1.29 (Fernandes et al., 1983) for developed slug flow. In this work, the value of 1.29 showed better results.

Figure 4-21 illustrates the comparison between the experimental and the estimated values of Taylor bubble velocity. The results are within an acceptable agreement. Taylor bubble velocity is underestimated by Nicklin et al. (1962) correlation with an average absolute error of 17.12% and standard deviation of 2.07. The discrepancy is more likely to be attributed to the effect of entrained bubbles within the liquid slug.

The rise velocity of Taylor bubble increases in the presence of bubbles in liquid slug (Mao and Dukler, 1985). It is evident that at the high superficial gas

velocity, the Taylor bubble velocity is closely predicted. This could be a result of high gas entrainment in liquid slugs at these conditions. Mao and Dukler (1985) correlation has slightly improved the velocity prediction at low gas superficial velocity since it takes into consideration the effect of entrained bubbles on the transitional velocity of Taylor bubble. However, it visibly overestimated the rise velocity at high gas flow. This is possibly due to the overcompensation of dispersed bubbles effect at high gas superficial velocity.

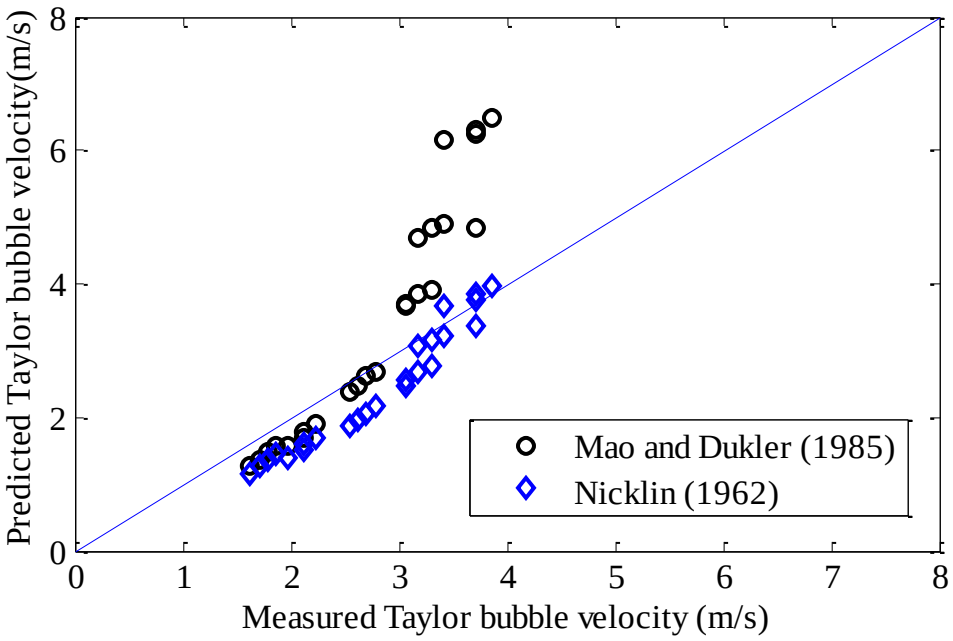


Figure 4-21: Experimental Taylor bubble velocity against the predicted values.

It could be said that at the low superficial gas velocity the entrained bubbles in liquid slugs are relatively large to flow down in the liquid film. Thus these bubbles will merge with the front of Taylor bubble causing an increase in the rise velocity of Taylor bubble. As the gas superficial velocity increases, the gas entrainment within the slug body increases. In this case, a swarm of tiny bubbles is entrained, and the liquid slug can be treated as a turbulent bubbly flow in which, buoyancy decreases with the increase of void fraction as reported by

(Zuber and Hench, 1962). The relative velocity of the entrained bubbles to the liquid is negligible; therefore the effect of entrained bubbles on the Taylor bubble velocity is expected to be negligible.

It must be mentioned that the distribution parameter (C_0) is highly dependent on the flow patterns and it is a function of the inclination angle as well as other parameters, such as pipe diameter and mixture velocity. It is expected to increase due to the increase in pipe diameter due to the effect of gas expansion as reported by (Fernandes et al., 1983). Therefore in this work the value 1.3 showed better prediction than the common value of 1.2.

4.6 Summary

In this chapter, experimental data from a 68mm ID vertical riser section, in which an air-silicone oil mixture flow upward is presented. Wire Mesh Sensor (WMS) and Electrical Capacitance Tomography (ECT) were used to provide cross-sectional averaged void fraction at three locations downstream of the mixing section. The corresponding flow patterns were visually identified, as well as, using the probability density function (PDF) of the averaged void fraction time series. Several flow parameters were estimated from the void fraction data of the WMS and the ECT, including cross-sectional averaged void fraction, slug length, slug frequency, void fraction in liquid slugs and Taylor bubble velocity. The experimental results were then compared to the predicted values of the available correlations. The key findings were summarised below:

- The ECT system and WMS tomography provide similar mean void fraction data. This is in agreement with previous studies is this field. It is

not simple to favour one technique over the other. The combination of both sensors can generate useful information about the flow structure. Since the WMS gives more detailed information on the flow structure, the ECT system can obtain the structure velocity.

- The flow development can be achieved in a vertical riser of 68mm ID within 65 pipe diameter lengths. This is in agreement with several previous studies.
- The cross-sectional averaged void fraction increases with the increase in gas superficial velocity for constant liquid flow rate. This increase in the void fraction is associated with flow transition.
- Developed slug flow occurs in a vertical 68 mm ID pipes for gas superficial velocity between 0.36 $m.s^{-1}$ and 1.83 $m.s^{-1}$ and liquid superficial velocity up to 0.53 $m.s^{-1}$. Undeveloped slug flow is also observed at the pipe exit. These slugs occur near the transition to churn flow at high gas superficial velocity.
- Slug length increases in the axial direction and with the rise of gas superficial velocity. This increase is due to the emerging process between two consecutive slug units.
- The frequency of liquid slugs decreases along the axial direction and with the increase in gas superficial velocity. Slug length and frequency are interchangeable parameter, if one increases the other should decline. Therefore, the reduction of slug frequency is also due to slug coalescence.
- Void fraction within the liquid slug continuously increases with the increase of gas superficial velocity. The lowest and highest value within

slug flow range corresponds to the transition from bubble to slug and from slug to churn respectively. Silicone oil seems to have higher void fraction than water, due to the higher viscosity.

- Taylor bubble tends to accelerate with the increase in superficial gas velocity and rise in the height of the vertical pipe. This is mainly due to the emerging process of two slug units, in addition to gas expansion and decrease in pressure with altitude.
- The available correlations for gas-liquid flow in vertical pipes are essentially based on air-water experiments. Most of them are empirical correlations that were developed by simply data fitting for a limited range of flow rates. Some have been derived from correlations originally developed for horizontal flows. Therefore the accuracy of these available models was diverse. Some models showed good agreement with the experimental results such as; drift-flux model and Nicklin et al. (1962) correlation for Taylor bubble velocity. Whereas some correlations have poorly predicted the experimental flow parameters including; Legius et al. (1997) and Zabaras (2000), for slug frequency. Table 4-1 summarise the statistical performance comparison of the two-phase flow correlations used in this chapter.
- In order to develop more robust correlations, several flow parameters, i.e. inclination angle, physical properties and pipe geometry, should be considered for a wide range of flow conditions.

Table 4-1: The statistical results for the applied two-phase flow correlations.

Source; Correlation	Pipe (ID); Fluids	Statistical measures		
		APE	AAPE	SD
(Nicklin et al., 1962) $\varepsilon_d = \frac{U_{gs}}{C_0 U_m + U_d}$	26mm air/water	-2.37	2.88	0.58
(Khatib and Richardson, 1984) $L_S = \frac{C_0 U_m + U_0}{f_S}\left[\frac{\varepsilon - \varepsilon_{gTB}}{\varepsilon_{gsl} - \varepsilon_{gTB}}\right]$	38.8mm air/water air/slurry	-15.58	16.85	2.09
Sylvester (1987) $f_s = \frac{U_{tb}(1-\beta)}{L_{ls}}$	25mm to 75mm gas/water gas/oil	0.34	0.37	0.05
Zabaras (2000) $f_s = 0.0226\left[\frac{u_{sl}}{gd}\left(\frac{212.6}{u_m} + u_m\right)\right]^{1.2}[0.836 + 2.75\sin(\Theta)]$	25mm, 100mm air/water	-95.82	95.82	0.24
(Legius et al., 1997) $f_s = 0.0543\frac{u_{ls}}{u_m}\left(\frac{2.02}{D} + \frac{u_m^2}{gD}\right)^{1.02}$	50mm air/water	-79.84	79.84	1.23
(Akagawa and Sakaguchi, 1966), $\varepsilon_{gsl} = \varepsilon_g^{1.8}$	27.6 mm air/water	-47.65	47.65	2.34
(Sylvester, 1987) $\varepsilon_{gSL} = \frac{u_{gs}}{C_2 + C_3(u_{gs} + u_{ls})}$	25mm to 75mm gas/water gas/oil	-46.59	46.60	0.72
Mori et al. (1999) $\varepsilon_{gsl} = 0.523\varepsilon_g$	25.8mm air/water	-47.70	47.70	0
Nicklin (1962) $u_{gTB} = C_0(u_{gs} + u_{ls}) + U_d$	26mm air/water	-15.86	17.11	2.07
Mao and Dukler (1985) $u_{gTB} = [(C_0 - \Phi)(u_m - U_o\varepsilon_{gSL} + U_d - U_o\Phi)](1-\Phi)^{-1}$	50mm air/water	15.46	28.99	6.04

Chapter 5

Influence of vertical to horizontal 90◦ bend on gas-liquid flows development

Most of the process industries have long pipe lines to transport the process fluids from one place to another. These pipelines have bends to change the orientation of the pipes as warranted by the layout of the process equipment and vessels. Single phase flows in such pipelines have been studied and a good understanding of the flow behaviour has been established making hydraulic designs robust and trustworthy. However, two-phase flows that occur in transportation of oil and gas from wells to the production platforms or boiler tubes in power generation are complex and the development of such flows around bends were not well understood. The complexity of the flow behaviour is increased due to the effects of centrifugal force induced by the curvature of the bend and the existence of the two phases with significantly different densities. As the fluid passes through curved pipes or bends, a considerable centrifugal force is applied to the mixture forcing it to separate. Separation is affected by the orientation of the bend giving rise to complications such as void fraction fluctuation and formation of dryout zones.

The effects of the bends on the two-phase flow is a common issue in a wide range of industrial applications, nevertheless, a low number of studies is available on this subject compared to single phase flow around bends.

Even though some literature is available on phase distribution at bends they are mainly restricted to small diameter pipes and fluids with physical properties significantly different from these of industrial fluids. In contrast, this work considers the air-silicone oil two-phase flows in relatively large pipes (68mm I D) in order to overcome the limitations of the previous studies and provide a reliable database by employing advanced instrumentations.

In this chapter, results of air-silicone oil experiments around a vertical to horizontal 90° bend are presented. In these experiments, the ECT was located at 5D upstream of the bend and the WMS was moved at different locations downstream of the bend (5D, 10D, 40D, 69D, 98D, and 128D). The time series of the local void fraction data from both devices were used to obtain several flow characteristics including; flow patterns, cross-sectional averaged void fraction, structure velocity and structure frequency. Slug flow was studied in more details and the common slug features were identified. The reported results were used to validate the available slug flow correlations. A comparison between the results at upstream and downstream of the bend is conducted, in order to quantify the influence of the bend on flow development.

It should be noted that the measurements were not made simultaneously but at same inlet conditions. This approach is necessary due to the fact that the WMS downstream of the bend has been moved to various locations as mentioned above. The ECT was placed 5D before the bend for all cases and the measurements were used to check the flow conditions for the different experiments in order to make sure the data at different locations downstream of the bend are comparable. The

PDFs for the inlet conditions at 5D upstream of the bend shows very little variation and separate measurements can be justified on that basis.

5.1 Flow patterns

The PDFs plots of the cross-sectional averaged void fraction are used to identify the flow patterns in the vertical riser prior to the bend and the horizontal section downstream of the bend. Based on the work of Jones and Zuber (1975) and Costigan and Whalley (1997), it is widely known that each flow regime has a unique PDF signature. The PDFs were compared with a series of visual observations through the transparent test section. Flow patterns observed, in the riser, during this study are mainly bubbly, cap bubble, slug and churn flow (Figure 5-1) for gas superficial velocity (U_{gs}) ranges from 0.045 to 3.2 m s^{-1} and liquid superficial velocity (U_{ls}) varying between 0.15 and 0.53 m s^{-1}.

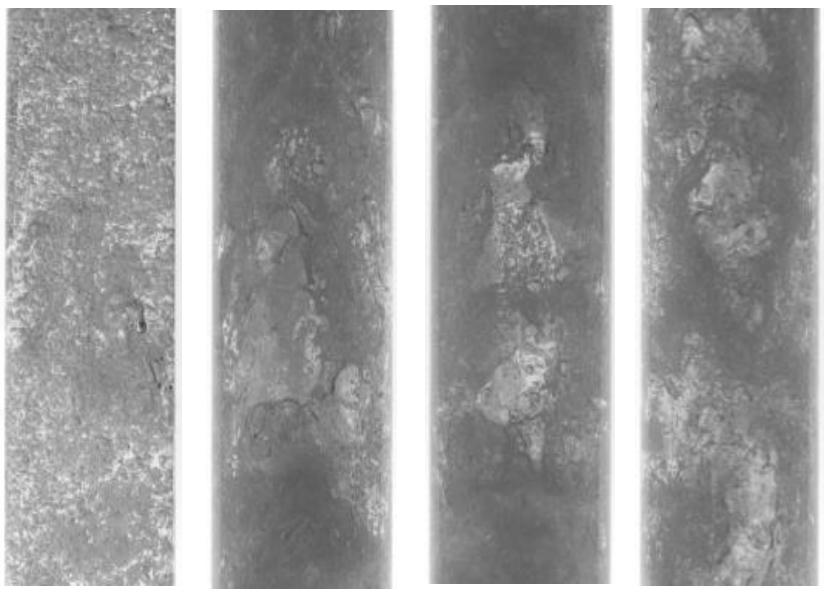


Figure 5-1: Flow patterns observed in the riser.

The flow patterns in the horizontal section at same flow conditions are stratified, wavy stratified, (disturbance waves) and slug flow as shown in Figure 5-2.

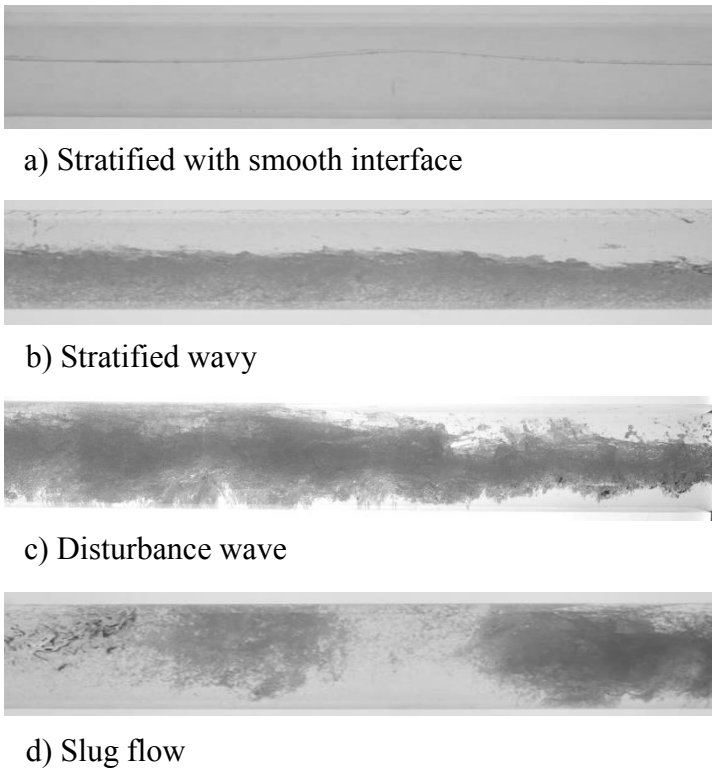


Figure 5-2: Flow patterns observed in the horizontal section.

The combinations of the tested flow conditions are superimposed over Taitel et al. (1980) flow pattern map as shown in Figure 5-3. The transitional borders of the map were corrected to the current experimental parameters. Although this flow pattern map was developed for air-water flow in vertical 50 mm pipe, the PDFs, as well as the visual observation in the riser, showed a good agreement with this flow map, except at the transitional boundaries where the decision is subject to personal judgment.

It can be seen that the transition between bubbly flow, including cap bubbles, and slug flow is in disagreement with the visual observations. The cap bubble flow conditions are mostly shown in the slug flow region. The discrepancy at the

transition line could be due to the assumption that was adopted for the flow transition boundary. Taitel et al. (1980) have considered the transition from bubbly to slug flow to occur when the void fraction reaches 0.25 and the equation (5.1) is used to plot the transition border.

$$U_{LS} = 3U_{GS} - 1.15\left[\frac{g(\rho_l - \rho_g)\sigma}{\rho_l^2}\right]^{0.25} \tag{5.1}$$

However, in these experiments, the void fraction in bubbly flow region can reach up to 0.35, before the transition to slug flow can take effect. This is a direct consequence of the viscosity and low surface tension of the silicone oil used in this work. Therefore equation (5.1) was modified, using a void fraction value equal to 0.35, as following:

$$U_{LS} = 1.86U_{GS} - \left[\frac{g(\rho_l - \rho_g)\sigma}{\rho_l^2}\right]^{0.25} \tag{5.2}$$

In Figure 5-3 the dashed line represents the new transitional border, using equation (5.2). It is clear that the new transition border has improved the prediction of the experimental results. Slug-churn transition has been a controversial subject. Taitel et al. (1980) considered churn flow as an entrance phenomenon, they claim that churn flow in vertical pipes will persist only to the point where stable slug can take place. The length of this entry effect region depends on mixture velocity and the pipe diameter. Therefore, there was no clear transition boundary between slug and churn. Brauner and Barnea (1986) suggested that slug-churn transition occurs when the void fraction in a liquid slug is 0.52 which is the maximum volumetric packing of bubbles within liquid slug. They considered churn flow as a developed flow pattern that can persist

throughout the whole length of the pipe. On the other hand, Mao and Dukler (1993) claimed that churn flow is a manifestation of slug flow and may not exist as independent flow pattern.

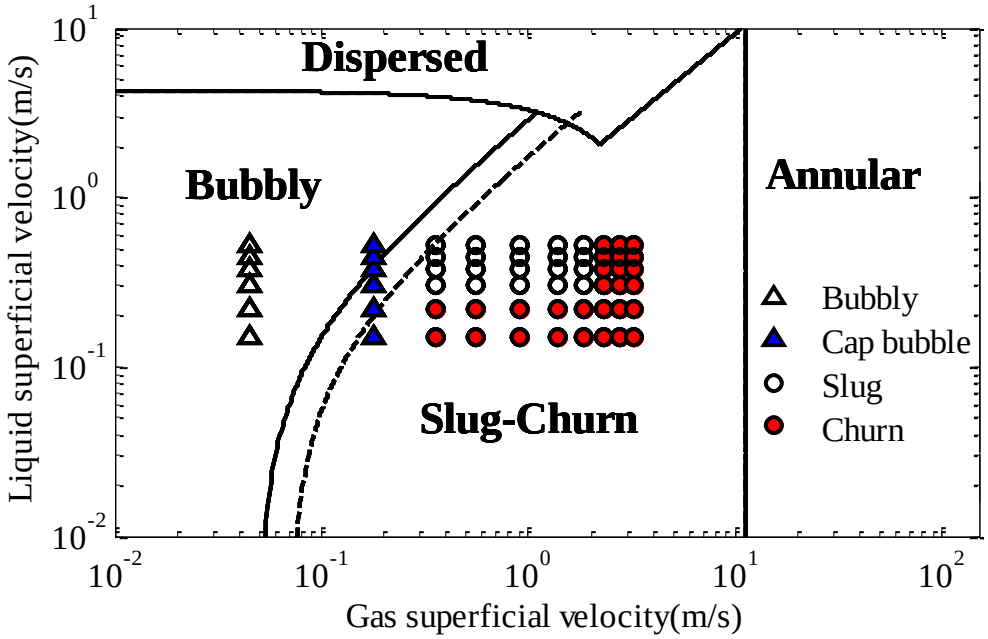


Figure 5-3:Flow condition in the riser superimposed on the flow patterns map of (Taitel et al., 1980).

It can be seen from Figure 5-3 churn flow conditions, in red colour, cannot be separated from slug flow using a continuous straight line or a smooth curve. Therefore it can be said that churn flow can be either an entry phenomenon or a separate and intermediate region between slug and annular flow as reported by (Hewitt and Jayanti, 1993).

For the horizontal section downstream of the bend, the flow pattern map suggested by Mandhane et al. (1974) was used to compare the experimental observations. This map is based on the largest amount of data and is the most widely used amongst the other available flow pattern maps. The map by Mandhane assumes that the changes in pipe diameter and in fluid properties have

no dramatic effects on the transition boundaries, if superficial gas velocity and superficial liquid velocity are used as axes. The flow patterns observed from the experiments with those predicted by Mandhane flow patterns map are compared as illustrated in Figure 5-4. The observed flow regimes are predicted well, except transition from smooth to wavy stratified which was poorly anticipated. This is due to the inherent discrepancy of the data originally used to generate the flow map. The data sets used by Mandhane showed inconsistency in predicting the wavy region (Mandhane et al., 1974).

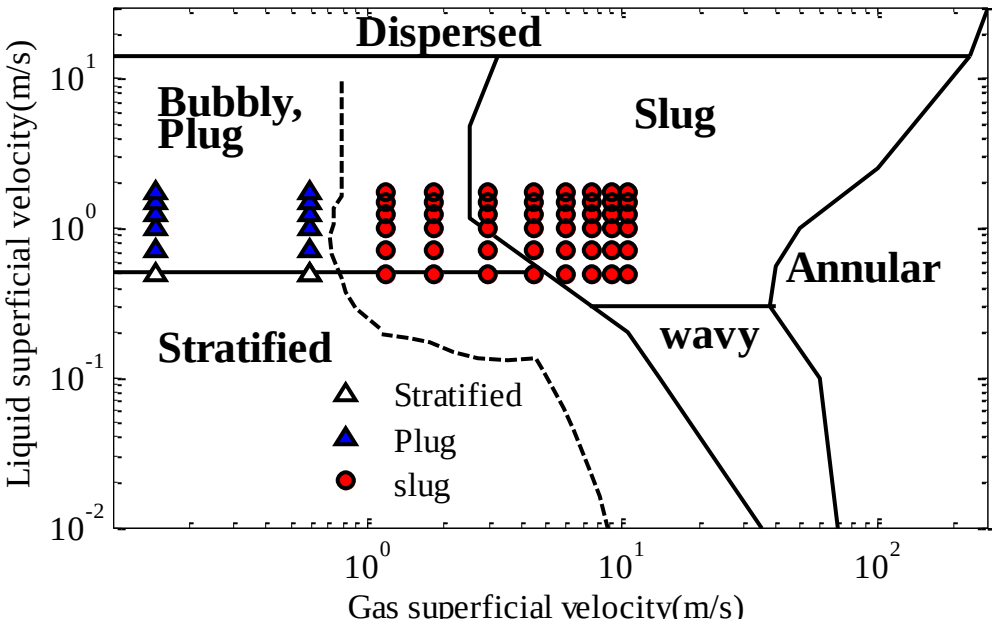


Figure 5-4: Flow condition in the riser superimposed on the flow patterns map of (Mandhane et al., 1974).

In slug flow region, 70% of the experimental conditions were accurately predicted, whereas in some cases slug conditions are predicted as plug flow. It was observed that transition from smooth stratified to either wavy stratified or slug at high gas superficial velocity occurs at lower liquid flow rate than in the Mandhane map. A new transition curve from smooth stratified to wavy stratified

and also from plug to slug flow was plotted as a dashed line in Figure 5-4. This transition curve is based on the current observations and the work of Lin and Hanratty (1986) for air water flow in horizontal pipe of 95.3 mm ID. Although, Mandhane map suggests that transition boundaries are least sensitive to the change in pipe size and physical properties of working fluids, it has been already reported that the pipe diameter and liquid viscosity can significantly alter the transition to slug flow, particularly at low gas superficial velocities (Taitel and Dukler, 1976; Lin and Hanratty, 1987b).

In the horizontal section, downstream of the bend large amplitude waves are observed. These waves have been identified by several researchers as slugs (Wallis and Dodson, 1973), roll wave (Lin, 1985), large disturbance waves (Andreussi and Persen, 1987) and Pseudo slugs as described by (Lin and Hanratty, 1987b). These are large disturbance waves which touch the top wall of the pipe. They differ from slugs in that they dissipate as they move downstream, they are not associated with high pressure pulsations and also do not travel at the gas velocity. Lin and Hanratty (1987b) has identified the so called pseudo slugs as independent flow pattern and the added the transition boundary of this region on the Mandhane flow pattern map. In this work the large disturbance waves (pseudo slugs) has been observed to occur within the slug region and more frequently at high gas superficial velocity and low liquid level. After the passage of liquid slug, the liquid level in the pipe decreases and hence several large disturbance waves can appear in between two consecutive liquid slugs. Therefore, in this work the disturbance waves that touch the upper wall of the pipe is not considered as independent flow pattern and its region is not marked on the flow map.

5.2 Axial flow development

To investigate the influence of the upstream conditions on determining the flow downstream of the bend, void fraction data has been obtained at different locations on the horizontal pipe section (5D, 10D, 40D, 69D, 98D and 128D) away from the bend using the WMS. It should be noted that the measurements were not made simultaneously but at same inlet conditions. The ECT was placed immediately (5D) before the bend in each experiments, due to its non-intrusiveness nature.

The flow patterns before and after the bend were compared using the PDFs plots of the cross sectional averaged void fraction. The PDFs of the averaged void fraction that obtained from the ECT system was used to identify the flow patterns prior to the bend, while the WMS PDFs were used to identify the flow downstream of the bend. The flow patterns identified upstream are bubbly, spherical cap bubbles, slug and churn flow, while the main flow patterns observed downstream the bend are stratified and stratified wavy, plug and slug. For gas superficial velocity ranges between 0.045 and 3.21 m s^{-1} and liquid superficial velocity of 0.15 to 0.53 m s^{-1}, it was observed that the flow at 10D downstream of the bend was mainly stratified and wavy stratified flow, whereas further downstream at 40D and beyond the flow ranges from stratified, wavy stratified, large disturbance waves and slug flow.

These direct visual observations were confirmed by WMS images of cross-section distribution of the phases and the PDF data of the void fraction time series obtained from ETC and WMS sensors. The evolution of the flow is shown in

Figure 5-6 and Figure 5-5 respectively for a lower flow condition and in Figure 5-8 and Figure 5-7 for moderate flow condition. The highest flow condition studied, liquid superficial velocity of 0.53 m s^{-1} and gas superficial velocity of 3.21 m s^{-1}, are illustrated in Figure 5-10 Figure 5-9 respectively. The images obtained from the WMS are shown relative to the position at which they were obtained, where blue and red colours represent the liquid phase and gas phase respectively.

At the lowest gas superficial velocity (0.05 m s^{-1}) and liquid superficial velocity of 0.22 m s^{-1}, bubbly flow was dominant in the riser before the vertical bend, as can be seen from Figure 5-5. As the phases passed around the bend to the horizontal section, the liquid phase was drained to the bottom of the pipe due to the effect of gravity and stratified flow was dominant for the whole length of the horizontal section. This is confirmed by the equivalent plots of the PDFs of the cross-sectionally averaged void fraction illustrated in Figure 5-6. Further downstream of the bend the PDFs show a two peak shape. These normally would be a sign of slug flow, however, direct observation indicates that the liquid level did not touch the top of the pipe and the two peaks were more a manifestation of a wavy stratified flow (Zhao et al., 2017) .

The liquid level in the pipe increases with the increase of liquid flow rate. When the gas superficial velocity increased to (U_{gs} = 0.18 m s^{-1}) the transition to cap bubble occurs. In this case, slow moving slugs were observed in the horizontal section since the liquid level was high enough to bridge the pipe. The body of

those slugs contained a low population of air bubbles. Slugs increased in length as they moved down the horizontal pipe.

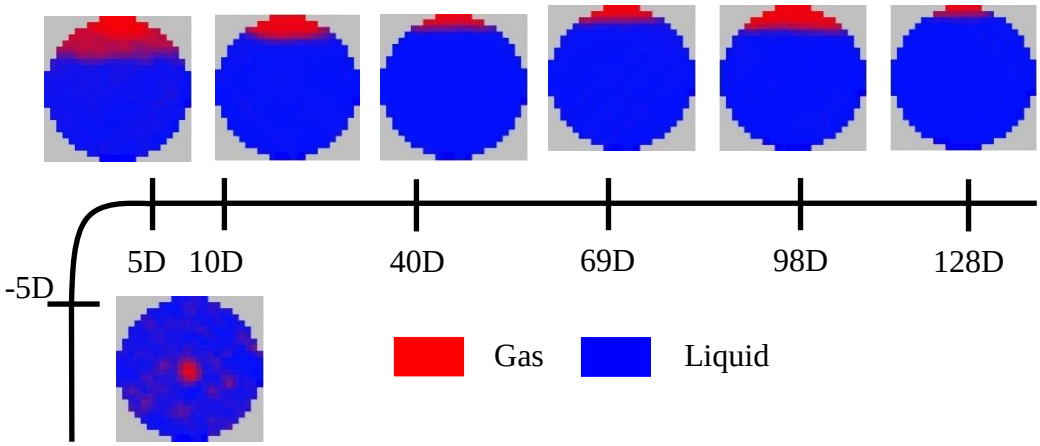


Figure 5-5: Tomographic images from positions along the pipe system. Liquid superficial velocity = 0.22 m s^{-1} and gas superficial velocity = 0.05 m s^{-1}.

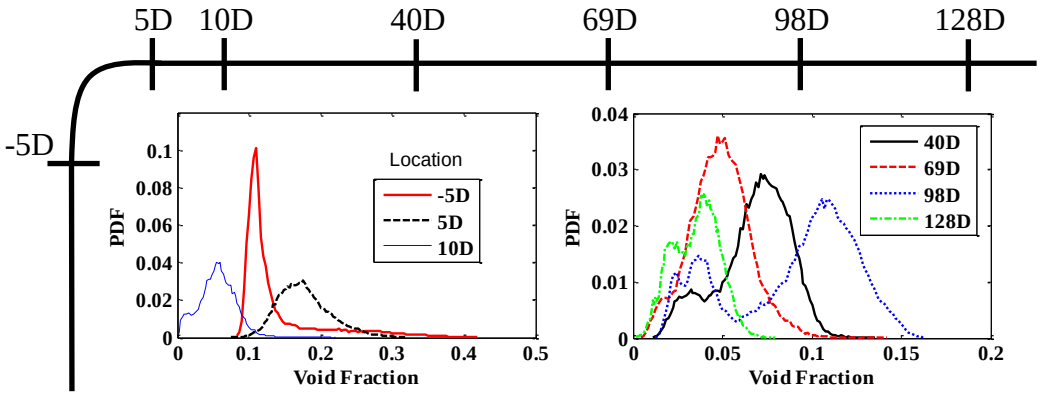


Figure 5-6: Probability Density Function of void fraction time series at axial positions along the pipeline. Liquid superficial velocity = 0.15 m s^{-1} and gas superficial velocity = 0.05 m s^{-1}.

At relatively higher gas superficial velocity (U_{ls} = 0.53 m s^{-1}, U_{gs} = 0.45 m s^{-1}), slug flow was dominant in the vertical pipe. As the slugs approach the bend, the liquid phase was moved to the outer wall of the bend at first due to the effect of centrifugal force. Further around the bend, the liquid is drained to the inside of the bend due to gravity effects leaving a dry patch on top, until a new slug unit cover the dry zone occupied by the gas phase. In this case, the flow in the horizontal

section was stratified near the bend with a slightly disturbed interface while hydrodynamic slugs formed at around ~40D downstream of the bend. This can be clearly seen from the WMS images in Figure 5-7 and PDFs plots in Figure 5-8. The body of the slug at these conditions was occupied with more dispersed bubbles. One remarkable feature, at this condition, is that some slugs are more likely to break up before leaving the test section.

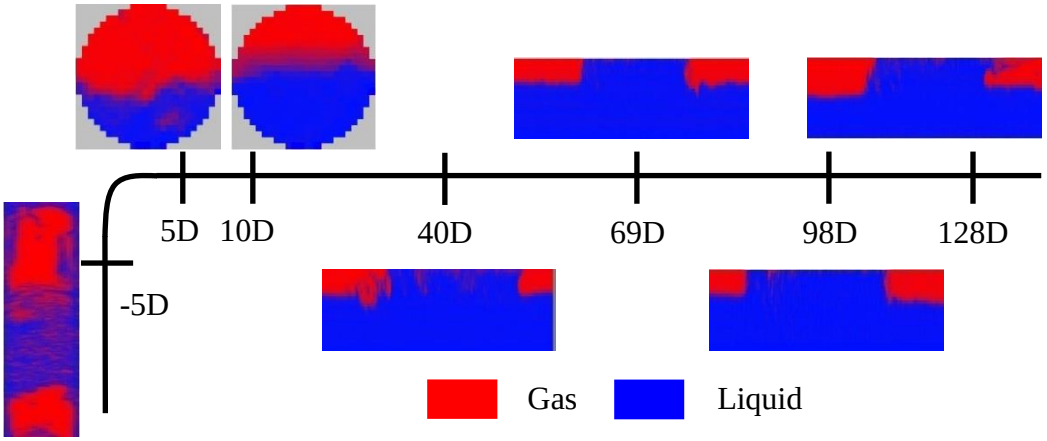


Figure 5-7: Tomographic images from positions along the pipe system. Liquid superficial velocity = 0.53 m s^{-1} and gas superficial velocity = 0.45 m s^{-1}.

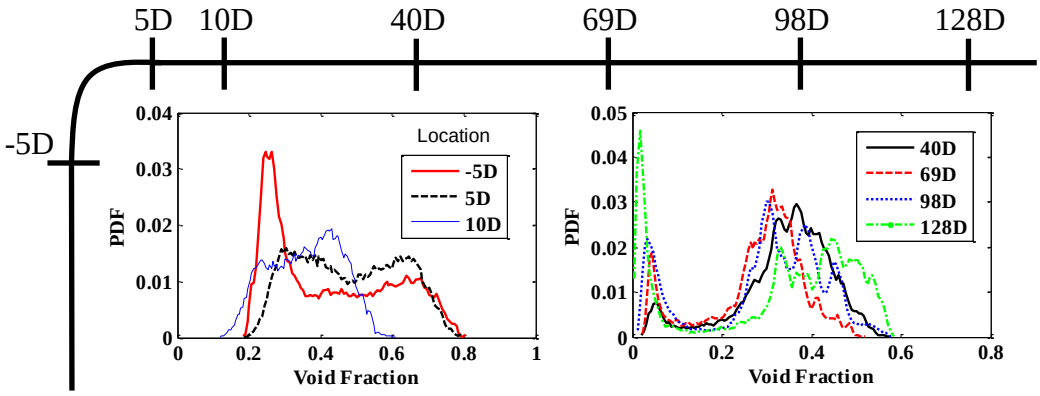


Figure 5-8: Probability Density Function of void fraction time series at axial positions along the pipeline. Liquid superficial velocity = 0.53 m s^{-1} and gas superficial velocity = 0.45 m s^{-1}.

At the maximum liquid and gas superficial velocities (U_{ls} = 0.53 m s^{-1} ,U_{gs} = 3.21 m s^{-1}) the flow in the riser was churn while stratified wavy was dominant up to around 55D downstream the bend, then slug flow become dominant for the rest of

the horizontal section length, as illustrated in Figure 5-9. It can be noticed from Figure 5-10 that the PDFs signature of churn flow in the riser and the slug flow in the horizontal section are similar in shape. This is for the reason that the hydrodynamic slugs formed at these conditions contain a very high dispersed bubbles population where the gas holdup reaches a maximum value of around 0.7.

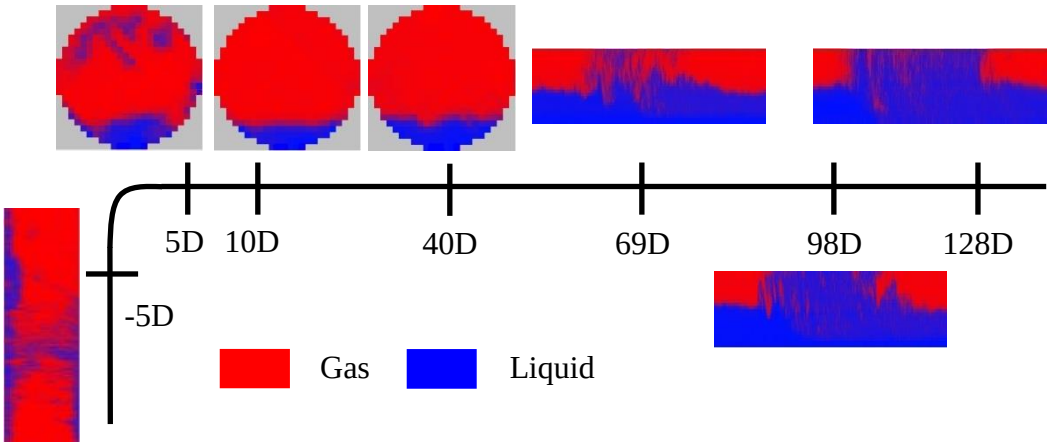


Figure 5-9: Tomographic images from positions along the pipe system. Liquid superficial velocity = 0.53 m s^{-1} and gas superficial velocity = 3.21 m s^{-1}.

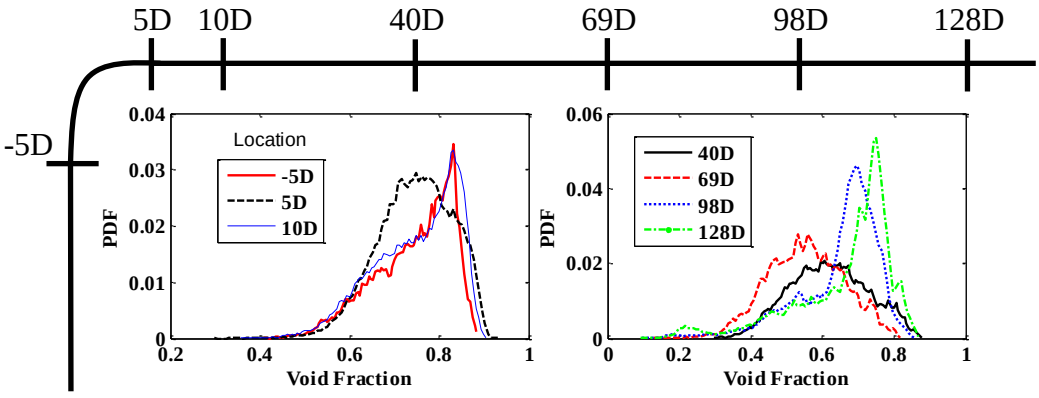


Figure 5-10: Probability Density Function of void fraction time series at axial positions along the pipeline. Liquid superficial velocity = 0.53 m s^{-1} and gas superficial velocity = 3.21 m s^{-1}.

5.3 Cross-sectional averaged void fraction

The cross-sectional averaged void fraction was obtained, using ECT at 5D upstream of the bend and WMS at six locations (5D, 10D, 40D, 69D, 98D and

128D) downstream of the bend. The cross-sectional averaged void fraction data was averaged over a period of 60 seconds at an acquisition rate of 1 kHz. The effects of the gas and liquid superficial velocities on the mean void fraction along the axial distance of pipe system are illustrated in Figure 5-11 and Figure 5-12 respectively. The dashed line in the figures indicates the location of the bend.

For constant liquid superficial velocity (Figure 5-11) the void fraction increases with the rise of the gas superficial velocity as expected. It is obvious that at U_{gs}=0.045 m s^{-1} the void fraction continuously decreases after the bend except at the first location (D=5) at which a slight increase in voidage was observed.

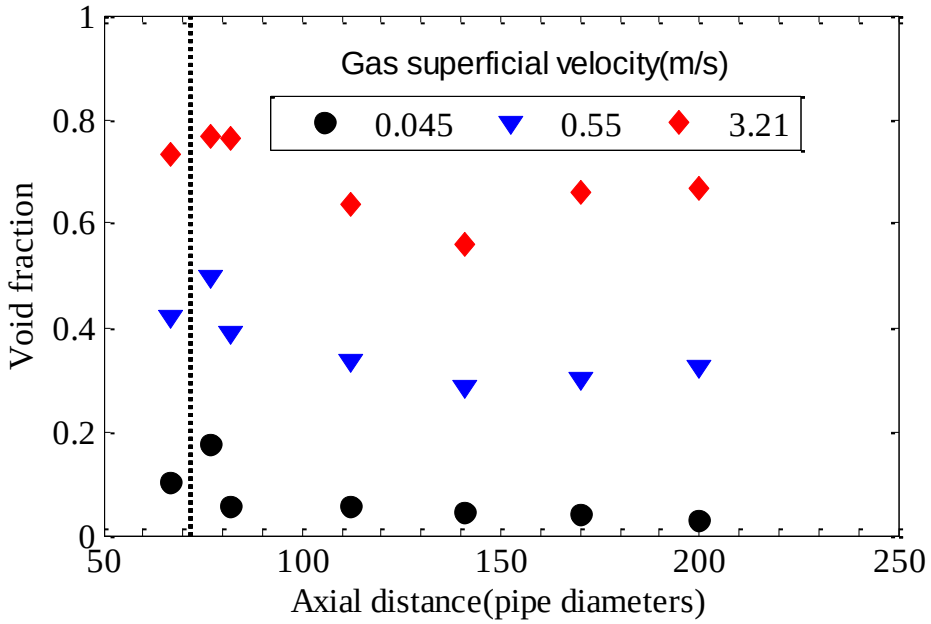


Figure 5-11: Effect of gas flow rate on the Cross-sectional averaged void fraction along the pipe system. Liquid superficial velocity = 0.45 m s^{-1}.

This due to that the liquid phase immediately after the bend was drained to the bottom of the pipe and the liquid film was highly agitated causing more bubble to entrain and hence the void fraction to increase. As the flow moved downstream, the liquid film was more stable and the gas content was released. Plug flow was

formed with low gas entrainment, resulting in a decrease in void fraction along the pipe. At high gas superficial velocity (U_{gs}=3.21 m s^{-1}), there was an insignificant change in void fraction before and after the bend. In this case, the flow is more chaotic before and after the bend. The flow was churn at the top of the vertical section and wavy stratified flow up to around ~55D downstream of the bend and then highly aerated slugs and disturbance waves were formed.

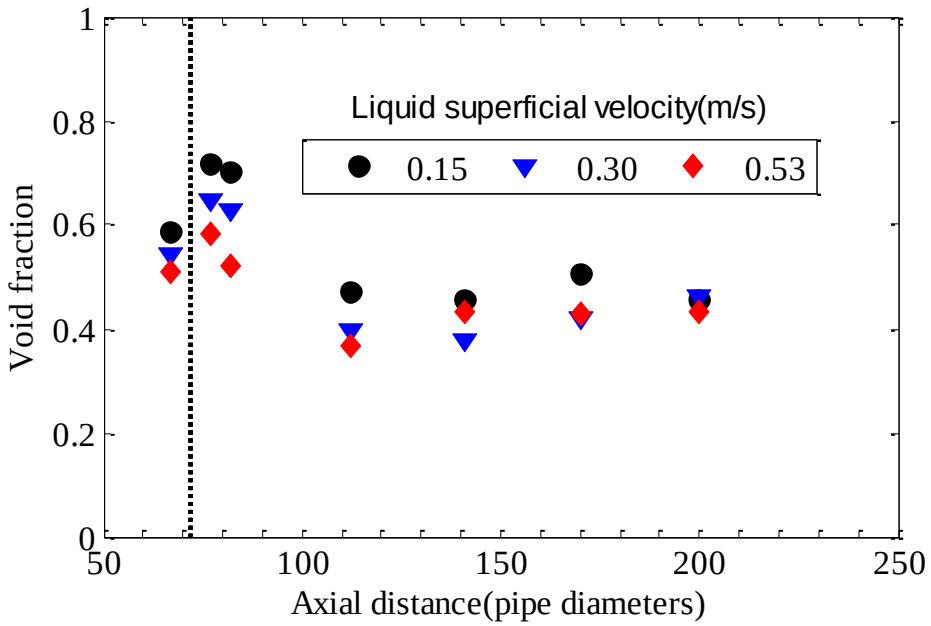
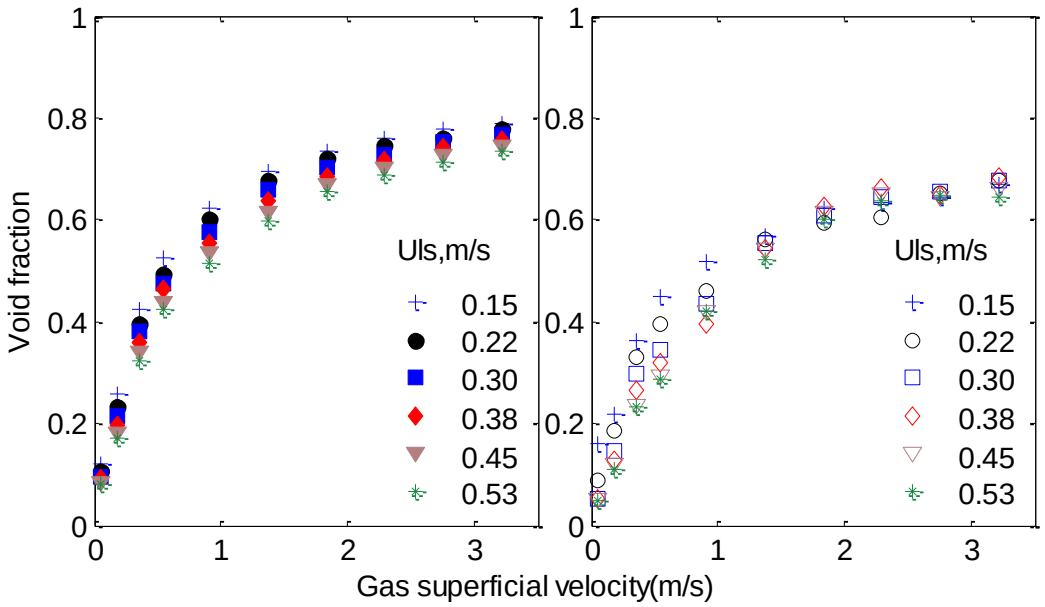


Figure 5-12: Effect of liquid flow rate on the cross-sectional averaged void fraction along the pipe system. Gas superficial velocity = 0.91 m s^{-1}.

Figure 5-12 shows that the cross-sectional averaged void fraction decreases with the increase of liquid velocity and also along the pipe system. It seems that void fraction is less sensitive to the effect of liquid superficial velocity, especially at further downstream of the bend. Beyond 69 D after the bend the void fraction was almost constant along the axial direction due to the formation of slugs.

The gas superficial velocity has a major influence on the subsequent flow development and transition. To quantify the variations, void fraction at 5D before

and at 98D after the bend is presented for a number of gas and liquid superficial velocities. The effect of gas superficial velocity on the cross-sectional averaged void fraction is illustrated in Figure 5-13.



(a) 5D before the bend (b) 98D after the bend

Figure 5-13: The variation of the averaged void fraction with gas superficial velocity at 5D upstream (a) and 98D downstream (b) of the vertical bend.

Figure 5-13 shows the mean void fraction for (U_{gs}=0.045 to 3.21 m s^{-1} and U_{ls}= 0.15 to 0.53 m s^{-1}) at 5D upstream (a) and 98D downstream of the bend (b). Figure 5-13-a obviously indicates a smooth and continuous increase in void fraction with increasing gas superficial velocity. It can be seen that the void fraction is sensitive to the change of superficial gas velocity at low values. The figure clearly indicates that the curves tend to level off beyond the superficial gas velocity 1.5 m s^{-1}. This trend can be interpreted as the change in flow patterns with the increase of gas superficial velocity. Transition from bubbly to slug flow associates with considerable change in void fraction, this explains the sharpness in the curve (up to U_{gs} = 0.55 m s^{-1}), whereas the transition from slug to churn

incorporates a slight change in void fraction (U_{gs} > 0.91 m s^{-1}). If the gas superficial velocity increases further the curve is expected to have another distinguished increase at the annular flow tarnation.

At 98D downstream of the bend (Figure 5-13-b) the void fraction variation maintained a generally similar trend to that upstream of the bend only at 0.15 and 0.22 m s^{-1} liquid superficial velocities, these flow ranges represent mostly stratified wavy flow and plug flow. Within this range of flow conditions, the phases were separated and redistributed in the horizontal section without any significant change in void fraction.

At higher liquid velocity, beyond 0.3 m s^{-1}, the void variation showed an inconsistent trend where it reaches the peak at U_{gs} = 2.29 m s^{-1} and then decreases. This unusual trend of variation in void fraction is more likely due to the formation of hydrodynamic slugs at gas superficial velocity of 0.91 m s^{-1} and above.

At first the liquid slugs are irregular and separated by wavy stratified flow which corresponds to the highest void fraction, as the gas superficial velocity increases the slugs become more regular causing the void fraction to decrease. At the maximum gas superficial velocity of 3.21 m s^{-1} the body of the slugs is mainly fine dispersed bubbles resulting in increase of void fraction again.

Generally, the effect of liquid superficial velocity is highly influenced by the gas superficial velocity. The void fraction decreases with the increase of liquid superficial velocity, however, the variation of void fraction with liquid superficial velocity at 98D downstream the bend showed relatively different behaviour to that

before the bend. This is more likely due to the backflow upstream of the bend, in addition to slug formation after certain length downstream the bend.

5.4 Structure Frequency

The power spectrum spectral density (PSD) analysis was applied to the void fraction time series in order to estimate the frequency of the flow structure, mainly slugs and disturbance waves in the horizontal pipe after the bend and includes spherical cap bubbles in the vertical pipe section. The results were compared to the method used by Hazuku et al. (2008) as detailed in Chapter 2. The structure frequencies from both methods were in a good agreement with each other and with the manual method of counting the peaks in the void fraction time series. The results of Hazuku et al. (2008) approach are presented here. The characteristic frequencies of the flow structure were obtained using ECT time series, at 5D upstream of the bend and WMS signal, at six locations (5D, 10D, 40D, 69D, 98D and 128D) downstream of the bend. The results that show the effect of gas and liquid flow rates are presented in Figure 5-14 and Figure 5-15 respectively.

The structure frequencies decrease with the increase of gas flow rates as illustrated in Figure 5-14. The more dominant trend is the continuous decrease of frequency along the downstream positions. These results are significantly different from those reported by Saidj et al. (2014) for horizontal to vertical pipe system. They indicate that there is no persistence of frequency and reinforces the point that structure frequency is preserved only if a flow pattern, particularly slug flow is maintained across the bend. In this case, the vertical to horizontal bend destroys slug flow and it takes around ~40 to ~55D for slug flow to reinitiate at

downstream of the bend (only beyond certain gas superficial velocity) (Zhao et al., 2017).

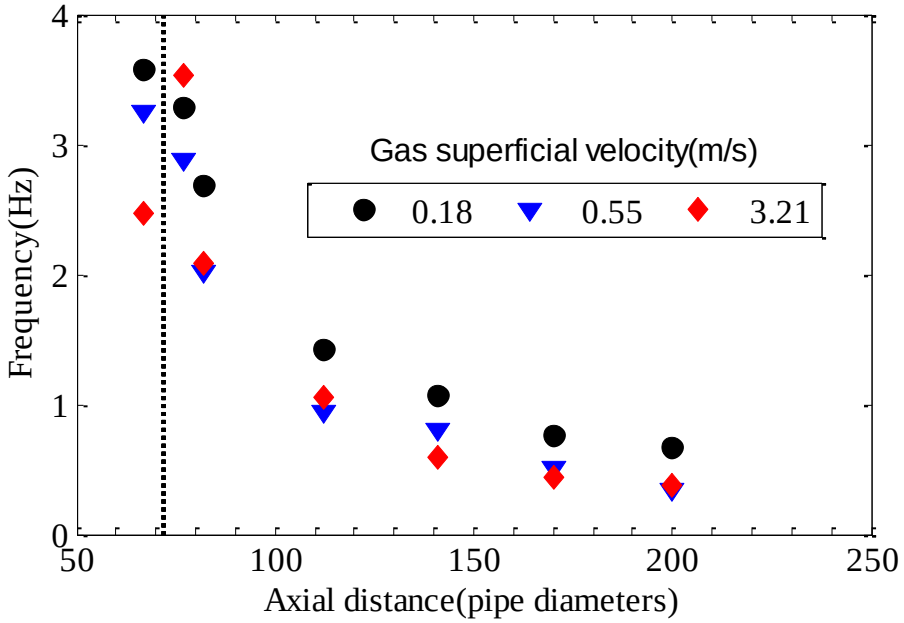


Figure 5-14: Effect of gas flow rate on the characteristic frequency along the pipe system. Liquid superficial velocity = 0.45 m s^{-1}.

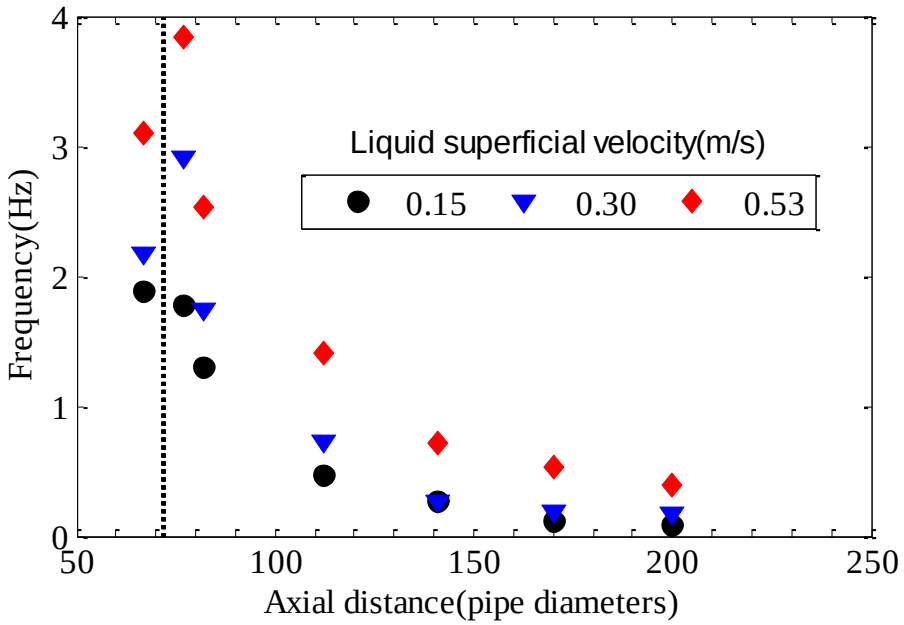


Figure 5-15: Effect of liquid flow rate on the characteristic frequency along the pipe system. Gas superficial velocity = 1.83 m s^{-1}.

The liquid flow rate has an opposite effect whereby the frequency increases with the increase of the liquid superficial velocities as explained in Figure 5-15. The frequencies at all conditions decreases along the pipe system from before to after the bend, though, there is a rise from just before to just after the vertical to horizontal bend. This is due to that the flow at 5D downstream of the bend being chaotic and has no clear structure.

The effect of gas superficial velocity on the frequency of periodic structure, including slugs and large disturbance waves is illustrated in Figure 5-16 for the vertical bend. In general the structure frequency exhibits a steady decrease with the increase of gas superficial velocities. This is attributed to the occurrence of large structure, provoked by coalescences of small structures. For the vertical pipe section (Figure 5-16-a), at superficial gas velocity 0.18 m s^{-1} cap bubbles were dominant, as the gas superficial velocity increases slugs and disturbance waves were formed respectively, which explains the continuous drop in frequency. Generally, the structure frequency increases with increase in liquid superficial velocity for all the cases considered. At the horizontal section after the bend the structure frequency, namely slugs decreases with the rise of gas superficial velocity and increases with the increase of liquid superficial velocity as shown in Figure 5-16-b. The frequency value seems to decline to below half of the frequency upstream of the bend.

It is noted that the frequency variation with the gas superficial velocity tends to level off beyond a gas superficial velocity of 0.91m s^{-1}. This is more likely to be related to the development of slugs.

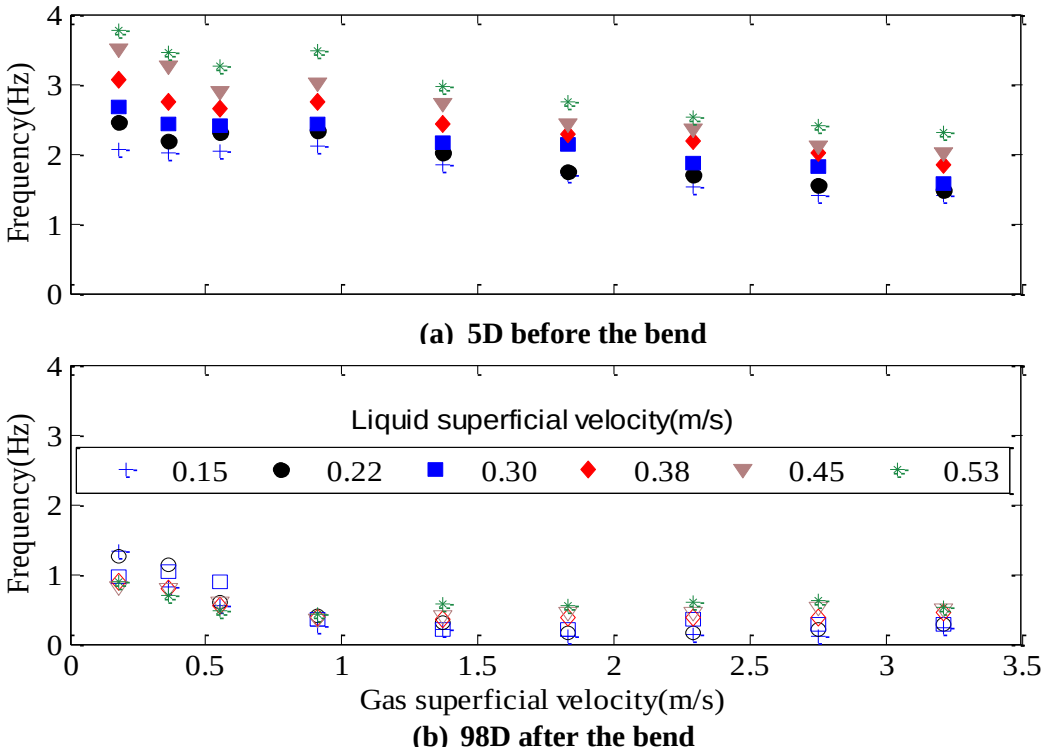


Figure 5-16: Frequency variation with air and oil superficial velocity at 5D (a) upstream and 98D (b) downstream of the vertical bend.

5.5 Structure Velocity

The effect of the gas superficial velocity on the structure velocity, mainly slugs and disturbance waves, upstream and downstream of the vertical bend is presented in Figure 5-17. Cross-correlation between the void fractions time series signals collected from the dual plane ECT were used to compute the structure velocity. In these experiments it was assumed that the slug unit is traveling at same velocity, however in reality the Taylor bubble and liquid slug may travel at slightly different velocities, which is usually considered to be small and has negligible effect, since the gas entrainment into and out of the Taylor bubble should be equal (Fernandes et al., 1983). The plot shows, as expected, an increase in structure velocity with the increase in both, the gas and the liquid superficial velocities. It was noticed that the effect of the liquid superficial velocity is more pronounced at

high gas superficial velocity. It can be said that the liquid superficial velocity has a weaker effect on the structure velocity comparing to that of the gas superficial velocity.

Figure 5-17 shows that the structure velocity seems to decrease downstream of the bend, particularly at low gas superficial velocities. This is due to the gravity effect in the horizontal section downstream of the bend. At low gas flow rate, the viscous force is more dominant than inertia, and hence the structure velocity is decrease downstream of the bend, due to the increase in shear rate with the inner walls of the pipe.

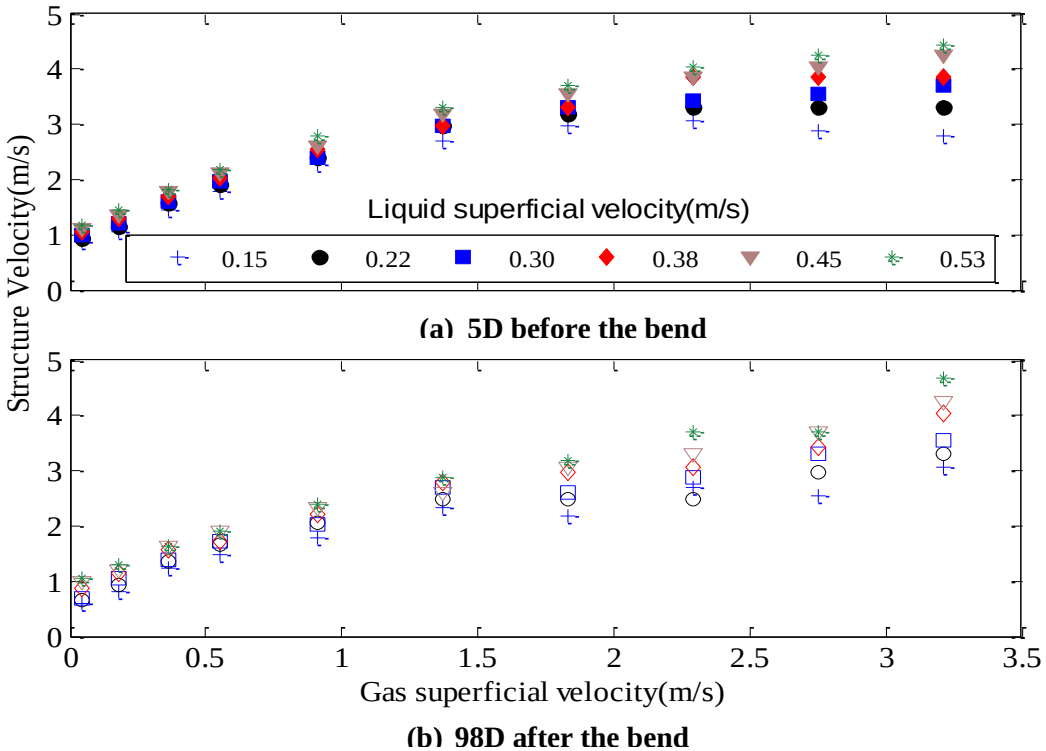


Figure 5-17: Structure velocity for several air and oil superficial velocities at 5D upstream (a) and 98D downstream (b) of the vertical bend.

5.6 Slug unit characterisation

As explained in the previous chapters, Slug flow is a crucial gas-liquid flow regime that persists for a wide range of flow conditions in several industrial applications. It is associated with an intermittent structure of aerated liquid slugs flowed by large gas bubbles which is called slug unit. In horizontal pipes, slug features are asymmetric around the axis. The dispersed bubbles within liquid slugs are agglomerated at the top part of the pipe, while in the gas bubbles region the liquid film in collected at the bottom of the pipe, forming a liquid layer that has either smooth or wavy interface. Slug flow in horizontal pipes can be described as a succession of dispersed bubbly flow by stratified configuration. The prediction of the quasiperiodic behaviour of slugging phenomenon has been a challenging task for industry. Several attempts to model slug flow have been reported (Nicholson et al., 1978; Andreussi and Bendiksen, 1989; Taitel and Barnea, 1990; Andreussi et al., 1993) most of which are based on the unit cell model that was first introduced by (Dukler and Hubbard, 1975). This approach simplifies the slugging phenomenon to a sequence of slug units through several assumptions and then a mass balance around a slug unit can be achieved.

The mechanism by which gas entrained into liquid slug is rather complex, however, a simplified approach has been always employed in modelling continuous slug flow. In horizontal pipes, slug aeration mechanisms are slightly different from that of vertical slug, since the symmetry of the Taylor bubble and liquid film around the pipe wall is lost. As the liquid slug moves along the pipe, liquid is continuously scooped from the slow liquid film in the front into the body of the slug. The slug is considered stable when the picking up rate is equal to the

shedding rate at the back. The penetration of the slow liquid film into the fast moving slug results in highly aerated mixing vertex at the slug front. Essentially bubbles are dispersed into the body of the slug forming a more stabilised region. The gas bubbles can also be rejected to the leading Taylor bubble, due to the circulation of the mixing zone, or absorbed by the trailing Taylor bubble. In developed flow, the rate of bubbles generation and loss is considered equal (Dukler and Hubbard, 1975).

In the following subsections, the effect of vertical to horizontal bend on the evolution of slug flow is investigated. Direct comparison between the developed slugs upstream and downstream of the bend is presented. The results examine the effects of gas and liquid superficial velocities on the slug features, Tayler bubble velocity, slug length, the frequency of slug and void fraction in liquid slugs. Finally, the predictability of the current correlations for horizontal slug flow is validated against the experimental data.

5.6.1 Taylor bubble velocity

The structure velocity of slugs was determined by cross correlating the time averaged void fraction distribution of the twin-plane ECT sensor. The ECT sensor was placed at a sufficient distance downstream of the bend (128D) to allow the flow development.

Figure 5-18 demonstrates the change in the slug velocity at 5D before and 128D after the bend. It can be clearly seen that the velocity increases with the increase of gas and liquid superficial velocities. The slug velocity is visibly lower at

downstream of the bend than the velocity of slugs upstream of the bend. This can be mainly due to the gravitational effects in the horizontal section.

The decrease in slug velocity after the bend seems to be more pronounced at high gas superficial velocity. It can be said that that the slug velocity upstream of the bend might influence the distance at which the slugging initiates, based on the required liquid level, but it seems to have no significant influence on the slug velocity in the horizontal section. This is mostly due to the separation of phases after the bend.

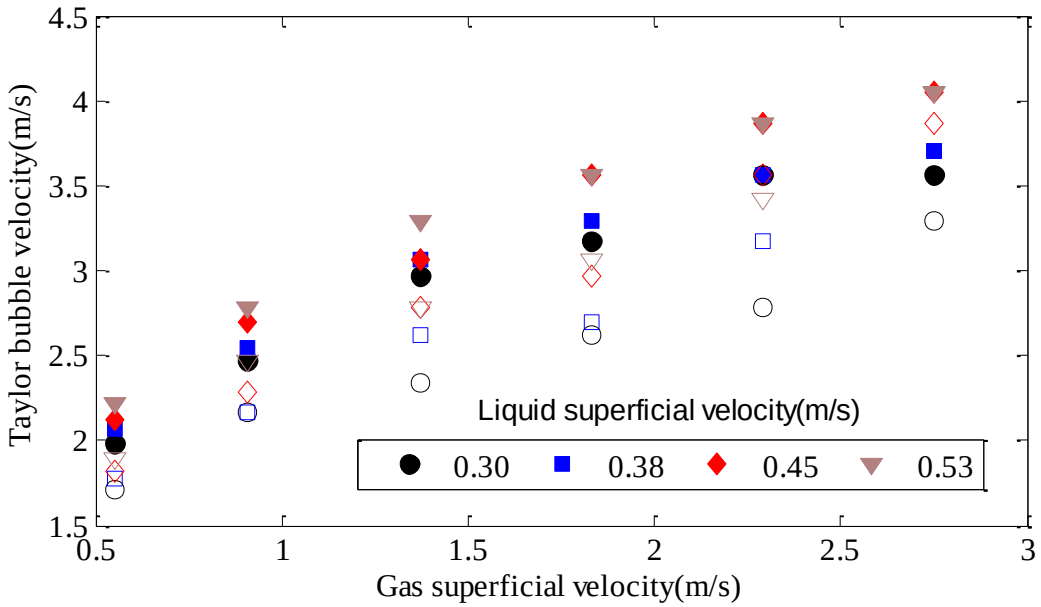


Figure 5-18: Slugs velocity variation at 5D upstream of the bend (filled symbols) and 128D downstream of the bend (empty symbols).

The correlation of Nicklin et al. (1962) has been widely accepted to correlate Taylor bubble velocity in continuous slug flow at different pipe inclination.

$$u_{gTB} = C_0 U_m + U_d \tag{5.3}$$

Where, U_d is the drift velocity, U_m is the mixture velocity and C_0 is the distribution parameter. A nonzero drift velocity in horizontal pipes has been a controversial topic amongst two-phase flow researchers. Based on physical justification, zero drift velocity has been reported by Dukler and Hubbard (1975) Gregory and Scott (1969), while other investigators have claimed that a nonzero drift velocity can exists in horizontal pipes (Mattar and Gregory, 1974; Nicholson et al., 1978; Weber, 1981).

The intuitiveness of physics would suggest that in horizontal flow, Taylor bubbles as well as dispersed bubbles in liquid slug migrate to the upper wall of the pipe. This should make the bubbles stationary with no slip velocity in the direction of the flow. Conversely, Zukoski (1966) showed experimentally that the drift velocity exists in horizontal pipes, he conducted experiment in pipes of a closed ends at different inclination. The drift velocity in those experiments was equal to the velocity of the air pocket moving in the opposite direction of a drained liquid out of a horizontal pipe. Benjamin (1968) has proved theoretically (in his paper page 22) the work of Zukoski. The drift velocity derived from Benjamin's work can be presented as a function of pipe diameter as in eq.(5.4) (Weber, 1981; Van Hout et al., 2002a; Fabre, 2003).

$$U_d = 0.54\sqrt{gD} \tag{5.4}$$

Where g is the gravitational constant and D is the diameter of the pipe. The existence of drift velocity in horizontal pipes was justified by the difference in static head that induced by the liquid level in the pipe cross-section as reported by

(Nicholson et al., 1978). Weber (1981) claimed that the drift velocity approaches zero in small pipes (< 5 mm). He correlated Zukoski's results in term of Eotvos number (E_{Ov}) and suggested that drift velocity is zero at $E_{Ov} \leq 12$.

Form Nicklin equation, the drift velocity can simply be obtained by extrapolating the experimental values to $U_m = 0$ as shown in Figure 5-19**.** It is obvious that the current data can be fitted with a straight line (the black dotted line) that has an intercept of 1.1 with $R^2 = 0.9$. This value corresponds to the drift velocity and should have a physical significant. The deviation from the fitted line increases at high mixture velocity.

The estimated drift velocity for the whole range of slug flow conditions in this work is equal to $\left(1.34\sqrt{gD}\right)$. It is significantly higher than the velocity of single bubble in stagnant liquid for both horizontal and vertical flows, similar observation is reported by Van Hout et al. (2002a) form inclinable 54mm pipe with water as liquid phase. This is due to the contribution of the dispersed bubbles in the liquid slug to the velocity of Taylor bubble where the coalescence of the dispersed bubbles to the nose of Taylor bubble enhances its velocity. According to Bendiksen (1984) the drift velocity approaches zero at high mixture velocities. He suggested a critical Froude number equal to 3.5 for the transition from a nonzero to zero drift velocity. When this criterion was applied to the current data and the high mixture velocities were excluded, the drift velocity obtained by extrapolating the best fit (the red dotted line) was equal to $\left(0.7\sqrt{gD}\right)$. This appears a great improvement, where the predicted drift velocity is slightly higher than the theoretical value. The overestimation of drift velocity in this work

is more likely due to highly aerated slugs particularly at high flow velocities that cause the transitional velocity of Taylor bubble to increase as a result of bubbles coalescence. The estimated distribution parameter at low mixture velocity is in agreement with the value suggested by Nicklin et al. (1962) C_0=1.2, while for the whole range of slug conditions, C_0 was equal to 0.82.

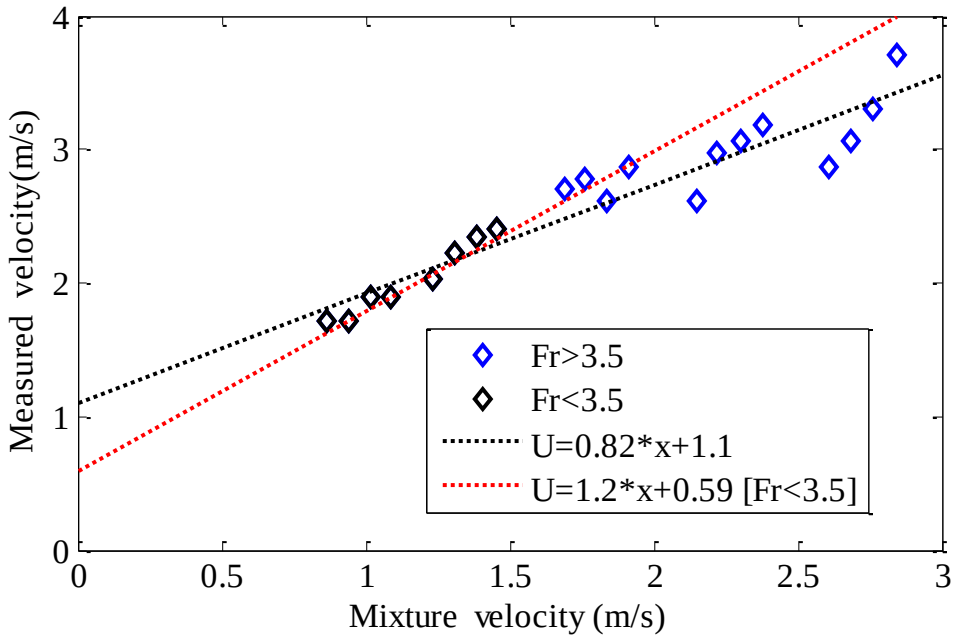


Figure 5-19: Regression analysis on the measured Taylor bubble velocity in the horizontal section downstream of the bend.

In this work, the correlation of Gregory and Scott (1969) eq.(5.5) for a zero drift velocity was used to predict the experimental results, while eq.(5.6) was used to examine the existence of drift velocity.

$$U_{gTB} = 1.35U_m \tag{5.5}$$

$$U_{gTB} = 1.35U_m + 0.54\sqrt{gD} \tag{5.6}$$

It should be noted that there is no agreement in the literature on a single value for the distribution parameter C_0. Bendiksen (1984) has suggested that C_0 is strongly dependent on Froude Number, where C_0 =1.05 for (Fr < 3.5) and C_0 =1.2 for (Fr ≥ 3.5). Other values of C_0 were also reported for horizontal slug flow, varying from 1.28 to 1.35 (Gregory and Scott, 1969; Mattar and Gregory, 1974; Dukler and Hubbard, 1975)). The value of C_0 =1.35, reported in Gregory and Scott (1969) was used in this work, since it gave the best estimation. In fact, when the current data was fitted with a line passing through the origin, almost similar value of (C_0=1.36) was obtained.

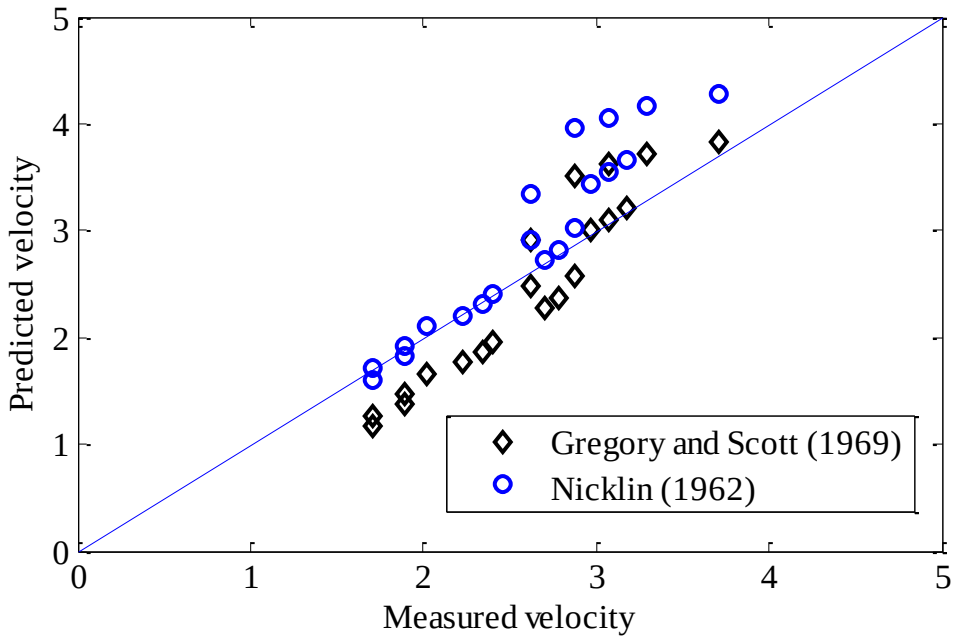


Figure 5-20: Theoretical prediction of the experimental Taylor bubble velocity.

Figure 5-20 illustrates the theoretical prediction of Taylor bubble velocity in horizontal pipe downstream of the vertical to horizontal bend. The figure shows that the correlation of Gregory and Scott (1969) under predicts the experimental data with an average absolute error of 15% and standard deviation of 3.15. Nicklin's equation showed a better anticipation of the Taylor bubble velocity,

particularly at lower velocities with an average absolute error of 11.1% and standard deviation of 2.5. The equation of Nicklin, employing the theoretical drift velocity, seems to accurately predict the experimental results at low mixture velocities (Fr < 3.5) with an average absolute error of 5% and standard deviation of 1.6. For high velocities, the correlation started to deviate and clearly overpredicts the experimental values. This due to overestimation of drift velocity at this conditions which is in agreement with the results of Bendiksen (1984) who reported that U_d approaches zero at high Froude number (Fr > 3.5). The equation of Gregory and Scott that considers zero drift velocity confirms this finding, since it underpredicted the experimental values at low mixture velocities and notably improved at high velocities where the drift velocity is expected to be negligible. Wang et al. (2007) reported similar observation on the critical Froude number, using air-water in a horizontal 50 mm ID pipe of 133 m long. They also suggested that axial location has an influence on the distribution parameter. They found that C_0 changed from 1.35 to 1.726 at 1157D and 2609D respectively.

Although it seems instinctively not convincing that drift velocity in horizontal pipes can be greater than that in vertical pipes, the current results and the reported data in the literature indicate the existence of some sort of unsteady velocity profile in horizontal pipes which is usually related to the drift velocity. This drift velocity is explained as the difference in static head between the top and the bottom of Taylor bubble nose in a horizontal pipe. At high mixture velocity, the contribution of drift velocity to Taylor bubble velocity seems negligible.

5.6.2 Slug length

The length of slugs was estimated through multiplying the averaged transitional velocity of slugs by the resident time of slugs at the sensor. The velocity was assumed to be constant throughout the test section.

At the horizontal pipe downstream of the bend, the slug lengths seem to increase in the axial direction. Figure 5-21 illustrates the growth of the slug lengths along the pipeline. The first measuring location after the bend is at 69D. The slugs at this position are not fully developed yet.

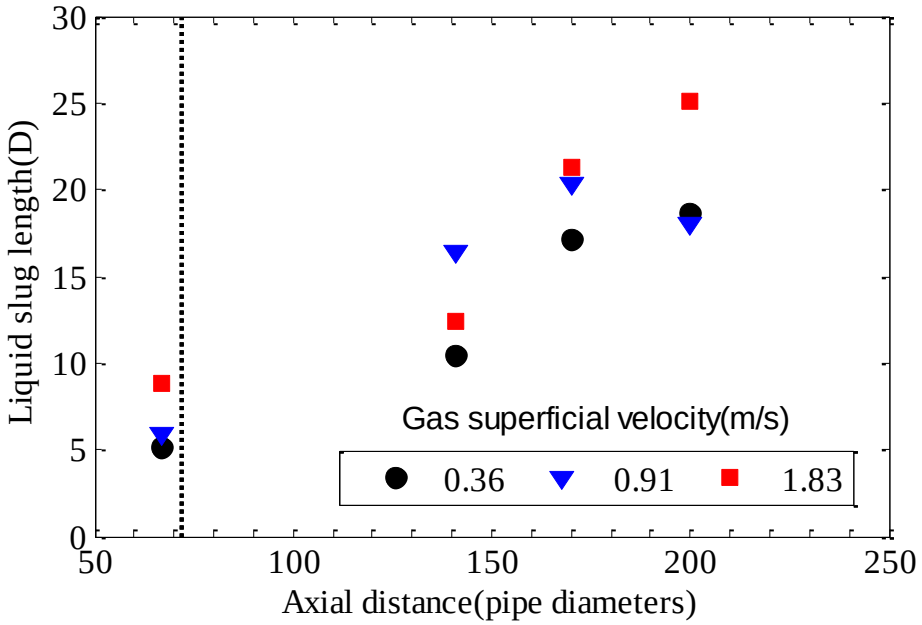


Figure 5-21: The axial development of the mean liquid slug length at the horizontal section, liquid superficial velocity=0.53 m s^{-1}.

It is obvious from Figure 5-21 that the mean length increases along the pipe in the direction of the flow downstream of the bend. This is clearly due to that slugs pick up more liquid as they travel further downstream. The fast moving slugs scoop the liquid film and the slow moving waves in front and shed liquid at the back. When the rate of liquid accumulation in the body of slugs is higher than the shedding

rate at the back, the slugs develop longer. The rate of growth increases at high gas velocities within the range of the flow conditions of this work. This mainly due to the fact that slugs formed at these conditions move faster and hence quickly overriding preceding waves and liquid film. Consequently, slugs appeared longer for high gas superficial velocities at the same axial location. According to Scott et al. (1989), there two mechanisms of slug growth, the first is what has been described here and it is called developing slug growth and the other is long-term growth. The former causes a rapid growth; while the latter is slower and has a long-term effect. The long-term growth occurs when the liquid film region between slugs becomes smooth. This growth mechanism can be noticed only if the slugs travel very long distance; since it was reported for field experiments of 5 km long pipes.

It was also observed that the length of slugs increases with the increase of gas superficial velocity. This is in agreement with the work of Ferré (1979) for air-water flow within the range of 0.5 to 4 m s^{-1} gas velocities in a 45 mm diameter pipe of 50m length and Wang et al. (2006) for air-oil flow in a 50 mm diameter pipe of 133m length at gas superficial velocity below 6 m s^{-1}. More recently, Losi et al. (2016) have reported a strong dependency of slug length on gas superficial velocity, using air and high viscosity oil (37 to 804mPa.s) in relatively small pipe (22 mm I.D.) of 9 m long. Based on their explanation, turbulence at higher gas velocity provokes an expansion of the mixing eddies at the front of the slug, and consequently causes longer slugs; however no clear interpretation was given on how the expansion of the turbulent region should make the slug longer. This perhaps means a lower pressure drop at the front of the slug and hence faster

traveling velocity which can increase the rate of liquid pick up. Scott et al. (1989) has also reported the increase of slug length with gas superficial velocity for 5km long and 410 mm to 610 mm ID pipes respectively, they related the increase of slug length to the increase of gas holdup within the liquid slug.

The length of slugs seems less sensitive to liquid superficial velocities; the length slightly decreases with the increase in liquid flow at constant gas velocity, similar to the trend reported by (Wang et al., 2006). Several experimental investigations suggest that the slug length is insensitive to the change in gas and liquid superficial velocity, including (Nicholson et al., 1978; Woods et al., 2006; Nydal et al., 1992). The gas velocities reported in those papers extended from 0.5 to 20 m s^{-1}, therefore if the conditions similar to this work, 0.5 to 3 m s^{-1} gas superficial velocity, was considered a clear accumulative trend of slug length can be observed from their data.

The length of slugs further away from the bend seems to reach a quasi-stable condition where the length is almost constant and the rate of change in length with the axial direction become notably small. The slug lengths in the horizontal section ranges from 9D to 30D, while in the vertical section it varies between 5D and 12D as shown in Figure 5-22. The measured slug length in this work is comparable to the stable length reported in the literature for vertical pipes (8D-16D) (Moissis and Griffith, 1962; Akagawa and Sakaguchi, 1966; Barnea and Shemer, 1989) and horizontal flow (12D-30D) (Dukler and Hubbard, 1975; Nicholson et al., 1978; Barnea and Brauner, 1985; Andreussi and Bendiksen, 1989; Nydal et al., 1992). This indicates that the stable slug length in the

horizontal slugs flow is almost double that of vertical slugs. It is evident that the length of the horizontal section downstream of the bend was sufficient for sustaining stable slugs. The length of slugs before and after the bend was within the stable length values reported for vertical and horizontal flows respectively at similar flow conditions. Therefore; it can be said that the effect of the bend on the flow evolution was mainly phase redistribution and separation. The flow after the bend was mainly introduced as a stratified configuration similar to most of the experimental work of horizontal gas-liquid flow. The current data is in agreement with Scott et al. (1989) conclusion for long pipes, that slug it is not completely an entrance effect since at certain flow conditions slugs were observed to form further away downstream of the bend.

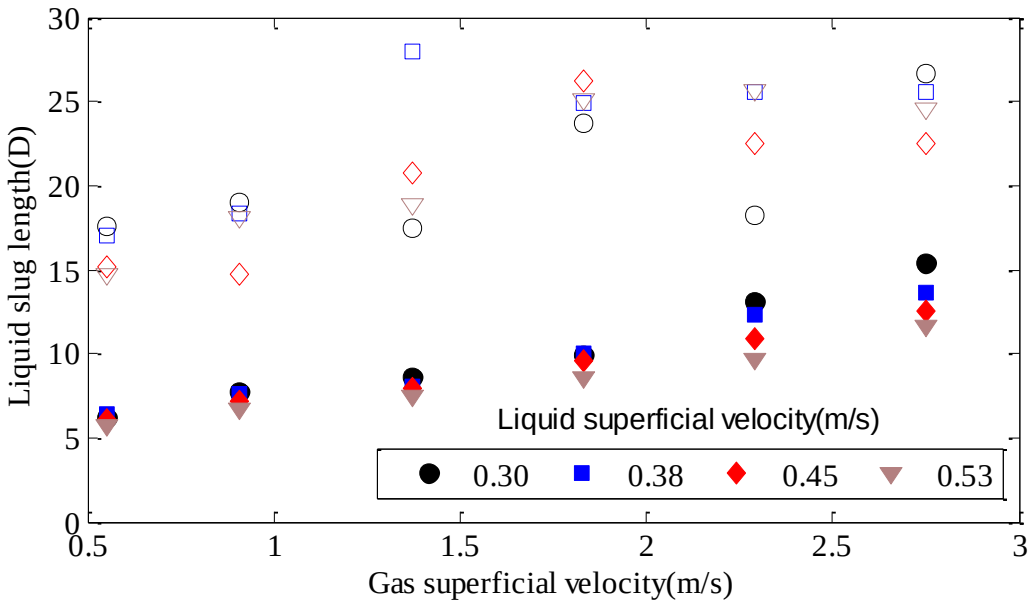


Figure 5-22: Slug length variation at 5D upstream of the bend (filled symbols) and 128D downstream of the bend (empty symbols).

It should be noted that the error in estimating slug length might be higher at high gas flowrate; where liquid slugs are highly aerated and it becomes difficult to

distinguish between the Taylor bubble region and the wake zone within the liquid slug.

5.6.3 Slug frequency

Slug frequency is a crucial factor in the design of the downstream equipment since it gives a direct representation to the flow instability. Slug frequency and slug length are interrelated slug features and both can be used alternatively. The method proposed Hazuku et al. (2008) was employed to identify the liquid slugs from the void fraction time series as described in Chapter 3. In this method certain threshold of void fraction was used to separate slugs from Taylor bubbles as well as waves. Then the frequency was estimated from dividing the number of slugs by the time interval of the measurement. The results from this method was crosschecked by the PSD method as well as the hand counting and a perfect agreement was achieved, although, the results of the former method are presented here.

Figure 5-23 illustrates how the frequency of slugs varies along the pipe line. It is clear that the frequency decreases along the pipe line from after to before the bend and to a less extent it decreases with the increase of gas superficial velocities. The reduction in the frequency in this case is due to the dissipation of some slugs before they exit the pipe. At high gas superficial velocities, the liquid level behind the formed slugs dropped sharply and longer time is taking for the liquid layer to reform to the equilibrium level, consequently longer time is required for the slug formation. In addition, large disturbance waves became more frequent at these conditions. The visual observation showed that liquid level became lower at high

gas velocities for constant liquid flow rate and hence the initial liquid layer was below that required to generate stable slugs.

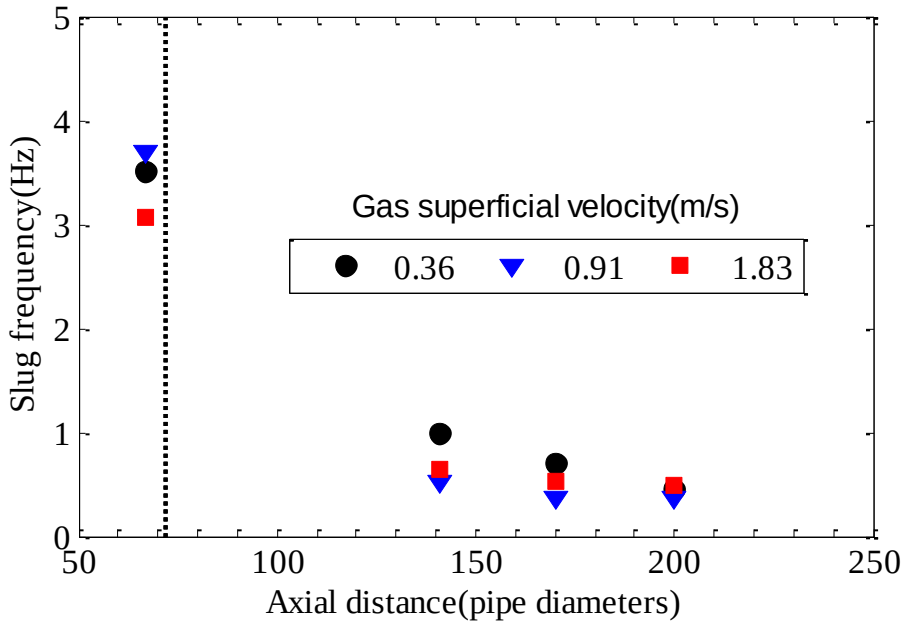


Figure 5-23: Frequency variation as a function of gas superficial velocity along the pipe system. Liquid superficial velocity=0.53 m s^{-1}.

In the horizontal section after the bend, the change in frequency of slugs at the axial positions became steady at high gas flows. At 128D downstream of the bend, the frequency is more stable and less sensitive to the change in gas superficial velocity. Liquid slugs are considered stable at the end of the horizontal section. Wang et al. (2007) and Al-Safran (2009a) reported that slug frequency is weakly sensitive to the pipe length, although, more recently Thaker and Banerjee (2015) observed a decrease in frequency with pipe length. Al-Safran (2009a) has also cited other works that disagree with his findings, including (Taitel, 1987) and (Shea et al., 2004). Taitel (1987) suggested that since the slug length increases in long pipes, due to the merging of successive slugs, the frequency of slugs should decrease.

The variations in the frequency of slugs upstream and downstream of the bend are presented in Figure 5-24. At 5D upstream of the bend the frequency tends to decline as the gas superficial velocity increases. This is due to the increase in the rate of coalescence between slug units with the increase in gas flow rates. The liquid superficial velocity seems to have an opposite effect. The frequency of slugs increases as the liquid flow increases.

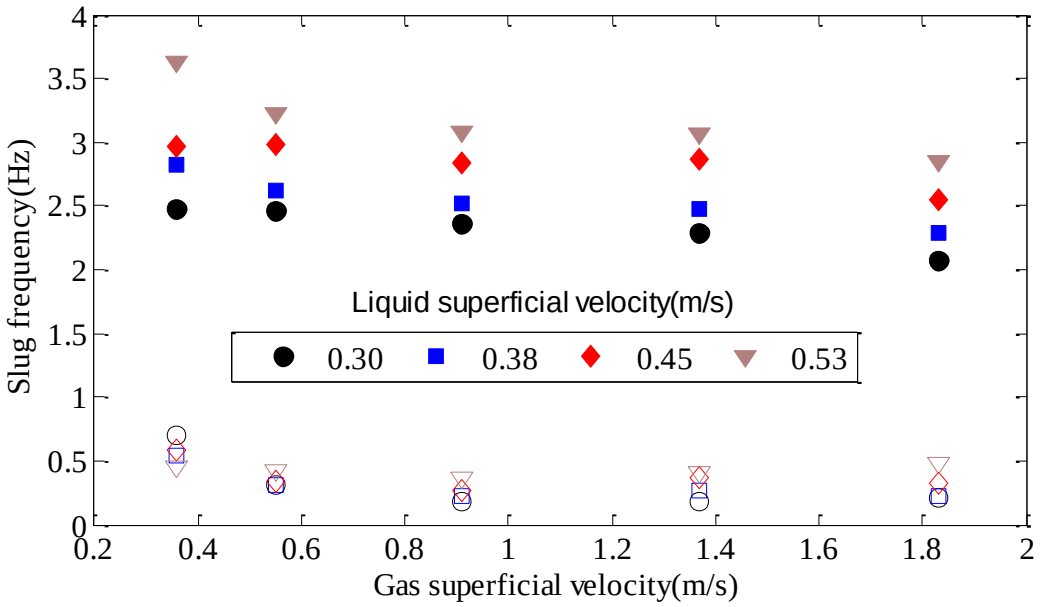


Figure 5-24: Frequency variation at 5D upstream of the bend (filled symbols) and 128D downstream of the bend (empty symbols).

Further downstream of the bend at 128D the frequency tends to decrease slightly as the gas superficial velocity increases then it stays almost constant. The decrease in frequency in this case is due to the breakup of some slugs and also due to the generation of disturbance wave that dissipated further downstream instead of developing into liquid slugs. The effect of liquid flow rate seems more significant than the gas flow rate in the horizontal section, the frequency increases with the rise of liquid flow which is in agreement with the work of Wang et al. (2007). The frequency variation showed a significant difference before and after the bend.

It is obvious from Figure 5-24 that the frequency of slugs downstream of the bend decline to almost one fifth of that upstream of the bend. It is evident that the phase separation at the vertical bend and the redistribution of the phases caused a significant alteration of the flow structure. It can be noticed also that the frequency after the bend become almost constant at high gas superficial velocity. This gives an indication that the onset of slugging downstream of the bend can be completely independent of the flow conditions upstream.

The estimation the frequency of liquid slug is significantly necessary in a wide range of industrial processes, particularly in oil and gas transportation. An accurate prediction of slug frequency is crucial to avoid serious operation issues such as flooding in gas-liquid separators and the failure of pipe system due to instabilities. Slug frequency is also required to predict pressure drop fluctuations. Several correlations have been proposed to estimate the frequency fluctuation of slugs. The main correlations are reviewed in Chapter 2. In this section three correlations are used to predict the frequency of slugs at 128D downstream of the bend, namely Gregory and Scott (1969), Nydal (1991) and Zabaras (2000) correlations.

Figure 5-25 shows the accuracy of three different correlations in estimating the slug frequency. Zabaras (2000) and Gregory and Scott (1969) correlations showed a better prediction of the frequency than Nydal (1991) correlation which clearly overpredicted the measured frequency. Both correlations produced an average percentage error of -1.03% and 17.26% respectively. This is considered a good performance in comparison to the reported in the literature. The averaged absolute

error of Zabaras (2000), Gregory and Scott (1969) andNydal (1991) correlations is 32.41%, 34.12% and 69.28% respectively.

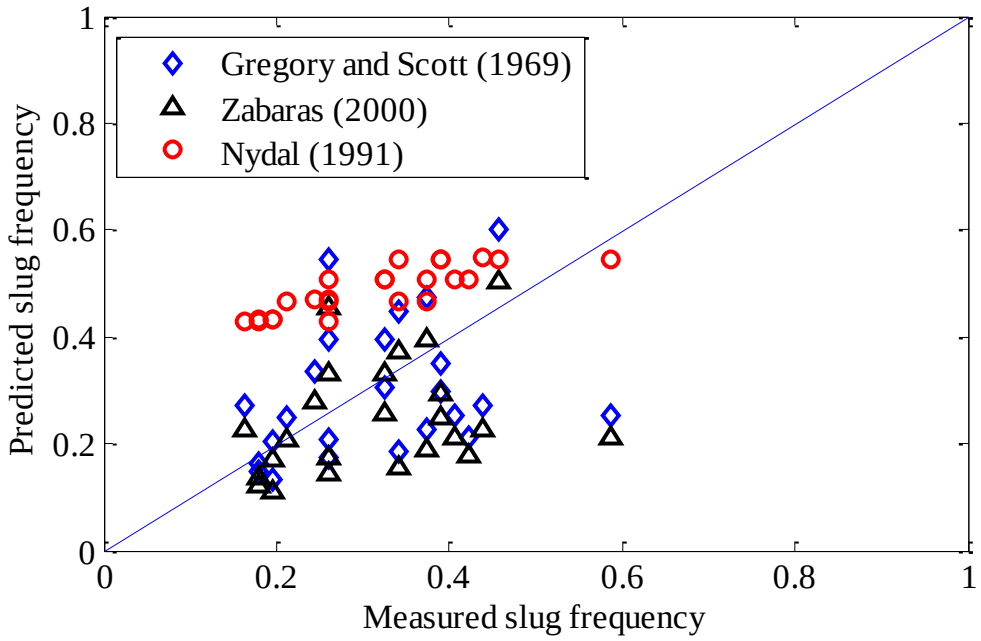


Figure 5-25: prediction of slug frequency at 128D downstream of the bend.

It is expected that the first two correlations should give similar results, since the former is an altered form of the later, except that Zabaras (2000) included the effect of slight inclination on the slug frequency. The Zabaras (2000) and Gregory and Scott (1969) correlations showed a wide fluctuation around the mean of the predicted values, with an average standard deviation of 5.91 and 7.07 respectively. This is directly related to the complex nature of slug frequency.

In general, none of the studied correlations seem to produce a close agreement with the experimental values. This is acceptable since that there is no single correlation that can be applied to all flow conditions. The three applied correlations have considered pipe diameter and liquid flow rate as the main parameters influencing the slug frequency. However each correlation was limited

to a specific flow conditions. Gregory and Scott (1969) correlation was developed for carbon dioxide and water experiments in 20mm ID pipe. The slug frequency was correlated with Froude number, based on the slug velocity at the minimum frequency. Zabaras (2000) used a 399 data point that collected from pipes in the range of 25mm to 200mm ID. Although Zabaras claimed that his correlation gives zero averaged error, his validation included only the same data that was used originally in developing the correlation. In order to develop more general correlation, the parameters that influence the slug frequency should be identified and then the effect of each parameter should be investigated.

The understating of the mechanisms that control slug initiation is essential in estimating the slug frequency. Taitel and Dukler (1977) define the slug frequency as the inverse of the time required for a slug to be formed near the pipe entrance. Therefore, investigating the factors that influence this mechanism is required. Al-Safran (2009a) has recently investigated the effect of the formation mechanism of hydrodynamic and terrain slugging on the frequency of slugs. He considered the slip velocity between gas and liquid phases to be strongly related to slug frequency. The validation of his proposed model against independent experimental data, showed an average percentage error of 43% and absolute average error of 47% with high standard deviation. This is obviously higher than the discrepancy obtained in this work form more simpler correlations. Therefore more work is needed in order to propose more accurate and general correlation. All the independent variables that might affect the frequency of slug should be considered such as; the development length that was neglected in some studies, including (Al-Safran, 2009a).

5.6.4 Void fraction in liquid slug

The void fraction in the liquid slugs (ε_{gSL}) is a critical parameter for anticipating the liquid holdup in the downstream facilities and for predicting pressure drop in the pipe system in oil and gas production. It is also required as an input value for slug flow mechanistic models such as the models developed by Dukler and Hubbard (1975) and Nicholson et al. (1978). Over the past decades, there has been an attempt to develop correlations that are applicable for wide range of flow conditions, yet none of the available correlations in the literature seem to attain success.

Slug aeration is governed by serval mechanisms, a good understanding of the aeration process is critical in predicting the gas holdup within liquid slug. Bubbles are entrapped into the liquid slug from the leading Taylor bubble and detached into the trailing liquid film or Taylor bubble. Bubbles entrainment occurs through; the jet effect at the slug front, the mixing eddies at the mixing region and the leading aerated liquid film (Al-Safran et al., 2015). The relatively fast speed of the slug with respect to the slow moving liquid film results in a jet effect where the film penetrates the slug to a certain distance before it is absorbed. Consequently a highly turbulent region at the front of the slug called mixing region is formed; the length of this region depends on the relative velocity of the slug. Bubbles are entrained due to the high shear rate between the slug front and the leading liquid film and also due to the turbulence circulation. For viscous fluids, bubbles trapped in the liquid film are absorbed by the slug body. Dispersed bubbles are then transferred from the mixing zone into the main body of the slug,

the bubbles size and distribution are related to the dominant forces, either turbulence or viscous, within the slug body.

In this section, the effects of axial flow development, gas superficial velocities and liquid superficial velocities on the void fraction in the liquid slug are investigated. The influence of a vertical to horizontal bend on the void fraction within the slug body is also examined. At last the experimental results are used to validate the available correlations for predicting the void fraction in the liquid slug.

Figure 5-26 illustrates the effect of axial distance on the change in the void fraction within liquid slugs. For a given set of gas and liquid superficial velocities, the void fraction in liquid slugs seems slightly higher at upstream of the bend, particularly at U_{gs}= 0.36 m s^{-1}, and almost constant along the pipeline downstream of the bend. In the case of U_{gs}= 0.36 m s^{-1} the slugs were slightly aerated before the bend and as they passed the bend the liquid was drained down in the horizontal section immediately after the bend and the gas content was mostly released. The slug formed downstream of the horizontal section were less aerated due to the low gas flow and the consequent low interfacial share stress between phases. As the gas flow rate increases the difference in the gas holdup at before and after the bend is reduced. The results indicate that the vertical bend effect is more pronounced at low gas flow rates whereby gravity is dominant in the horizontal section. The change in gas holdup along the horizontal section seems slight and showed a nontangible effect of the pipe length.

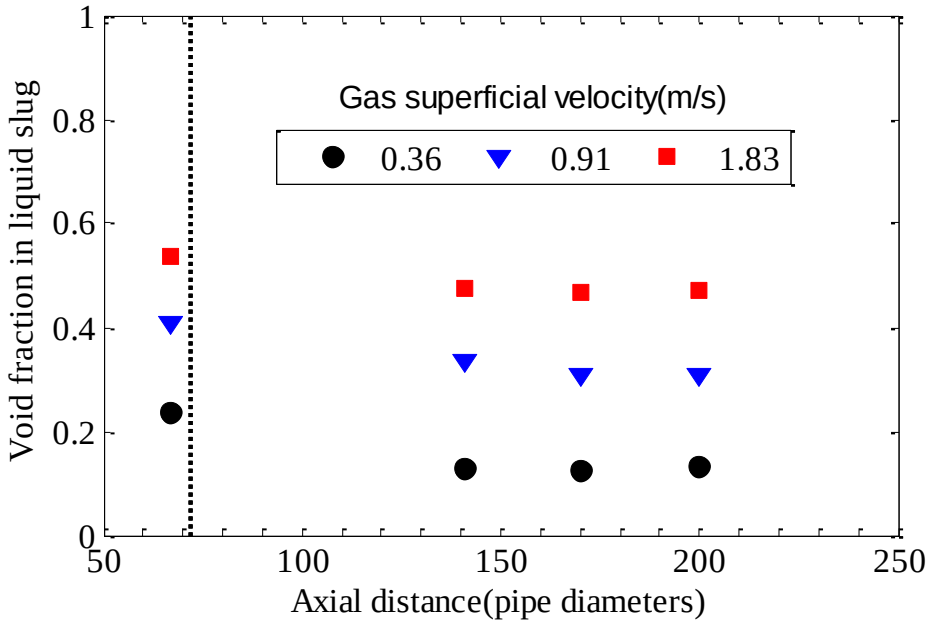


Figure 5-26: Axial development of the void fraction in slug length at the horizontal section, Uls=0.53 m s^{-1}.

The effects of the bend and of flow conditions on the gas void within liquid slugs are presented in Figure 5-27. In all cases the gas hold up of slugs in the vertical section upstream of the bend is higher than that at the horizontal section downstream. This directly related to the effect inclination angle on the velocity of Taylor bubble. The Taylor bubble velocity in the horizontal section is lower than that of the vertical section, and consequently the relative velocity between the liquid film and the slug is lower causing a smaller production rate of bubbles in the this case. This is in accordance with the results of Andreussi and Bendiksen (1989) for air-water flow in slightly inclined (-3° to +5°) pipes.

Felizola and Shoham (1995) and Gomez et al. (2000) examine the effect of inclination angle on the liquid holdup, for wide range of experimental data in the full range of inclination, from horizontal to vertical. They reported that void fraction increases as the inclination angle increase from horizontal to vertical.

Similarly,Barnea et al. (2013) reported strong dependency of gas holdup in liquid slug on the inclination angle ranging from 2° to 90°. The gas holdup increases with the increase of inclination due to the high shear rate between the liquid film and the slug body that causes a higher rate of gas entrainment from the preceding Taylor bubble.

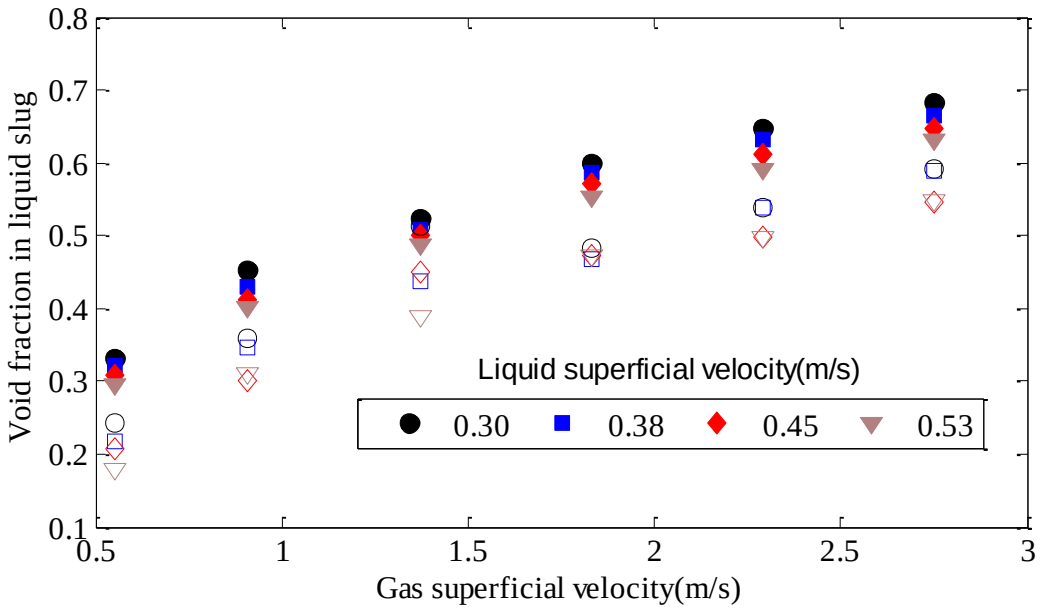


Figure 5-27: Void fraction in liquid slug variation at 5D upstream of the bend (filled symbols) and 128D downstream of the bend (empty symbols).

It is also obvious that the gas content within the slug body increases with the increase of gas superficial velocities, while liquid superficial velocity has an opposite effect. The effect of liquid superficial velocity seems insignificant as reported by (Nydal et al., 1992). At high gas flow rate the ε_{gSL} was almost reached 0.7 which is higher than the value suggested by the theory of maximum gas packing presented by (Brauner and Barnea, 1986). Similar observations reported by Brandt and Fuchs (1989) for large scale experiments of nitrogen-diesel flow at high pressure where a minimum liquid holdup of 0.26 was reported. They argued that maximum packing theory may not be applicable for liquids such

as diesel where frothy highly turbulent mixture of nonhomogeneous bubbles is generated. Indeed this is the case for the current experiments, where smaller bubbles filled the space between slightly larger bubbles within liquid slug.

Figure 5-28 indicates the frothy nature of the liquid slugs in this work, especially at high gas flow rates. It presents the ratio of void fraction between the liquid slug and the film region. As can be seen from the figure that the ratio increases with the increase of gas superficial velocity and it approaches near unity at the highest gas flow rate in these experiments.

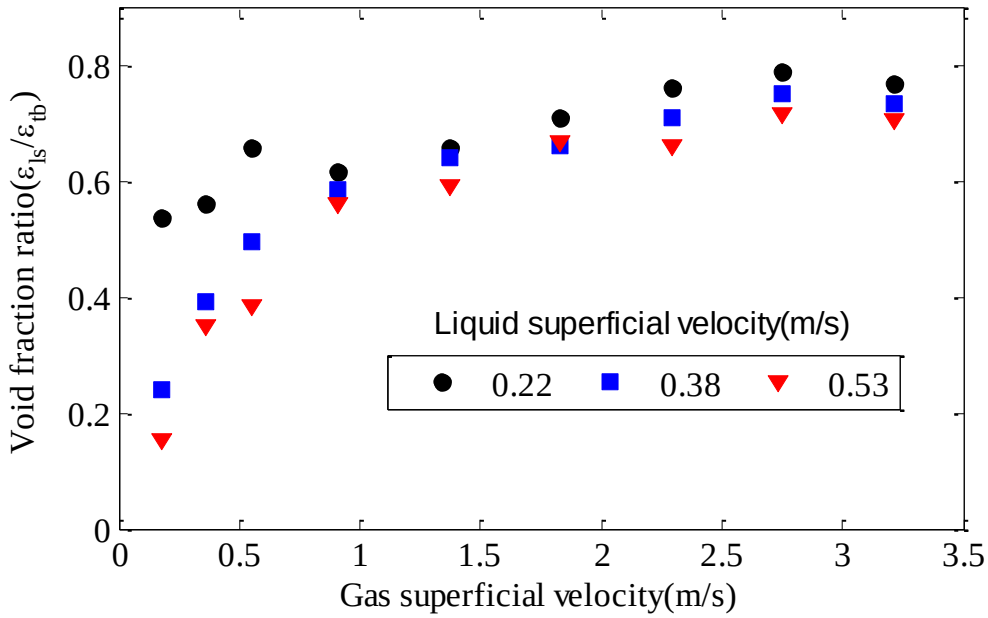


Figure 5-28: Void fraction ratio between liquid slug and Taylor bubble against gas superficial velocities.

The high void fraction in this case is mainly due to the effect of physical properties such as viscosity and surface tension. Nädler and Mewes (1995) experimentally showed that the gas holdup in air-oil flow is higher than in air-water flow. Their experiments were conducted with water and oil of 14 mPa.s and 37 mPa.s viscosity in 59 mm ID pipe. They suggested that the effect of surface

tension and density difference are the main cause of the increase in void fraction. The effect of surface tension on the gas holdup within liquid slugs is also reported by Andreussi and Bendiksen (1989) and Nydal et al. (1992) where gas holdup decreases with the increase of surface tension. The surface tension of oil is lower than water, producing smaller bubbles size in air-silicone oil flows. The smaller bubbles disperse in the body of the slug and take longer time to migrate to the top wall of the pipe which reduces the loss rate of bubbles from the liquid slug and consequently increases the void fraction.

The void fraction in liquid slug was predicted using the available correlations in the literature. Figure 5-29 illustrate the performance of four correlations based on the relative accuracy of the predicted data. Statistical analysis was applied to measure the reliability of the available correlations. The void fraction in liquid slug was poorly underpredicted by (Malnes, 1983; Marcano et al., 1998; Gregory et al., 1978; Andreussi and Bendiksen, 1989) with an average percentage error of -60.28%, -65.86%, -72.67%, and -94.02% respectively. All correlations showed a small deviation from the mean. Indeed, the poor performance of Gregory et al. (1978) was surprising at the beginning, since the correlation was originally developed using experimental data almost similar to this work. Their experiments were conducted in 50mmID pipe with of air and light oil of viscosity and density of 6.7mPa.s and 858kg/m3 respectively. However, this discrepancy was later justified by the difference in the reported void fraction measurements. Gregory et al. data showed maximum void fraction of 0.25 within the range of gas and liquid flow rates of the current work, which is below the half of the value reported in this

work. This should be due to the difference in the measurements techniques used in both studies.

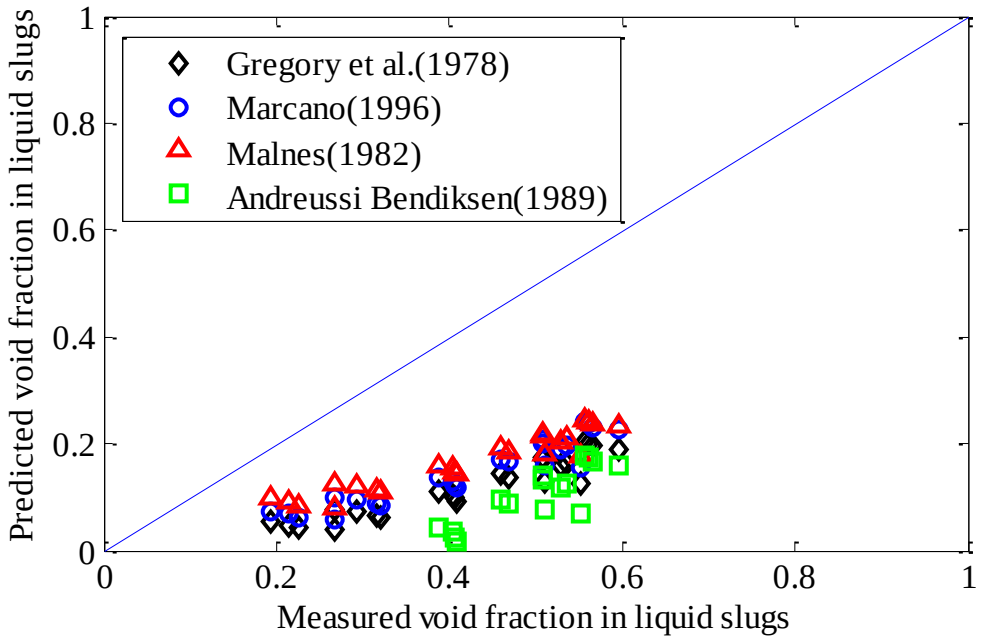


Figure 5-29: Predicted void fraction in liquid slug using the available correlations.

Pereyra et al. (2012) examine the performance of the same correlations based on the measuring technique; there seem to be tangible difference in the relative accuracy for data generated by different devices, though, Gregory et al. (1978) correlation was reported as the best correlation for horizontal pipes. In general, it has been always considered as simple and reasonable reliable correlation for horizontal pipes (Abdul-Majeed, 2000; Al-Safran, 2009b; Pereyra et al., 2012), however, it could be argued that this results are biased by the fact that the Gregory et al. data has always dominated the data bank, with (156 data points) almost 50% of the data used for models validation.

It should be noted that Gregory et al. (1978) and Marcano et al. (1998) correlated the liquid holdup in liquid slugs in term of mixture velocity only, therefore it is

expected that the produce similar results. This absence of physical properties and geometrical effects on the void fraction in liquid slugs may justify the limited accuracy of those models. Malnes (1983) used Gregory et al. data and proposed a correlation as a function of mixture velocity, pipe diameter and liquid properties, however, only a slight improvement is observed in this this work in comparison to Gregorey correlation. It is more likely due to the inherent discrepancy in void fraction data obtained by Gregory in comparison to this work. Andreussi and Bendiksen (1989) presented their correlation as a function of the pipe inclination and diameter, using water as liquid phase. As explained earlier the gas holdup of silicone oil used in this work is much higher than that reported for water. This is due to the difference in viscosity and surface tension that causes the production of smaller bubbles and increase the holdup time of dispersed bubbles with in liquid slug.

The data indicates that the void fraction in liquid slug is a complex slug flow feature that is a function of several independent parameters. The void fraction in liquid slug has been mainly correlated in term of mixture velocity. Several correlations considered the effect of operational conditions, physical properties and pipe geometry, though; they are applicable to a limited range of flow conditions, close to the range used to develop those correlations. None of the reported correlations in the literature can be extended to the entire range of operation conditions. In order to generate a unified model that can overcome the limitation of the current correlations, an enormous data base that includes a vast range of experimental and filed data is required. A great attention should be paid to the measuring techniques used to estimate the gas holdup in liquid slugs, since

different measuring devices cloud produce different results for same flow conditions.

5.7 Summary

Gas-liquid flow experiments were conducted in an open system, in which the air and 5 mPa.s silicone oil flow rates were changed from 0.045 to 3.21 m s^{-1} and 0.15 to 0.53 m s^{-1} respectively. Electrical Capacitance Tomography (ECT) and Wire Mesh Sensor (WMS) were used to provide cross sectional averaged void fraction at upstream and downstream of the bend respectively. The ECT was kept immediately upstream while the WMS was moved at six positions after the bend. The probability density functions (PDF) of the averaged void fraction time series were estimated in order to identify the corresponding flow regime, the results were visually confirmed using high speed camera. The void fraction time series were used to identify the main characteristics of the flow such as; structure velocity and frequency, Taylor bubble velocity, slug length, slug frequency and the void fraction in liquid slugs. The main findings of this work concluded as below:

- For the range of flow rates considered bubbly, cap bubble, slug and churn flows were observed in the vertical riser upstream of the bend while in the horizontal section downstream of the bend slug flow was dominant, in addition to the stratified and plug flows at low gas and liquid flow rates.
- Stratified flow was dominant up to (~40D) downstream of the bend for most of the flow conditions, except at low gas flow rate (< 0.36 m.s^{-1}) and

high liquid flow rate (> 0.22 $m.s^{-1}$) where the liquid level is high enough to bridge the pipe and form either plug or slug flow near the bend.

- Slugs were observed further away from the bend for certain flow conditions (gas superficial velocity > 0.55 $m.s^{-1}$). This might indicate that slug flow is not totally an entrance phenomenon.
- The Flow patterns observed from experiments were compared with those predicted by flow patterns maps. The transitional borders were corrected to the corresponding experimental parameters. All of the observed flow regimes are predicted well, except the wavy flow in the horizontal section which was poorly expected by Mandhane et al. (1974) flow map. This is due to the inherent discrepancy of the data used to generate the original map.
- Liquid slugs are destroyed at the bend and the phases are completely separated shortly downstream. Therefore, the formation of slug in the horizontal section is directly associated with the necessary conditions for slug occurrence in horizontal pipes.
- The velocity of Taylor bubble and liquid slug increases with the increase of gas superficial velocity. The velocity downstream of the bend is lower than the velocity upstream. This is mainly due to the gravity effect in the horizontal section.
- A non-zero drift velocity in horizontal pipes is justified only at low mixture velocity. While at high mixture velocities zero drift velocity should be implemented.

- Slug length increases in the axial direction in both the vertical and horizontal sections. This mainly due to the emerging process of consecutive slug units along the vertical pipe. While in the horizontal pipe the entrainment rate of liquid in front is higher than the shedding rate at the back of the slug. The reported slug length is within the range of stable slugs in both vertical and horizontal sections respectively. Generally, the length of slugs increases with the increase of gas superficial velocity.
- The frequency of liquid slugs decreases along the vertical and horizontal pipes; this is due to the coalescence of slug units and the breakup of liquids slugs in the vertical and horizontal sections respectively. The frequency of liquid slugs downstream of the bend was declined to almost one fifth of the frequency upstream of the bend.
- Void fraction in liquid slug increases with the increase of gas superficial velocity. The gas holdup was higher in the vertical section upstream of the bend in comparison to that of downstream of the bend. Silicone oil showed that surface tension and viscosity have a great influence on the gas holdup in liquid slugs. The void fraction in liquid slugs in these experiments was higher than that predicted by the maximum packing theory.
- The flow development can be achieved in a vertical riser and horizontal section of 68 mm ID within 65 and 128 pipe diameter lengths respectively.
- The flow behaviour at further downstream of the 90° bend, including void fraction and frequency variations, give an indication that the formation of hydrodynamic slugs further downstream of the bend is independent of the inlet conditions at upstream of the bend.

- The majority of the available correlations for predicting slug flow parameters are limited to a certain range of flow conditions. None of these correlations can be generalised for the entire range of operation conditions. Some correlations seemed more reliable such as Nicklin et al. (1962) correlation to estimate the velocity of Taylor bubble, while others have poorly predicted the experimental results such as the correlation proposed for void fraction estimation in the liquid slug. Table 5-1 presents the statistical measures that were used to compare the correlations employed in this work.
- A great and unified effort is needed in order to develop more general correlations that consider all the independent flow variables. A balance between the accuracy and simplicity might be achieved if all sources of possible measurement errors were eliminated.

Table 5-1: The statistical measures for the employed two-phase flow correlations.

Source; Correlation	Pipe (ID); Fluids	Statistical measures		
		APE	AAPE	SD
Nicklin et al. (1962) $u_{gTB} = 1.35(u_{gs} + u_{ls}) + U_d$	26mm Air/water	9.87	11.14	2.5
Gregory and Scott (1969) $U_{gTB} = 1.35U_m$	19mm Carbon dioxide/ water	-7.94	15.07	3.15
Gregory and Scott (1969) $f_s = 0.0226\left[\frac{u_{sl}}{gd}\left(\frac{19.75}{u_m} + u_m\right)\right]$	19mm Carbon dioxide/ water	-1.04	34.12	7.08
Zabaras (2000) $f_s = 0.0226\left[\frac{u_{sl}}{gd}\left(\frac{212.6}{u_m} + u_m\right)\right]^{1.2}[0.836 + 2.75\sin(\Theta)]$	25mm, 100mm air/water	-17.27	32.41	5.92
Nydal (1991) $f_s = 0.088\frac{(u_{ls} + 1.5)^2}{gd}$	53mm, 90mm air/water	68.71	69.28	8.13
Gregory et al. (1978) $\varepsilon_{gSL} = \frac{1}{1 + \left(\frac{u_m}{8.66}\right)^{1.39}}$	51.2mm, 25.8mm air/light oil	-72.67	72.67	0.99
Marcano et al. (1998) $\varepsilon_{gsl} = \frac{1}{(1.001 + 0.0179u_m + 0.0011u_m^2)}$	77.9 mm air/ kerosene	-65.86	65.86	0.99
Malnes (1983) $\varepsilon_{gSL} = 1 - \frac{u_m}{\left[83\left(\frac{g\sigma_{gl}}{\rho_l}\right)^{0.25} + u_m\right]}$	51.2mm, 25.8mm air/light oil	-60.28	60.28	0.75
Andreussi and Bendiksen (1989) $\varepsilon_{gSL} = \frac{Fr_m - F_0}{Fr_m - F_1}$	50mm, 90mm Air/water	-94.02	94.02	3.86

Chapter 6

Experimental characterisation of air-silicone oil slug flow through a horizontal 90° bend

Slug flow is a common occurrence in a broad variety of industrial applications, over a wide range of liquid and gas flow rates. In horizontal pipes, slug flow is characterised by a repeated pattern of aerated liquid surges that is separated by a wavy stratified configuration. It is considered as an intermittent flow pattern that is associated with fluctuations in void fraction, velocity and pressure. The pipeline system in the oil and gas industries consists of risers, horizontal and inclined pipes, in addition to fittings such as bends and T-junctions. This can make slugging phenomenon even more complex and unpredicted. Therefore the occurrence of slug flow, in such pipelines, is a fundamental challenge in terms of the damage that can cause at pipe fittings due vibration and the generation of dryout zones. Moreover, predicting the size of slugs is a crucial factor in equipment designed and control, particularly gas-liquid separators due to the continuous change in the volume of liquid and gas received at the vessel.

Developed slug flow in straight pipes has been the focus of researchers over the past years. In contrast, the effects of obstructions and fittings, such as bends, on the evolution of slug flow have been only investigated in a limited number of

publications. Moreover those publications that considered slug characteristics through bends were mostly conducted in relatively small pipes and with water as the liquid phase. Therefore, this work aims to investigate the influence of a horizontal to horizontal 90° bend on the evolution of slug flow in 68 mm ID pipes. It provides more detailed analysis of slug characteristics before and after the bend in order to evaluate the significance of horizontal bends on flow alteration.

The following sections present detailed experimental results for air-silicone two-phase flows through a horizontal bend. The ECT was located at 5D upstream of the bend, while the WMS was moved at 10D, 40D, 69D and 75D downstream of the bend. The WMS measurements at different locations were done separately, though the repeatability of the measurements at upstream of the test section is justified through random uncertainty analysis and PDF plots, as described in Chapter 3.

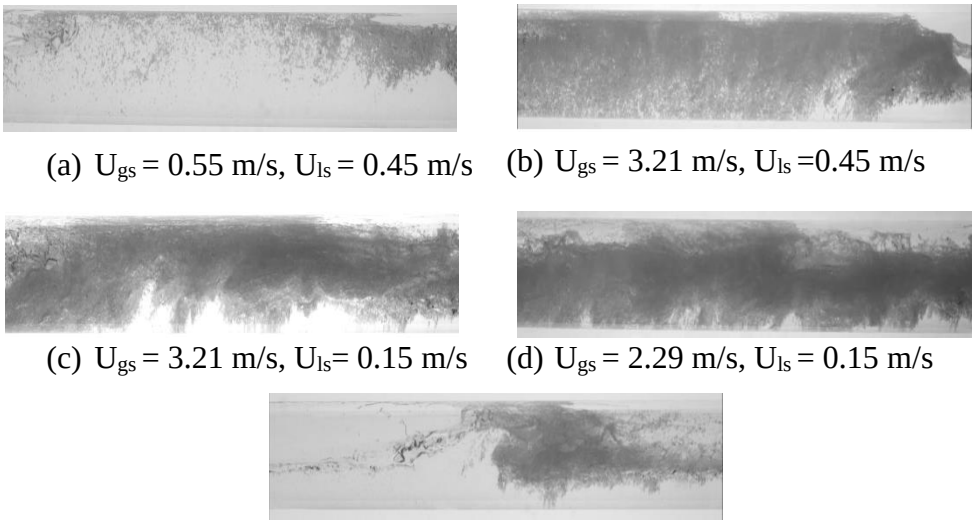
The flow patterns were identified through visual observations with the assistance of high-speed imaging. Slug formation and the required conditions for transition from stratified to slug flow were reported. The void fraction data was used to estimate slug flow characteristics such as slug frequency, slug velocity and gas holdup in liquid slug. The experimental results were used to evaluate the performance of several slug flow correlations; the predictions of those correlations before and after the bend were compared.

6.1 Onset of Hydrodynamic slugging

Hydrodynamic slugging is generated by a growing disturbance of a stratified liquid layer. As the gas flows over a smooth liquid layer at a sufficiently high

velocity, a low pressure zone is generated at any upward perturbation of the interface due to Bernoulli effect. This tends to initiate a suction force that overcomes the stabilising effect of gravity, consequently a wave is formed which can then grow to bridge the pipe and forms a slug. This is widely known as Kelvin-Helmholtz instability, (Taitel and Dukler, 1976).

In this work, hydrodynamic slugging was observed over a range of gas and liquid superficial velocities of 0.36 $m.s^{-1}$ to 3.21 $m.s^{-1}$ and 0.15 $m.s^{-1}$ to 0.53 $m.s^{-1}$ respectively. Disturbance waves and roll waves as described by Hanratty and Hershman (1961) were also observed. Figure 6-1 shows the observed liquid structures.



(a) U_{gs} = 0.55 m/s, U_{ls} = 0.45 m/s (b) U_{gs} = 3.21 m/s, U_{ls} =0.45 m/s

(c) U_{gs} = 3.21 m/s, U_{ls}= 0.15 m/s (d) U_{gs} = 2.29 m/s, U_{ls} = 0.15 m/s

(e) U_{gs}= 2.99 m/s, U_{ls} = 0.15 m/s

Figure 6-1: Slug flow and disturbance waves observed during the experiments.

It was observed that as the air superficial velocity rate increases from 0.55 $m.s^{-1}$ to 3.21 $m.s^{-1}$ at constant liquid flow, the gas holdup in the liquid slug increases (Figure 6-1 a and b). At high gas flow rate and low liquid flow rate a short and foamy slugs were observed similar to the undeveloped slugs described by (Nydal

et al., 1992) (Figure 6-1 c). At similar flow conditions, more waves are observed between successive slugs; including large disturbance waves, and roll waves (Figure 6-1 d and e).

6.1.1 Visual observations

For all liquid flows, as the gas superficial velocity increases, the flow in the horizontal pipe changes from smooth stratified to wavy stratified and then to slug flow. Waves were observed between slugs. The location at which slug flow was initiated ranged from around 5 m (74D) to 4 m (60D) as the liquid superficial velocity increases for a constant gas superficial velocity.Lin and Hanratty (1987b) and Woods and Hanratty (1999) reported that slugs generate closer to the inlet(< 40D) as the liquid superficial velocity increases, for air-water flow in a 76mm ID pipe. They suggested that at high liquid flow slug formation is influenced by the large waves formed near the entry. Lin and Hanratty (1987b) reported that slug forms near the inlet when the liquid level at upstream part of the pipe is higher than that required for the onset of slugging. In this work, the flow after the bend maintained stratified configuration up to L/D > 55, hence the formation of slugs are not expected to be influenced by the inlet conditions.

Slug flow was found to originate directly from long wavelength waves as suggested by Kelvin-Helmholtz instability for low liquid superficial velocity (0.15 $m.s^{-1}$) and gas superficial velocity below 2.29 $m.s^{-1}$. Figure 6-2 illustrates the slug formation mechanism at gas superficial velocity of 1.37 $m.s^{-1}$ and liquid superficial velocity of 0.15 $m.s^{-1}$. Eight consecutive frames are presented with a time interval of 1/60 s where 20 cm of the pipe length is captured. It is worth

mentioning that, the original videos were recorded at time resolution of 2000 frame per second, and then appropriate frames were extracted.

Frames (a) to (d) in Figure 6-2 show how the wave grows in height as it flows from left to right, due to the suction force generated by the pressure variation at the interface. The velocity of the wave increases suddenly during this process. Frame (e) captures the moment at which the wave blocks the pipe cross-section and starts rolling as in frame (f). The entire process occurs rapidly and takes less than a second for the wave to propagate and form a slug.

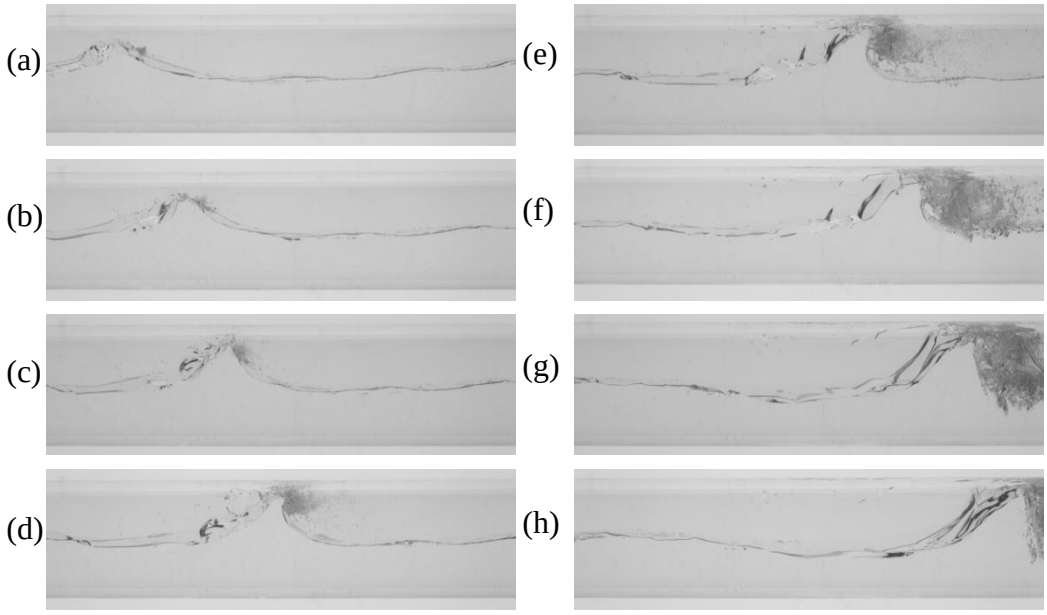


Figure 6-2: Photographs illustrating the onset of a slug at; U_{ls} = 0.15 m.s^{-1}, U_{gs} = 1.37 m.s^{-1}.The direction of the flow from left to right.

Once the wave bridges the cross-section, the liquid layer upstream decreases as in frame (g and h). Further downstream, the originated slug grows in length as more liquid scooped in from the slower downstream liquid layer. This slug mechanism is similar to that reported by Woods and Hanratty (1999) for Froude number below unity. Conversely, Fan et al. (1993) for air-water system of 95 mm ID ,

reported that at gas superficial velocity $\leq$ 3 m.s^{-1}, slug flow forms from short wavelength waves, that double in length as the flow moves downstream, instead of growing directly from long wavelength waves. This could be due to the difference in the nature of the fluids and the size of the pipe used in both experiments. It is reported that the diameter of the pipe influences the critical gas velocity required for slug formation (Lin and Hanratty, 1986; Lin and Hanratty, 1987a).

Another noteworthy observation is reported in Figure 6-3. The figure shows the effect of the generated slugs on the downstream waves. Eight frames are extracted sequentially at a time interval of around 1/100 s, from a high seeped video that captures the flow in a pipe length of around 20 cm. Frames (a and b) illustrate the growth of the wave as it moves downstream from left to right. The wave suddenly jumps to block the pipe, immediately after the initiation of unseen slug from the left side of the frames. Frames (c and d) show the growing wave and the foamy front of the upstream slug. Shortly afterwards the downstream slug propagates further forming a longer liquid bridge while the upstream slug comes to appearance as in (e and f).

It is noticeable that an aerated region is trapped between the upstream slug and the newly formed slug downstream. As the flow propagates downstream, the two slugs are expected to merge. This observation suggests that the formation of slug may influence the wave growth upstream. This is mainly due to a sudden decrease in pressure and consequently an increase in the suction force in the region downstream of the slug.

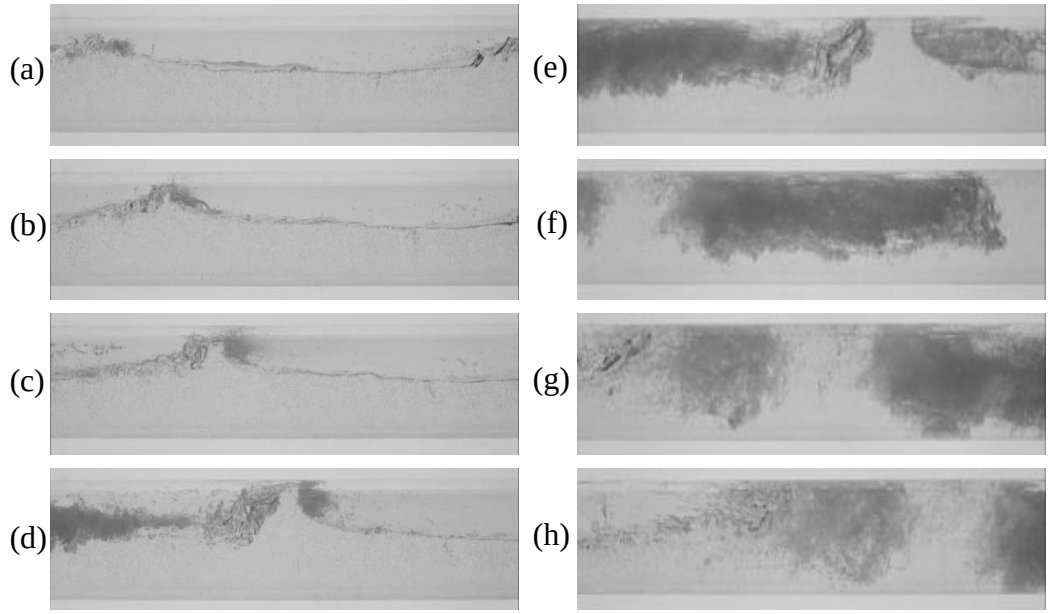


Figure 6-3: Photographs illustrating the onset of a slug at; U_{ls} = 0.45 m.s^{-1}, U_{gs} = 1.37 m.s^{-1}. The direction of the flow from left to right.

At high gas superficial velocities (> 2.29 m.s^{-1}), the slug formation mechanism seems to be similar to that reported by (Lin and Hanratty, 1987b; Andritsos et al., 1989; Fan et al., 1993). The Kelvin–Helmholtz waves are generated over the interface. These waves travel at different velocity and seem to overtake each other and rapidly evolve to form a slug. The 2D gravity waves evolve to a roll wave that is combined with a thinner liquid layer. Therefore, slugs cannot from directly from the growth of the roll wave and the coalescence of consecutive waves is required to supply enough liquid to bridge the pipe (Lin and Hanratty, 1987b). The slugs generated with this mechanism are very fast and highly aerated. It was not easy to capture the whole process due to the high speed of the flow and the limited focal length of the lens, we have at our disposal.

6.1.2 Necessary conditions for slug initiation

The wavy stratified region where the slugs are first formed was estimated using the void fraction matrices from the WMS as explained in Chapter 3. Figure6-4

illustrates the liquid height measurements at liquid superficial velocity of 0.53 $m.s^{-1}$ and four gas superficial velocities of 0.36, 0.91, 1.83 and 2.75 $m.s^{-1}$. The liquid height during the presence of slugs at the measuring sensor is lower than one, due to the gas holdup within the liquid slug. The figure indicates the reduction of liquid layer with the increase of gas superficial velocity from h/D = 0.6 to h/D = 0.3 for Figure6-4 (a) and Figure6-4 (d) respectively. The interface between slugs is smooth at low gas flow rate and becomes wavy as the gas flow increases. The number of slugs decreases with the increase of gas flow, more waves are observed at high gas flow as can be observed in Figure6-4 (d). These measurements were made at 69D from the vertical bend, slightly downstream the location at which slugs are initiated, therefore the axial development measurement is required to evaluate the change of liquid height along the pipe.

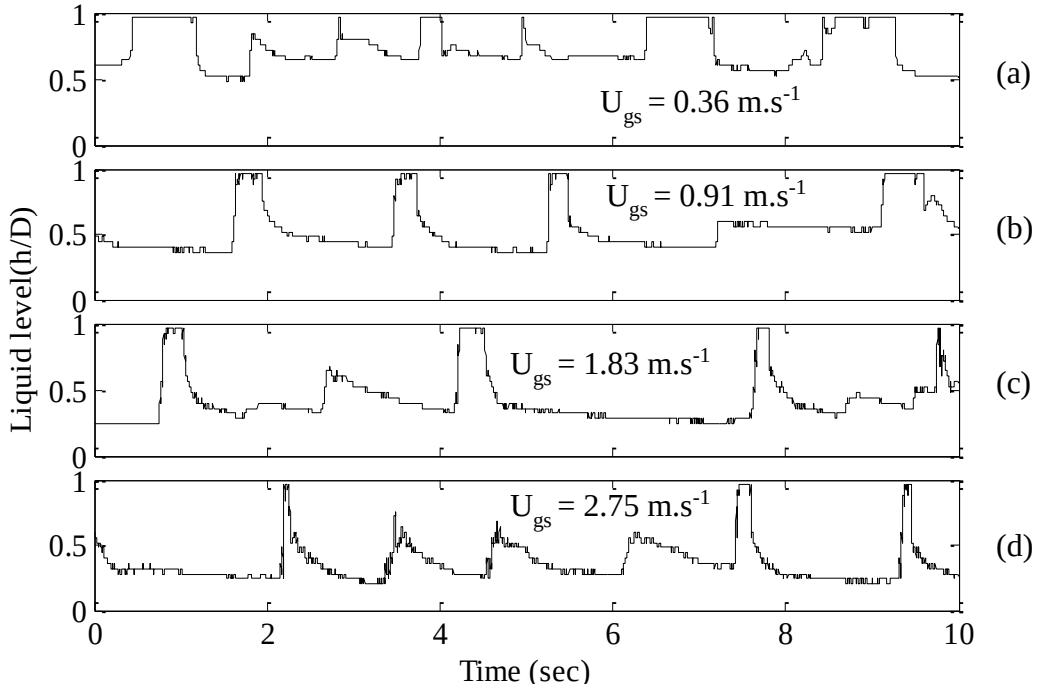


Figure6-4: Liquid height measurements at L/D = 69 and U_{ls} = 0.53 $m.s^{-1}$: (a) U_{gs} = 0.36 $m.s^{-1}$,(b) U_{gs} = 0.91 $m.s^{-1}$, (c) U_{gs} = 1.83 $m.s^{-1}$, (d) U_{gs} = 2.75 $m.s^{-1}$.

Figure 6-5 shows the liquid level measurements at three different locations for gas superficial velocity of 1.37 $m.s^{-1}$ and liquid superficial velocity of 0.53 $m.s^{-1}$. At L/D = 69, the liquid holdup measurements show highly disturbed interface with several waves in-between of slugs. The number of slugs decreases along the pipeline at L/D = 98 and L/D = 128. The disturbance of the interface between successive slugs decreases along the axial direction. This difference can be seen between axial locations of L/D = 69 and L/D = 128. The slug at L/D = 128 is fully developed and the wavy interface is partially absorbed by survived slugs along the axial direction. It is evident that the liquid level notably drops behind passing slugs.

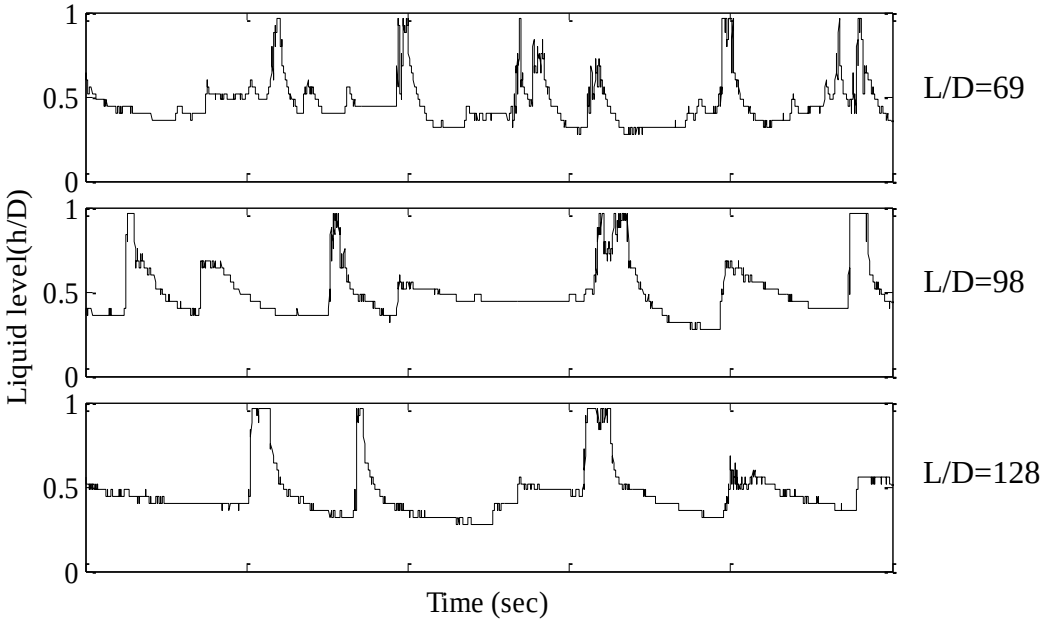


Figure 6-5: Liquid height at three different locations from the vertical 90° bend; U_{gs} = 1.37 $m.s^{-1}$, U_{ls} = 0.53 $m.s^{-1}$.

It is known that slugs decay if the shedding rate of liquid at the back is higher than the pickup rate at the front of the slug. The height of the interface of the stratified flow and the liquid layer behind the slugs is a critical parameter in evaluating the

necessary conditions of slug formation and the development of stable slugs. Figure 6-6 shows the change in the liquid height required to initiate slugs. The average liquid height was identified from the time series of liquid holdup measured at L/D = 69. It is obvious that the liquid height decreases with the increase of gas superficial velocity up to 1.83 $m.s^{-1}$ and then remains almost constant at around 0.4. The liquid superficial velocity has no pronounced effects of the liquid level, although, the liquid level slightly increases with a noticeable increase of liquid flow. The difference in liquid height at low and high gas superficial velocities suggests that slugs are formed by different mechanism as explained earlier. At gas superficial velocity above 2 $m.s^{-1}$, the interface is shallow and aerated. The amount of available liquid is not sufficient for the waves to grow and from slugs. Therefore, the required liquid for transition comes alternatively from coalescence of consecutive waves.

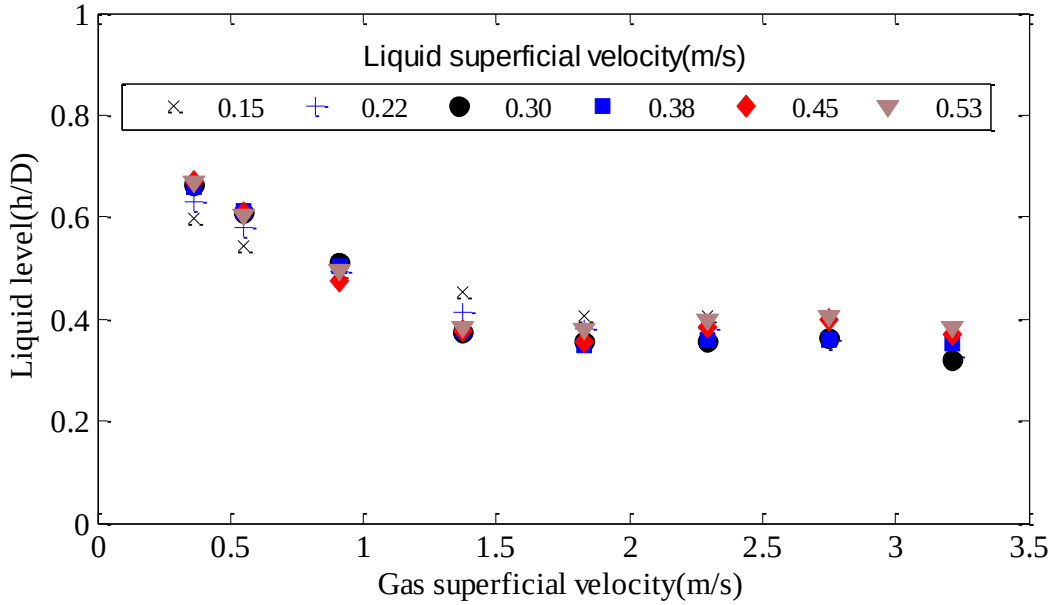


Figure 6-6: The variation of liquid height with the increase of gas superficial velocity at L/D=69.

6.2 Axial flow development

The effect of the horizontal bend on the axial flow development was investigated through measuring the cross-sectional averaged void fraction at several locations before and after the bend. The ECT was located at 5D upstream of the bend while the WMS was relocated at 10D, 40D, 69D and 75D downstream of the bend. The void fraction measurements from both instruments were used to evaluate the flow evolution around the bend.

Slug flow was observed at liquid superficial velocities of 0.15 to 0.53 $m.s^{-1}$ and gas superficial velocities between 0.36 and 3.21 $m.s^{-1}$. At low gas superficial velocities plug and stratified flows were observed. The PDF plots of the cross-sectional void fraction distribution were used to compare the flow behaviour at the different locations with the aid of visual observations and the WMS images as illustrated in Figure 6-7 to Figure 6-10. The blue colour represents liquid phase while the red colour corresponds to the gas phase in the WMS images.

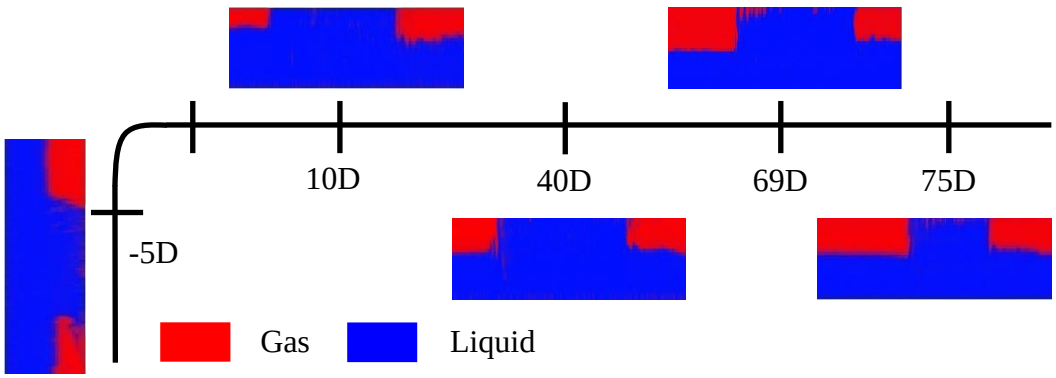


Figure 6-7: Tomographic images from positions along the horizontal pipe system. Liquid superficial velocity = 0.53 m s^{-1} and gas superficial velocity = 0.55 m s^{-1}.

At a low range of gas superficial velocities, slug flow was easily recognised. It is characterised by a slow moving liquid slugs with small gas hold up as shown in Figure 6-7. There was no significant change in the behaviour of the slug body as it

passes through the bend. The PDF plots in Figure 6-8 exhibit similar PDF signature that is associated with conventional slug pattern. More than one slug unit was observed in the pipeline at the same time. Slugs are more likely to grow faster in length along the pipeline at these conditions.

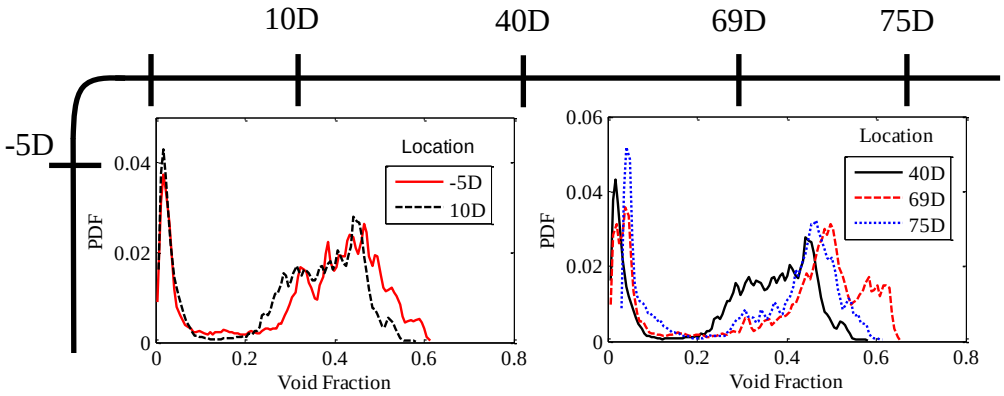


Figure 6-8: Probability Density Function of void fraction time series from positions along the horizontal pipe system. Liquid superficial velocity = 0.53 m s^{-1} and gas superficial velocity = 0.55 m s^{-1}.

At high gas superficial velocities, the formed slugs are highly aerated and travel at high velocity almost equal to the velocity of the gas behind the slugs. Figure 6-9 presents WMS images of the cross-section distribution between phases. Slug originated at high gas flow are hardly distinguished from disturbance waves, particularly in term of PDF plots as can be seen in Figure 6-10. In most cases, only one slug is observed in the pipeline at the time and rarely two slugs may occur sequentially. In contrast, waves become more frequent between slugs, those waves are more likely to break before developing into slugs. The space between consecutive slugs is longer than that of slugs formed at low gas flow rate. As a slug passes, the liquid layer upstream reaches its lowest level. Thus, it takes more time for the liquid height to build up to the required level for slug generation. In

the meantime, the formed waves may contribute to increase the liquid height through coalescence.

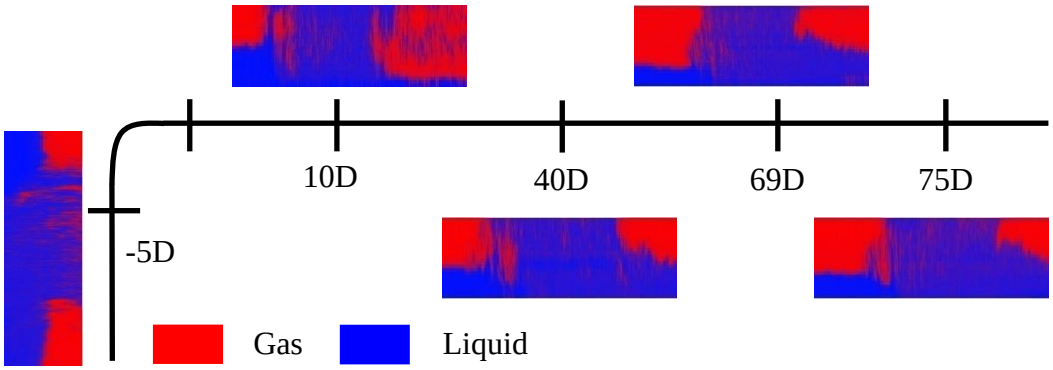


Figure 6-9: Tomographic images from positions along the horizontal pipe system. Liquid superficial velocity = 0.53 m s^{-1} and gas superficial velocity = 3.21 m s^{-1}.

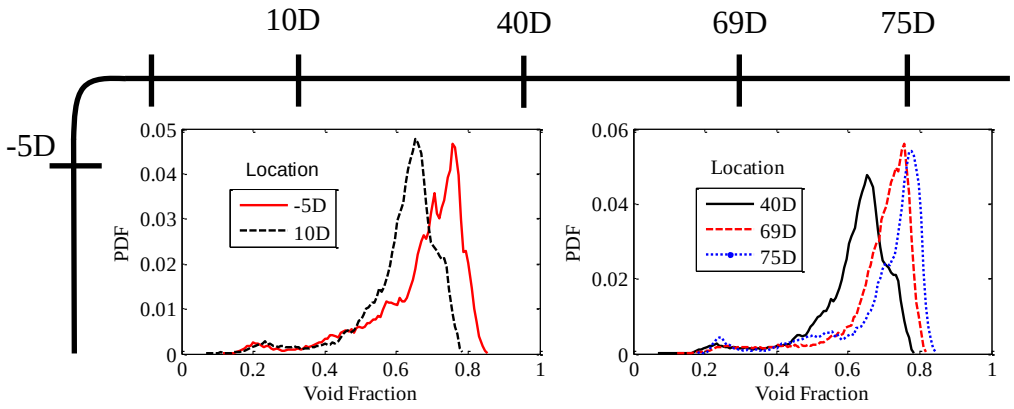


Figure 6-10: Probability Density Function of void fraction time series from positions along the horizontal pipe system. Liquid superficial velocity = 0.53 m s^{-1} and gas superficial velocity = 3.21 m s^{-1}.

Slugs occasionally dissipate before they leave the pipe system. This is mainly caused by the amount of liquid available being lower than that required for stable slugs. Gas superficial velocity is a critical parameter that alters the liquid level at constant liquid flow. The effect of the horizontal bend on the slug formation or breakup is not highly pronounced. Some slugs break up shortly downstream of the bend, while new slugs may be created after the bend. However, this is an irregular process.

6.3 Slug frequency

The frequency of slugs is a critical challenge for the design and operation of downstream facilities in the oil and gas industries. The unstable nature of slug flow is directly characterised by the frequency of liquid slugs or interchangeably its length.

In these experiments, the slug frequency at upstream and downstream of a horizontal bend is estimated in order to evaluate the influence of the bend on the behaviour of liquid slugs at different gas and liquid superficial velocities. The frequency was obtained from the time series of the cross-sectional averaged void fraction using the methods described in Chapter 3.

Figure 6-11 illustrates the change in slug frequency along the pipeline at different gas superficial velocities; the dashed line corresponds to the bend location. The frequency at three locations upstream and four locations downstream of the bend are presented. The clear trend is that frequency of the slug decreases along the axial distance for the upstream positions.

Beyond the bend the frequency seems to be independent of the axial position, particularly at high gas flow, although, at further downstream of the bend the frequency is almost equal to the frequency before the bend. The frequency of slugs also decreases with the increase of gas superficial velocity, however, at high gas flow rate the effect is less obvious and inconsistent.

Slugs are formed at just before the measurement station 69D downstream of the inlet to the horizontal pipe (after the vertical bend), at this positions slugs are not

fully developed. Therefore some of the generated slugs are dissipated along the pipeline upstream of the bend. Slugs that pass through the bend usually persist to the exit of the system. Though it is not always the case, weak slugs vanish shortly after the bend. This is mainly due to the momentum transfer and the energy dissipation at the bend. This effect seems random and insignificant except at high gas flow. Generally, the frequency at before and further downstream of the bend is almost invariant.

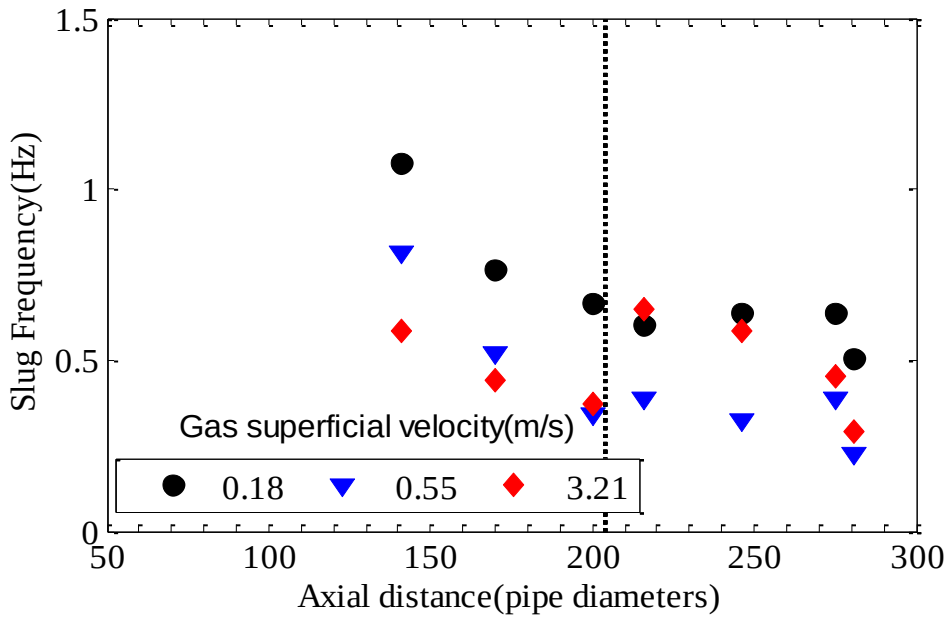


Figure 6-11: Frequency variation against the gas superficial velocity along the pipe system. Liquid superficial velocity=0.45 m s^{-1}.

At gas superficial velocity of 3.21 $m.s^{-1}$, the frequency downstream of the bend appears more arbitrary. The high gas flow is associated with low liquid layer and more waves; subsequently the formation mechanism of slugs is rather complicated. The shallow liquid layer is not sufficient to initiate slugs, although, waves may coalesce before or rarely after the bend and form highly aerated and mostly unstable slugs.

At the horizontal bend the slug frequency experienced a minor change as shown in Figure 6-12. The frequency tends to decrease and then remain constant as the gas superficial velocity increases. An increase in liquid flow rate has a noticeable effect on slug formation, the number of slugs increases with increase of liquid flow rate at constant gas superficial velocity. The frequency decreases slightly after the bend. This small reduction in the frequency after the horizontal bend is a direct consequence of the dissipation of some slugs after the bend, along the pipeline. Occasionally, few developing slugs are destroyed at the bend, due to the direct impact with the outer wall of the bend. It is undoubtedly that the bend enhances the dissipation of the slugs due to momentum transfer and phase separation although, as Figure 6-11 suggested, the change in the axial position of the measurements might be another reason to consider.

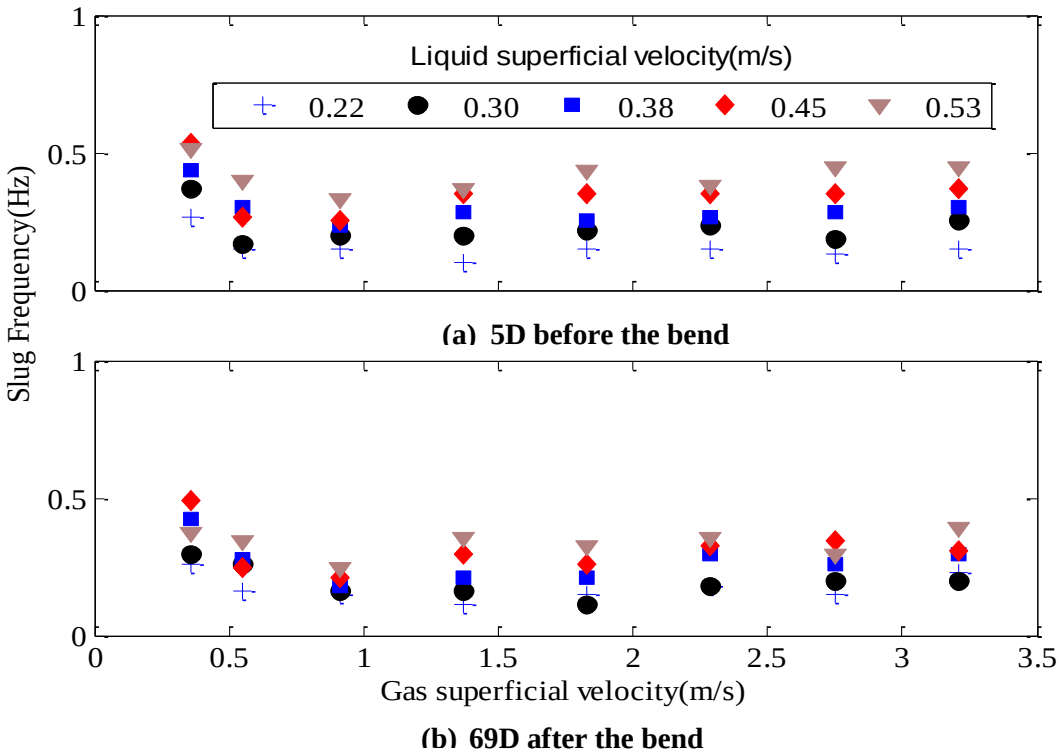


Figure 6-12: Frequency variation at 5D upstream of the bend (a) and 69D downstream of the bend (b).

A precise estimation of the frequency of slugs is highly necessary in most of the industrial processes, in order to avoid oversizing of the downstream equipment. Several empirical correlations and two-phase flow models are developed to predict the frequency of slugs, (Gregory and Scott, 1969; Taitel and Dukler, 1977; Zabaras, 2000), none of which has been shown to apply for all flow conditions.

The accuracy of the available correlation was tested, using the measurements obtained at 5D upstream and 69 downstream of the bend. The performance of Gregory and Scott (1969), Nydal (1991), Zabaras (2000) and Fossa et al. (2003) correlations is presented in Figure 6-13. Most of these correlations are developed from air-water data obtained at various pipe diameters.

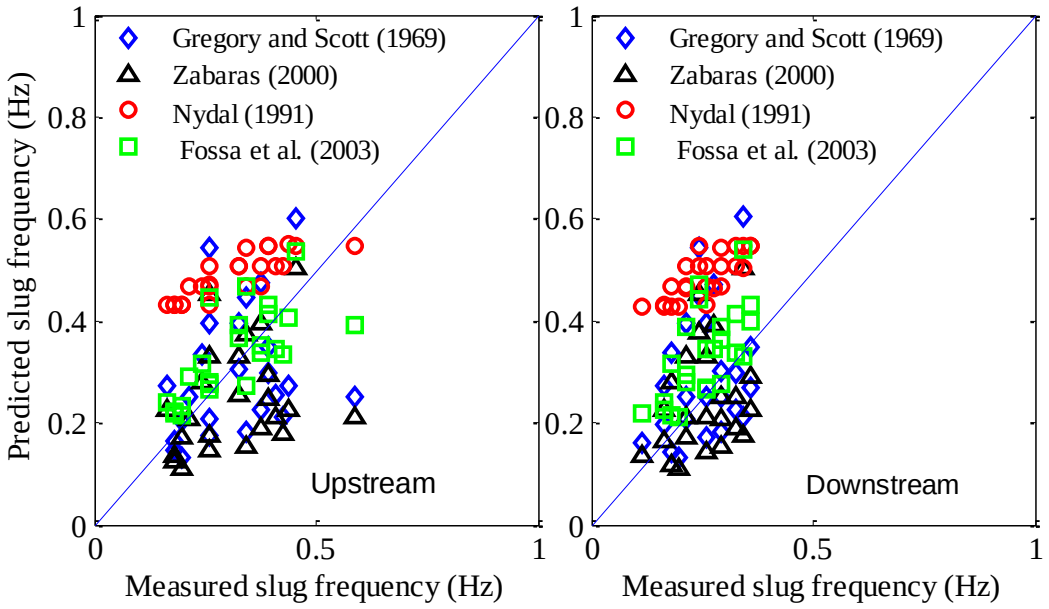


Figure 6-13: Prediction of slug frequency at 5D upstream and 69D downstream of the bend.

The results show a slight difference in the estimated frequency at upstream and downstream of the bend. In general, none of the tested correlations has illustrated a perfect agreement with the experimental results neither before nor after the

bend. However, Fossa et al. (2003) seems to correlate the frequency of slugs with an acceptable uncertainty. Table 6-1 summaries the uncertainty associated with each correlation at upstream and downstream of the bend.

Table 6-1: Statistical results of the slug frequency correlations (top values are for upstream and bottom values are for downstream)

Source; Correlation	Pipe (ID); Fluids	Statistical measures		
		APE	AAPE	SD
Fossa et al. (2003) $St = \frac{f_s D}{u_{gs}} = \frac{0.044 X_L}{1 - 1.71 X_L + 0.70 (X_L)^2}$ $X_L = \frac{u_{ls}}{u_{ls} + u_{gs}}$	40mm' 60mm air/ water	-7.94 13.29	15.07 15.34	3.15 2.29
(Gregory and Scott, 1969) $f_s = 0.0226 \left[\frac{u_{sl}}{gd}\left(\frac{19.75}{u_m} + u_m\right)\right]$	19mm Carbon dioxide/ water	-1.04 20.03	34.12 40.93	7.08 8.85
(Zabaras, 2000) $f_s = 0.0226 \left[\frac{u_{sl}}{gd}\left(\frac{212.6}{u_m} + u_m\right)\right]^{1.2} [0.836 + 2.75 \sin(\Theta)]$	25mm, 100mm air/water	-17.27 0.35	32.41 35.44	5.92 7.40
Nydal (1991) $f_s = 0.088 \frac{(u_{ls} + 1.5)^2}{gd}$	53mm, 90mm air/water	68.71 103	69.28 103.9	8.13 8.54

Table 6-1 shows that the correlation of Nydal (1991) poorly overpredicts the experimental frequency at before and after the bend. All other correlations showed higher average percentage error after the bend. This could be related to the increase in the rate of slug dissipation downstream of the bend, in addition to the immediate destruction of few slugs at the bend.

It was noticed that the frequency is well correlated in term of Strouhal number as suggested first by (Nedderman and Shearer, 1963). Therefore the experimental

frequency at 69D downstream of the bend was presented in term of the dimensionless Strouhal number against liquid volume fraction as reported by Fossa et al. (2003). The parameters associated with the equation of Fossa et al. were slightly adjusted to fit the current results as in eq.(6.1):

$$St = \frac{f_s D}{u_{sg}} = \frac{0.04 X_L}{1 - 1.5 X_L + 0.4 (X_L)^2} \tag{6.1}$$

Figure 6-14 shows a satisfactory agreement between the experimental results and the correlation of Fossa et al. and eq.(6.1), similar findings are reported by (Wang et al., 2007; Abdulkadir et al., 2016).

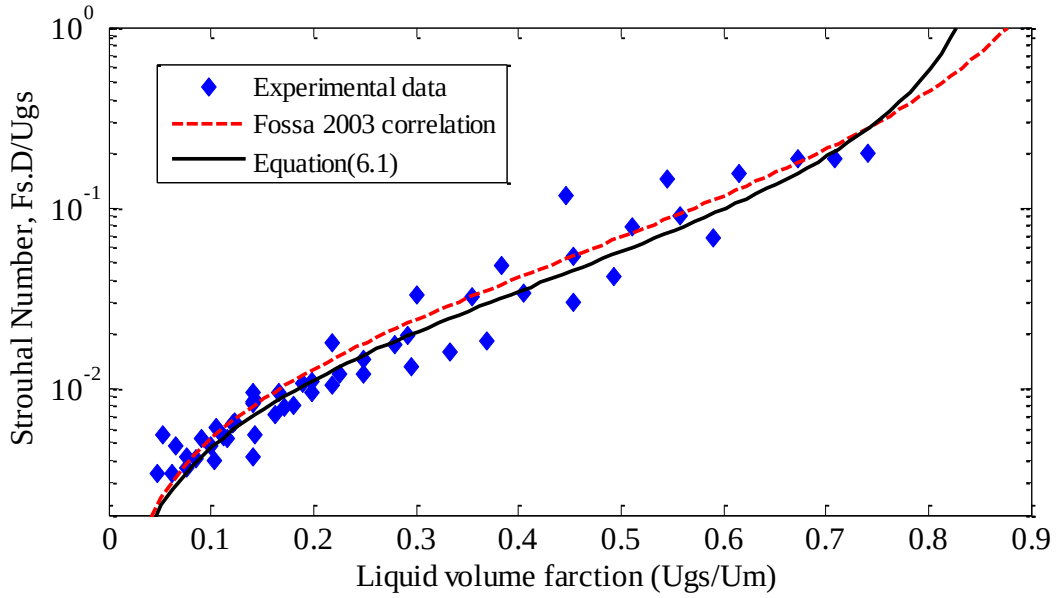


Figure 6-14: Experimental slug frequency at 69D downstream of a horizontal bend is correlated in term of Strouhal number.

The frequency of slugs has been commonly correlated in term of pipe diameter and liquid superficial velocity, where a neglected change with axial position is suggested. This work, in accordance with to (Fossa et al., 2003; Wang et al., 2007; Abdulkadir et al., 2016), indicates the frequency seems to be better correlated in term of Strouhal number as a function of liquid volume fraction. However, this

approach needs to be tested against a wide range of experimental data before a final conclusion can be reached.

It seems that the horizontal bend has a slight influence on the slug frequency in comparison to that of the vertical bend which was reported in the previous chapter. The destruction of low momentum slugs at the bend is the main cause of reduction in frequency at downstream of the bend. The effect of the bend was also evident in the performance of the available frequency correlations.

6.4 Slug bubble velocity

Slug bubble velocity was determined by cross correlating the void fraction time series obtained from the twin-plane ECT sensor. The mean velocity is equal to the distance between the two measuring planes divided by the time delay estimated from the cross-correlation. The ECT was located at 5D upstream of the bend and at 69D downstream of the bend respectively. Repeatable experiments are achievable as discussed in Chapter 3.

The variation of slug bubble velocity with the increase of gas superficial velocity is illustrated in Figure 6-15. The plot shows an expected increase in velocity with the increase of the gas and liquid superficial velocities. Slug bubble velocity encountered a slight increase after the horizontal bend at the low gas superficial velocity, below 1.5 m s^{-1}. This is due to the gas expansion that is caused by the pressure drop after the bend. At high gas superficial velocity, the pressure drop increases across the bend and hence, the velocity of slug bubble notably increases. It is acknowledged that liquid slugs move at velocity equal to the gas velocity upstream while waves and undeveloped slugs travel at velocity almost 30% lower

than the velocity of gas flow (Andritsos et al., 1989). The destruction of some slugs and dissipation of waves at the bend could increase the averaged velocity of slug bubbles predicted experimentally.

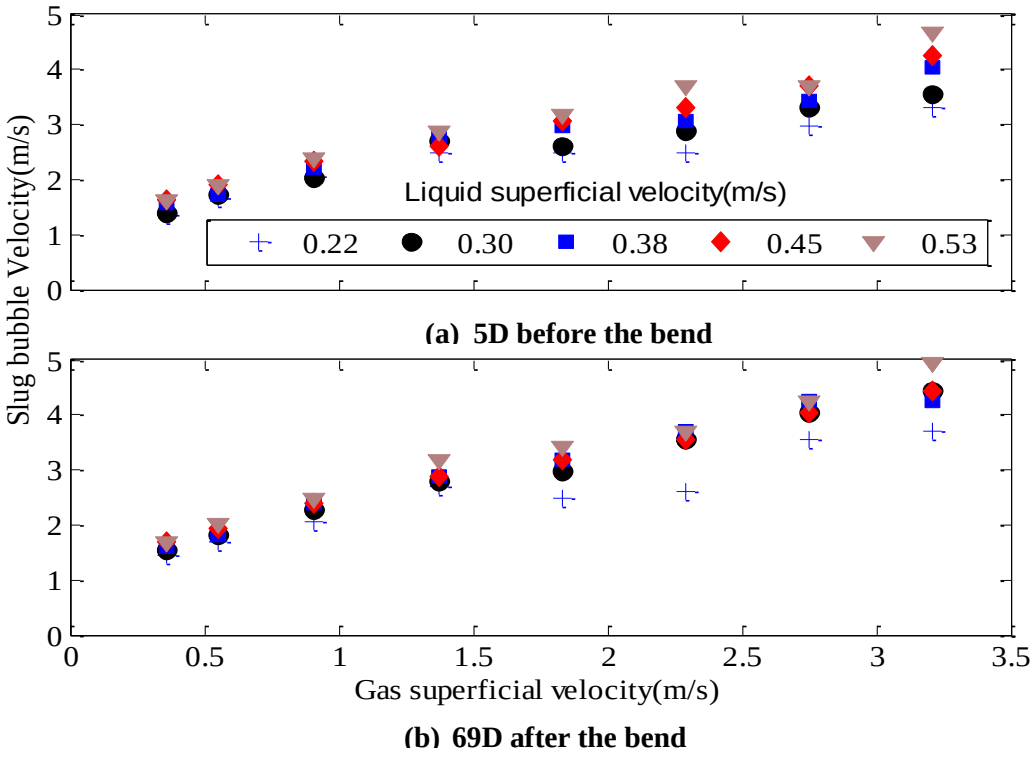


Figure 6-15: Slug bubble velocity variation at 5D upstream of the bend (a) and 69D downstream of the bend (b).

Nicklin et al. (1962) correlation is commonly accepted as the best theoretical estimate of the transitional velocity of slug bubble in continuous slug flow.

$$u_{gTB} = C_0 U_m + U_d \tag{6.2}$$

Where, U_d is the drift velocity, U_m is the mixture velocity and C_0 is the distribution parameter. The value of C_0 is equal to the relative maximum velocity at the nose of the bubble to the mixture velocity(U_{max}/U_m). The value of this parameter varies from 1.2 for fully developed turbulent flow to 2 for laminar flow (Nicklin et al., 1962). The drift velocity is a function of the buoyancy force and

thus, it mainly depends on the inclination angle of the pipe and gas superficial velocity, as it was experimentally shown by (Bendiksen, 1984).

For a horizontal flow a none zero drift velocity is usually considered (Mattar and Gregory, 1974; Nicholson et al., 1978; Weber, 1981), although, several works suggested a negligible drift velocity due to the absence of bouncy in the horizontal configuration (Dukler and Hubbard, 1975; Gregory and Scott, 1969). The drift velocity in horizontal pipe is usually presented as the propagation velocity of an air bubble created by a drained liquid from a horizontal pipe closed at one end (Zukoski, 1966). The widely accepted equation for drift velocity in horizontal pipes is:

$$U_d = 0.54\sqrt{gD} \tag{6.3}$$

The drift velocity of the experimental data is estimated by extrapolating the fitted line of the experimental values to a zero mixture velocity as illustrated in Figure 6-16. The whole range of the measured velocity is fitted with a black dotted line. The intercept represents the drift velocity which was 1.1 and 0.95 for upstream and downstream and can be represented as $1.4\sqrt{gD}$ and $1.16\sqrt{gD}$ respectively. These values are dramatically higher than the reported value for a single bubble in stagnant liquid. This is mainly due to the contribution of small bubbles in the aerated slugs to the velocity of slug bubble, during coalescence (Nydal et al., 1992; Van Hout et al., 2002a).

The drift velocity becomes negligible beyond a Froude number value of 3.5 as reported by (Bendiksen, 1984). Therefore, the drift velocity was estimated using

the experimental values at Froude number below 3.5. The results are represented by the red dotted line as in Figure 6-16. The drift velocity with the imposed conditions was greatly improved to $0.7\sqrt{gD}$ and $0.68\sqrt{gD}$ for upstream and downstream of the bend respectively, however, it is still greater than the theoretical value in eq.(6.3). This is more likely due to the influence of the coalescence with small bubbles from the aerated front and back of slugs which boost the transitional velocity.

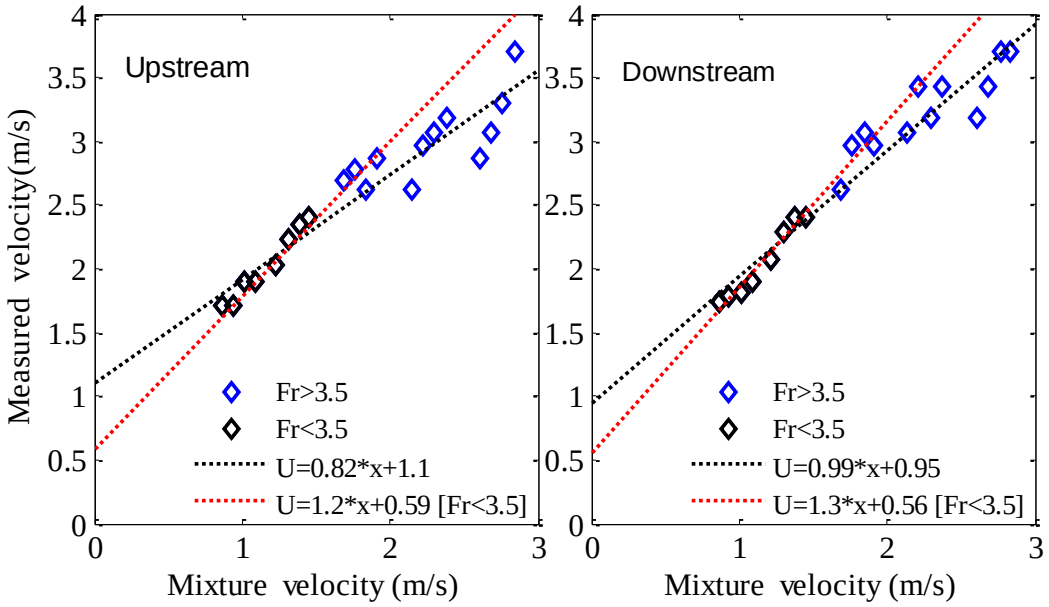


Figure 6-16: Regression analysis on the measured slug bubble velocity at 5D upstream and 69D downstream of the horizontal bend.

The distribution parameter for the horizontal flow reportedly varies from 1.05 to 1.35 (Bendiksen, 1984; Gregory and Scott, 1969). In this work, $C_0 = 1.35$ was used, since it provides the best estimation. Gregory and Scott (1969) and Nicklin et al. (1962) correlations were used for a zero and none zero drift velocity respectively:

$$U_{gTB} = 1.35U_m \tag{6.4}$$

$$U_{gTB} = 1.35U_m + 0.54\sqrt{gD} \tag{6.5}$$

The results for 5D upstream and 69D downstream of the bend are illustrated in Figure 6-17. Similar findings to that discussed in Chapter 5 are obtained, for both upstream and downstream of the bend. Nicklin's correlation demonstrated a better prediction of the transitional velocity of slug bubble, especially at a low Froude number. As the Froude number increases beyond 3.5 the predicted values start to deviate from the measured values. The Gregory and Scott (1969) correlation clearly underestimates the measured values at low gas and liquid velocities while the prediction improves at high mixture velocities. These results are in agreement with the critical Froude number of 3.5 reported by (Bendiksen, 1984). Thus, it could be said that drift velocity should be only considered at low mixture velocity since it approaches zero at high velocities.

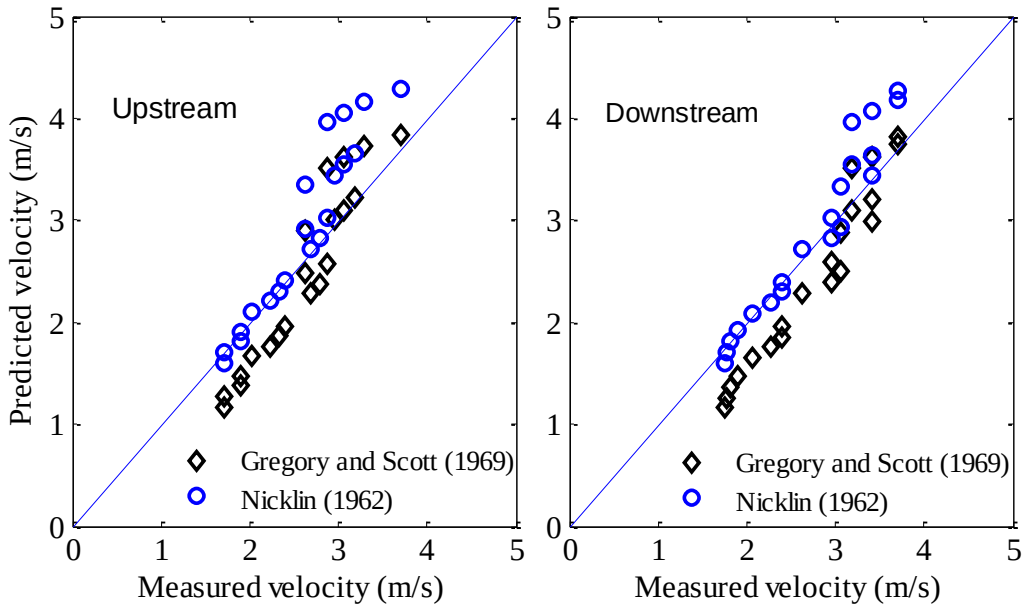


Figure 6-17: Theoretical prediction of the experimental slug bubble velocity at 5D upstream and 69D downstream of the horizontal bend.

The bend seems to have a minor influence on the prediction of both correlations. The performance of Nicklin's correlation was slightly improved from average absolute percentage error of 11.14% before the bend to 6.79% after the bend with standard deviation of 2.5 and 1.63 respectively. Gregory and Scott (1969) showed almost similar accuracy with an average absolute error of 15% for both upstream and downstream of the bend with standard deviation below 3.5.

It seems that the bend influence the drift velocity of the slug bubble. This could be due to the dissipation of some undeveloped and highly aerated slugs at the bend. The gas expansion after the bend is another reason to consider.

In general, the change in slug bubble velocity after the horizontal bend is dramatically smaller than the change at the vertical bend. This is mainly due to the negligible effect of gravity force on the horizontal to horizontal configuration.

6.5 Slug length

Slug length is estimated from the measured residence time of each slug at the sensor and its transitional velocity as detailed in Chapter 3. A uniform velocity profile was assumed along the test section.

The variation of slug length along the axial direction of the flow from upstream to downstream of the bend at different gas superficial velocities is illustrated in Figure 6-18. Slugs at upstream of the horizontal bend are considered to be developed as discussed in Chapter 5. The averaged slug length experienced an insignificant change after the horizontal bend. Although, a small decrease in

length is observed at immediately upstream, the slug length at further downstream is almost equal to that upstream of the bend.

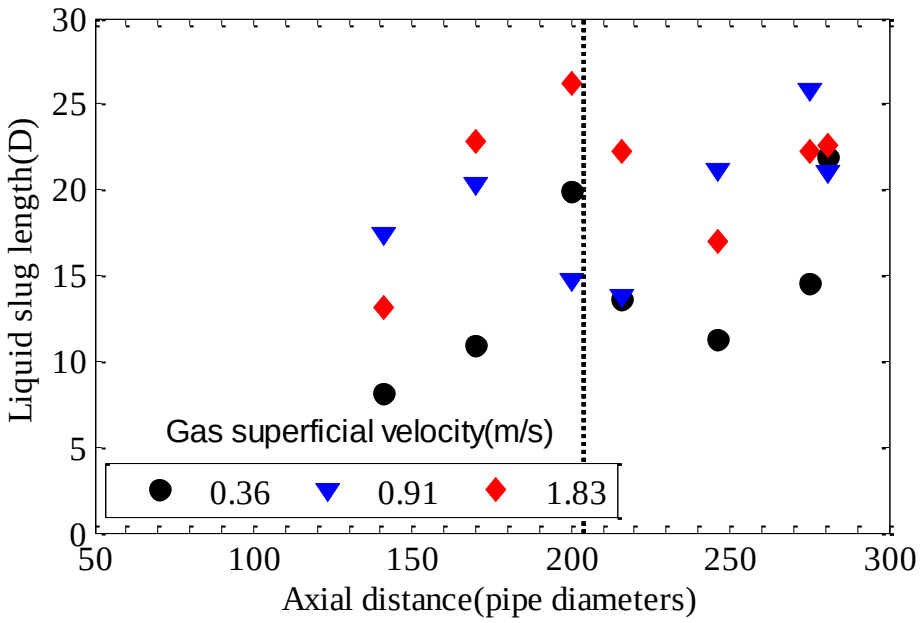


Figure 6-18: The axial development of the mean liquid slug length around the horizontal bend, liquid superficial velocity = 0.45 m.s^{-1}.

The slug velocity is considered constant throughout the test section and it was measured only at 5D upstream and 69D downstream of the bend. Therefore, the change in the slug velocity along the pipe downstream of the bend is highly suspected to be the main cause of the reduction in the length of slug. The acceleration is expected to be higher immediately after the bend than at 69D downstream of the bend since slugs are expected to decelerate further downstream, due to the wall resistance and gravity force. Thus the measured slug length shortly after the bend is expected to be slightly lower than the actual slug length.

The slug length increases as the gas superficial velocity increases, similar observations are reported by (Ferré, 1979; Wang et al., 2006; Losi et al., 2016). At

high gas superficial velocity, the change in slug length seems insignificant. The liquid superficial velocity showed an intangible effect on the slug length, as suggested by (Woods et al., 2006; Nydal et al., 1992).

The averaged slug length at after and before the bend varies from 12D to 30D as shown in Figure 6-19. This is similar to the range of stable slug length that is reported in literature (Dukler and Hubbard, 1975; Nicholson et al., 1978; Barnea and Brauner, 1985; Andreussi and Bendiksen, 1989; Nydal et al., 1992).

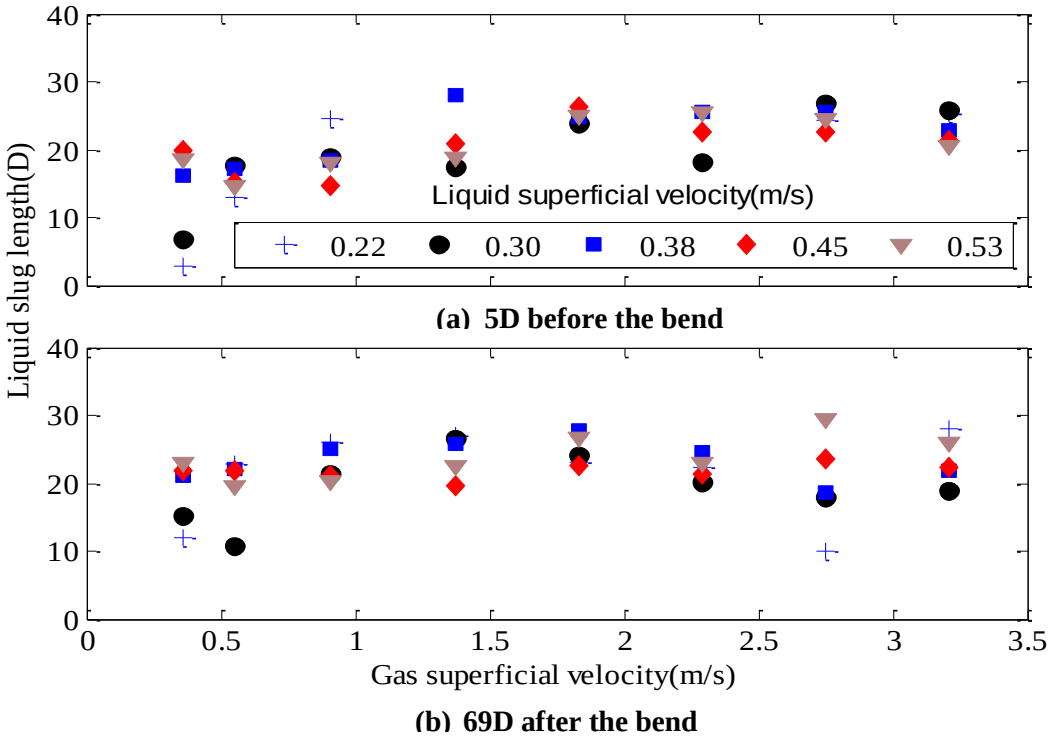


Figure 6-19: Slug length variation at 5D upstream of the horizontal bend (a) and 69D downstream of the horizontal bend (b).

The horizontal bend appears to have a minor effect on the length of slugs passing from upstream to downstream. A slight increase in the average length at 69D upstream is reported. The increase in length after the bend might be related to the destruction of some slugs after the bend which enhances the rate of liquid pickup

and hence growth of the trailing slugs. This agrees with the long-term growth mechanism reported by Scott et al. (1989) for experimental data obtained from sufficiently long pipes of Prudhoe Bay field.

The inconsistency in the trend of the Figure 6-19 is manly related to the intermittent behaviour of liquid slugs as mentioned in chapter 4. It is worth mentioning that discrimination between slugs and disturbance waves becomes harder at high gas flow rate. The body of the slug resembles a foamy structure where the PDF plots signatures of slugs and waves are similar in shape. Therefore, a higher uncertainty is expected at these flow conditions. In addition, the variation of the propagation velocity of slugs downstream of the bend can possibly contribute to the uncertainty of the length estimation.

6.6 Void fraction in liquid slug

The void fraction in liquid slug is used interchangeably to describe the liquid holdup within the body of liquid slugs. It is regularly needed to solve the available slug flow models such as the one suggested by Dukler and Hubbard (1975). The gas is entrained into the liquid slug essentially due to the turbulence caused by the jet effect at the front of the slug. This is essentially caused by the high relative velocity of slugs with respect to the slower downstream liquid layer.

The effect of gas and liquid superficial velocities on the void fraction within liquid slugs is demonstrated in Figure 6-20 and Figure 6-21. The measurements were taken at three positions upstream and four positions downstream of the horizontal bend. Figure 6-20 illustrates that the gas holdup remains almost constant along the pipeline for all gas superficial velocities. At 0.36 $m.s^{-1}$ gas

superficial velocity, the void fraction decreases slightly with axial position upstream of the bend. At low gas flow, the slug moves slowly and has very low gas holdup, thus the entrained bubbles are expected to migrate to the top of the pipe and then escape at the back of the slug.

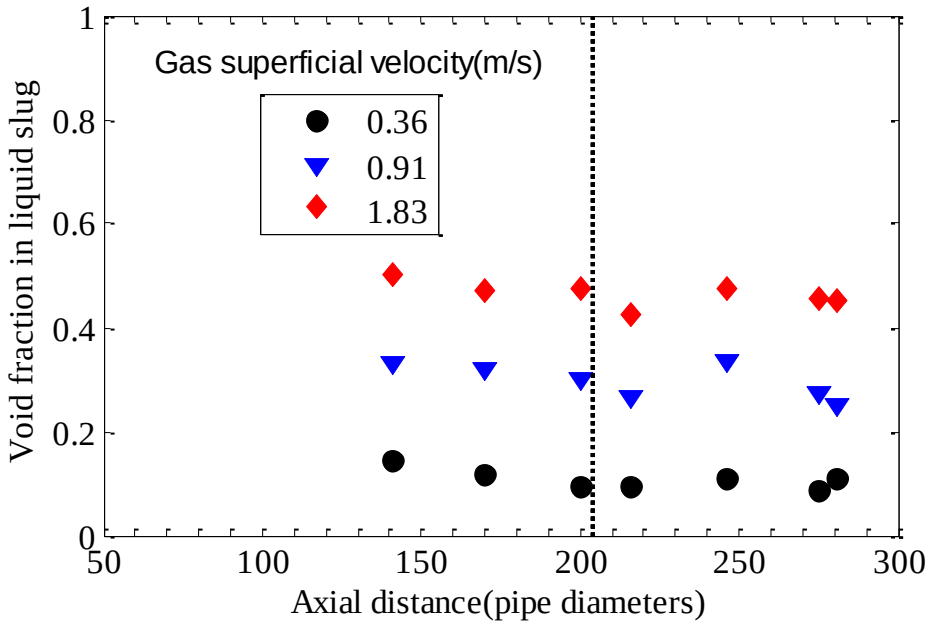


Figure 6-20: Axial development of the void fraction in liquid slug around the horizontal bend. Liquid superficial velocity = 0.45 m.s^{-1}.

As the gas flow increases, the length of the mixing region at the front of the slug increases and the liquid slug becomes highly aerated. The void fraction is expected to increase after the bend due to gas expansion, though; it was only the case at low gas flow rate. In fact, in some cases of high gas flow, the void fraction was slightly higher at upstream of the bend than that of downstream. This is possibly due the random nature of the frequency of slugs after the bend, since few liquid slugs may not persist to the exit of the pipe.

The effect of liquid superficial velocity along the pipeline is illustrated in Figure 6-21. The gas holdup within the liquid slugs seems constant along the axial

positions around the bend. The void fraction within the slugs decreases with the increase of liquid flow rate.

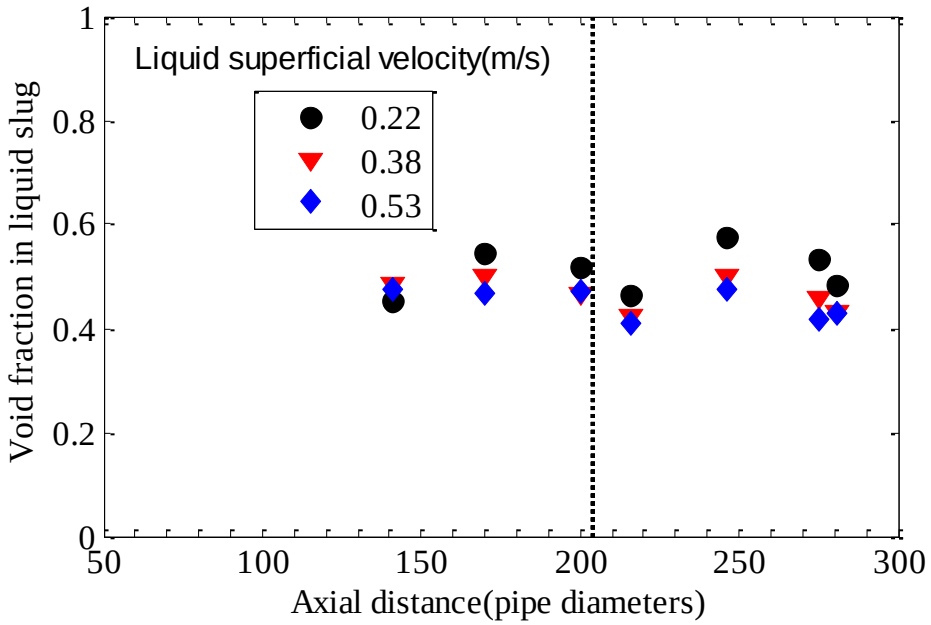
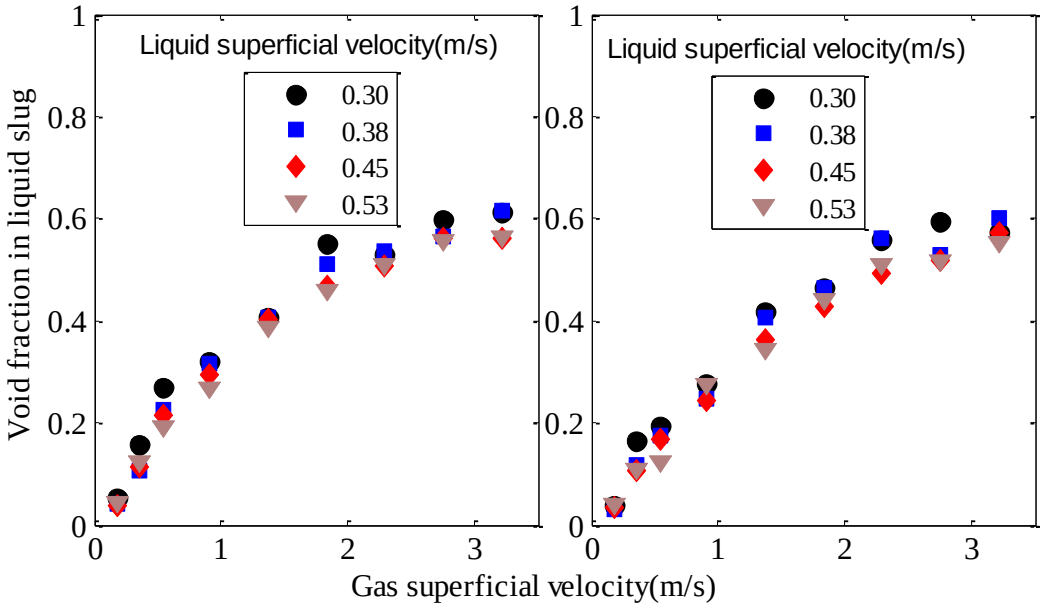


Figure 6-21: Axial development of the void fraction in liquid slug around the horizontal bend. Gas superficial velocity = 1.83 m.s^{-1}.

The effect of the bend on the void fraction within the body of liquid slug was to some extent negligible. The void values at 5D upstream and 69D downstream of the bend was plotted to evaluate the difference as shown in Figure 6-22. It was not possible to plot both cases in one figure since most of the values were overlapping. It is evident that the gas superficial velocity enhances the gas holdup in liquid slugs, this is clearly due to the increase of the slug velocity and hence the turbulence generated at the front of the slug. On the other hand, the increase of the liquid superficial velocity raises the liquid holdup of the slugs. This effect is more tangible at low gas superficial velocities.

The bend has minimal effect on the void fraction. At low gas flow rate (U_{gs} < 0.55 m.s^{-1}), the gas holdup slightly increases after the bend which is mainly due to the

gas expansion associated with energy dissipation and pressure drop at the bend. This observation is in agreement with Silva et al. (1999) for 41 mm ID elbow.



(a) 5D before the bend (b) 69D after the bend

Figure 6-22: Void fraction in liquid slug variation at 5D upstream (a) and 69D downstream (b) of the horizontal bend.

At high gas flow, the undeveloped slug and waves become more frequent at upstream of the bend. The bend has a negligible effect at these conditions. In some cases, the gas holdup in liquid slugs was higher at upstream than that of downstream of the bend. This can be principally due to the dissipation of some slugs and waves at the bend. The undeveloped slugs are more likely to dissipate than the developed slugs, thus the averaged void fraction in liquid slug is expected to decreases after the bend.

The accurate estimation of the liquid holdup, during the conditions of slugging, is critically essential for the sizing and operation of two-phase separators. Several correlations were proposed to predict the void fraction in liquid slug at different

flow conditions. Some of those correlations were used to predict the experimental void fraction of slugs in this work and their performance, around the bend, was evaluate. Figure 6-23 illustrates the performance of the employed correlations at 5D upstream and 69D upstream of the bend.

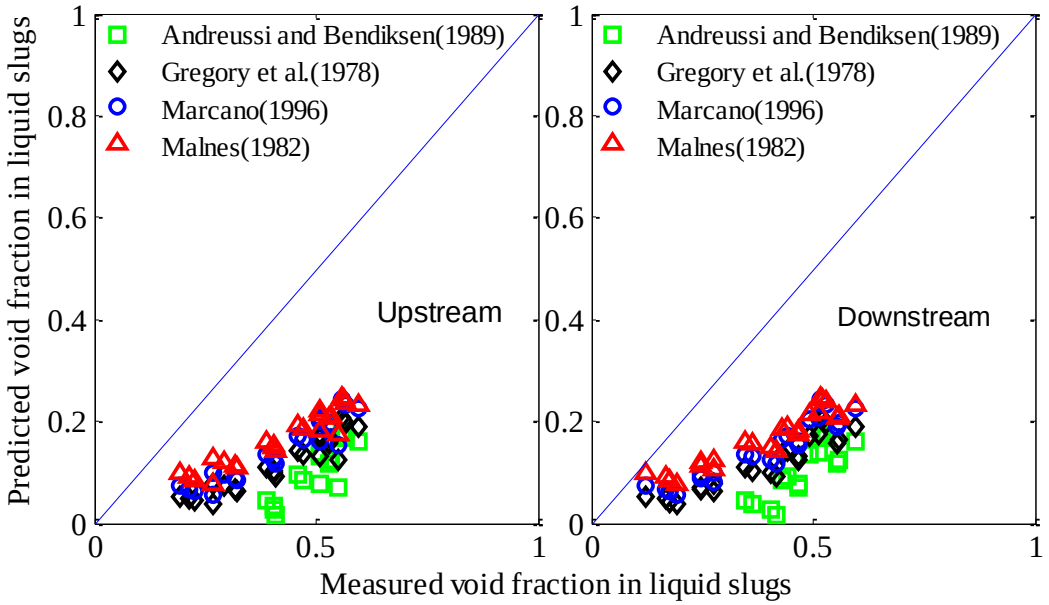


Figure 6-23: Predicted void fraction in liquid slug at 5D upstream and 69D downstream of the horizontal bend, using the available correlations.

None of the applied correlations has shown a close agreement with the experimental results. All correlations have poorly estimated the gas holdup within the liquid slug at upstream and downstream of the bend. The statistical analysis employed to evaluate the performance of the correlation is summarised in Table 6-2. It can be seen from the table that there is no significant change in the relative accuracy of all correlations at before and after the bend.

The reliability of these correlations has been discussed in details in Chapter 5, therefore in this chapter; the comparison between upstream and downstream of the bend is of primary interest. The horizontal bend showed a minor effect on the

gas holdup of liquid slugs. The effect was random and the void fraction was higher at downstream of the bend only at low gas flow rate. The accuracy of the correlations is visibly poor, due to the inherent limitations discussed in Chapter 5. The perdition of the correlation of Malnes (1983) was slightly improved after the bend, this possibly due to the reduction in void fraction after the bend at high gas flow rate as explained earlier.

Table 6-2: Statistical results of the estimated void fraction in liquid slugs (top values are for upstream and bottom values are for downstream)

Source; Correlation	Pipe (ID); Fluids	Statistical measures		
		APE	AAPE	SD
Gregory et al. (1978) $\varepsilon_{gSL} = \frac{1}{1+\left(\frac{u_m}{8.66}\right)^{1.39}}$	51.2mm, 25.8mm air/light oil	-72.67 -60.68	72.67 69.86	0.99 0.93
Marcano et al. (1998) $\varepsilon_{gsl} = \frac{1}{(1.001 + 0.0179u_m + 0.0011u_m^2)}$	77.9 mm air/ kerosene	-65.86 -62.13	65.86 62.13	0.99 0.98
Malnes (1983) $\varepsilon_{gSL} = 1 - \frac{u_m}{\left[83\left(\frac{g\sigma_{gl}}{\rho_l}\right)^{0.25} + u_m\right]}$	51.2mm, 25.8mm air/light oil	-60.28 -55.54	60.28 55.54	0.75 1.11
Andreussi and Bendiksen (1989) $\varepsilon_{gSL} = \frac{Fr_m - F_0}{Fr_m - F_1}$ $Fr_m = \frac{U_m}{\sqrt{gD}}$, $F_0 = 2.6\left(1 - 2\frac{D_0^2}{D^2}\right)$ $F_1 = 2400\left(1 - \frac{\sin\Theta}{3}\right)Bo^{-0.75}$	50mm, 90mm Air/water	-94.02 -95.90	94.02 95.9	3.86 4.62

In general, the effect of momentum transfer and phase separation on the void fraction of liquid slugs at the horizontal bend was clearly lower than that of the vertical bend. The acceleration of the slugs after the bend has not sharply influenced the entrainment of the gas into liquid slugs.

6.7 Summary

A detailed study of slug flow evolution around a horizontal to horizontal 90° bend and downstream was conducted in an open system of 69 mm ID pipes. The axial development of slugs was investigated, in the horizontal sections before and after the bend, using WMS and ECT. The ECT was kept at 5D upstream while the WMS was moved at four positions after the bend. The velocity of the slugs was measured using the ECT at 5D upstream and 69D downstream of the bend. The slug flow was studied at gas and liquid superficial velocities of 0.36 to 3.21 $m.s^{-1}$ and 0.15 to 0.53 $m.s^{-1}$ respectively. The void fraction data was obtained at three locations upstream and four locations downstream of the bend. The time series of the cross-sectional averaged void fraction from both devices was used to characterise the behaviour of slugs around the bend. The main slug features were experimentally estimated including; the slug length and frequency, slug bubble velocity and gas holdup in liquid slug. The experimental results were compared with theoretically estimated values using the available slug flow correlations. A high-speed camera was used to observe the formation and the behaviour of slug flow. The main observations of these experiments are concluded in the following points:

- Slug flow upstream of the bend is mainly generated due to growing waves; as described by the Kelvin-Helmholtz instability. At high gas superficial velocities (> 2.29 $m.s^{-1}$), the liquid layer becomes thinner than the required height to initiate slugs. At these conditions, slugs were evolved from the coalescence of roll waves travelling at different velocities.

- Waves are more frequent at high gas superficial velocity. Slugs formed at high gas flow rates are highly aerated and can be hardly discriminated from disturbance waves.
- Slugs formed at a location closer to the inlet as liquid flow increases at constant gas flow. The formation of slug can influence the growth of upstream waves, due to the sudden change in pressure.
- The necessary liquid height for slug initiation decreases with the increases of gas superficial velocity. It remains constant beyond gas superficial velocity of 2 $m.s^{-1}$. The interface is disturbed at high gas flow and more waves are observed between consecutive slugs.
- At low gas flow, slug flow has a distinctive PDF signature with two peaks one at low void fraction and the other at high void fraction. At high gas flow, the PDF plot of slugs is almost similar in shape to that of disturbance waves.
- The horizontal bend, unlike the vertical bend, has a minor influence on the frequency of liquid slugs. It was observed that the slight reduction in the frequency after the horizontal bend is associated with the breakup of some slugs shortly after the bend.
- The frequency of slugs is well correlated in term of Strouhal number as a function of liquid volume fraction.
- The velocity of slug bubble increases with the increase of gas and liquid superficial velocities. It also experiences a slight change when the two-phase mixture passes through the bend. The slug bubble seems to accelerate after the horizontal bend, possibly due to the gas expansion

caused by the pressure drop at the bend. As the gas superficial velocity increases the effect of the bend becomes more evident.

- The slug length was in the range of developed slug (12D to 30D). The horizontal bend showed an insignificant effect on the length of liquid slugs.
- The void fraction in liquid slug encountered an inconsiderable change around the horizontal bend. The gas holdup is observed to slightly increase after the bend, especially at low gas flows.
- The available correlations of slug flow endorse that the horizontal bend has insignificant effect on the main features of slug flow. In addition, none of the employed correlations has shown a good agreement with the experimental results at after or before the bend.
- The horizontal 90° bends have inconsiderable effects on the behaviour of slugs in comparison to the vertical bends. This is due to that the phase separation and momentum transfer being higher at the vertical bends. The horizontal bend has a minimum influence on the velocity and frequency of the flow structure.

Chapter 7

Conclusion and future wok

7.1 Conclusions

Gas-liquid flow experiments were conducted in an open system that consists of a vertical riser, a vertical upward 90° bend and two horizontal sections with a 90° bend in between. The air and 5 mPa.s silicone oil flow rates were varied from 0.045 $m.s^{-1}$ to 3.21 $m.s^{-1}$ and 0.15 $m.s^{-1}$ to 0.53 $m.s^{-1}$ respectively. A Wire Mesh Sensor (WMS) and Electrical Capacitance Tomography (ECT) were used to provide cross-sectional averaged void fraction at several location along the test sections. At the vertical section, both sensors were placed in series in order to compare their performance and then moved at three axial locations (15D, 30D and 45D) downstream of the mixing section to study the flow development in the riser. To investigate the flow evolution around the vertical upward and the horizontal 90° bends, the ECT was kept immediately (5D) upstream while the WMS was moved at six and four positions downstream of the bend respectively. The dual plane ECT was used to obtain data for velocity measurements at after and before both bends.

The probability density functions (PDF) of the averaged void fraction time series were estimated in order to identify the corresponding flow patterns. Those PDF signatures were justified by visual observations, using high speed imaging. The frequency of the flow structure, mainly slugs, was estimated using the power spectral density (PSD) and the technique developed for disturbance wave as

reported by (Hazuku et al., 2008). The results from both methods were in a good agreement with the manual counting of the major peaks in the time series signal of the cross-sectional averaged void fraction. The structure velocity was obtained by applying the cross-correlation function to the void fraction signal from the twin plane ECT system.

Several flow parameters were estimated from the void fraction data of the WMS and the ECT including cross-sectional averaged void fraction, bubble size distribution, radial void fraction profiles, slug length, slug frequency, void fraction in liquid slugs, and slug bubble velocity. The experimental results were then used to validate the available slug flow correlations.

The main findings of this work are summarised in the following points.

- The ECT system and WMS tomography provide similar mean void fraction data. The WMS offers detailed information about the flow structure, while the ECT system obtains the structure velocity without disturbing the flow. A combination of both can be a powerful measuring tool.
- The vertical 90° bends considerably alert the flow behaviour in comparison to the horizontal bends. This is due to that the phase separation and momentum transfer being higher at the vertical bends. The flow downstream of the vertical bend was mainly stratified or wavy stratified up to (~40D), for most of the flow conditions, while slug flow was initiated at further downstream of the bend. At the horizontal bend the flow was either stratified or slug.

- It can be said that the vertical bend has a significant influence of the flow evolution downstream of the bend. It is apparent that the hydrodynamic formation of slugs downstream of the vertical bend is completely independent of the flow conditions upstream. The horizontal bend has a minimum influence on the velocity and frequency of the flow structure.
- Void fraction in liquid slug increases with the increase of gas superficial velocity. The Void fraction was higher in the riser upstream of the vertical upward bend in comparison to that of downstream of the bend. The void fraction in liquid slug encountered an inconsiderable change around the horizontal bend. The gas holdup is observed to slightly increase after the bend, especially at low gas flows. This might be due to the gas expansion downstream of the bend.
- The velocity of liquid slugs increases with the increase of gas and liquid superficial velocities. It experiences a slight change when the two phase mixture passes through the bends, particularly at low gas superficial velocity. After the vertical bend the structure velocity tends to decrease slightly which could be due to the gravity effects in the horizontal section. On the other hand liquid slugs seem to accelerate after the horizontal bend, possibly due to the gas expansion caused by the pressure drop at the bend.
- Structure frequency encountered a dramatic change after the vertical bend. It was declined to almost one fifth of the frequency upstream of the bend. The frequency of slugs decreases along the vertical and horizontal pipes; this is due to the coalescence of slug units and the breakup of liquids slugs in the vertical and horizontal section respectively. The

horizontal bend, unlike the vertical bend, has a minor influence on the frequency of liquid slugs. It was observed that the slight reduction in the frequency after the horizontal bend is associated with the breakup of some slugs due to the direct impact on the outer wall of the bend.

- The frequency of slugs in the horizontal pipes is well correlated in term of Strouhal number as a function of liquid volume fraction.
- Silicone oil has higher gas holdup than water due to the lower surface tension and relatively higher viscosity. The void fraction in liquid slugs in these experiments was higher than that predicted by the maximum packing theory.
- A non-zero drift velocity in horizontal pipes is justified only at low mixture velocity. While at high mixture velocities zero drift velocity should be implemented.
- Slug flow in the horizontal pipe sections is mainly generated due to growing waves; as described by the Kelvin-Helmholtz instability. At high gas superficial velocities (> 2.29 $m.s^{-1}$), the liquid layer becomes thinner than the required height to initiate slugs. At these conditions, slugs were evolved from the coalescence of roll waves travelling at different velocities.
- The necessary liquid height for slug initiation decreases with the increases of gas superficial velocity. It remains constant beyond gas superficial velocity of 2 $m.s^{-1}$. The interface is disturbed at high gas flow and more waves are observed between consecutive slugs.

- The majority of the available correlations for predicting slug flow parameters are limited to a certain range of flow conditions. This due to that most of the correlations are developed empirically for a limited range of experimental data, where water was mainly the liquid phase.

7.2 Recommendations for future work

The flow rig constructed in this work can be employed to investigate the influence of additional flow parameters on the flow evolution around 90° bends, particularly within slug flow region. A comprehensive study, on gas-liquid flow evolution through bends, has been conducted in this project, though there is still a room for improvements and future work:

- The effect of the curvature radius of the bends can be evaluated using bends with different curvature ratios.
- More viscous fluids can be used in order to examine the effects of the physical properties of the fluids. A wide range of industrial relevant data can be generated.
- Detailed experiments on the pressure drop across bends can be conducted; using the current system. A differential pressure transducer with a suitable pressure range should be used for sensitive response and accurate pressure drop measurements.
- The designed pressure system can be used to accurately identify the liquid slugs. The pressure signals can be used efficiently to discriminate between liquid slugs and Taylor bubbles.

- Since the measurements in this work were not made simultaneously, further work should consider the use of affordable probes that can be located along the pipeline. For instance, developing capacitance ring probes would allow simultaneous measurements of the averaged void fraction. While the current available instruments (ECT and WMS) can offer more detailed information.

BIBLIOGRAPHY

Abdul-Majeed, G. H. (2000). Liquid slug holdup in horizontal and slightly inclined two-phase slug flow. *Journal of Petroleum Science and Engineering,* **27**, 27-32.

Abdulkadir, M. (2011). *Experimental and Computational Fluid Dynamics (CFD) Studies of Gas-Liquid Flow in Bends.* PhD thesis, The University of Nottingham.

Abdulkadir, M., Hernandez-Perez, V., Lowndes, I. S., Azzopardi, B. J. & Sam-Mbomah, E. (2016). Experimental study of the hydrodynamic behaviour of slug flow in a horizontal pipe. *Chemical Engineering Science,* **156**, 147-161.

Abdulkadir, M., Zhao, D., Azzi, A., Lowndes, I. S. & Azzopardi, B. J. (2012). Two-phase air–water flow through a large diameter vertical 180° return bend. *Chemical Engineering Science,* **79**, 138-152.

Abdulkadir, M., Zhao, D., Sharaf, S., Abdulkareem, L., Lowndes, I. S. & Azzopardi, B. J. (2011). Interrogating the effect of 90° bends on air–silicone oil flows using advanced instrumentation. *Chemical Engineering Science,* **66**, 2453-2467.

Akagawa, K. & Sakaguchi, T. (1966). Fluctuation of Void Ratio in Two-Phase Flow : 2nd Report, Analysis of Flow Configuration Considering the Existence of Small Bubbles in Liquid Slugs. *Bulletin of JSME,* **9**, 104-110.

Al-Safran, E. (2009a). Investigation and prediction of slug frequency in gas/liquid horizontal pipe flow. *Journal of Petroleum Science and Engineering,* **69**, 143-155.

Al-Safran, E. (2009b). Prediction of slug liquid holdup in horizontal pipes. *Journal of Energy Resources Technology,* **131**, 023001.

Al-Safran, E., Kora, C. & Sarica, C. (Year). Prediction of liquid volume fraction in slugs in two-phase horizontal pipe flow with high viscosity liquid. *In:* 16th International Conference on Multiphase Production Technology, 2013a. BHR Group.

Al-Safran, E., Kora, C. & Sarica, C. (2015). Prediction of slug liquid holdup in high viscosity liquid and gas two-phase flow in horizontal pipes. *Journal of Petroleum Science and Engineering,* **133**, 566-575.

Al-Safran, E., Sarica, C., Zhang, H. Q. & Brill, J. (2005). Investigation of slug flow characteristics in the valley of a hilly-terrain pipeline. *International Journal of Multiphase Flow,* **31**, 337-357.

Al-Safran, E. M. (2016). Probabilistic modeling of slug frequency in gas/liquid pipe flow using the Poisson probability theory. *Journal of Petroleum Science and Engineering,* **138**, 88-96.

Al-safran, E. M., Gokcal, B. & Sarica, C. (2013b). Investigation and Prediction of High-Viscosity Liquid Effect on Two-Phase Slug Length in Horizontal Pipelines. *SPE Production & Operations,* **28**, 296-305.

Alves, G. F. (1954). Cocurrent Liquid-Gas Flow in a Pipeline Contractor. *Chem. Eng. Progress,* **50**, 449-456.

Andreussi, P. & Bendiksen, K. (1989). An investigation of void fraction in liquid slugs for horizontal and inclined gas—liquid pipe flow. *International Journal of Multiphase Flow,* **15**, 937-946.

Andreussi, P., Minervini, A. & Paglianti, A. (1993). Mechanistic model of slug flow in near-horizontal pipes. *AIChE Journal,* **39**, 1281-1291.

Andreussi, P. & Persen, L. N. (1987). Stratified gas-liquid flow in downwardly inclined pipes. *International Journal of Multiphase Flow,* **13**, 565-575.

Andritsos, N. & Hanratty, T. J. (1987). Interfacial instabilities for horizontal gas-liquid flows in pipelines. *International Journal of Multiphase Flow,* **13**, 583-603.

Andritsos, N., Williams, L. & Hanratty, T. J. (1989). Effect of liquid viscosity on the stratified-slug transition in horizontal pipe flow. *International Journal of Multiphase Flow,* **15**, 877-892.

Azzi, A., Belaadi, S. & Friedel, L. (1999). Two-phase gas/liquid flow pressure loss in bends. *Forschung im Ingenieurwesen,* **65**, 309-318.

Azzi, A. & Friedel, L. (2005). Two-phase upward flow 90° bend pressure loss model. *Forschung im Ingenieurwesen,* **69**, 120-130.

Azzi, A., Friedel, L., Kibboua, R. & Shannak, B. (2002). Reproductive accuracy of two-phase flow pressure loss correlations for vertical 90° bends. *Forschung im Ingenieurwesen,* **67**, 109-116.

Azzopardi, B. J. (2006). *Gas-liquid flows.* Begell House New York.

Azzopardi, B. J., Abdulkareem, L. A., Zhao, D., Thiele, S., da Silva, M. J., Beyer, M. & Hunt, A. (2010). Comparison between Electrical Capacitance Tomography and Wire Mesh Sensor Output for Air/Silicone Oil Flow in a Vertical Pipe. *Industrial & Engineering Chemistry Research,* **49**, 8805-8811.

Azzopardi, B. J., Jackson, K., Robinson, J. P., Kaji, R., Byars, M. & Hunt, A. (2008). Fluctuations in dense phase pneumatic conveying of pulverised coal measured using electrical capacitance tomography. *Chemical Engineering Science,* **63**, 2548-2558.

Baker, G. (2003). *Separation and control of gas-liquid flows at horizontal T-junctions.* University of Nottingham.

Baker, O. (1954). Simultaneous Flow of Oil and Gas. *The oil and gas journal,* **53**, 185-195.

Banerjee, S., Rhodes, E. & Scott, D. S. (1967). Film inversion of cocurrent two-phase flow in helical coils. *AIChE Journal,* **13**, 189-191.

Banowski, M., Beyer, M., Szalinski, L., Lucas, D. & Hampel, U. (2016). Comparative study of ultrafast X-ray tomography and wire-mesh sensors for vertical gas-liquid pipe flows. *Flow Measurement and Instrumentation*.

Barnea, D. & Brauner, N. (1985). Holdup of the liquid slug in two phase intermittent flow. *International Journal of Multiphase Flow,* **11**, 43-49.

Barnea, D., Roitberg, E. & Shemer, L. (2013). Spatial distribution of void fraction in the liquid slug in the whole range of pipe inclinations. *International Journal of Multiphase Flow,* **52**, 92-101.

Barnea, D. & Shemer, L. (1989). Void fraction measurements in vertical slug flow: applications to slug characteristics and transition. *International Journal of Multiphase Flow,* **15**, 495-504.

Barnea, D. & Taitel, Y. (1993). A model for slug length distribution in gas-liquid slug flow. *International Journal of Multiphase Flow,* **19**, 829-838.

Beck, M. S. & Williams, R. A. (1995). *Process tomography: principles, techniques, and applications.* Butterworth-Heinemann.

Beij, K. H. (1938). Pressure Loss For Fluid flow in 90° Pipe Bends. *Journal of Research of the National Bureau of Standards,* **21**, 18.

Benbella, S., Al-Shannag, M. & Al-Anber, Z. A. (2009). Gas–liquid pressure drop in vertical internally wavy 90° bend. *Experimental Thermal and Fluid Science,* **33**, 340-347.

Bendat, J. S. & Piersol, A. G. (1980). *Engineering applications of correlation and spectral analysis.*

Bendat, J. S. & Piersol, A. G. (2011). *Random data: analysis and measurement procedures.* John Wiley & Sons.

Bendiksen, K. H. (1984). An experimental investigation of the motion of long bubbles in inclined tubes. *International Journal of Multiphase Flow,* **10**, 467-483.

Benjamin, T. B. (1968). Gravity currents and related phenomena. *Journal of Fluid Mechanics,* **31**, 209-248.

Berger, S. A., Talbot, L. & Yao, L. S. (1983). Flow in Curved Pipes. *Annual Review of Fluid Mechanics,* **15**, 461-512.

Bhagwat, S. M. & Ghajar, A. J. (2014). A flow pattern independent drift flux model based void fraction correlation for a wide range of gas–liquid two phase flow. *International Journal of Multiphase Flow,* **59**, 186-205.

Brandt, I. & Fuchs, P. (1989). Liquid holdup in slugs: some experimental results from the SINTEF two-phase flow laboratory. *BHRA Multiphase Proceedings, Nice, France*.

Brauner, N. & Barnea, D. (1986). Slug/Churn transition in upward gas-liquid flow. *Chemical Engineering Science,* **41**, 159-163.

Brill, J. P., Schmidt, Z., Coberly, W. A., Herring, J. D. & Moore, D. W. (1981). Analysis of two-phase tests in large-diameter flow lines in Prudhoe Bay field. *Society of Petroleum Engineers Journal,* **21**, 363-378.

Carver, M. B. (1984). Numerical Computation of Phase Separation in Two Fluid Flow. *Journal of Fluids Engineering,* **106**, 147-153.

Carver, M. B. & Salcudean, M. (1986). THREE-DIMENSIONAL NUMERICAL MODELING OF PHASE DISTRIBUTION OF TWO-FLUID FLOW IN ELBOWS AND RETURN BENDS. *Numerical heat transfer,* **10**, 229-251.

Chaplin, G. & Pugsley, T. (2005). Application of electrical capacitance tomography to the fluidized bed drying of pharmaceutical granule. *Chemical Engineering Science,* **60**, 7022-7033.

Chisholm, D. (1967). *Pressure losses in bends and tees during steam-water flow*. National Engineering Laboratory.

Chisholm, D. (Year). Prediction of pressure drop at pipe fittings during two-phase flow. *In:* Proceedings of the 13th International Congress on Refrigeration, 1971. 781.

Chisholm, D. (1980). Two-phase flow in bends. *International Journal of Multiphase Flow,* **6**, 363-367.

Costigan, G. & Whalley, P. B. (1997). Slug flow regime identification from dynamic void fraction measurements in vertical air-water flows. *International Journal of Multiphase Flow,* **23**, 263-282.

Da Silva, M., Schleicher, E. & Hampel, U. (2007). Capacitance wire-mesh sensor for fast measurement of phase fraction distributions. *Measurement Science and Technology,* **18**, 2245.

Da Silva, M. J., Thiele, S., Abdulkareem, L., Azzopardi, B. J. & Hampel, U. (2010). High-resolution gas–oil two-phase flow visualization with a capacitance wire-mesh sensor. *Flow Measurement and Instrumentation,* **21**, 191-197.

Das, S. K., Biswas, M. N. & Mitra, A. K. (1991). Friction factor for gas-non-newtonian liquid flow in horizontal bends. *The Canadian Journal of Chemical Engineering,* **69**, 179-187.

Davies, R. M. & Taylor, G. (1950). The Mechanics of Large Bubbles Rising through Extended Liquids and through Liquids in Tubes. *Proceedings of the Royal Society of London A: Mathematical, Physical and Engineering Sciences,* **200**, 375-390.

De Oliveira, P. M., Strle, E. & Barbosa Jr, J. R. (2014). Developing air–water flow downstream of a vertical 180° return bend. *International Journal of Multiphase Flow,* **67, Supplement**, 32-41.

Dean, W. R. (1927). XVI. Note on the motion of fluid in a curved pipe. *Philosophical Magazine Series 7,* **4**, 208-223.

Dukler, A. E. & Hubbard, M. G. (1975). A model for gas-liquid slug flow in horizontal and near horizontal tubes. *Industrial & Engineering Chemistry Fundamentals,* **14**, 337-347.

Dukler, A. E., Moalem Maron, D. & Brauner, N. (1985). A physical model for predicting the minimum stable slug length. *Chemical Engineering Science,* **40**, 1379-1385.

Dumitrescu, D. T. (1943). Strömung an einer Luftblase im senkrechten Rohr. *ZAMM - Journal of Applied Mathematics and Mechanics / Zeitschrift für Angewandte Mathematik und Mechanik,* **23**, 139-149.

Dyakowski, T., Jeanmeure, L. F. C. & Jaworski, A. J. (2000). Applications of electrical tomography for gas–solids and liquid–solids flows — a review. *Powder Technology,* **112**, 174-192.

Eustice, J. (1910). Flow of water in curved pipes. *Proceedings of the Royal Society,* **84**, 107-118.

Eustice, J. (1911). Experiments on stream-line motion in curved pipes. *Proceedings of the Royal Society of London. Series A,* **85**, 119-131.

Fabre, J. (2003). Gas-Liquid Slug Flow. *In:* Bertola, V. (ed.) *Modelling and Experimentation in Two-Phase Flow*. Springer Vienna.

Fan, Z., Lusseyran, F. & Hanratty, T. J. (1993). Initiation of slugs in horizontal gas-liquid flows. *AIChE Journal,* **39**, 1741-1753.

Felizola, H. & Shoham, O. (1995). A Unified Model for Slug Flow in Upward Inclined Pipes. *Journal of Energy Resources Technology,* **117**, 7-12.

Fernandes, R. C. (1981). *Experimental and theoretical studies of isothermal upward gas-liquid flows in vertical tubes.* PhD, University of Houston.

Fernandes, R. C., Semiat, R. & Dukler, A. E. (1983). Hydrodynamic model for gas-liquid slug flow in vertical tubes. *AIChE Journal,* **29**, 981-989.

Ferré, D. (1979). Ecoulements Diphasiques à poches en conduite horizontale. *La Houille Blanche*, 378-381.

Fitzsimmons, D. E. (1964). Two-phase pressure drop in piping components. General Electric Co. Hanford Atomic Products Operation, Richland, Wash.

Fossa, M., Guglielmini, G. & Marchitto, A. (2003). Intermittent flow parameters from void fraction analysis. *Flow Measurement and Instrumentation,* **14**, 161-168.

Gardner, G. C. & Neller, P. H. (1969). Phase Distributions in Flow of an Air-Water Mixture round Bends and past Obstructions at the Wall of a 76-mm Bore Tube. *Proceedings of the Institution of Mechanical Engineers, Conference Proceedings,* **184**, 93-101.

Gomez, L. E., Shoham, O. & Taitel, Y. (2000). Prediction of slug liquid holdup: horizontal to upward vertical flow. *International Journal of Multiphase Flow,* **26**, 517-521.

Gopal, M., Kaul, A. & Jepson, W. (1995). Mechanisms contributing to enhanced corrosion in three phase slug flow in horizontal pipes.

Gregory, G. A., Nicholson, M. K. & Aziz, K. (1978). Correlation of the liquid volume fraction in the slug for horizontal gas-liquid slug flow. *International Journal of Multiphase Flow,* **4**, 33-39.

Gregory, G. A. & Scott, D. S. (1969). Correlation of liquid slug velocity and frequency in horizontal cocurrent gas-liquid slug flow. *AIChE Journal,* **15**, 933-935.

Grenier, P., Fabre, J. & Fagundes Netto, J. (Year). Slug flow in pipelines: recent advances and future developments. *In:* BHRG Multiphase Production Technology Proceedings, 1997. Cannes, France.

Greskovich, E. J. & Shrier, A. L. (1972). Slug frequency in horizontal gas-liquid slug flow. *Industrial & Engineering Chemistry Process Design and Development,* **11**, 317-318.

Griffith, P. & Snyder, G. A. (1964). The bubbly-slug transition in a high velocity two phase flow. Cambridge, Mass.: MIT Division of Sponsored Research,[1964].

Hamad, F. A., He, S., Khan, M. K. & Bruun, H. H. (2013). Development of kerosene–water two-phase up-flow in a vertical pipe downstream of A 90° bend. *The Canadian Journal of Chemical Engineering,* **91**, 354-367.

Hammer, E. A. (1983). *Three-component flow measurement in oil/gas/water mixtures using capacitance transducers.* PhD, University of Manchester.

Hanratty, T. J. & Hershman, A. (1961). Initiation of roll waves. *AIChE Journal,* **7**, 488-497.

Hazuku, T., Takamasa, T. & Matsumoto, Y. (2008). Experimental study on axial development of liquid film in vertical upward annular two-phase flow. *International Journal of Multiphase Flow,* **34**, 111-127.

Hernandez-Perez, V., Abdulkadir, M. & Azzopardi, B. (2010). Slugging frequency correlation for inclined gas–liquid flow. *World Acad. Sci., Eng. Technol,* **6**, 44-51.

Hewitt, G. F. & Hall-Taylor, N. (1970). *Annular two-phase flow.* (Pergamon Press, Oxford).

Hewitt, G. F. & Jayanti, S. (1993). To churn or not to churn. *International Journal of Multiphase Flow,* **19**, 527-529.

Hewitt, G. F. & Roberts, D. (1969). Studies of two-phase flow patterns by simultaneous X-ray and flash photography. ATOMIC ENERGY RESEARCH ESTABLISHMENT HARWELL (ENGLAND).

Heywood, N. I. & Richardson, J. F. (1979). Slug flow of air—water mixtures in a horizontal pipe: Determination of liquid holdup by γ-ray absorption. *Chemical Engineering Science,* **34**, 17-30.

Hibiki, T. & Ishii, M. (2003). One-dimensional drift-flux model and constitutive equations for relative motion between phases in various two-phase flow regimes. *International Journal of Heat and Mass Transfer,* **46**, 4935-4948.

Hsu, L.-C., Chen, I. Y., Chyu, C.-M. & Wang, C.-C. (2015). Two-phase pressure drops and flow pattern observations in 90° bends subject to upward, downward and horizontal arrangements. *Experimental Thermal and Fluid Science,* **68**, 484-492.

Huang, S. (1986). *Capacitance transducers for concentration measurement in multi-component flow processes.* University of Manchester, Institute of Science and Technology.

Huang, S., Plaskowski, A., Xie, C. & Beck, M. (1989). Tomographic imaging of two-component flow using capacitance sensors. *Journal of Physics E: Scientific Instruments,* **22**, 173.

Huang, S., Stott, A., Green, R. & Beck, M. (1988). Electronic transducers for industrial measurement of low value capacitances. *Journal of Physics E: Scientific Instruments,* **21**, 242.

Huang, S., Xie, C., Beck, M., Thorn, R. & Snowden, D. (1992). Design of sensor electronics for electrical capacitance tomography. *IEE Proceedings G (Circuits, Devices and Systems),* **139**, 83-88.

Huang, Z., Wang, B. & Li, H. (2003). Application of electrical capacitance tomography to the void fraction measurement of two-phase flow. *Instrumentation and Measurement, IEEE Transactions on,* **52**, 7-12.

Isaksen, Ø. (1996). A review of reconstruction techniques for capacitance tomography. *Measurement Science and Technology,* **7**, 325.

Ito, D., Prasser, H. M., Kikura, H. & Aritomi, M. (2011). Uncertainty and intrusiveness of three-layer wire-mesh sensor. *Flow Measurement and Instrumentation,* **22**, 249-256.

Itō, H. (1987). Flow in curved pipes. *JSME international journal: bulletin of the JSME,* **30**, 543-552.

Jayanti, S. & Hewitt, G. F. (1992). Prediction of the slug-to-churn flow transition in vertical two-phase flow. *International Journal of Multiphase Flow,* **18**, 847-860.

Johnson, I. D. (1987). *Method and apparatus for measuring water in crude oil*. United States patent application 4,644,263. Feb. 17, 1987.

Jones, O. C. & Zuber, N. (1975). The interrelation between void fraction fluctuations and flow patterns in two-phase flow. *International Journal of Multiphase Flow,* **2**, 273-306.

Khatib, Z. & Richardson, J. (1984). Vertical co-current flow of air and shear thinning suspensions of kaolin. *Chemical engineering research and design,* **62**, 139-154.

Kim, S., Kojasoy, G. & Guo, T. (2010). Two-phase minor loss in horizontal bubbly flow with elbows: 45° and 90° elbows. *Nuclear Engineering and Design*, **240**, 284-289.

Kim, S., Park, J. H., Kojasoy, G. & Kelly, J. M. (2006). Local Interfacial Structures in Horizontal Bubbly Flow with 90-Degree Bend. The ASME Foundation, Inc., Three Park Avenue, New York, NY 10016-5990 (United States).

Kim, S., Park, J. H., Kojasoy, G., Kelly, J. M. & Marshall, S. O. (2007). Geometric effects of 90-degree Elbow in the development of interfacial structures in horizontal bubbly flow. *Nuclear Engineering and Design*, **237**, 2105-2113.

Kipping, R., Brito, R., Scheicher, E. & Hampel, U. (2016). Developments for the application of the Wire-Mesh Sensor in industries. *International Journal of Multiphase Flow*, **85**, 86-95.

Kirkup, L. & Frenkel, R. B. (2006). *An Introduction to Uncertainty in Measurement: Using the GUM (Guide to the Expression of Uncertainty in Measurement).* Cambridge University Press.

Kora, C., Sarica, C., Zhang, H.-q., Al-Sarkhi, A. & Al-Safran, E. (Year). Effects of high oil viscosity on slug liquid holdup in horizontal pipes. *In:* Canadian Unconventional Resources Conference, 2011. Society of Petroleum Engineers.

Legius, H. J. W. M., van den Akker, H. E. A. & Narumo, T. (1997). Measurements on wave propagation and bubble and slug velocities in cocurrent upward two-phase flow. *Experimental Thermal and Fluid Science,* **15**, 267-278.

Lin, P.-Y. (1985). *Flow regime transitions in horizontal gas-liquid flow.* PhD, University of Illinois at Urbana-Champaign.

Lin, P. Y. & Hanratty, T. J. (1986). Prediction of the initiation of slugs with linear stability theory. *International Journal of Multiphase Flow*, **12**, 79-98.

Lin, P. Y. & Hanratty, T. J. (1987a). Detection of slug flow from pressure measurements. *International Journal of Multiphase Flow,* **13**, 13-21.

Lin, P. Y. & Hanratty, T. J. (1987b). Effect of pipe diameter on flow patterns for air-water flow in horizontal pipes. *International Journal of Multiphase Flow,* **13**, 549-563.

Lizarraga-Garcia, E., Buongiorno, J., Al-Safran, E. & Lakehal, D. (2017). A broadly-applicable unified closure relation for Taylor bubble rise velocity in pipes with stagnant liquid. *International Journal of Multiphase Flow*, **89**, 345-358.

Losi, G., Arnone, D., Correra, S. & Poesio, P. (2016). Modelling and statistical analysis of high viscosity oil/air slug flow characteristics in a small diameter horizontal pipe. *Chemical Engineering Science,* **148**, 190-202.

Lucas, D., Beyer, M., Szalinski, L. & Schütz, P. (2010). A new database on the evolution of air–water flows along a large vertical pipe. *International Journal of Thermal Sciences,* **49**, 664-674.

Lucas, D., Krepper, E. & Prasser, H. M. (2005). Development of co-current air–water flow in a vertical pipe. *International Journal of Multiphase Flow,* **31**, 1304-1328.

Malnes, D. (1983). Slug flow in vertical, horizontal and inclined pipes. *Tech. Rep. IFE/KR/E-83/002 Rev. 1987*. Institute for Energy Technology.

Mandal, S. N. & Das, S. K. (2001). Pressure Losses in Bends during Two-Phase Gas−Newtonian Liquid Flow. *Industrial & Engineering Chemistry Research,* **40**, 2340-2351.

Mandhane, J. M., Gregory, G. A. & Aziz, K. (1974). A flow pattern map for gas—liquid flow in horizontal pipes. *International Journal of Multiphase Flow,* **1**, 537-553.

Manera, A., Ozar, B., Paranjape, S., Ishii, M. & Prasser, H. M. (2009). Comparison between wire-mesh sensors and conductive needle-probes for measurements of two-phase flow parameters. *Nuclear Engineering and Design,* **239**, 1718-1724.

Mansouri, A., Arabnejad, H., Karimi, S., Shirazi, S. A. & McLaury, B. S. (2015). Improved CFD modeling and validation of erosion damage due to fine sand particles. *Wear,* **338–339**, 339-350.

Mao, Z.-S. & Dukler, A. E. (1985). Rise velocity of a Taylor bubble in a train of such bubbles in a flowing liquid. *Chemical Engineering Science,* **40**, 2158-2160.

Mao, Z.-S. & Dukler, A. E. (1991). The motion of Taylor bubbles in vertical tubes—II. Experimental data and simulations for laminar and turbulent flow. *Chemical Engineering Science,* **46**, 2055-2064.

Mao, Z. S. & Dukler, A. E. (1993). The myth of churn flow? *International Journal of Multiphase Flow,* **19**, 377-383.

Marcano, R., Chen, X., Sarica, C. & Brill, J. (Year). A study of slug characteristics for two-phase horizontal flow. *In:* International Petroleum Conference and Exhibition of Mexico, 1998.

Mattar, L. & Gregory, G. (1974). Air-oil slug flow in an upward-inclined pipe-I: Slug velocity, holdup and pressure gradient. *Journal of Canadian Petroleum Technology,* **13**, 69-76.

Mazhar, H., Ewing, D., Cotton, J. S. & Ching, C. Y. (2014). Mass Transfer in Single Bends Under Annular Two Phase Flow Conditions. *Journal of Heat Transfer,* **136**, 043001-043001.

Mazumder, Q. H. (2012). CFD Analysis of Single and Multiphase Flow Chracteristics in Elbow. *Engineering,* **04**, 210-214.

Miwa, S., Mori, M. & Hibiki, T. (2015). Two-phase flow induced vibration in piping systems. *Progress in Nuclear Energy,* **78**, 270-284.

Mohamad, E. J., Rahim, R. A., Rahiman, M. H. F., Ameran, H. L. M., Muji, S. Z. M. & Marwah, O. M. F. (2016). Measurement and analysis of water/oil multiphase flow using Electrical Capacitance Tomography sensor. *Flow Measurement and Instrumentation,* **47**, 62-70.

Moissis, R. & Griffith, P. (1962). Entrance Effects in a Two-Phase Slug Flow. *Journal of Heat Transfer,* **84**, 29-38.

Morgado, A. O., Miranda, J. M., Araujo, J. D. P. & Campos, J. B. L. M. (2016). Review on vertical gas-liquid slug flow. *International Journal of Multiphase Flow,* **85**, 348-368.

Mori, K., Kaji, M., Miwa, M. & Sekoguchi, K. (1999). Interfacial structure and void fraction of liquid slug for upward gas–liquid two-phase slug flow. *Two Phase Flow Modelling and Experimentation. Edizioni ETS, Pisa*.

Nädler, M. & Mewes, D. (1995). Effects of the liquid viscosity on the phase distributions in horizontal gas-liquid slug flow. *International Journal of Multiphase Flow*, **21**, 253-266.

Nedderman, R. M. & Shearer, C. J. (1963). The motion and frequency of large disturbance waves in annular two-phase flow of air-water mixtures. *Chemical Engineering Science*, **18**, 661-670.

Nicholson, M. K., Aziz, K. & Gregory, G. A. (1978). Intermittent two phase flow in horizontal pipes: Predictive models. *The Canadian Journal of Chemical Engineering*, **56**, 653-663.

Nicklin, D. J., Wilkes, J. O. & Davidson, J. F. (1962). Two-phase flow in vertical tubes. *Transaction of Institution of Chemical Engineers*, **40**, 61-68.

Norris, L. (1982). Correlation of Prudhoe Bay Liquid Slug Lengths and Holdups Including 1981 Large Diameter Flow Line Tests. *Exxon Production Research Co., Houston, TX*.

Nydal, O. J. (1991). *An Experimental Investigation on Slug Flow*. PhD Thesis, University of Oslo.

Nydal, O. J., Pintus, S. & Andreussi, P. (1992). Statistical characterization of slug flow in horizontal pipes. *International Journal of Multiphase Flow*, **18**, 439-453.

Ohnuki, A. & Akimoto, H. (2000). Experimental study on transition of flow pattern and phase distribution in upward air–water two-phase flow along a large vertical pipe. *International Journal of Multiphase Flow*, **26**, 367-386.

Oka, Y. I., Okamura, K. & Yoshida, T. (2005). Practical estimation of erosion damage caused by solid particle impact: Part 1: Effects of impact parameters on a predictive equation. *Wear*, **259**, 95-101.

Omar, R., Azzopardi, B. & Hewakandamby, B. (Year). Air-Silicone Oil Flow Around a Vertical to Horizontal 90° Bend. *In:* 17th International Conference on Multiphase 2015 10-12th June 2015 Cannes, France BHR Group.

Omebere-Iyari, N. K., Azzopardi, B. J. & Ladam, Y. (2007). Two-phase flow patterns in large diameter vertical pipes at high pressures. *AIChE Journal*, **53**, 2493-2504.

Omebere-Iyari, N. K., Azzopardi, B. J., Lucas, D., Beyer, M. & Prasser, H. M. (2008). The characteristics of gas/liquid flow in large risers at high pressures. *International Journal of Multiphase Flow*, **34**, 461-476.

Oshinowo, T. & Charles, M. E. (1974). Vertical two-phase flow part I. Flow pattern correlations. *The Canadian Journal of Chemical Engineering*, **52**, 25-35.

Paliwoda, A. (1992). Generalized method of pressure drop calculation across pipe components containing two-phase flow of refrigerants. *International Journal of Refrigeration*, **15**, 119-125.

Pereira, G. C., de Souza, F. J. & de Moro Martins, D. A. (2014). Numerical prediction of the erosion due to particles in elbows. *Powder Technology*, **261**, 105-117.

Pereyra, E., Arismendi, R., Gomez, L. E., Mohan, R. S., Shoham, O. & Kouba, G. E. (2012). State of the Art of Experimental Studies and Predictive Methods for Slug Liquid Holdup. *Journal of Energy Resources Technology*, **134**, 023001-023001.

Pietruske, H. & Prasser, H.-M. (2007). Wire-mesh sensors for high-resolving two-phase flow studies at high pressures and temperatures. *Flow Measurement and Instrumentation,* **18**, 87-94.

Polonsky, S., Shemer, L. & Barnea, D. (1999). The relation between the Taylor bubble motion and the velocity field ahead of it. *International Journal of Multiphase Flow,* **25**, 957-975.

Prasser, H.-M., Krepper, E. & Lucas, D. (2002). Evolution of the two-phase flow in a vertical tube—decomposition of gas fraction profiles according to bubble size classes using wire-mesh sensors. *International Journal of Thermal Sciences,* **41**, 17-28.

Prasser, H. (Year). High-speed measurement of the void fraction distribution in ducts by wire-mesh sensors. *In:* International Meeting on Reactor Noise, 2000.

Prasser, H. M., Böttger, A. & Zschau, J. (1998). A new electrode-mesh tomograph for gas–liquid flows. *Flow Measurement and Instrumentation,* **9**, 111-119.

Prasser, H. M., Misawa, M. & Tiseanu, I. (2005). Comparison between wire-mesh sensor and ultra-fast X-ray tomograph for an air–water flow in a vertical pipe. *Flow Measurement and Instrumentation,* **16**, 73-83.

Prasser, H. M., Scholz, D. & Zippe, C. (2001). Bubble size measurement using wire-mesh sensors. *Flow Measurement and Instrumentation,* **12**, 299-312.

Pringle, C. C. T., Ambrose, S., Azzopardi, B. J. & Rust, A. C. (2015). The existence and behaviour of large diameter Taylor bubbles. *International Journal of Multiphase Flow,* **72**, 318-323.

Qiao, S. & Kim, S. (2016). Interfacial area transport across a 90° vertical-upward elbow in air–water bubbly two-phase flow. *International Journal of Multiphase Flow,* **85**, 110-122.

Rasteiro, M., Silva, R., Garcia, F. & Faia, P. (2011). Electrical Tomography: a review of Configurations and Applications to Particulate Processes. *Kona,* **29**, 2011.

Rautenbach, C., Mudde, R. F., Yang, X., Melaaen, M. C. & Halvorsen, B. M. (2013). A comparative study between electrical capacitance tomography and time-resolved X-ray tomography. *Flow Measurement and Instrumentation*.

Recktenwald, G. (2013). *Wiring of the Solenoid Valves*. URL: http://web.cecs.pdx.edu/~eas199/B/howto/fishtank/wiring/solenoid_wiring.html [1 November 2016].

Reinecke, N. & Mewes, D. (1996). Recent developments and industrial/research applications of capacitance tomography. *Measurement Science and Technology,* **7**, 233.

Reinecke, N., Petritsch, G., Boddem, M. & Mewes, D. (1998). Tomographic imaging of the phase distribution in two-phase slug flow. *International Journal of Multiphase Flow,* **24**, 617-634.

Rodriguez, I. H., Velasco Peña, H. F., Bonilla Riaño, A., Henkes, R. A. W. M. & Rodriguez, O. M. H. (2015). Experiments with a Wire-Mesh Sensor for stratified and dispersed oil-brine pipe flow. *International Journal of Multiphase Flow,* **70**, 113-125.

Saidj, F., Kibboua, R., Azzi, A., Ababou, N. & Azzopardi, B. J. (2014). Experimental investigation of air–water two-phase flow through vertical 90° bend. *Experimental Thermal and Fluid Science,* **57**, 226-234.

Salve, M. D., Monni, G. & Panella, B. (2012). Horizontal Air-Water Flow Analysis with Wire Mesh Sensor. *Journal of Physics: Conference Series,* **395**, 012179.

Sánchez Silva, F., Luna Resendiz, J. C., Carvajal Mariscal, I. & Tolentino Eslava, R. (2010). Pressure Drop Models Evaluation for Two-Phase Flow in 90 Degree Horizontal Elbows. *Ingeniería mecánica, tecnología y desarrollo,* **3**, 115-122.

Sardeshpande, M. V., Harinarayan, S. & Ranade, V. V. (2015). Void fraction measurement using electrical capacitance tomography and high speed photography. *Chemical Engineering Research and Design,* **94**, 1-11.

Schmidt, Ž. (1977). *Experimental study of two-phase slug flow in a pipeline-riser pipe system.* PhD, University of Tulsa,.

Schmidt, Z., Brill, J. P. & Beggs, H. D. (1980). Experimental study of severe slugging in a two-phase-flow pipeline-riser pipe system. *Society of Petroleum Engineers Journal,* **20**, 407-414.

Scott, G. F. (1963). Properties of Co-Current Gas-Liquid Flow Patterns. *Advances in Chem. Eng.,* **4**.

Scott, S., Shoham, O. & Brill, J. (Year). Modeling slug growth in large diameter pipes. *In:* Proceedings of the 3rd International Conference Multi-Phase Flow, Hague, 1987. 55-63.

Scott, S. L., Shoham, O. & Brill, J. P. (1989). Prediction of slug length in horizontal, large-diameter pipes. *SPE Production Engineering,* **4**, 335-340.

Sharaf, S., Da Silva, M., Hampel, U., Zippe, C., Beyer, M. & Azzopardi, B. (2011). Comparison between wire mesh sensor and gamma densitometry void measurements in two-phase flows. *Measurement Science and Technology,* **22**, 104019.

Shea, R., Eidsmoen, H., Nordsveen, M., Rasmussen, J., Xu, Z. & Nossen, J. (Year). Slug frequency prediction method comparison. *In:* Proceedings of the 4th North American Conference on Multiphase Technology, 2004. 227-237.

Silva, F. S., Gómez, A. H. & Velázquez, M. T. (1999). Experimental characterization of air water slug flow through a 90º horizontal elbow. *Two Phase Flow Modeling and Experimentation*, 827-834.

Solnordal, C. B., Wong, C. Y. & Boulanger, J. (2015). An experimental and numerical analysis of erosion caused by sand pneumatically conveyed through a standard pipe elbow. *Wear,* **336–337**, 43-57.

Spedding, P. L. & Benard, E. (2007). Gas–liquid two phase flow through a vertical 90° elbow bend. *Experimental Thermal and Fluid Science,* **31**, 761-769.

Spedding, P. L., Benard, E. & McNally, G. M. (2004). Fluid Flow through 90 Degree Bends. *Developments in Chemical Engineering and Mineral Processing*, **12**, 107-128.

Spedding, P. L. & Nguyen, V. T. (1980). Regime maps for air water two phase flow. *Chemical Engineering Science,* **35**, 779-793.

Spedding, P. L. & Spence, D. R. (1993). Flow regimes in two-phase gas-liquid flow. *International Journal of Multiphase Flow,* **19**, 245-280.

Spedding, P. L., Woods, G. S., Raghunathan, R. S. & Watterson, J. K. (1998). Vertical Two-Phase Flow: Part I: Flow Regimes. *Chemical Engineering Research and Design,* **76**, 612-619.

Sun, J. & Jepson, P. (1992). Slug flow characteristics and their effect on corrosion rates in horizontal oil and gas pipelines, SPE 24787. *SPE ATCE, Washington, DC*.

Sun, M., Liu, S., Li, Z. & Lei, J. (2008). Application of Electrical Capacitance Tomography to the Concentration Measurement in a Cyclone Dipleg. *Chinese Journal of Chemical Engineering,* **16**, 635-639.

Sylvester, N. (1987). A mechanistic model for two-phase vertical slug flow in pipes. *Journal of energy resources technology*, **109**, 206-213.

Taitel, Y. (1987). Effect of gas expansion on slug length in long pipelines. *International Journal of Multiphase Flow,* **13**, 629-637.

Taitel, Y. & Barnea, D. (1990). Two-phase slug flow. *Advances in heat transfer,* **20**, 83-132.

Taitel, Y., Bornea, D. & Dukler, A. (1980). Modelling flow pattern transitions for steady upward gas-liquid flow in vertical tubes. *AIChE Journal,* **26**, 345-354.

Taitel, Y. & Dukler, A. E. (1976). A model for predicting flow regime transitions in horizontal and near horizontal gas-liquid flow. *AIChE Journal,* **22**, 47-55.

Taitel, Y. & Dukler, A. E. (1977). A model for slug frequency during gas-liquid flow in horizontal and near horizontal pipes. *International Journal of Multiphase Flow,* **3**, 585-596.

Taitel, Y., Lee, N. & Dukler, A. E. (1978). Transient gas-liquid flow in horizontal pipes: Modeling the flow pattern transitions. *AIChE Journal,* **24**, 920-934.

Tay, B. L. & Thorpe, R. B. (2014). Hydrodynamic forces acting on pipe bends in gas–liquid slug flow. *Chemical Engineering Research and Design,* **92**, 812-825.

Tay, B. L. & Thorpe, R. B. (2015). Statistical analysis of the hydrodynamic forces acting on pipe bends in gas–liquid slug flow and their relation to fatigue. *Chemical Engineering Research and Design,* **104**, 457-471.

Taylor, J. (1997). *Introduction to error analysis, the study of uncertainties in physical measurements.* 2nd ed ed. California: University Science Books.

Thaker, J. & Banerjee, J. (2015). Characterization of two-phase slug flow sub-regimes using flow visualization. *Journal of Petroleum Science and Engineering,* **135**, 561-576.

Thomson, J. (1876). On the origin of windings of rivers in alluvial plains, with remarks on the flow of water round bends in pipes. *Proceedings of the Royal Society of London,* **25**, 5-8.

Tomiyama, A. (1998). Struggle with computational bubble dynamics. *Multiphase Science and Technology,* **10**, 369-405.

Traviss, D. P. & Rohsenow, W. M. (1971). The influence of return bends on the downstream pressure drop and condensation heat transfer in tubes. Cambridge, Mass.: MIT Heat Transfer Laboratory,[1971].

Trononi, E. (1990). Prediction of slug frequency in horizontal two-phase slug flow. *AIChE Journal*, **36**, 701-709.

Usui, K., Aoki, S. & Inoue, A. (1980). Flow Behavior and Pressure Drop of Two-Phase Flow through C-Shaped Bend in Vertical Plane, (I). *Journal of Nuclear Science and Technology*, **17**, 875-887.

Usui, K., Aoki, S. & Inoue, A. (1981). Flow Behavior and Pressure Drop of Two-Phase Flow through C-Shaped Bend in Vertical Plane, (II). *Journal of Nuclear Science and Technology*, **18**, 179-190.

Usui, K., Aoki, S. & Inoue, A. (1983). Flow Behavior and Phase Distribution in Two-Phase Flow around Inverted U-Bend. *Journal of Nuclear Science and Technology*, **20**, 915-928.

Van Hout, R., Barnea, D. & Shemer, L. (2002a). Translational velocities of elongated bubbles in continuous slug flow. *International Journal of Multiphase Flow*, **28**, 1333-1350.

Van Hout, R., Gulitski, A., Barnea, D. & Shemer, L. (2002b). Experimental investigation of the velocity field induced by a Taylor bubble rising in stagnant water. *International Journal of Multiphase Flow*, **28**, 579-596.

Van Hout, R., Shemer, L. & Barnea, D. (1992). Spatial distribution of void fraction within a liquid slug and some other related slug parameters. *International Journal of Multiphase Flow*, **18**, 831-845.

Velasco Peña, H. F. & Rodriguez, O. M. H. (2015). Applications of wire-mesh sensors in multiphase flows. *Flow Measurement and Instrumentation*, **45**, 255-273.

Vieira, R. E., Mansouri, A., McLaury, B. S. & Shirazi, S. A. (2016). Experimental and computational study of erosion in elbows due to sand particles in air flow. *Powder Technology*, **288**, 339-353.

Wallis, G. B. (1969). *One-dimensional two-phase flow*. McGraw-Hill Companies.

Wallis, G. B. & Dodson, J. E. (1973). The onset of slugging in horizontal stratified air-water flow. *International Journal of Multiphase Flow*, **1**, 173-193.

Wang, S. J., Dyakowski, T., Xie, C. G., Williams, R. A. & Beck, M. S. (1995). Real time capacitance imaging of bubble formation at the distributor of a fluidized bed. *The Chemical Engineering Journal and the Biochemical Engineering Journal*, **56**, 95-100.

Wang, X., Guo, L. & Zhang, X. (2006). Development of Liquid Slug Length in Gas-Liquid Slug Flow along Horizontal Pipeline: Experiment and Simulation1 1Supported by the National Natural Science Foundation of China (No.50536020 and 50323001). *Chinese Journal of Chemical Engineering*, **14**, 626-633.

Wang, X., Guo, L. & Zhang, X. (2007). An experimental study of the statistical parameters of gas–liquid two-phase slug flow in horizontal pipeline. *International Journal of Heat and Mass Transfer*, **50**, 2439-2443.

Weber, M. E. (1981). Drift in intermittent two-phase flow in horizontal pipes. *The Canadian Journal of Chemical Engineering*, **59**, 398-399.

Woods, B. D., Fan, Z. & Hanratty, T. J. (2006). Frequency and development of slugs in a horizontal pipe at large liquid flows. *International Journal of Multiphase Flow*, **32**, 902-925.

Woods, B. D. & Hanratty, T. J. (1999). Influence of Froude number on physical processes determining frequency of slugging in horizontal gas–liquid flows. *International Journal of Multiphase Flow*, **25**, 1195-1223.

Xie, C., Huang, S., Beck, M., Hoyle, B., Thorn, R., Lenn, C. & Snowden, D. (1992). Electrical capacitance tomography for flow imaging: system model for development of image reconstruction algorithms and design of primary sensors. *IEE Proceedings G (Circuits, Devices and Systems)*, **139**, 89-98.

Yadav, M. S., Kim, S., Tien, K. & Bajorek, S. M. (2014a). Experiments on geometric effects of 90-degree vertical-upward elbow in air water two-phase flow. *International Journal of Multiphase Flow*, **65**, 98-107.

Yadav, M. S., Worosz, T., Kim, S., Tien, K. & Bajorek, S. M. (2014b). Characterization of the dissipation of elbow effects in bubbly two-phase flows. *International Journal of Multiphase Flow*, **66**, 101-109.

Yang, W. & Peng, L. (2003). Image reconstruction algorithms for electrical capacitance tomography. *Measurement Science and Technology*, **14**, R1.

Yang, W., Stott, A., Beck, M. & Xie, C. (1995). Development of capacitance tomographic imaging systems for oil pipeline measurements. *Review of scientific instruments*, **66**, 4326-4332.

York, T. (2001). Status of electrical tomography in industrial applications. *Journal of Electronic Imaging*, **10**, 608-619.

Zabaras, G. (2000). Prediction of slug frequency for gas/liquid flows. *SPE Journal*, **5**, 252-258.

Zhang, H.-Q., Wang, Q., Sarica, C. & Brill, J. P. (2003). A unified mechanistic model for slug liquid holdup and transition between slug and dispersed bubble flows. *International Journal of Multiphase Flow*, **29**, 97-107.

Zhang, Z., Bieberle, M., Barthel, F., Szalinski, L. & Hampel, U. (2013). Investigation of upward cocurrent gas–liquid pipe flow using ultrafast X-ray tomography and wire-mesh sensor. *Flow Measurement and Instrumentation*, **32**, 111-118.

Zhao, D., Omar, R., Abdulkadir, M., Abdulkareem, L. A., Azzi, A., Saidj, F., Hernandez Perez, V., Hewakandamby, B. N. & Azzopardi, B. J. (2017). The control and maintenance of desired flow patterns in bends of different orientations. *Flow Measurement and Instrumentation*, **53, Part B**, 230-242.

Zhao, Y., Lao, L. & Yeung, H. (2015). Investigation and prediction of slug flow characteristics in highly viscous liquid and gas flows in horizontal pipes. *Chemical Engineering Research and Design*, **102**, 124-137.

Zheng, G., Brill, J. P. & Taitel, Y. (1994). Slug flow behavior in a hilly terrain pipeline. *International Journal of Multiphase Flow*, **20**, 63-79.

Zuber, N. & Hench, J. (1962). Steady state and transient void fraction of bubbling systems and their operating limits (Part I, Steady State Operation). *General Electric Report 62GL100*.

Zukoski, E. (1966). Influence of viscosity, surface tension, and inclination angle on motion of long bubbles in closed tubes. *Journal of Fluid Mechanics*, **25**, 821-837.

Appendix A

Experimental arrangements

A.1 Experimental matrix

The table below shows the experimental matrix that was conducted for each axial location along the test section. The matrix of the test runs is not included.

Table A-1: The experimental matrix.

Run	U_{ls} [m/s] Air / Oil U_{gs} [m/s]	0.15	0.22	0.30	0.38	0.45	0.53
1	0.045	a	b	c	d	e	f
2	0.18	a	b	c	d	e	f
3	0.36	a	b	c	d	e	f
4	0.55	a	b	c	d	e	f
5	0.91	a	b	c	d	e	f
6	1.37	a	b	c	d	e	f
7	1.83	a	b	c	d	e	f
8	2.29	a	b	c	d	e	f
9	2.75	a	b	c	d	e	f
10	3.21	a	b	c	d	e	f

A.2 Start-up and shutdown procedure

A.2.1 Start-up procedures:

1. Check the silicone oil level in the tank to ensure that it contains enough silicone oil.
2. Make sure that the feed valve before the pump is open (V10).
3. Make sure the feed valve of the inclined rig (V9) is close.
4. Ensure that the air inlet Valves (V1, V2 and V3) are closed while the liquid bypass valve (V11) is open.
5. Check that all devices are connected to the test section and ready to use.
6. Turn the pump on while main liquid inlet valve is closed to allow the flow to stabilise in the recycle loop first before it is passed to the mixer.
7. Open the liquid inlet valve (V12) and start with low flow rate ($1m^3$/hr) that can fill the pipe section with oil, in order to check for leaks.
8. Increase the liquid flow rate gradually to the flow rate required (1 to $6m^3$/hr) and check for any possible leaks.
9. When it is confirmed that the rig is ready to use, open the air inlet slightly to form a bubble column.
10. Increase the gas flow rate to the desirable value (50 to 500 l/min).
11. Allow sufficient time for the flow to stabilise and then start taking the measurements.(it is known that the structure of the flow keep changing with time. This change should stabilise with time and can be ignored).
12. Set the air and the liquid flow rates to the ranges of interest, by controlling the air inlet valve (V3) and the bypass valve (V11) respectively. the flow should reach steady state before taking measurements.

13. During the experiments check the rig for leaks and excessive vibration, in which case follow shutdown procedure.
14. The temperature of the fluids should be monitored during the operation. This is only to make sure that the oil properties are not affected. The cooling system in the tank should be turned on if the temperature increased by 6 degrees Celsius from the ambient temperatures.
15. For emergency shutdown, press the upper level emergency stop for the pump if safe to do so.

A.2.2Shut-down procedures:

1. Gradually open the liquid bypass valve (V11).
2. Close the air inlet valves (V3, V2 and V1) respectively.
3. Turn the pump off from the switch next to the pump.
4. Drain the oil back to the tank by blowing pressurized air through the pipe section. A pressurized air hose will be attached to the valve in the horizontal section (V4 or V5), made for this purpose. This will not drain the whole amount back to the tank, especially in the vertical section. The rest of the oil can be drained from the drain valve (V-drain)
5. Turn off all the electronic devices. Switch the ECT and wire mesh boxes, through the buttons at the back of each box. Turn off the Pc normally and then turn off the DAQ device by turning the switch of the extension lead off. Finally unplug the extension lead.

A.2.3Emergency shutdown

If it is safe;

1. Press the emergency button for a quick shutdown of the pump. (Two shutdown buttons are available at the upper and lower platform).
2. Stop the air flow by closing the air inlet valve (V1).It is located near the operating plat form and can be accessed in a comfortable way.
3. Switch all measuring devices off. This can be done by turning the switch of the extension lead off
4. Otherwise evacuate the area

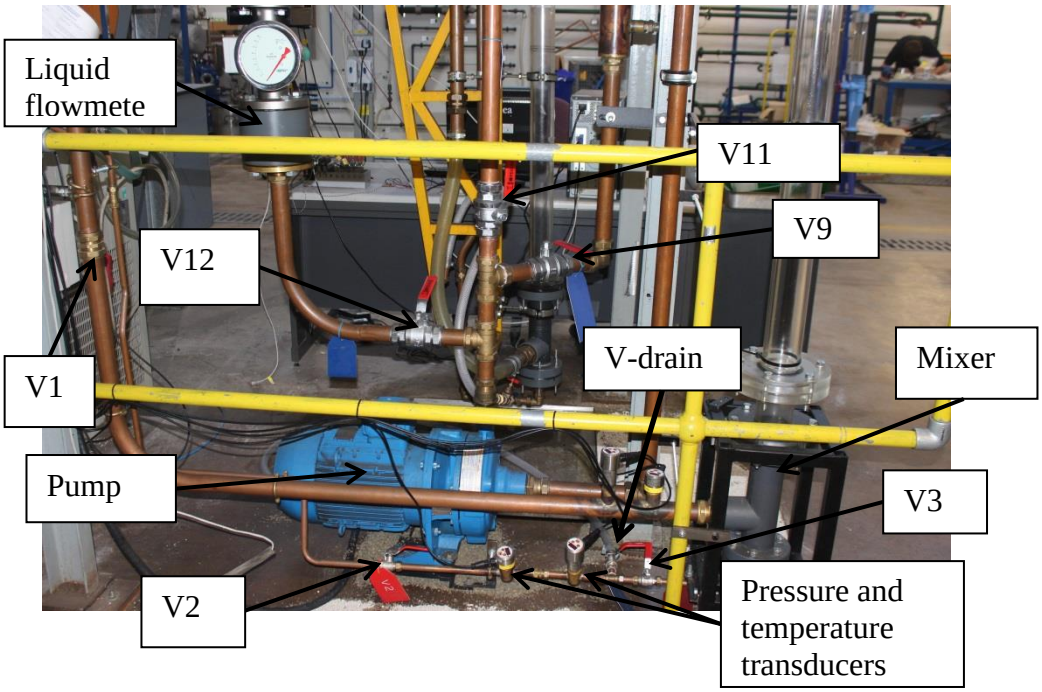


Figure A-1: The main valves of the flow rig.



Figure A-2: Silicone oil tank.



Figure A-3: Shutdown buttons at the upper platform (left) and the lower platform (right).

A.3 Camera system

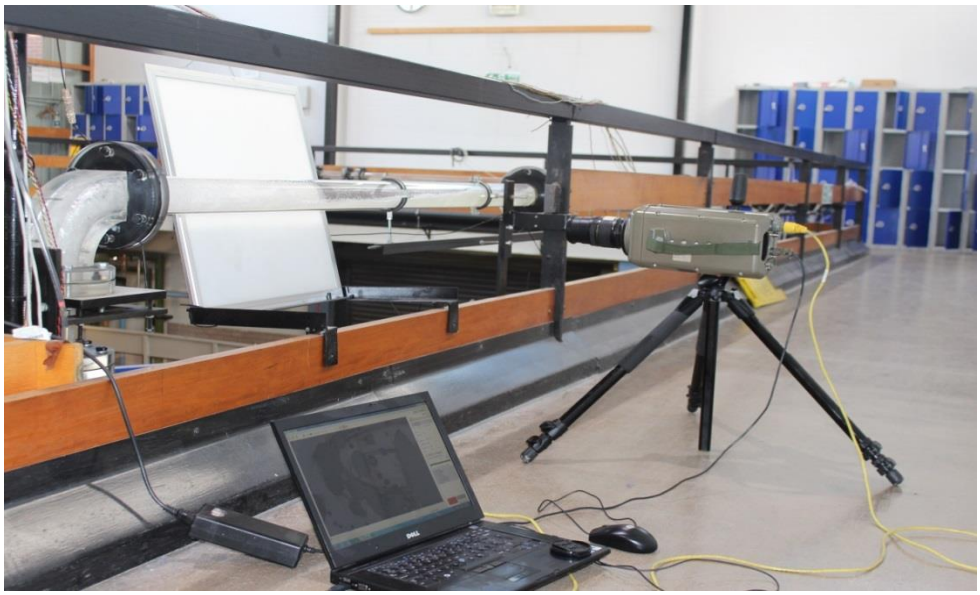
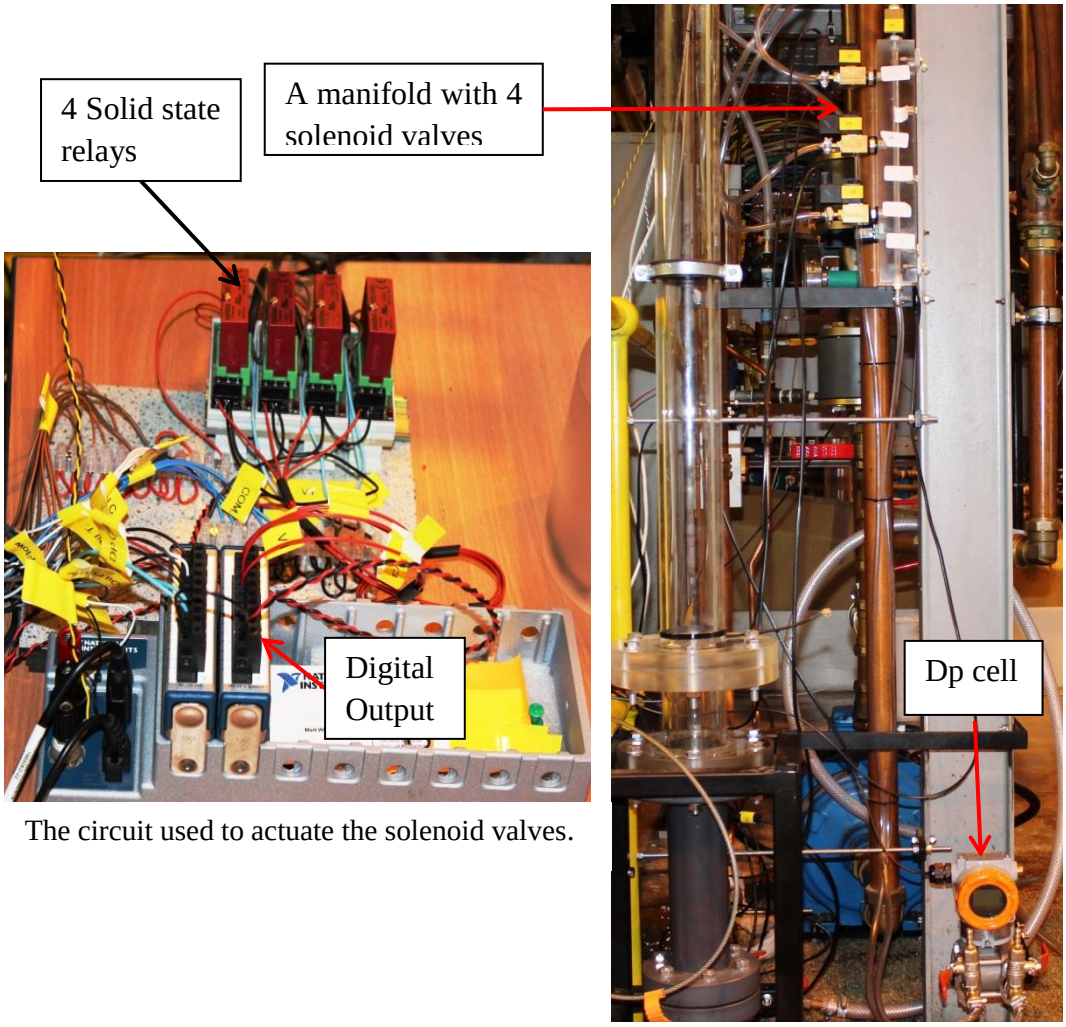


Figure A-4: High speed imaging system.

A.4 Differential pressure measurements system



The circuit used to actuate the solenoid valves.

Figure A-5: The differential pressure measurements system.

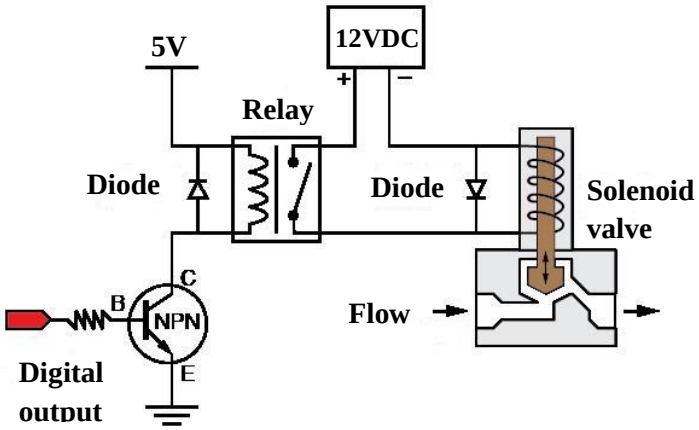
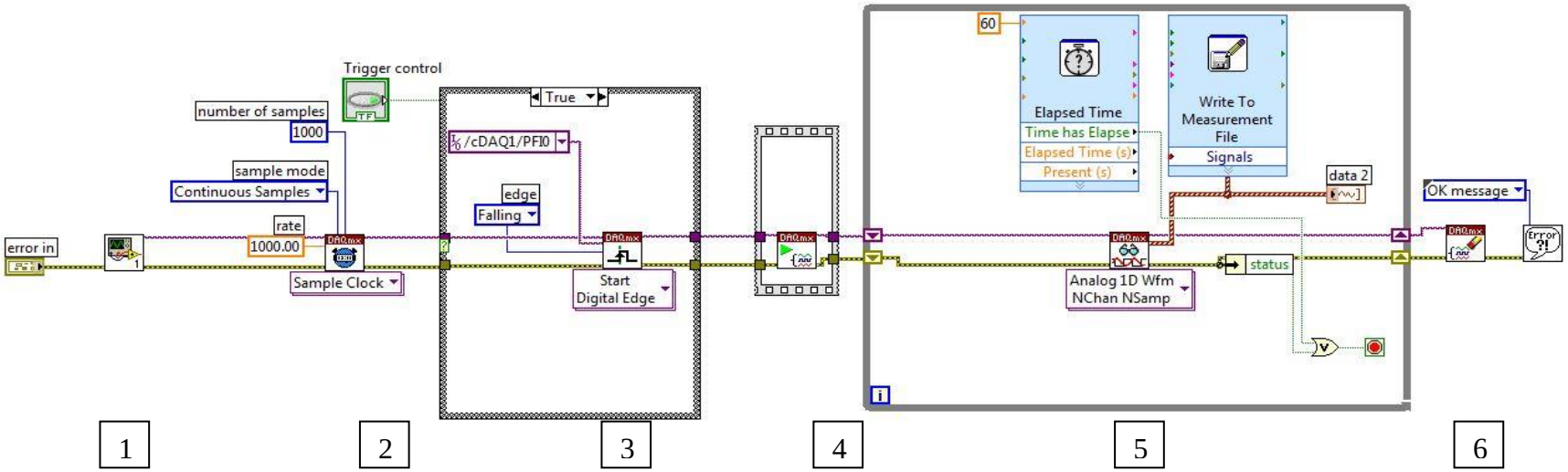


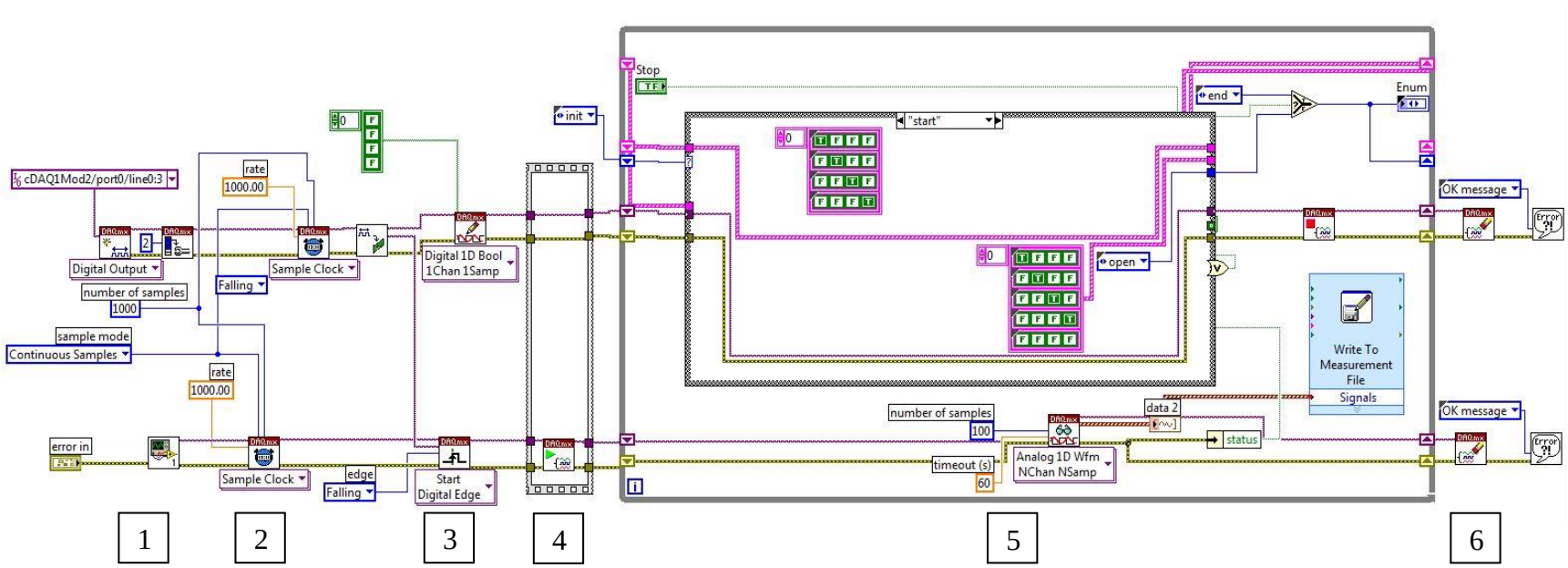
Figure A-6: A schematic of the circuit showed in figure A-5, adopted from Recktenwald (2013).

A.5 LabVIEW block diagrams



1. Create an Analog input channels.
2. Set the rate of the sample clock rate and mode.
3. Use the trigger signal to simultaneously start the measurements.
4. Start the acquisition.
5. Read the data and open the solenoid valves sequentially/ Write the measurements to excel file.
6. Clear the task and check for errors.

Figure A-7: The LabVIEW block diagram used for data acquisition.



1. Create an Analog input channels.
2. Set the rate of the sample clock rate and mode.
3. Use the trigger signal to simultaneously start the measurements.
4. Start the acquisition.
5. Read the data and open the solenoid valves sequentially/ Write the measurements to excel file.
6. Clear the task and check for errors.

Figure A-8: The LabVIEW block diagram used for data acquisition and valve control.

Appendix B

Uncertainty analysis

The measurements of any physical quantities are represented in term of the best estimate as:

$$\text{Measured value (x)} = x_{best} \pm \delta x \tag{B.1}$$

Where; δx is the uncertainty interval or margin of the best estimate x. This means that the measured value can fall anywhere between $x_{best} + \delta x$ and $x_{best} - \delta x$. It is acknowledge that the uncertainty δx alone may not provide a comprehensible interpretation of the measurements precision. Therefore the fractional uncertainty is often used instead.

$$\text{Fractional uncertainty} = \frac{\delta x}{|x_{best}|} \tag{B.2}$$

In the following sections, the uncertainty associated with the measurements reported in this thesis is estimated based on statistical analysis, as informatively explained by Taylor (1997) and Kirkup and Frenkel (2006). The equations applied are listed and the results are presented. More details about error analysis and uncertainty propagation can be found in (Taylor, 1997; ; Kirkup and Frenkel, 2006).

B.1 The systematic error of the void fraction measurements

The systematic error was not provided for both the WMS and the ECT system. Therefore, experimental comparison was carried out to estimate the discrepancy between both sensors at identical flow conditions. The results are considered as the approximate systematic error of the sensors, though, it is not claimed as the maximum uncertainty of the void fraction measurements.

Figure B-1 illustrates the difference in void fraction values that were obtained simultaneously from WMS and ECT, for the full range of flow conditions. The results showed a good agreement between both sensors with an average percentage error of 5% and standard deviation of 1.02, while the averaged absolute percentage error is 6.7%. It is noticeable that the voidage data obtained from WMS are higher than those from the ECT at low flow rates, while the discrepancy is reversed as the gas superficial velocity increases.

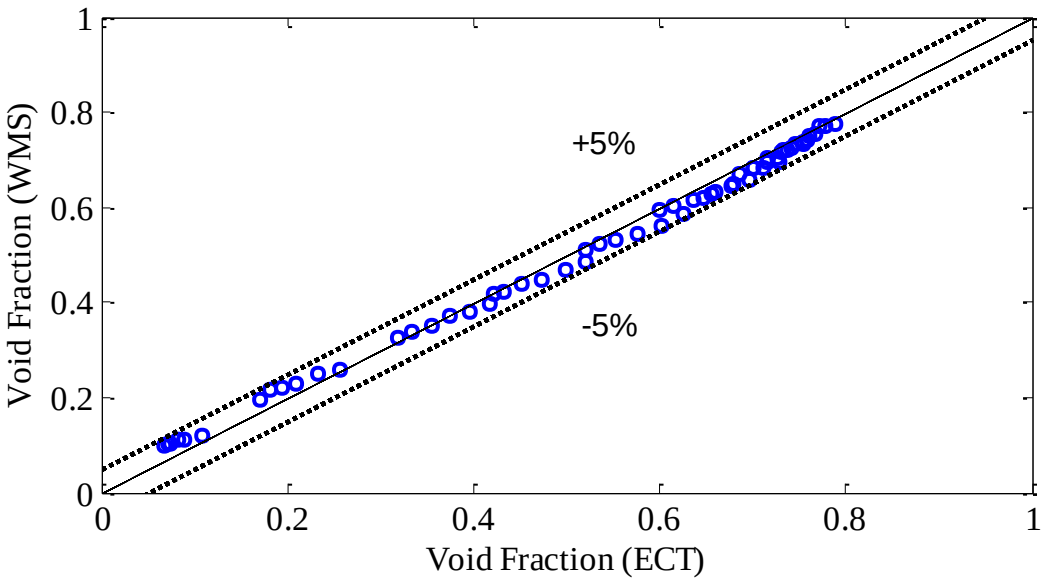


Figure B-1: The discrepancy of void fraction measurements between the WMS and the ECT.

Figure B-2 shows the variation of the average error with the increase of gas superficial velocity where the error bars represents the standard deviation of the measurements. It is evident that the error is highest at low gas superficial velocity (U_{gs} = 0.045 m.s^{-1}). As the gas superficial velocity increases the average error decreases to slightly below zero and the standard deviation approaches zero.

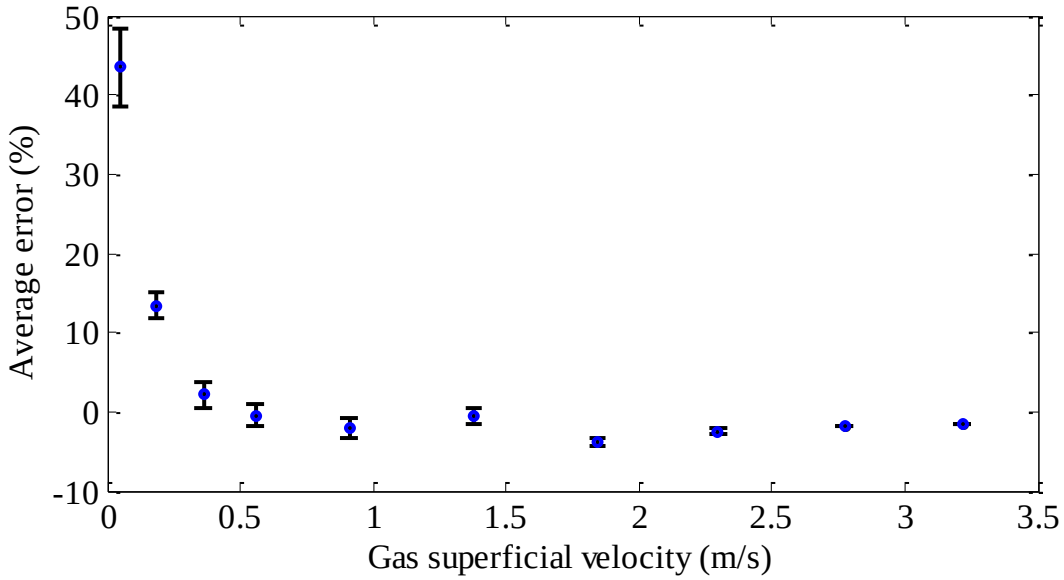


Figure B-2: The effect of gas superficial velocity on the average error.

B.2 Random uncertainty calculation

After the systematic uncertainty was corrected through calibration procedure, the random uncertainty is reduced by repeating the runs. The random uncertainty of the independent flow parameters, including gas and liquid flow, pressure, frequency and void fraction measurements, was estimated through statistical analysis. The mean value is considered the best estimate while the standard deviation of the mean is taken as the uncertainty of the best estimate that describes the reliability and repeatability of the experimental measurements. The following equations are used for the statistical analysis:

$$\bar{x} = \frac{\sum_{i=1}^{N} xi}{N} \tag{B.3}$$

$$\sigma_x = \sqrt{\frac{\sum_{i=1}^{N}(xi - \bar{x})}{N-1}} \tag{B.4}$$

$$\sigma_{\bar{x}} = \frac{\sigma_x}{\sqrt{N}} \tag{B.5}$$

Where; $\bar{x}$ is the mean and is considered the best estimate for repeated runs. While σ_x and $\sigma_{\bar{x}}$ is the standard deviation and the standard deviation of the mean respectively. Random uncertainties more often have Gaussian distribution (i.e. bell shaped distribution) and hence the mean is justified as the best estimate, while the standard deviation of the mean as the uncertainty of the best estimate with 68% confidence (Taylor, 1997). The results of random uncertainty of all flow parameters are summarised in Table B-1.

These results indicate the minimum, maximum and average deviation from the best estimate of the entire flow range. For instance, the minimum and maximum random error associated with the gas flow can be written as:

$$10 \pm 7 \times 10^{-3}(l/min) \tag{B.6}$$

$$700 \pm 0.3(l/min) \tag{B.7}$$

The uncertainty of each individual flow parameter can be represented as in equation (B.8) or (B.9) for entire range of flow conditions. It is clear that the

random uncertainty, Table B-1, is sufficiently small and hence; the repeatability of the experimental runs is confidently expected.

Table B-1: Random uncertainty of the measured flow parameters

Measurement	Random uncertainty (δx)	The mean of δx
Gas flow	$7 \times 10^{-3} \leq \sigma_x \leq 0.3$	0.15
Liquid flow	$8 \times 10^{-3} \leq \sigma_x \leq 2 \times 10^{-3}$	5×10^{-3}
pressure	$4 \times 10^{-4} \leq \sigma_x \leq 5 \times 10^{-3}$	2×10^{-3}
Void fraction	$1 \times 10^{-4} \leq \sigma_x \leq 1 \times 10^{-3}$	5×10^{-4}
Frequency	$3 \times 10^{-3} \leq \sigma_x \leq 2 \times 10^{-2}$	9×10^{-2}

B.3 Uncertainty propagation estimation

The uncertainty propagation is estimated for the parameters that were measured indirectly; such as liquid, gas and mixture velocities.

In general, if q is a computed value from several measured values x, y ... and z, then q can be written as;

$$q = f(x, y \ldots, z) \tag{B.8}$$

The uncertainty in q (δq) is a combination of the uncertainties of the independent input variables (δx), (δy)… (δz).

For independent and random errors:

$$\delta q = \sqrt{\left(\frac{\partial q}{\partial x}\delta x\right)^2 + \left(\frac{\partial q}{\partial y}\delta y\right)^2 + \cdots . + \left(\frac{\partial q}{\partial z}\delta z\right)^2} \tag{B.9}$$

According to Taylor (1997) , δq should be always smaller than the ordinary sum of the partial errors of the independent inputs:

$$\delta q \leq \left|\frac{\partial q}{\partial x}\right| \delta x + \left|\frac{\partial q}{\partial y}\right| \delta y + \cdots . \left|\frac{\partial q}{\partial z}\right| \delta z \tag{B.10}$$

B.3.1 Combined uncertainty calculations

The gas superficial velocity is given as

$$u_{gs} = \frac{4Q_A}{\pi D^2} \tag{B.11}$$

Where; Q_A is the air flow rate and D is the pipe diameter. The equation (B.9) is applied and the calculations are detailed in the following steps:

The error in u_{gs} due to D alone is:

$$\delta u_{gs(D)} = \left|\frac{\partial u_{gs}}{\partial D}\right| \delta D \tag{B.12}$$

$$\delta u_{gs(D)} = \left|\frac{(\pi D^2 * 0) - (4Q_A * 2\pi D)}{(\pi D^2)^2}\right| \delta D \tag{B.13}$$

$$\delta u_{gs(D)} = \left|\frac{-(8\pi D Q_A)}{(\pi D^2)^2}\right| \delta D \tag{B.14}$$

$$\delta u_{gs(D)} = \left|\frac{-8Q_A}{\pi D^3}\right| \delta D \tag{B.15}$$

The error in u_{gs} due to Q_A alone is:

$$\delta u_{gs(QA)} = \left|\frac{\partial u_{gs}}{\partial Q_A}\right| \delta Q_A \tag{B.16}$$

$$\delta u_{gs(QA)} = \left|\frac{(\pi D^2 * 4) - (4Q_A * 0)}{(\pi D^2)^2}\right| \delta Q_A \tag{B.17}$$

$$\delta u_{gs(QA)} = \left|\frac{(4\pi D^2)}{(\pi D^2)^2}\right| \delta Q_A \tag{B.18}$$

$$\delta u_{gs(QA)} = \left|\frac{4}{\pi D^2}\right| \delta Q_A \tag{B.19}$$

The total uncertainty of u_{gs} is

$$\delta u_{gs=}\sqrt{\left(\delta u_{gs(D)}\right)^2 + \left(\delta u_{gs(QA)}\right)^2} \tag{B.20}$$

$$\delta u_{gs=}\sqrt{\left(\frac{8Q_A}{\pi D^3}\delta D\right)^2 + \left(\frac{4}{\pi D^2}\delta Q_A\right)^2} \tag{B.21}$$

Since the uncertainty in pipe diameter is $\delta D = \pm 5 \times 10^{-4}$mm and the uncertainty of the gas flow rate ($\delta Q_A = \pm 1.17 \times 10^{-4}$ m^3.s^{-1}), the combined uncertainty of gas superficial velocity is calculated from equation (B.21). The results are illustrated in Figure B-3.

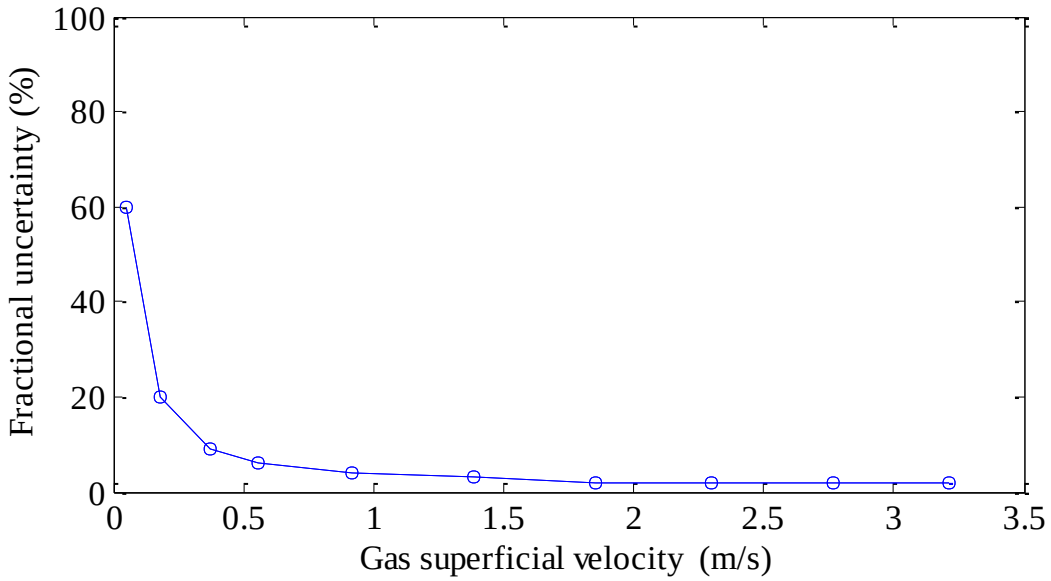


Figure B-3: The fractional uncertainty of gas superficial velocities.

It is certain that the fractional uncertainty decays exponentially as the gas superficial velocity increases. The fractional uncertainty is 60% at the lowest gas

velocity (0.045 m.s^{-1}) and it approaches 2% at gas superficial velocity of (U_{gs}=1.83 m.s^{-1}). As the gas superficial velocity increases further the relative uncertainty remains constant at 2%.

The combined uncertainty of liquid superficial velocities was estimated in a similar way to the gas superficial velocities, where($\delta Q_l = \pm 1.94 \times 10^{-5} \mathrm{m}^3.\mathrm{s}^{-1}$). The results are shown in Figure B-4. The uncertainty in liquid superficial velocities is much smaller than that of gas superficial velocities. It is slightly higher at low liquid flow rate and then it levels off as the liquid flow increases.

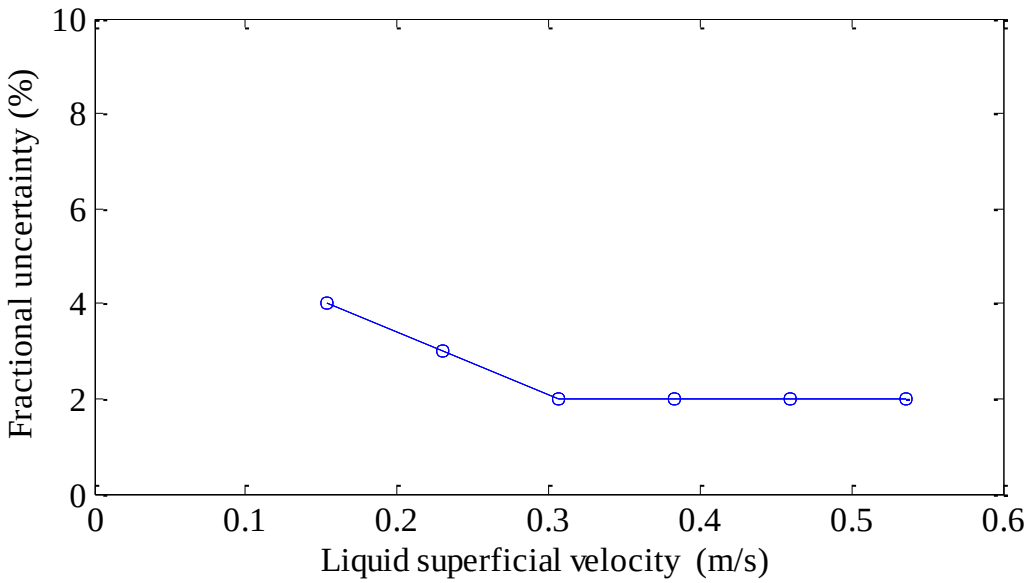


Figure B-4: The fractional uncertainty of gas superficial velocities.

The mixture velocity is given as:

$$u_m = u_{gs} + u_{ls} \tag{B.22}$$

In the case of summation, the combined uncertainty is given by the quadrate sum of the independent uncertainties Taylor (1997), hence the uncertainty of the mixture velocity can be estimated by:

$$\delta u_{m=}\sqrt{\left(\delta u_{gs}\right)^2+(\delta u_{ls})^2} \tag{B.23}$$

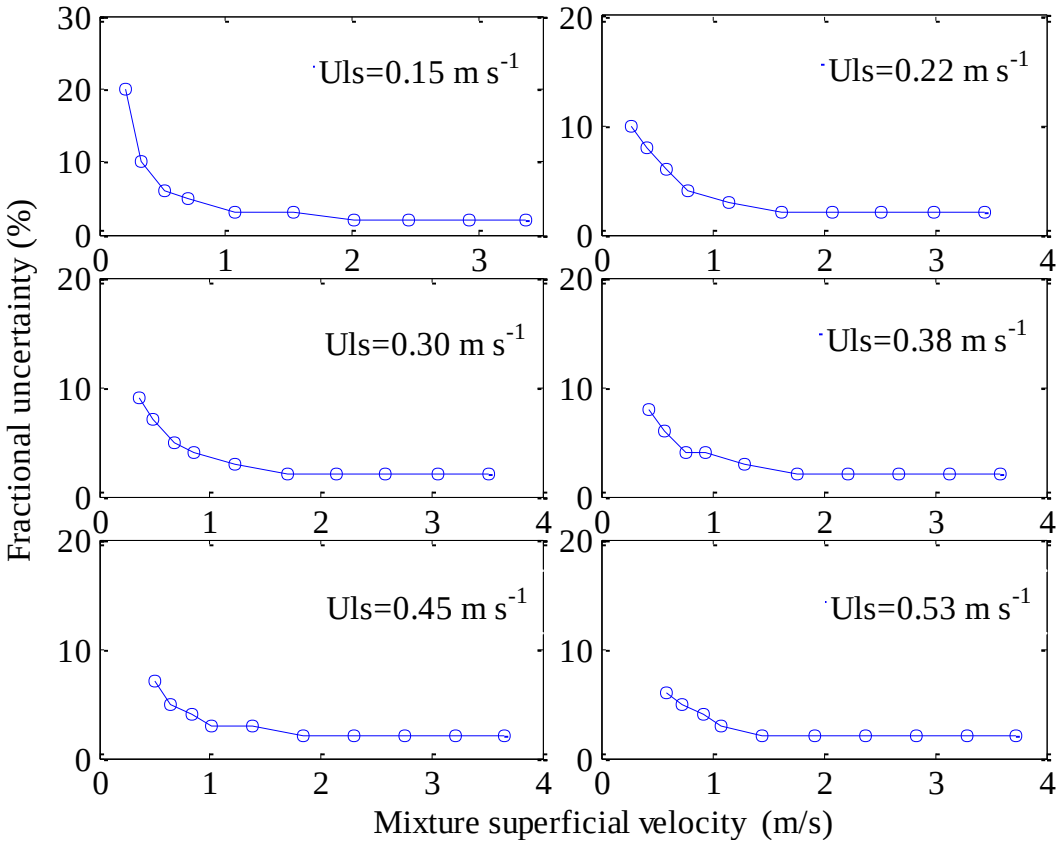


Figure B-5: The fractional uncertainty of mixture superficial velocities.

Figure B-5 shows the fractional uncertainty of the mixture velocities for different liquid superficial velocities. The fractional uncertainty decreases exponentially as the mixture velocity increases for all liquid superficial velocities. The highest uncertainty value is recorded at the lowest liquid superficial velocity (U_{ls}=0.15 m.s^{-1}). As the liquid superficial velocity increases the uncertainty in mixture velocity decreases. The uncertainty also decreases with the increase of gas superficial velocity and it levels off as the gas superficial velocity rises beyond (U_{gs}=0.91 m.s^{-1}).

B.4 Statistical analysis of the relative accuracy

The relative accuracy of the ECT and WMS was obtained through a series of statistical measures. Similar measures were used to quantify the accuracy and reliability of slug flow theoretical models against the experimental results. The statistical parameters that were estimated to evaluate theoretically predicted values are given by the following equations:

1. The percentage error $(\%E)$:

$$\%E = \frac{calculated\ value - measred\ value}{measred\ value} \times 100 \tag{B.24}$$

2. The average percentage error (%AE):

$$\%AE = \frac{\sum_{i=1}^{N} \%E}{N} \tag{B.25}$$

3. Standard deviation of the error(STD):

$$STD = \sqrt{\frac{\sum_{i=1}^{N} \left(\%E - \%E_{avg}\right)^2}{N-1}} \tag{B.26}$$

4. The average absolute error (%AAE):

$$\%\text{AAE} = \frac{\sum_{i=1}^{N} |\%E|}{N} \tag{B.27}$$

B.5 Calibration curves and calibration certificate

Calibration procedure was conducted for the temperature transducers and pressure transmitters; whereas calibration certificates were supplied, by the manufacturer, for the flow meters the differential pressure transmitter.

B.5.1 Temperature sensors

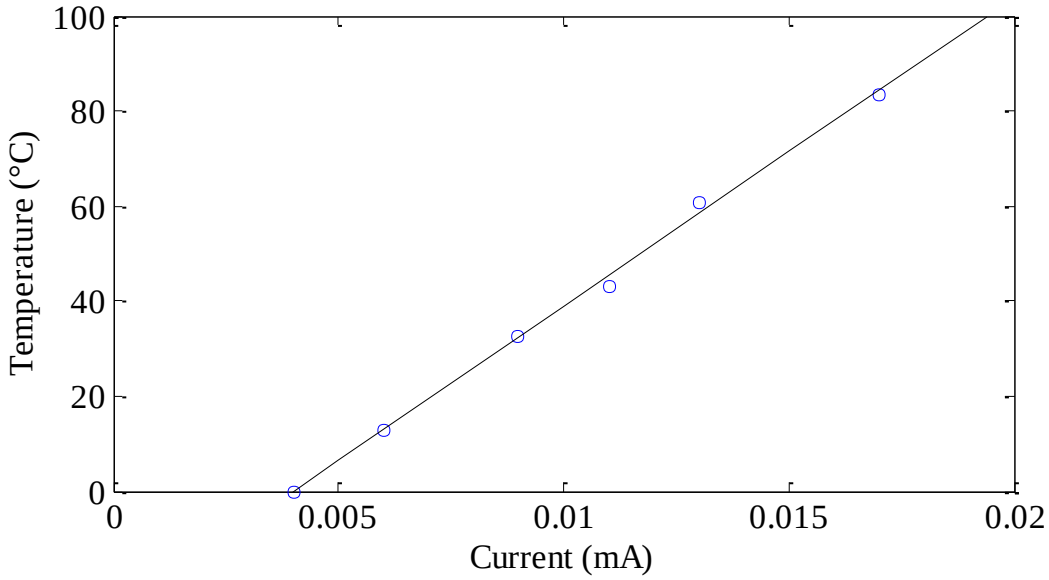


Figure B-6: Calibration curve of a temperature sensor.

B.5.2 Pressure transmitters

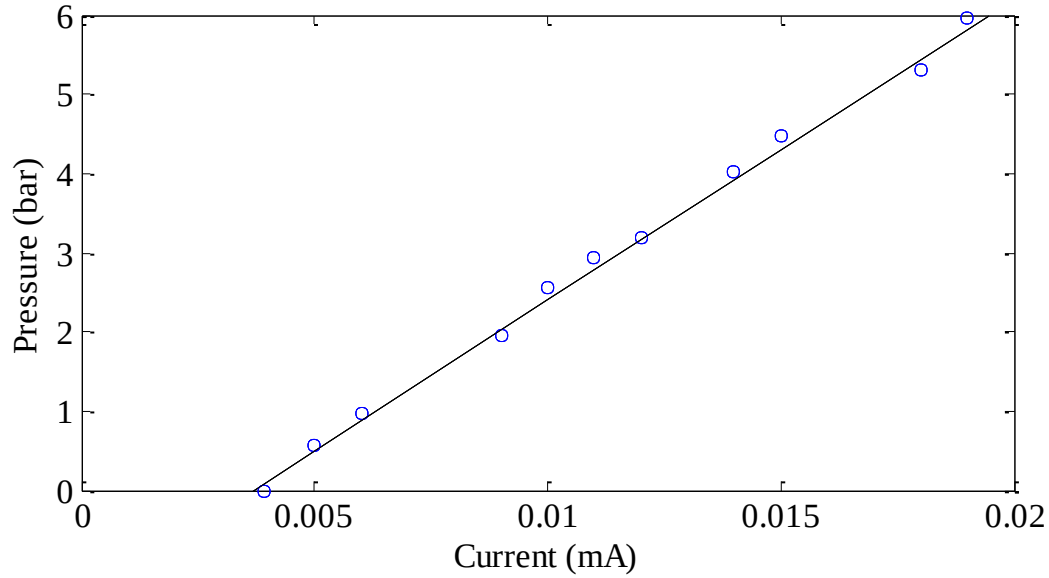


Figure B-7: Calibration curve of a pressure transmitter.

B.5.3 Calibration certificates

1. Liquid flowmeter (m^3. hr^{-1})

INFLUX MEASUREMENTS LTD

1a Bennett House, The Dean, Alresford, Hampshire, SO24 9BQ, U.K.
T: +44 (0)1962 736736 E: sales@influxmeasurements.com

Quality Systems Certificate No. 464
Assessed to ISO 9001:2008

Certificate of Calibration

Faculty of Engineering
University of Nottingham
University Park
Nottingham
NG7 2RD

Certificate No. S21589/1

Customer Order No.: T12770/24829 **Serial No.**: 21589/1

Flowmeter Type: Metal tube variable area flowmeter **Flow Range: 2-16 m3/h Silicon Oil SG 0.9 Visc 5cP**

The above flowmeter was calibrated using equivalent flowrates of Water by series comparison, using a master flowmeter traceable to National Standards.
Master serial number – IMT 197/201

Indicated Flow Silicon Oil SG 0.9 Visc 5cP	Actual Flow Silicon Oil SG 0.9 Visc 5cP	mA
2	2.06	6.14
4	4.11	8.22
6	6.15	10.22
8	8.08	12.11
10	10.04	14.05
12	12.11	16.13
14	14.02	17.97
16	16.02	19.95

The best measurement capability expressed as an uncertainty does not exceed 1%.

The uncertainties are for a confidence probability of not less than 95%.

Observation:

Signed: J Fox

Date: 19/6/2014

For Influx Measurements Ltd

2. Air flowmeter (l/min):

INFLUX MEASUREMENTS LTD

1a Bennett House, The Dean, Alresford, Hampshire, SO24 9BQ, U.K.
T: +44 (0)1962 736736 E: sales@influxmeasurements.com

Quality Systems Certificate No. 464
Assessed to ISO 9001:2008

Certificate of Calibration

Faculty of Engineering
University of Nottingham
University Park
Nottingham
NG7 2RD

Certificate No. S21589/2

Customer Order No.: T12770/24829 **Serial No.**: 21589/2

Flowmeter Type: Azbil Corp – MFC 151 AGN D01 0000 **Flow Range: 1000L/min Air or N2 at STP**
Thermal mass flowmeter

The above flowmeter was calibrated using equivalent flowrates of Air by series comparison, using a master flowmeter traceable to National Standards.
Master serial number – IMT 232/181

Indicated Flow STP L/min	Actual Flow STP L/min
86	93.18
172	186.36
262	279.53
354	372.71
448	465.89
542	559.07
634	652.24
730	745.42
830	838.60
924	931.78

The best measurement capability expressed as an uncertainty does not exceed 1%.

The uncertainties are for a confidence probability of not less than 95%.

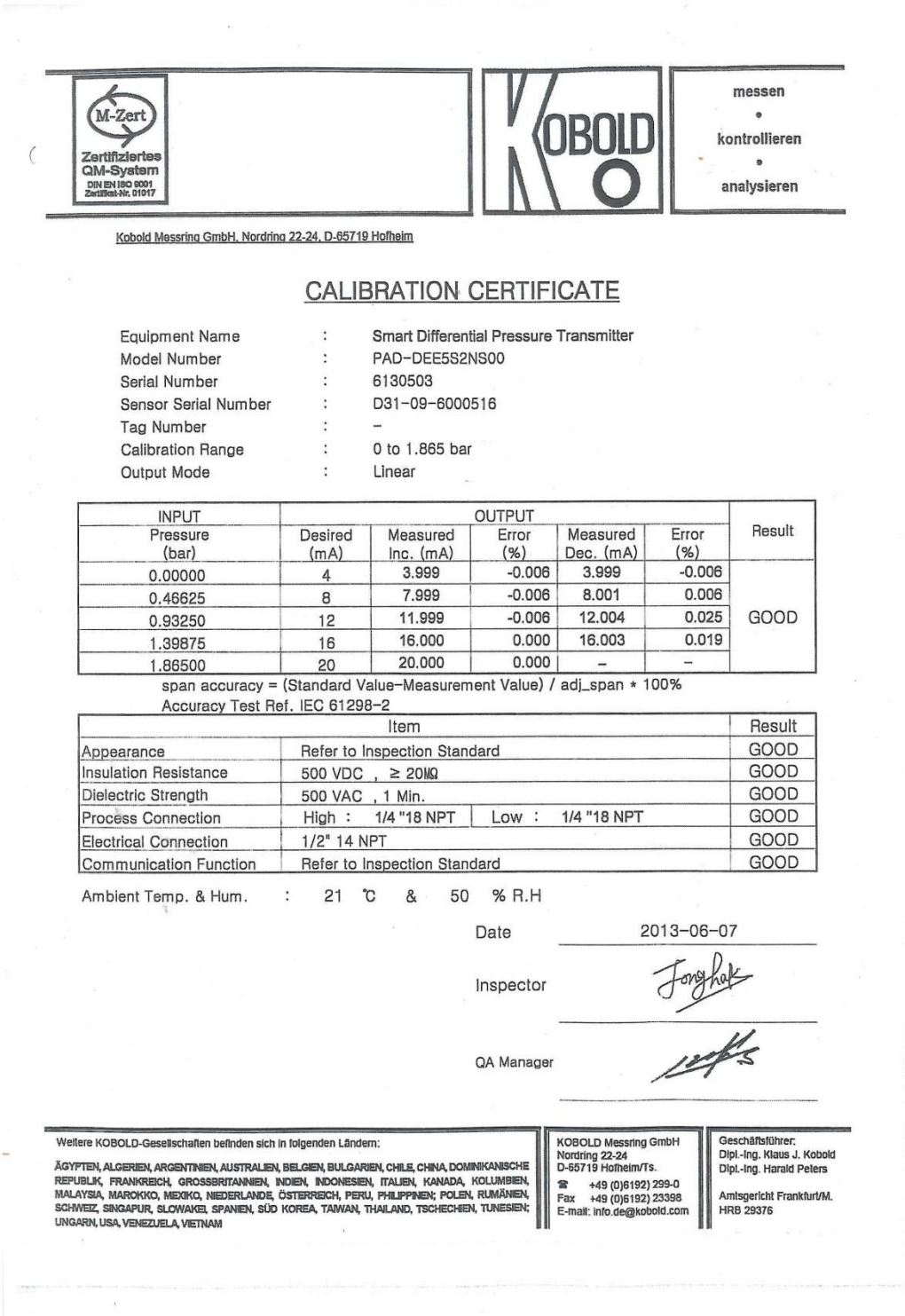
Observation: The 4-20mA outputs correspond as expected to display

Signed: J Fox

Date: 19/6/2014

For Influx Measurements Ltd

3. Differential pressure transmitter (bar)



M-Zert
Zertifiziertes QM-System
DIN EN ISO 9001
Zertifikat-Nr. 01017

KOBOLD

messen
•
kontrollieren
•
analysieren

Kobold Messring GmbH, Nordring 22-24, D-65719 Hofheim

CALIBRATION CERTIFICATE

Equipment Name	:	Smart Differential Pressure Transmitter
Model Number	:	PAD-DEE5S2NS00
Serial Number	:	6130503
Sensor Serial Number	:	D31-09-6000516
Tag Number	:	-
Calibration Range	:	0 to 1.865 bar
Output Mode	:	Linear

INPUT	OUTPUT					Result
Pressure (bar)	Desired (mA)	Measured Inc. (mA)	Error (%)	Measured Dec. (mA)	Error (%)	
0.00000	4	3.999	-0.006	3.999	-0.006	GOOD
0.46625	8	7.999	-0.006	8.001	0.006	
0.93250	12	11.999	-0.006	12.004	0.025	
1.39875	16	16.000	0.000	16.003	0.019	
1.86500	20	20.000	0.000	-	-	

span accuracy = (Standard Value-Measurement Value) / adj_span * 100%
Accuracy Test Ref. IEC 61298-2

Item				Result
Appearance	Refer to Inspection Standard			GOOD
Insulation Resistance	500 VDC , ≥ 20MΩ			GOOD
Dielectric Strength	500 VAC , 1 Min.			GOOD
Process Connection	High : 1/4 "18 NPT	Low :	1/4 "18 NPT	GOOD
Electrical Connection	1/2" 14 NPT			GOOD
Communication Function	Refer to Inspection Standard			GOOD

Ambient Temp. & Hum. : 21 ℃ & 50 % R.H

Date 2013-06-07

Inspector

QA Manager

Weitere KOBOLD-Gesellschaften befinden sich in folgenden Ländern:
ÄGYPTEN, ALGERIEN, ARGENTINIEN, AUSTRALIEN, BELGIEN, BULGARIEN, CHILE, CHINA, DOMINIKANISCHE REPUBLIK, FRANKREICH, GROSSBRITANNIEN, INDIEN, INDONESIEN, ITALIEN, KANADA, KOLUMBIEN, MALAYSIA, MAROKKO, MEXIKO, NIEDERLANDE, ÖSTERREICH, PERU, PHILIPPINEN; POLEN, RUMÄNIEN, SCHWEIZ, SINGAPUR, SLOWAKEI, SPANIEN, SÜD KOREA, TAIWAN, THAILAND, TSCHECHIEN, TUNESIEN; UNGARN, USA, VENEZUELA, VIETNAM

KOBOLD Messring GmbH
Nordring 22-24
D-65719 Hofheim/Ts.
☎ +49 (0)6192) 299-0
Fax +49 (0)6192) 23398
E-mail: info.de@kobold.com

Geschäftsführer:
Dipl.-Ing. Klaus J. Kobold
Dipl.-Ing. Harald Peters

Amtsgericht Frankfurt/M.
HRB 29376